

INSTITUTE
FOR
COSMIC RAY RESEARCH
THE UNIVERSITY OF TOKYO

ANNUAL REPORT
(APRIL 2015 – MARCH 2016)



Editorial Board

MIYOKI, Shinji

YOSHIKOSHI, Takanori

TAKENAGA, Yumiko

FUKUDA, Hironobu

©**Institute for Cosmic Ray Research, The University of Tokyo**

5-1-5, Kashiwanoha, Kashiwa, Chiba 277-8582, Japan

Telephone: (81) 4-7136-3102

Facsimile: (81) 4-7136-3115

WWW URL: <http://www.icrr.u-tokyo.ac.jp/>

TABLE OF CONTENTS

Preface	
Research Divisions	1
Neutrino and Astroparticle Division	2
High Energy Cosmic Ray Division	28
Astrophysics and Gravity Division	50
Observatories and a Research Center	66
Norikura Observatory	67
Akeno Observatory	72
Kamioka Observatory	75
Research Center for Cosmic Neutrinos	76
Appendix A. ICRR Workshops and Ceremonies	78
Appendix B. ICRR Seminars	79
Appendix C. List of Publications	79
(a) Papers Published in Journals	
(b) Conference Papers	
(c) ICRR Reports	
Appendix D. Doctoral Theses	87
Appendix E. Public Relations	88
(a) ICRR News	
(b) Public Lectures	
(c) Visitors	
Appendix F. Inter-University Researches	92
Appendix G. List of Committee Members	97
(a) Board of Councillors	
(b) Advisory Committee	
(c) Inter-University Research Advisory Committee	
Appendix H. List of Personnel	98

PREFACE

This report summarizes the scientific activities of the Institute for Cosmic Ray Research (ICRR) of the University of Tokyo in the Japanese FY 2015.

ICRR is an inter-university research institute for studies of cosmic rays. The headquarters of ICRR is located in Kashiwa, Chiba prefecture, Japan. In order to promote various cosmic-ray-related studies efficiently, ICRR has three research divisions; Neutrino and Astroparticle division, High Energy Cosmic Ray division, and Astrophysics and Gravity division. ICRR has 3 observatories in Japan; Kamioka Observatory (Kamioka underground, Gifu prefecture), Norikura Observatory (2770 meters above sea level, Mt. Norikura, Gifu prefecture), and Akeno Observatory (Yamanashi prefecture), together with 1 research center; Research Center for Cosmic Neutrinos (Kashiwa, Chiba prefecture). Furthermore, Gravitational Wave Project Office has been established in 2011 in order to construct the KAGRA gravitational wave detector. In addition, there are 2 major experimental facilities outside of Japan. They are located in Utah in USA, and Yangbajing in Tibet, China.

Many researchers from various Japanese institutions as well as those from overseas are involved in the research programs of ICRR. It should be noted that most of the scientific outputs from this institute are the results of the collaborative efforts by many scientists from various institutions. In order to produce outstanding results, it is very important to carry out an experiment by an international collaboration composed of top-level researchers all over the world. Hence, most of the experimental collaborations that ICRR is involved are international ones. For example, the number of collaborators in the Super-Kamiokande experiment is about 130; about a half of them are from abroad (USA, Korea, China, Poland, Spain, Canada and United Kingdom).

Many exciting scientific activities of ICRR are described in this report. For example, the Super-Kamiokande and T2K (which uses Super-Kamiokande as the far detector) experiments have been continuously producing impressive results on neutrino oscillation physics. The neutrino oscillation studies by the Super-Kamiokande experiment were recognized by the 2015 Nobel Prize in Physics.

Some of the other highlights in JFY2015 are mentioned here: The gravitational wave telescope (KAGRA) had the initial operation in March-April 2016. KAGRA plans to begin operating the advanced interferometer in the Japanese FY 2017. The highest energy cosmic ray experiment TA (Telescope Array) has observed indication that the highest energy cosmic rays arrive from a particular direction of the sky, which may suggest the birth of a new research field, the highest energy cosmic ray astronomy.

As an inter-university research institute, ICRR is reviewed by the top-level researchers in the field. Furthermore, future projects of ICRR are evaluated by a committee composed of top-level researchers from various nearby fields. The report from the ICRR Future Project Evaluation Committee was released in September 2013. The Committee evaluated various possible future projects of ICRR. Several projects have been recommended highly. Among them, joining the CTA project, which is a global TeV gamma ray astronomy project, has been recommended as the top priority ICRR future project. The review report from the External Review Committee, which was released in May 2013 (please see the 2013 Annual Review), also supported joining CTA. ICRR is going to contribute to construct and operate the CTA observatory and carry out various researches with it as an important international partner of this project.

We hope that this report is useful for the understanding of the current research activities of ICRR. Finally, we appreciate very much the strong support of our colleagues in this research field, the University of Tokyo and the Japanese Ministry of Education, Culture, Sports, Science and Technology. They are indispensable for the continuing, and exciting scientific outcome of ICRR.



Takaaki Kajita,
Director,
Institute for Cosmic Ray Research,
The University of Tokyo

2015 Nobel Prize in Physics to Professor Takaaki Kajita

The Nobel prize in physics 2015 was awarded to Takaaki Kajita, the director of Institute for Cosmic Ray Research and Professor at University of Tokyo, and Professor Arthur B. McDonald, Professor Emeritus at Queen's University.

In 1998 Professor Kajita and collaborators discovered that the number of neutrinos created on the opposite side of the earth and that had traveled up through it was only half that of neutrinos raining down from above. This was a result of "neutrino oscillation", a phenomenon in which neutrinos change their type in flight. Since muon neutrinos created on the other side of the earth had changed into tau neutrinos while traveling through it, some of the muon neutrinos appeared to be missing. Neutrino oscillations can only occur if neutrinos have mass. For this reason the observation of neutrino oscillations became conclusive evidence that the neutrino's mass is non-zero. The discovery of atmospheric neutrino oscillations turned the then-accepted theory of elementary particles upside down and opened the door to new physics. Ultimately the significance of this discovery resulted in the 2015 Nobel Prize in Physics.



Awarding ceremony of 2015 Nobel Prize.

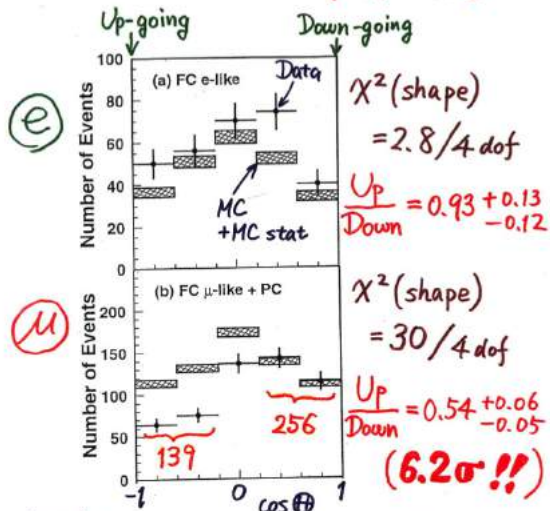


The Sweden King Carl XVI and Professor Kajita.



SK Collaborators.

Zenith angle dependence (Multi-GeV)



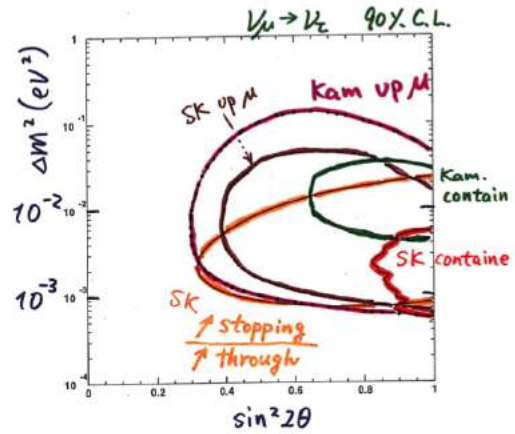
* Up/Down syst. error for μ -like

Prediction (flux calculation $\lesssim 1\%$
1km rock above SK 1.5%) 1.8%

Data (Energy calib. for $\uparrow\downarrow$ 0.7%
Non ν Background < 2%) 2.1%

Summary

Evidence for ν_μ oscillations



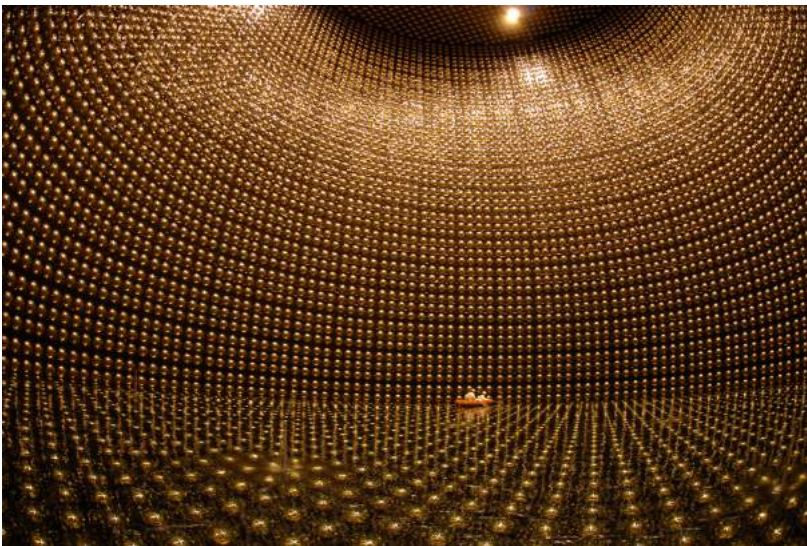
$$\bullet \begin{cases} \sin^2 2\theta > 0.8 \\ \Delta m^2 \sim 10^{-3} \sim 10^{-2} \end{cases}$$

(• $\nu_\mu \rightarrow \nu_\tau$ or $\nu_\mu \rightarrow \nu_s$?)

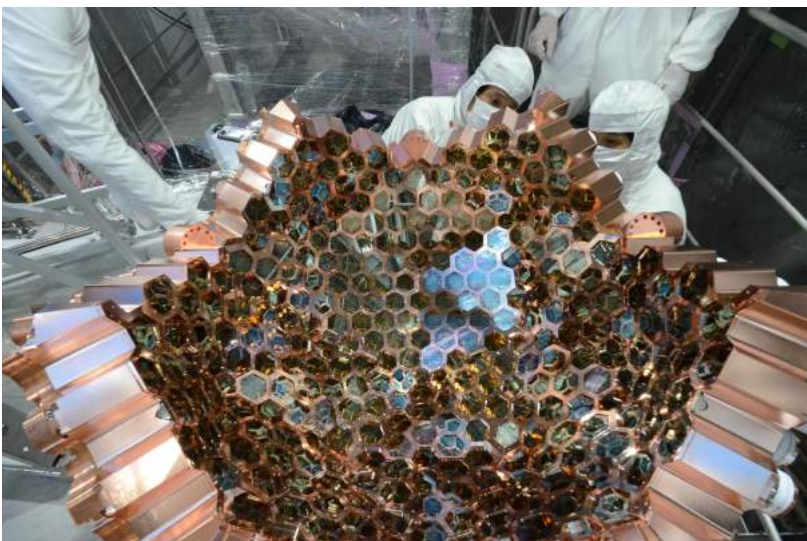
Neutrino oscillation evidence presented at Takayama in 1998.



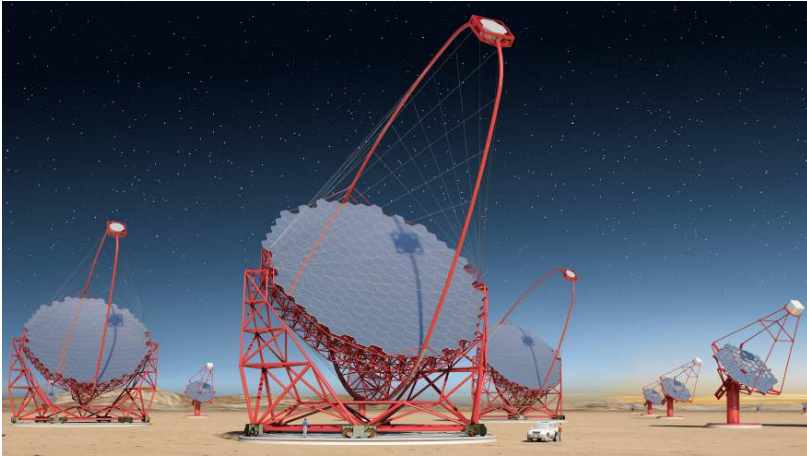
The ICRR building at Kashiwa, Chiba, Japan.



The Super-Kamiokande detector (the photo was taken during pure water fill in 2006).



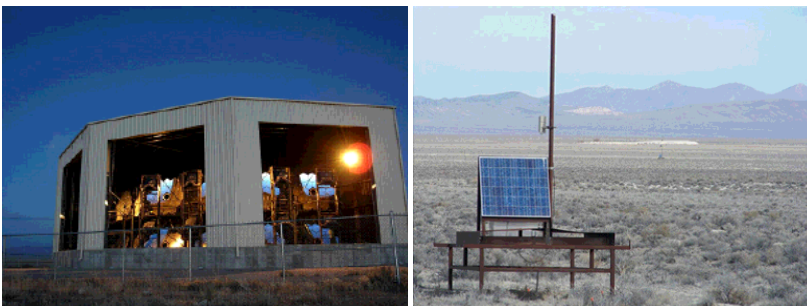
The XMASS detector (the photo was taken during the refurbishment work in 2013).



Artist view of the CTA observatory. CTA consists of three types of telescopes, Large Size Telescopes (23m diameter), Mid Size Telescopes (12m) and Small Size Telescopes (4m), and covers the broad energy band from 20GeV to 100TeV.



Tibet-III air shower array (37000 m²) at Yangbajing, Tibet (4300 m in altitude).



Air fluorescence telescopes (left) and a scintillator surface detector (right) of the Telescope Array experiment in Utah, USA to explore the origin of extremely high energy cosmic rays.

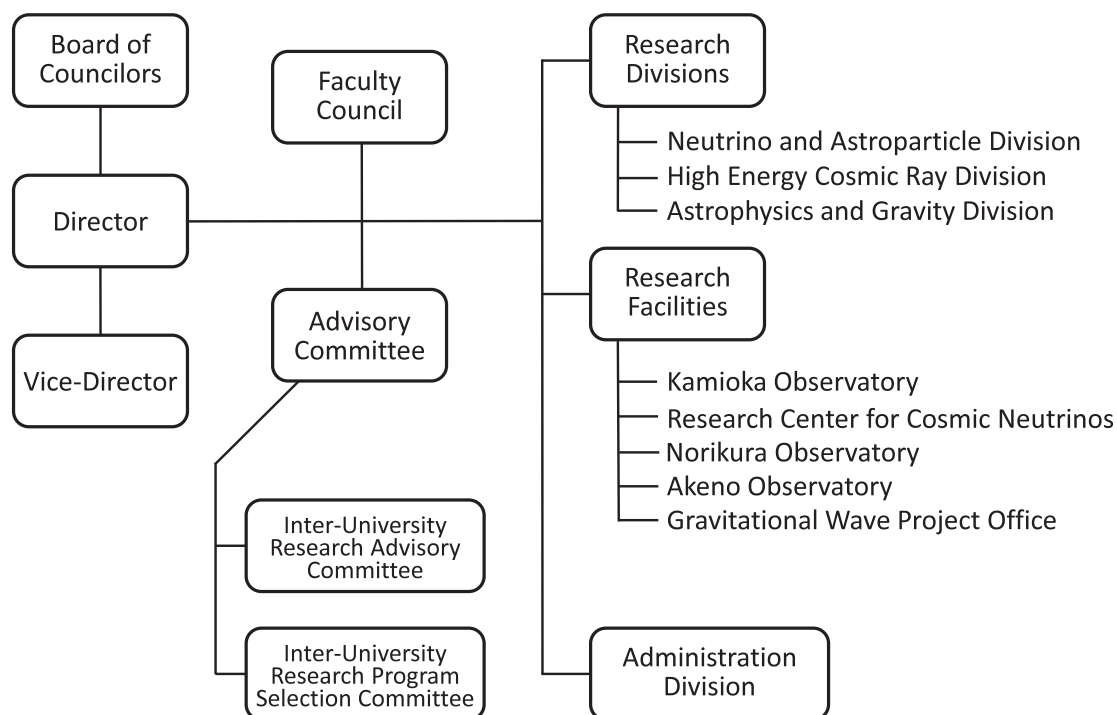


KAGRA X-arm tunnel.



A public lecture held by Research Center for Cosmic Neutrinos.

Organization



Number of Staff Members (As of May 1, 2015)

	Scientific Staff	Technical Staff	Research Fellows	Administrators and Secretaries	Total
Neutrino and Astroparticle Div.	24	4	1	18	47
High Energy Cosmic Ray Div.	17	14	4	2	37
Astrophysics and Gravity Div.	13	2	4	8	27
Administration	0	0	0	14	14
Total	54	20	9	42	125

FY 2008–2015 Budget

	2009	2010	2011	2012	2013	2014	2015
Personnel expenses	590 000	576 000	653 000	658 000	687 000	706 000	757 000
Non-personnel expenses	1 292 000	1 048 000	1 400 000	1 172 000	1 095 000	1 282 000	1 327 000
Total	1 882 000	1 624 000	2 053 000	1 830 000	1 782 000	1 988 000	2 084 000

(in 1 000 yen)

RESEARCH DIVISIONS

Neutrino and Astroparticle Division

Overview

Super-Kamiokande

T2K Experiment

XMASS Experiment

Hyper-Kamiokande

High Energy Cosmic Ray Division

Overview

Cherenkov Cosmic Gamma-Ray Group

TA: Telescope Array Experiment

Tibet AS γ Project

High Energy Astrophysics Group

Other Activities

Astrophysics and Gravity Division

Overview

Gravitational Wave Group

KAGRA Project

Observational Cosmology Group

Theory Group

Particle Phenomenology

Astrophysics and Cosmology

NEUTRINO AND ASTROPARTICLE DIVISION

Overview

This division aims to study particle physics with prime interests in physics of neutrinos and proton decay, and astroparticle physics with the use of underground experimental facilities.

Our most important facility is the Super-Kamiokande (SK) detector. It is a 50 kton water Cherenkov detector using 11,129 50 cm-diameter photomultipliers (PMTs) for its inner detector and 1,885 20 cm-diameter PMTs for its outer detector. The data taking of SK started in April 1996. The neutrino oscillations in atmospheric neutrinos were discovered in 1998 and thereby demonstrating that neutrinos have a finite mass. These findings became the research achievement for which the Nobel Prize in Physics was awarded in 2015. In 2001, the accurate measurements of the ^8B solar neutrino flux by SK and SNO discovered that neutrino oscillations are the solution of the solar neutrino problem beyond doubt. After those discoveries, precise measurements of atmospheric neutrinos and solar neutrinos have been performed and they unraveled various phenomena of neutrino oscillations. In the last few years, excess of events induced by ν_τ appearance was observed in atmospheric neutrinos, and the day/night difference of the solar neutrino flux, which is expected from the matter effect of neutrino oscillations, was observed in the precise solar neutrino measurement. At present, the most interesting subjects in those observations are the determination of neutrino mass hierarchy using atmospheric neutrinos and the consistency check of solar(ν_e) and reactor($\bar{\nu}_e$) oscillations.

A high intensity neutrino beam experiment using the J-PARC accelerator (T2K) was started in 2009. The T2K experiment uses the SK detector as the far detector. Electron neutrino appearance (the effect of the mixing angle θ_{13}) and the high precision measurement of oscillation parameters are main physics subjects in T2K. An indication of electron neutrino appearance was found in June 2011, and the significance of the appearance has been greatly improved in 2013. Since 2014, anti-neutrino beam data also has been taken in order to search for CP violation.

The search for nucleon decay is another important subject at SK because it gives a direct evidence for the Grand Unified Theories (GUTs). SK gives the current best limit which strongly constrains the GUT models.

If a supernova happens in our galaxy, many thousands of neutrino interactions are expected at SK and they will reveal detailed mechanism of the supernova explosion. SK is the only detector in the world that can identify the direction of the supernova. So, SK has been running all the time with small dead time and if a supernova is observed at SK, we will send burst information to astronomers as soon as it is detected. In addition, SK aims to observe supernova relic neutrinos, which is an accumulated supernova burst neutrinos from the beginning of the universe. For this purpose, it is planned to add 0.1% of gadolinium into the Super-K tank (called SK-Gd

project) in order to tag neutrons for $\bar{\nu}_e$ detection. A feasibility study for the SK-Gd project has been performed using a 200 ton tank which mimics the Super-K detector.

Another activity of the Neutrino and Astroparticle division is a multi-purpose experiment using liquid xenon aiming at the detection of cold dark matter, neutrino absolute mass using neutrinoless double beta decay, and low energy solar neutrinos. A 800 kg liquid xenon detector was constructed in an experimental hall near the SK site, and searches for dark matter interactions and rare phenomena in liquid xenon have been running in the last few years.

The Hyper-Kamiokande (Hyper-K) detector is proposed as a next generation underground water Cherenkov detector. The detector is an order of magnitude larger in volume than Super-K and has discovery potential of leptonic CP violation and proton decays. New photosensor R&D and physics potential studies for Hyper-K has been performed in 2015.

SUPER-KAMIOKANDE

[Spokesperson : Masayuki Nakahata
(Kamioka Observatory, ICRR, The University of Tokyo)]

Search for nucleon decay

Proton decays and bound neutron decays (nucleon decays in general) is the most dramatic prediction of Grand Unified Theories (GUTs) in which three fundamental forces of elementary particles are unified into a single force. Super-Kamiokande (SK) is the world's largest detector to search for nucleon decays. Various nucleon decay modes have been looked for, but we have found no significant signal excess so far.

A proton decay into one charged lepton and one neutral pion ($p \rightarrow e^+ \pi^0$, $p \rightarrow \mu^+ \pi^0$) is one of the most popular decay modes which have large detection efficiency. These decay mode is mediated by super-heavy gauge bosons and discovery of the signal would give us the information of the mass of the gauge bosons. To discriminate the signal from the atmospheric neutrino background, we reconstruct the number of particles (Cherenkov rings) and reconstruct the total visible energy corresponding to parent proton mass and total momentum corresponding to the proton's Fermi momentum and the signal region is defined as $800 < M_{tot} < 1050 \text{ MeV}/c^2$ and $P_{tot} < 250 \text{ MeV}/c$. There was an improvement in the analysis and the signal region was divided into free proton enriched region ($P_{tot} < 100 \text{ MeV}/c$) and bound proton enriched region ($100 \leq P_{tot} < 250 \text{ MeV}/c$). The free proton enriched region was almost background free and expected atmospheric neutrino background in 306 kt-year exposure which corresponds to entire SK running period until March 2015, is 0.07 events

for $p \rightarrow e^+\pi^0$ and 0.05 events for $p \rightarrow \mu^+\pi^0$. Also systematic uncertainties comes from proton kinematics and nuclear interaction on decayed particles can be suppressed in this region. On the other hand, more backgrounds and systematic uncertainties were expected in the bound proton enriched region and expected backgrounds in 306 kt-year exposure for $p \rightarrow e^+\pi^0$ and $p \rightarrow \mu^+\pi^0$ were 0.54 and 0.82 events, respectively. By separating signal box into two regions, both sensitivity and discovery potential have been improved.

There were no candidates in data until March 2015 for $p \rightarrow e^+\pi^0$ search and there were two events remained in the bound proton enriched region after all selection for $p \rightarrow \mu^+\pi^0$, as shown in Figure 1 and Figure 2. Both candidates were located very close to border of signal box. The first candidate had a reconstructed invariant mass of 903 MeV/c² and 248 MeV/c total momentum. The first candidate was categorized as a two-ring event; the e -like ring had momentum 375 MeV/c, the μ -like ring had 551 MeV/c momentum, and there was a 158 degree opening angle between the two rings. For the second candidate, the ring counting algorithm originally found one μ -like ring and two e -like rings. However, one of e -like rings (orange ring in Figure 2) was judged as a fake ring at the final stage of ring counting. This stage discards rings caused by multiple coulomb scattering of charged particles by examination of the ring angle relative to other rings and by visible energy. As a result, the second candidate was judged as a two-ring event. In the final result of the reconstruction, the second candidate had a reconstructed invariant mass of 832 MeV/c² and a total momentum of 238 MeV/c calculated from the e -like ring with 461 MeV/c, the μ -like ring with 391 MeV/c, and 149 degree angle between the two rings. If the third ring had not been rejected, the reconstructed invariant mass from the two e -like rings would be 104 MeV/c², which could be gammas from π^0 decay. However, the total momentum and invariant mass would increase to 289 MeV/c and 880 MeV/c², respectively, which would move the event outside of the defined signal region.

The probability to observe ≥ 2 events was calculated to be 23% by assuming Poisson distribution, thus lower limit of proton lifetime with 90% for $p \rightarrow e^+\pi^0$ and $p \rightarrow \mu^+\pi^0$ were estimated to be 1.6×10^{34} and 7.7×10^{33} years, respectively.

Several papers related to nucleon decay search breaking baryon number conservation by 2 have been published in 2015. Neutron-antineutron ($n - \bar{n}$) oscillation, a process violates B and B-L by two was first discussed by V. Kuzumin in 1970 [1]. The discovery of neutrino oscillations has renewed interests in theories with Majorana spinors which yield B and L symmetry breaking by two as a neutrinoless double beta decay and $n - \bar{n}$ oscillation. The observation of $n - \bar{n}$ oscillation signal at SK would imply new physics at a scale of 100 TeV. \bar{n} -nucleon annihilation makes several hadrons in the detector with small total momentum because of Fermi-momentum of nucleon. Also invariant mass from decayed particles should be close to mass of two nucleons. Thus we searched for multi-ring events with $P_{tot} < 450$ MeV/c and $750 < M_{tot} < 1800$ MeV/c² in 1489 live-day data (SK-I). As shown in Figure 3 24 candidates were found in signal region, which was consistent with expected background 24.1 events. Thus, the lower limit of lifetime for $n - \bar{n}$ oscillation and the free neutron oscillation time were es-

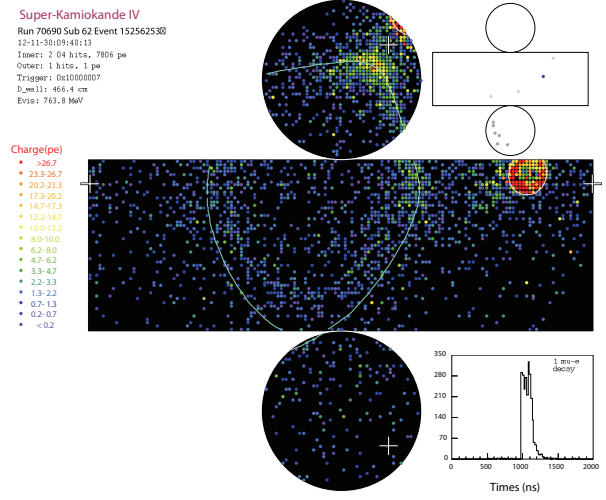


Fig. 1. Event display of the first observed event. The blue solid line and the yellow dashed line show the reconstructed e -like and μ -like ring, respectively.

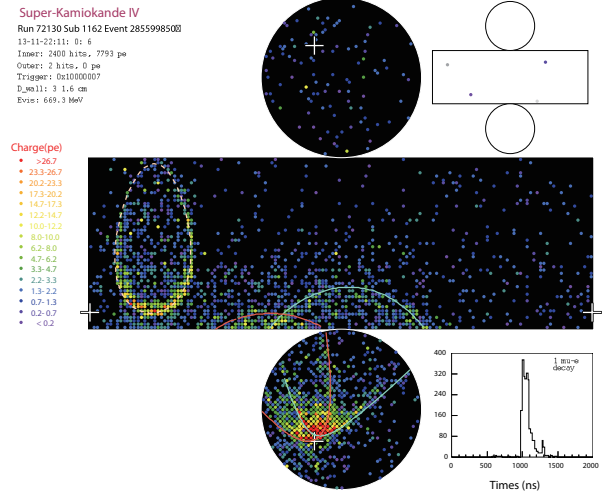


Fig. 2. Event display of the second observed event. The blue solid line and the yellow dashed line show the reconstructed e -like and μ -like ring, respectively. The orange solid line shows an additional e -like ring that was identified in the initial ring counting process, but it is rejected by the ring correction because it is too close in angle to the other e -like ring (blue line). As a result, this event is judged as a two-ring event.

timated to be 1.9×10^{32} years and 2.4×10^8 seconds [2].

Dinucleon decay is the name given to the process where the quarks of the two bound nucleons interact to produce a decay. This process could be occurred by the exchange of a heavy particle which is not predicted by the standard model. The first attempt has been done in SK that search for dinucleon decays into pions; $^{16}O(pp) \rightarrow ^{14}C\pi^+\pi^+$, $^{16}O(pn) \rightarrow ^{14}N\pi^+\pi^0$, and $^{16}O(nn) \rightarrow ^{14}O\pi^0\pi^0$ in 282 kton-year data. Pions from dinucleon decay are back-to-back, but high energy charged pions often make secondary particles in water, which makes the analysis difficult. To select signal candidates, a

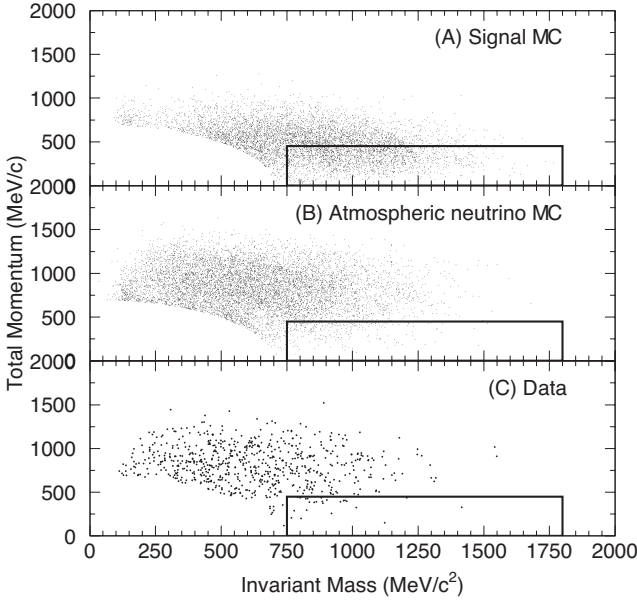


Fig. 3. Total momentum vs the invariant mass after applying the selection criteria (a)-(b) on the FC sample: (A) signal MC, (B) atmospheric neutrino MC, and (C) data. The boxed region in each panel shows the criterion (c)-(d) for the $n - \bar{n}$ oscillation signal.

boosted decision tree method was used for $^{16}O(pp) \rightarrow ^{14}C\pi^+\pi^+$ with 9 input variables and $^{16}O(pn) \rightarrow ^{14}N\pi^+\pi^0$ with 7 input variables. In those variables, angle between two leading μ -like rings had larger importance. For $^{16}O(pn) \rightarrow ^{14}N\pi^+\pi^0$, reconstructed π^0 mass and momentum were also used for input variable. In $^{16}O(pn) \rightarrow ^{14}N\pi^+\pi^0$ mode, all final particles can be observed by SK if π^0 s come out from nucleus. Thus, total mass and momentum cuts were applied; $1600 \leq M_{tot} \leq 2000$ MeV/c² and $P_{tot} \leq 600$ MeV/c. Observed events and expected background for $^{16}O(pp) \rightarrow ^{14}C\pi^+\pi^+$, $^{16}O(pn) \rightarrow ^{14}N\pi^+\pi^0$, and $^{16}O(nn) \rightarrow ^{14}O\pi^0\pi^0$ were 2 (background:4.5), 1 (0.75), and 0 (0.14) events, respectively. The observed events were consistent with the expected background and obtained lower limit of lifetime were estimated to be $\tau_{pp \rightarrow \pi^+\pi^+} > 7.22 \times 10^{31}$, $\tau_{pn \rightarrow \pi^+\pi^0} > 1.70 \times 10^{32}$, and $\tau_{nn \rightarrow \pi^0\pi^0} > 4.04 \times 10^{32}$ years, respectively [3].

Other new searches for nucleon decays into leptons and invisible massless particles X, $p \rightarrow e^+X$, $p \rightarrow \mu^+X$, $n \rightarrow \nu\gamma$, as well as dinucleon decays into leptons, $pn \rightarrow e^+\nu$, $pn \rightarrow \mu^+\nu$, and $pn \rightarrow \tau^+\nu$ have been carried out using 273 kton-year exposure. In this set of decay modes, one charged lepton ring should be found in the detector. In $pn \rightarrow \tau^+\nu$ case, τ has several decay modes but we used only leptonic decay modes, $\tau \rightarrow e\nu\nu$ and $\tau \rightarrow \mu\nu\nu$. Thus momentum distributions of fully-contained single ring e -like and μ -like were checked whether there were any distortions at momentum range expected from these decay modes. Figure 4 shows reconstructed momentum distribution of electron and muon. Top figures correspond to data and atmospheric ν MC. Middle figures correspond to difference between data and atmospheric ν MC and they agree well. Lower limits of lifetime for each mode were calculated by fitting data with momentum distribution of atmospheric ν MC and nucleon or dinucleon decay MC in bottom figures.

Obtained lower limits of lifetime with 90% confidence level were $\tau_{p \rightarrow e^+X} > 7.9 \times 10^{32}$, $\tau_{p \rightarrow \mu^+X} > 4.1 \times 10^{32}$, $\tau_{p \rightarrow \nu\gamma} > 5.5 \times 10^{32}$, $\tau_{pn \rightarrow e^+\nu} > 2.6 \times 10^{32}$, $\tau_{pn \rightarrow \mu^+\nu} > 2.2 \times 10^{32}$, and $\tau_{pn \rightarrow \tau^+\nu} > 2.9 \times 10^{31}$ years, respectively [4].

Bibliography

- [1] V. A. Kuzmin, Pis'ma Zh. E'ksp. Teor. Fiz. **12**, 335 (1970).
- [2] K. Abe *et al.* [Super-Kamiokande Collaboration], Phys. Rev. D **91**, 072006 (2015).
- [3] J. Gustafson *et al.* [Super-Kamiokande Collaboration], Phys. Rev. D **91**, 072009 (2015).
- [4] T. Takhistov *et al.* [Super-Kamiokande Collaboration], Phys. Rev. Lett. **115**, 121803 (2015).

Atmospheric neutrinos

Cosmic ray interactions in the atmosphere produce neutrinos via the decay products of secondary hadrons, such as pions and kaons, emerging from these interactions. The atmospheric neutrino flavor ratio, $(\nu_\mu + \bar{\nu}_\mu)/(\nu_e + \bar{\nu}_e)$, is expected to be approximately two based on the structure of the pion decay chain. Though the uncertainty on this ratio is estimated to be only 5 % or less, the absolute scale of the flux for all neutrino species is much less understood and its prediction carries an uncertainty of at least 20 %. It should be noted that despite this uncertainty, above a few GeV where the effects of the geomagnetic field are negligible, the fluxes of upward- and downward-going neutrinos are nearly equal and therefore provide a useful constraint in the study of these neutrinos. Super-Kamiokande has been observing atmospheric neutrinos since 1996 and has accordingly made several important measurements, including the discovery of neutrino oscillations [1, 2].

Three flavor oscillations and the neutrino mass hierarchy

The SK atmospheric neutrino data are described at leading order by two-flavor $\nu_\mu \rightarrow \nu_\tau$ oscillations with maximal mixing ($\theta_{23}=\pi/4$). However, sub-leading contributions via $\nu_\mu \rightarrow \nu_e$ oscillations induced by the mixing angle θ_{13} as well as the ‘‘solar’’ mixing parameters ($\Delta m_{12}^2, \theta_{12}$) provide the ability to probe currently unknown aspects of the standard neutrino oscillation paradigm, such as the existence of leptonic CP violation and the neutrino mass ordering (hierarchy). Understanding these open questions may bring important insight into larger questions, such as the origin and evolution of today's matter-dominated universe.

Several sub-leading oscillation effects are expected to appear in atmospheric neutrinos:

- Resonant enhancement of $\nu_\mu \rightarrow \nu_e$ oscillations due to the effects of matter occur at energies between 2 and 10 GeV and will manifest as an excess of upward-going electron-like events (e-like) in the atmospheric sample.
- This enhancement exists for either ν_e or $\bar{\nu}_e$ depending on the mass hierarchy. Therefore the mass hierarchy can be probed by understanding the relative amount of neutrino and antineutrino interactions in the detector.

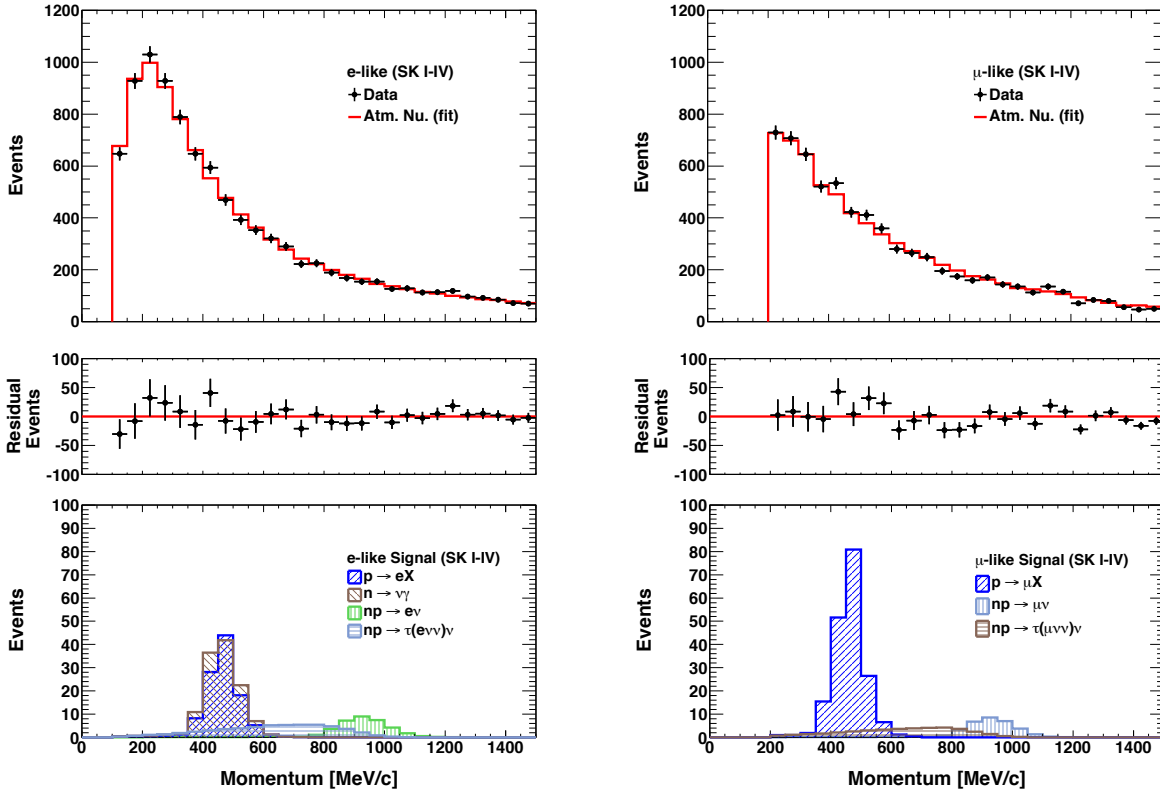


Fig. 4. [Top] Reconstructed momentum distribution for 273.4 kton · years of combined SK data (black dots) and the best-fit result for the atmospheric neutrino background Monte Carlo (solid line). The corresponding residuals are shown below, after fitted background subtraction from data. [Bottom] The 90% confidence level allowed nucleon decay signal (hatched histograms), from the signal and background MC fit to data. All modes are shown (overlaid), with e -like channels on the left and μ -like channels on the right.

- The combination of the solar oscillation parameters and the octant of $\sin^2 \theta_{23}$, may enhance or suppress the event rate, and to some extent alter the spectral shape, of Sub-GeV electron-like data due to $\nu_\mu \leftrightarrow \nu_e$ oscillations they induce.
- The CP violating term, δ_{cp} , induces several sub-dominant oscillation effects which are predicted to appear across many of the SK atmospheric neutrino samples.

Super-Kamiokande has studied the effects of these oscillations on atmospheric neutrino data separated into fully-contained (FC) events, partially-contained (PC) events, and upward-going muon topologies. Fully-contained events are characterized by a primary interaction vertex that is located inside the 22.5 kton fiducial volume of the detector and whose visible particles stop within the inner detector. On the other hand, though the primary vertex position of PC events is within the fiducial volume, they are characterized by having at least one charged particle escaping the inner detector and depositing light in the outer detector. In most cases the escaping particle is a muon. Upward-going muons originate from high energy muon-neutrino interactions in the rock surrounding the detector. Since all other particles are lost to interactions in the rock, only the muon is penetrating enough to reach the detector and be identified. The FC sample is separated into electron-like and muon-like (μ -like) subsamples by applying a particle identification algorithm to the most energetic Cherenkov ring

of each event. Since PC and upward-going events are predominantly produced by muon neutrinos, no particle identification is applied. Though SK cannot distinguish on an event-by-event basis neutrino and antineutrino interactions, since the effect of the mass hierarchy lies in the difference of their oscillations, statistical separation of multi-GeV electron-like subsamples is performed. A likelihood method designed to enhance the kinematic differences between neutrino and antineutrino interactions is applied to separate the events into ν_e -like and $\bar{\nu}_e$ -like subsamples.

The atmospheric neutrino data accumulated during SK-I, -II, -III, and -IV and corresponding to 1489+799+518+2339 days of FC/PC and 1646+828+636+2339 days of upward-going muon data have been analyzed. Zenith angle distributions for six data subsamples are shown in Figure 5. An oscillation analysis considering all mixing parameters from the PMNS framework, including the CP violating term, δ_{cp} , and the effects of the earth's matter on neutrino propagation, has been performed assuming that θ_{13} is constrained to the measured value from reactor neutrino experiments, $\sin^2 \theta_{13}=0.0238$. It should be noted, however, that the uncertainty on this measurement is included as a systematic uncertainty in this analysis. Figure 6 shows the allowed region of the atmospheric mass squared difference (Δm_{32}^2) and θ_{23} parameters obtained from the analysis. Though accelerator experiments such as T2K and MINOS give more stringent constraints, the atmospheric neutrino measurements are consistent with these re-

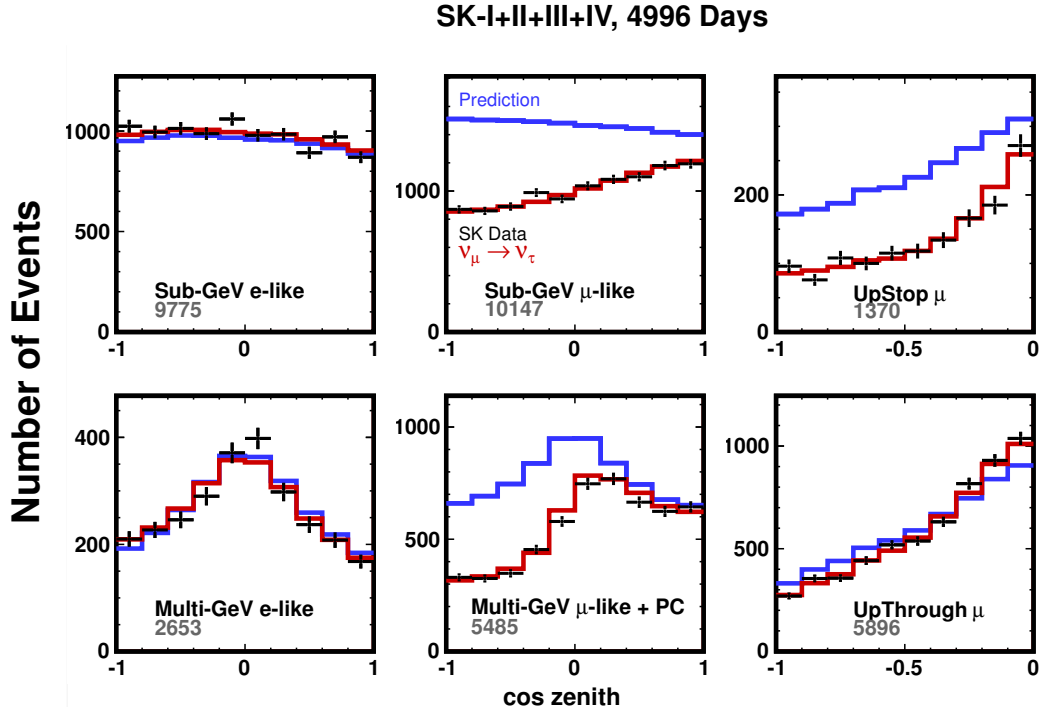


Fig. 5. Zenith angle distributions of SK atmospheric neutrino data. The horizontal axis indicates the cosine of the reconstructed zenith angle ($\cos \theta = -1$ corresponds to the upward-going direction). The data are shown by the black points with error bars and the MC predictions without oscillations and with two flavor $\nu_\mu \rightarrow \nu_\tau$ oscillations are shown by the blue and red lines, respectively.

sults. Comparing the minimum absolute χ^2 values between fits to the normal and inverted hierarchy hypotheses indicate that the Super-K data have a weak preference for the normal mass hierarchy, $\Delta\chi^2 = \chi_{NH}^2 - \chi_{IH}^2 = -3.0$. In order to improve sensitivity to the mass hierarchy the analysis has been extended to include external constraints from the T2K experiment. T2K is modeled using atmospheric neutrino MC reweighted to the beam spectrum and incorporates publicly available data and systematic error information for the analysis [4, 5]. The modeled T2K data samples are then fit in conjunction with the atmospheric neutrino data including relevant systematic error correlations. In this fit the normal hierarchy preference is strengthened to $\Delta\chi^2 = -3.2$. The best fit oscillation parameters and minimum χ^2 values from these analyses are shown in Table 1. It should be noted that the data show a slight preference for $\delta_{cp} = 220^\circ$ but include $\sin\delta_{cp} = 0$ at the 99% C.L. in all fits.

Atmospheric Neutrino Flux Measurement

Measurements of neutrino oscillations like the above and searches for rare processes subject to atmospheric neutrino backgrounds, such as searches for proton decay, are reliant on accurate modeling of the atmospheric neutrino flux. As a result measurements of the flux are a vital tool for establishing the validity of these models. While the computational accuracy and systematic uncertainties present in simulations used to build these flux models have improved dramatically over the last 20 years, atmospheric neutrino flux measurements, particularly at low energies are sparse; The Frejus experiment made the first flux measurements up to 10^4 GeV in 1995

and the cubic-kilometer ice Cherenkov experiments have extended these measurements beyond 10^5 GeV within the last five years. With its efficient particle identification and larger size relative to the Frejus experiments, Super-Kamiokande can provide high statistics measurements of both the $\nu_e + \bar{\nu}_e$ and $\nu_\mu + \bar{\nu}_\mu$ flux at energies below 100 GeV, which are inaccessible to current ice Cherenkov detectors, and thereby bridge the gap between existing measurements. The flux measurement at SK is performed using both the FC e-like data, FC μ -like interactions and the PC and upward-going muon data. The results are in good agreement with the predictions of modern flux models and are shown in Figure 7 [6].

Additionally, the presence of the geomagnetic field enforces a rigidity cutoff on the flux of primary cosmic rays. This cutoff manifests as a suppression of west-going cosmic rays and results in an east-west asymmetry in the flux of these particles, which should also be visible in the atmospheric neutrino flux. At lower energies the effect is expected to be strongest and weaken at higher energies. Though this asymmetry has been previously observed in Super-K's ν_e -dominated e-like samples, it was only seen with marginal significance in the μ -like data. However, in the 16 years since this analysis was performed Super-K has both improved its reconstruction and analysis as well as increased the data sample by a factor of more than six. Figure 8 shows the azimuthal distribution of the FC sub-GeV e-like and μ -like data from a 295 kiloton year exposure of the detector. The azimuthal angle is defined to be the angle measured clockwise from true south to the reconstructed lepton direction. Events reconstructed in the interval 0 to 180 (180 to 360) degrees are defined to west (east)-

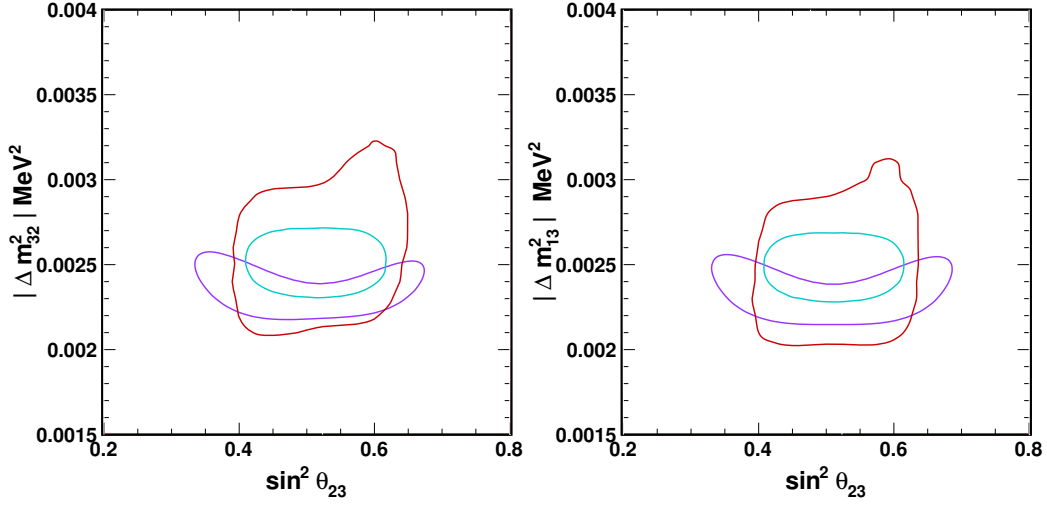


Fig. 6. Allowed regions in the atmospheric mixing plane, $\Delta m_{23,31}^2$ and $\sin^2 \theta_{23}$, at the 90% C.L. as measured by Super-Kamiokande atmospheric neutrinos (red), MINOS (purple) [3], and T2K [4] (cyan). Fits to the normal and inverted hierarchy hypotheses are shown in the left and right figures, respectively.

	$\sin^2 \theta_{13}$	δ_{CP}	$\sin^2 \theta_{23}$	$\Delta m_{32}^2 (\times 10^{-3})$	χ^2
SK only (NH)	0.0238	240	0.58	2.6	582.4
SK only (IH)	0.0238	220	0.58	2.5	585.4
SK+T2K (NH)	0.0238	280	0.53	2.5	651.5
SK+T2K (IH)	0.0238	240	0.55	2.4	654.7

Table 1. Best fit oscillation parameters obtained by the three flavor oscillation analysis. Fits are conducted for both the normal (NH) and inverted (IH) hierarchy assumptions for the atmospheric neutrino data (“SK only”) and including constraints from the T2K experiment (“SK+T2K”). All fits are performed assuming $\sin^2 \theta_{13}=0.0238$.

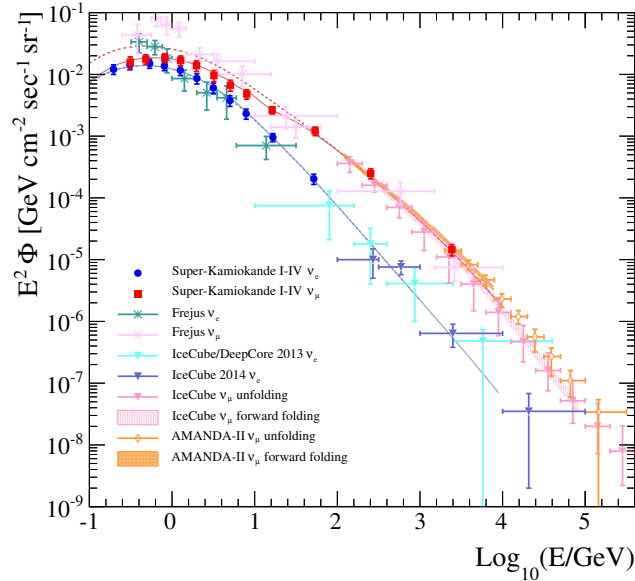


Fig. 7. The measured energy spectra of the atmospheric ν_e and ν_μ fluxes by Super-Kamiokande with measurements by other experiments, Frejus, AMANDA-II, and IceCube. The HKKM11 flux model predicted for Kamioka site are also shown in solid (with oscillation) and dashed (without oscillation) lines. The error bars on the SK measurement include all statistical and systematic uncertainties.

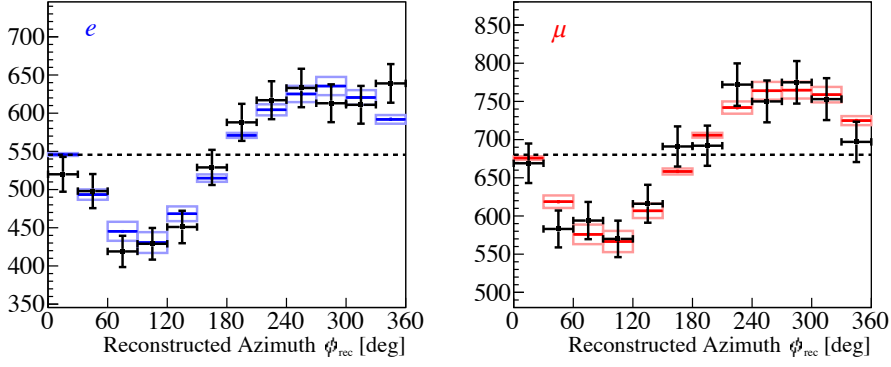


Fig. 8. Azimuthal distributions of sub-selection of e -like (left) and μ -like (right) events, from SK I-IV data (points with statistical error) and MC (boxes with systematic error). The sub-selection is optimized to obtain the highest significance of the final east-west asymmetry by using $0.4 < E_{rec} < 3.0$ GeV and $|\cos(\theta_{rec})| < 0.6$.

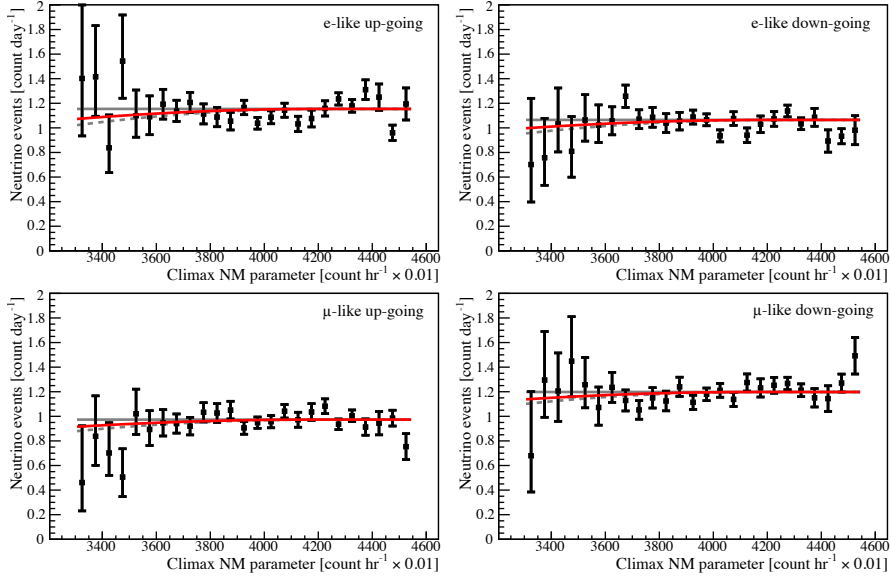


Fig. 9. The test for a solar modulation correlation using the SK I-IV data (points). The solar correlation hypotheses are shown for no correlation ($\alpha=0$, grey), best fit ($\alpha=0.62$, red) and the default prediction ($\alpha=1$, grey dotted) for each of the four data samples. The statistical error bars are also drawn on the data instead of the model.

going. Measurements of the asymmetry of the east-west event rate, $A = (N_{west} - N_{east}) / (N_{west} + N_{east})$, yield $A_e = 0.153 \pm (0.015)(stat) \pm (0.004)(syst)$ for e -like events and $A_\mu = 0.108 \pm (0.014)(stat) \pm (0.004)(syst)$ for μ -like events. These results indicate a clear observation of an east-west asymmetry with 8σ and 6σ significance, respectively [6]. Note that this is the first confirmation of this effect in the ν_μ flux. Further, it should be pointed out that the data in the figure are in good agreement with the predictions from the flux models.

The cosmic ray flux at Earth is well known to be anti-correlated with the solar activity. This is essentially because the plasma flux (or “solar wind”) from the sun can scatter cosmic rays entering the solar system, and therefore during periods of high solar activity the cosmic ray flux is relatively reduced. Consequently, the atmospheric neutrino flux is predicted to also be anti-correlated with the solar cycle, although this has not previously been measured. We test for the anti-correlation of the atmospheric neutrino flux with the solar cy-

cle, by searching for a correlation between the neutrino flux at SK and the neutron detection rates measured at Earth’s surface by various institutes, which are generally believed to be well-correlated with the primary cosmic ray activity. The data, summing over SK I-IV and dividing into the four sample types (e -like or μ -like, and up-going or down-going) are shown in Figure 9. To test for the correlation, we construct flux function to be scaled by a continuous parameter α , where $\alpha=0$ would represent no correlation between the neutrino flux and the neutron rate, and $\alpha=1$ represents the default correlation predicted by HKKM flux calculation. As a result of fit, the best fit value of alpha is $\alpha=0.62^{+0.57}_{-0.58}$. This is lower than the predicted value, but still a reasonably likely result with p -value of 0.26 [6].

Search for sterile neutrino

Though the standard three flavor oscillation scheme has been established by a wide range of experiments, there re-

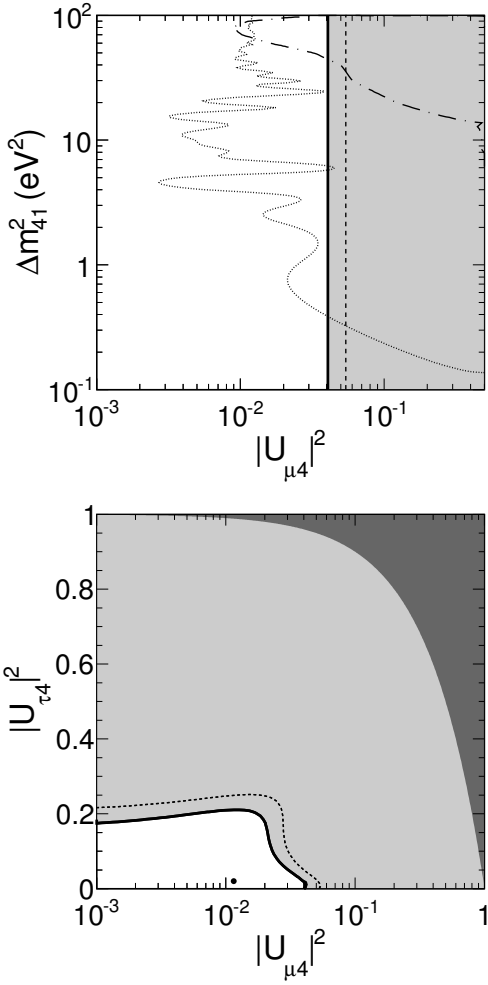


Fig. 10. (Top) Super-Kamiokande’s upper limits on $|U_{\mu 4}|^2$ and on $|U_{\tau 4}|^2$ vs $|U_{\mu 4}|^2$ (bottom). The 90% and 95% C.L. limits are shown by the solid and dashed lines, respectively. The light gray region is excluded at 90 % and the dark gray region is disallowed by unitarity.

main “anomalies” which are not consistent in this picture; For example, the LSND experiment observed $\bar{\nu}_e$ appearance over a short baselines, which when interpreted as an oscillation signal suggests a mass difference inconsistent with the results of solar and atmospheric neutrino measurements, $\Delta m_s^2 \sim 1\text{eV}^2$ [7]. The MiniBooNE experiment, which was designed to study this anomaly, reported a similar excess of $\bar{\nu}_e$ events [8]. Due to the strong constraint on the number of neutrinos from LEP measurements, the additional neutrino suggested by this new mass difference must not participate in weak interactions. These non-interacting neutrinos are therefore called “sterile.” If there is indeed a heavy fourth neutrino state, the effects of the extra oscillation channel atop the dominant $\nu_\mu \rightarrow \nu_\tau$ oscillations are expected to be visible in the atmospheric neutrino flux.

The atmospheric neutrino data has been fit searching for evidence of these oscillations. However, at large masses atmospheric neutrino oscillations become insensitive to the exact value of the mass splitting and are primarily sensitive to

the additional mixing matrix elements between the active and sterile states, $U_{\mu 4}$ and $U_{\tau 4}$. More importantly, the data are insensitive to the precise number of additional sterile neutrinos, a feature unique to atmospheric neutrino studies, so the analysis is performed using a model with only one additional neutrino (the “3+1” model) [10]. The results of two fits, one for $U_{\mu 4}$ with standard matter effects only and one for $U_{\mu 4}$ and $U_{\tau 4}$ including sterile matter effects only, are shown in Figure 10. Tight constraints on both parameters have been obtained, with $|U_{\mu 4}|^2 < 0.041$ and $|U_{\tau 4}|^2 < 0.18$ at 90% C.L., and a large portion of the allowed region from [10] has been ruled out [15].

Limits on Lorentz invariance violation

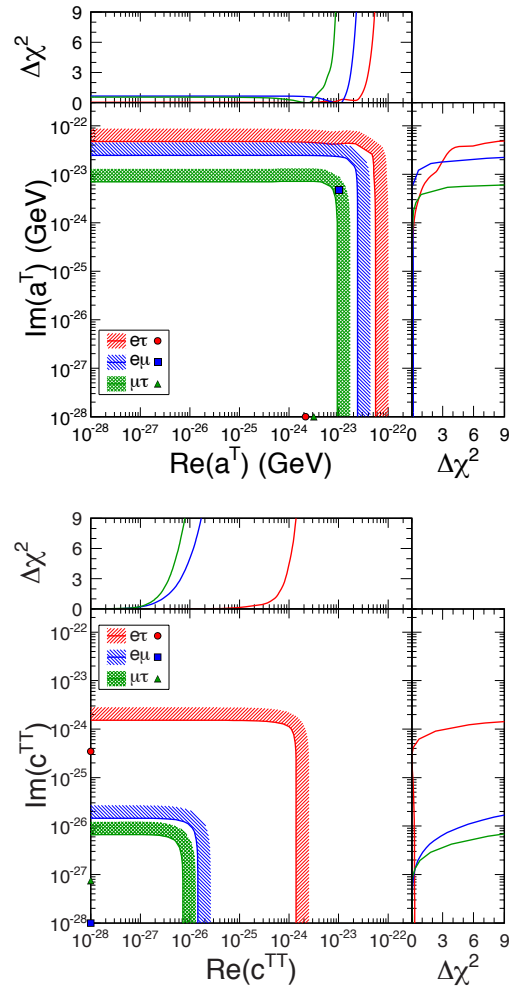


Fig. 11. Contours showing the 95 % confidence level allowed regions for the Lorentz invariance violating parameters $a_{e\tau}^T$ (red), $a_{e\mu}^T$ (blue), $a_{\mu\tau}^T$ (green) appear in the left figure and those for $c_{e\tau}^{TT}$ (red), $c_{e\mu}^{TT}$ (blue), $c_{\mu\tau}^{TT}$ (green) are shown in the right figure. Best fit points from the six fits are also shown.

Symmetry of physical systems under Lorentz transformations is a fundamental feature of both the Standard Model of particle physics and the General Theory of Relativity. Accordingly, violation of this symmetry, termed Lorentz invariance violation (LIV), would provide striking evidence for new physics and has been the focus of many experiments. Neu-

trino oscillations are sensitive to two types of LIV phenomena: sidereal effects, in which oscillations are seen to vary as the earth rotates through its sidereal day, and spectral anomalies, which induce oscillation effects whose frequency is proportional to the neutrino pathlength or the product of the neutrino pathlength with its energy. At Super-K LIV is studied within the context of the standard model extension (SME) [13] which introduces a LIV term, H_{LV} , into the standard neutrino Hamiltonian,

$$H = UMU^\dagger + V_e + H_{LV},$$

where U is the PMNS mixing matrix, M is the neutrino mass matrix and V_e is the earth matter potential. Though H_{LV} can have many possible complex coefficients corresponding to higher dimensional LIV operators, the present analysis focuses only on the isotropic dimension-three and dimension-four contributions,

$$H_{LV} = \pm \begin{pmatrix} 0 & a_{e\mu}^T & a_{e\tau}^T \\ (a_{e\mu}^T)^* & 0 & a_{\mu\tau}^T \\ (a_{e\tau}^T)^* & (a_{\mu\tau}^T)^* & 0 \end{pmatrix} - E \begin{pmatrix} 0 & c_{e\mu}^{TT} & c_{e\tau}^{TT} \\ (c_{e\mu}^{TT})^* & 0 & c_{\mu\tau}^{TT} \\ (c_{e\tau}^{TT})^* & (c_{\mu\tau}^{TT})^* & 0 \end{pmatrix}.$$

The diagonal elements of H_{LV} have been neglected since they cannot be observed in neutrino oscillations. Though this matrix represents the neutrino Hamiltonian, antineutrino propagation is described by changing the sign of the first matrix and taking the complex conjugate of the a^T and c^{TT} parameters.

It should be noted that this is the first analysis to approach the problem of LIV in the SME without introducing approximations. Indeed, the usual perturbative conditions introduced to simplify analysis in this framework are invalid for the high energy Super-K atmospheric neutrino data, so the complete neutrino evolution equation has been solved when computing oscillation probabilities. After performing oscillation fits including these effects, no evidence for LIV is seen. As a result, Super-K has set limits on the isotropic parameters a^T and c^{TT} in the $e\mu$, $\mu\tau$, and $e\tau$ sectors as shown in Figure 11. Despite the lack of a positive signal, the SK constraints on the existence of LIV phenomena in neutrino oscillations improve on existing limits [11] for a^T and c^{TT} by four and seven orders of magnitude, respectively [16].

Indirect WIMP searches

Astronomical and cosmological observations point conclusively to the existence of dark matter and though invisible to electromagnetic probes, it is thought to represent 26% of the matter-energy content of the universe. Weakly Interacting Massive Particles (WIMPs), GeV/c^2 -scale particles which have only gravitational and weak interactions, are a favored candidate to explain the existence of this as yet unknown matter. Though direct dark matter detection experiments search for the elastic scattering interactions of these proposed particles with ordinary baryonic matter, it is also possible that WIMPs decay or annihilate into Standard Model particles which can then be detected to give indirect evidence for WIMPs. If WIMPs become trapped in the gravitational potential of a massive system, such as the center of the Milky Way or the sun, their density may become sufficient for large numbers of these particles to annihilate into particles which then decay into neutrinos. In this case the neutrinos pass undeflected

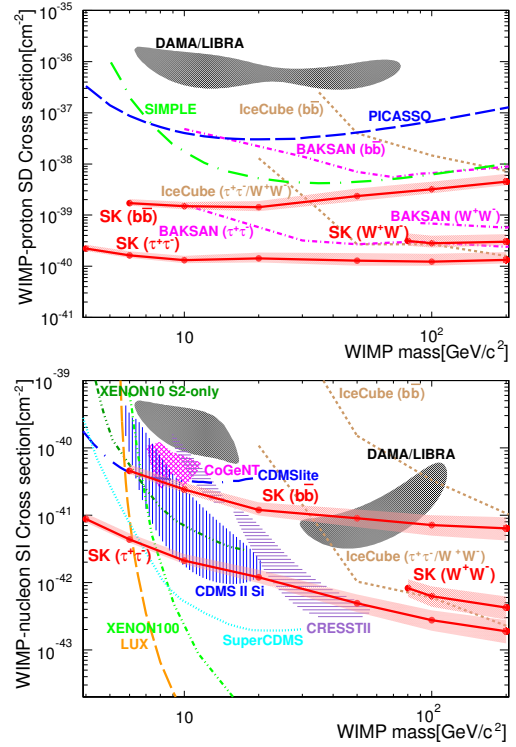


Fig. 12. The 90% C.L. upper limits on the spin-dependent (top) and spin-independent (bottom) WIMP-nucleon scattering cross section based on a search from WIMP-induced neutrinos coming from the direction of the sun are shown as a function of WIMP mass. These limits are calculated assuming WIMP annihilation into $\tau^+\tau^-$, $b\bar{b}$, and W^+W^- each with 100% branching fraction. Limits and allowed regions from other experiments are also shown.

through the universe and would therefore create an additional neutrino signal with a characteristic energy spectrum emerging from a common direction.

At Super-K, though the search for these particles is dominated by the atmospheric neutrino background, the expectation that they are produced at a common location in the sky is a powerful discriminant. Accordingly, the atmospheric neutrino data are binned in both lepton momentum and the reconstructed angle to either the galactic center or to the sun to search for the presence of an extra neutrino signal from those directions. Since there is no knowledge of WIMP interactions, the analysis proceeds by separately assuming annihilation into each of $\nu\bar{\nu}$, $b\bar{b}$, $t\bar{t}$, and W^+W^- with 100% branching fraction. For each assumed WIMP mass the expected neutrino energy distribution emerging from the decay chains of these particles is computed and used to define the signal spectrum at Super-K. In contrast to previous studies, the entire atmospheric neutrino data set is used and therefore gives access WIMP masses in the range of several GeV/c^2 to TeV/c^2 . No evidence for a neutrino signal on top of the atmospheric neutrino background has been found in the direction of either the galactic center or the sun. Limits on the WIMP-nucleon spin-dependent and spin-independent scattering cross sections from the search for events from the sun are shown in Figure 12 [17].

Bibliography

- [1] Y. Fukuda *et al.* [Super-Kamiokande Collaboration], Phys. Rev. Lett. **81** 1562 (1998).
- [2] Y. Fukuda *et al.* [Super-Kamiokande Collaboration], Phys. Rev. Lett. **81**, 1562 (1998) [arXiv:9807003 [hep-ex]].
- [3] P. Adamson *et al.* [MINOS Collaboration], Phys. Rev. Lett. **112**, 191801 (2014) [arXiv:1403.0867 [hep-ex]].
- [4] K. Abe *et al.* [T2K Collaboration], Phys. Rev. Lett. **112**, 181801 (2014) [arXiv:1403.1532 [hep-ex]].
- [5] K. Abe *et al.* [T2K Collaboration], Phys. Rev. Lett. **112**, 061802 (2014) [arXiv:1311.4750 [hep-ex]].
- [6] E. Richard, K. Okumura *et al.* [Super-Kamiokande Collaboration], to be published, [arXiv:1510.08127 [hep-ex]].
- [7] A. Aguilar-Arevalo *et al.* [LSND Collaboration], Phys.Rev. **D64**, 112007 (2001), [arXiv:0104049 [hep-ex]].
- [8] A. Aguilar-Arevalo *et al.* [MiniBooNE Collaboration], Phys.Rev.Lett. **110**, 161801 (2013).
- [9] P. Huber, Phys.Rev. **C84**, 024617 (2011), [arXiv:1106.0687 [hep-ph]].
- [10] J. Kopp, P. A. N. Machado, M. Maltoni, and T. Schwetz, JHEP **1305**, 050 (2013).
- [11] V. A. Kostelecky, N. Russell and R. Tso, Phys. Lett. B **716**, 470 (2012) [arXiv:1209.0750 [hep-th]].
- [12] R. Abbasi *et al.* [IceCube Collaboration], arXiv:1210.3557 [hep-ex].
- [13] V. A. Kostelecky, Phys. Rev. D **69**, 105009 (2004) [hep-th/0312310].
- [14] D. Cokinos and E. Melkonian, Phys. Rev. C **15**, 1636 (1977).
- [15] K. Abe *et al.* [Super-Kamiokande Collaboration], Phys. Rev. D **91**, 052019 (2015) [arXiv:1410.2008 [hep-ex]].
- [16] K. Abe *et al.* [Super-Kamiokande Collaboration], Phys. Rev. D **91**, no. 5, 052003 (2015) [arXiv:1410.4267 [hep-ex]].
- [17] K. Choi *et al.* [Super-Kamiokande Collaboration], Phys. Rev. Lett. **114**, no. 14, 141301 (2015) [arXiv:1503.04858 [hep-ex]].

Solar Neutrinos

Solar neutrino flux measurements from Super-Kamiokande (SK) [1] and the Sudbury Neutrino Observatory (SNO) [2] have provided direct evidence for solar neutrino flavour conversion. However, there is still no clear evidence that this solar neutrino flavour conversion is indeed due to neutrino oscillations and not caused by any other mechanism. Currently there are two testable signatures unique to neutrino oscillations. The

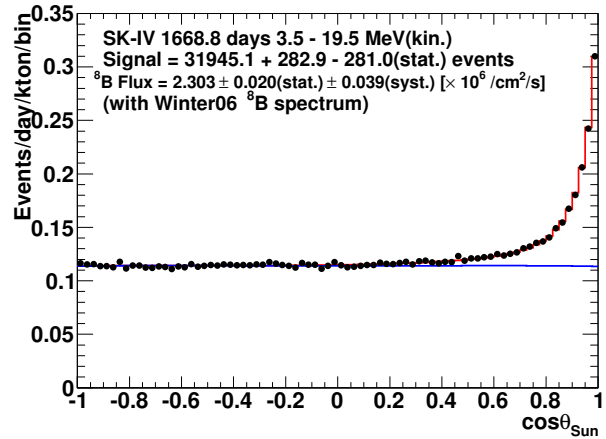


Fig. 13. Solar angle distribution for 3.5-19.5 MeV. θ_{sun} is the angle between the incoming neutrino direction and the reconstructed recoil electron direction. Black points are data while the blue and red histograms are best fits to the background and signal plus background, respectively.

first is the observation and precision test of the MSW resonance curve [3]. Based on oscillation parameters extracted from solar neutrino and reactor anti-neutrino measurements, there is an expected characteristic energy dependence of the flavour conversion. The higher energy solar neutrinos (higher energy ^8B and hep neutrinos) undergo complete resonant conversion within the sun, while the flavour changes of the lower energy solar neutrinos (pp, ^7Be , pep, CNO and lower energy ^8B neutrinos) arise only from vacuum oscillations, which limits the average electron flavour survival probability to exceed 50%. The transition from the matter dominated oscillations within the sun, to the vacuum dominated oscillations, should occur near 3 MeV, making ^8B neutrinos the best choice when looking for a transition point within the energy spectrum. A second signature unique to oscillations arises from the effect of the terrestrial matter density on solar neutrino oscillations. This effect is tested directly by comparing solar neutrinos which pass through the Earth at nighttime to those which do not during the daytime. Those neutrinos which pass through the Earth will in general have an enhanced electron neutrino content compared to those which do not, leading to an increase in the nighttime electron elastic scattering rate (or any charged-current interaction rate), and hence a negative “day/night asymmetry”. SK detects ^8B solar neutrinos over a wide energy range in real time, making it a prime detector to search for both solar neutrino oscillation signatures.

The start of physics data taking of SK-IV occurred on October 6th, 2008, with this report including data taken until January 31st, 2014. The total livetime is 1668.8 days. The entire data period was taken using the same low energy threshold, with about 85% triggering efficiency at 3.5-4.0 MeV kinetic energy, 99% at 4.0-4.5 MeV kinetic energy and 100% above 4.5 MeV kinetic energy. In the case of ν -e interactions of solar neutrinos in SK, the incident neutrino and recoil electron directions are highly correlated. Fig.13 shows the $\cos \theta_{\text{sun}}$ distribution for events between 3.5-19.5 MeV. In order to obtain the number of solar neutrino interactions, an extended maximum likelihood fit is used. This method is also used in the

SK-I [1], II [4], and III [5] analyses. The red line of Fig.13 is the best fit to the data. The blue line shows the background component of that best fit.

The combined systematic uncertainty of the total flux in SK-IV is found to be 1.7% as the quadratic sum of all components. This is the best value seen throughout all phases of SK, much improved over 2.2% in SK-III. The main contributions to the reduction come from improvements in the uncertainties arising from the energy-correlated uncertainties (energy scale and resolution), the vertex shift, trigger efficiency and the angular resolution. SK-III data below 6.0 MeV recoil electron kinetic energy has only about half the livetime as the data above, while SK-IV's livetime is the same for all energy bins. As a consequence, the energy scale and resolution uncertainties lead to a smaller systematic uncertainty of the flux in SK-IV than in SK-III. The higher efficiency of SK-IV between 5.0 and 6.0 MeV (kinetic) of SK-IV and the addition of the 3.5 to 4.5 MeV data lessens the impact of energy scale and resolution uncertainty on the flux determination even further. The number of solar neutrino events (between 3.5 and 19.5 MeV) is $31,945^{+283}_{-281}(\text{stat.}) \pm 543(\text{syst.})$. This number corresponds to a ${}^8\text{B}$ solar neutrino flux of $\Phi_{8\text{B}} = (2.303 \pm 0.020(\text{stat.}) \pm 0.039(\text{syst.})) \times 10^6 / (\text{cm}^2\text{sec})$, assuming a pure ν_e flavor content.

Fig.14 shows the resulting SK-IV energy spectrum. SK-IV has $N_{\text{bin}} = 23$ energy bins; 20 bins of 0.5 MeV width between 3.5-13.5 MeV, two energy bins of 1 MeV between 13.5 and 15.5 MeV, and one bin between 15.5 and 19.5 MeV.

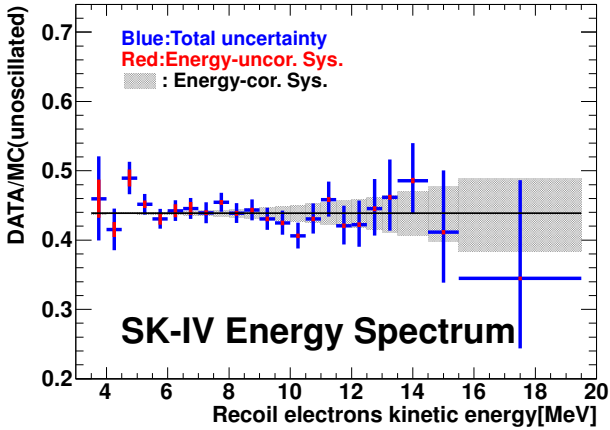


Fig. 14. SK-IV energy spectrum. The horizontal dashed line gives the SK-IV average. Error bars shown are statistical plus energy-uncorrelated systematic uncertainties. Energy-correlated systematic uncertainties are shown separately as shaded region.

To test the expected “upturn” below ~ 6 MeV from the MSW resonance effects, the best fit oscillation parameters of solar experiments and solar + KamLAND (described later) were fitted to all the SK-I to SK-IV spectra, and it is disfavored by 1σ and 1.7σ respectively so far. Fitted results are shown in Fig.15.

As SK has observed solar neutrinos for 17 years, about 1.5 solar activity cycles to date, an analysis regarding possible correlations between the solar neutrino flux and the 11 year solar activity cycle was conducted. A constant flux was fitted

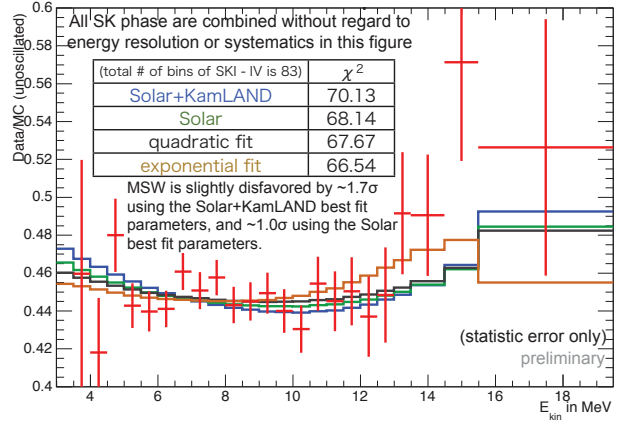


Fig. 15. All SK phase combined energy spectrum and fitted functions.

and results are shown in Fig.16. ($\chi^2/\text{dof} = 13.57/17$) Super-K solar rate measurements are fully consistent with a constant solar neutrino flux emitted by the Sun.

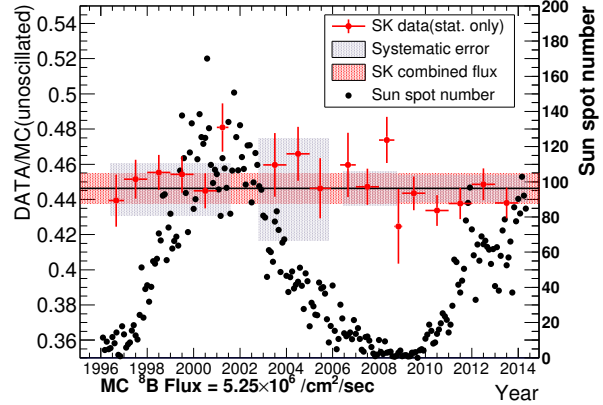


Fig. 16. Flux data from all SK phases as a function of time. Sun spot numbers [6] are also plotted

The SK-IV livetime during the day (night) is 799.7 days (869.1 days). The solar neutrino flux between 4.5 and 19.5 MeV and assuming no oscillations is measured as $\Phi_D = (2.25 \pm 0.03(\text{stat.}) \pm 0.38(\text{syst.})) \times 10^6 / (\text{cm}^2\text{sec})$ during the day and $\Phi_N = (2.36 \pm 0.03(\text{stat.}) \pm 0.40(\text{syst.})) \times 10^6 / (\text{cm}^2\text{sec})$ during the night. A more sophisticated method to test the day/night effect is given in [1, 7]. For a given set of oscillation parameters, the interaction rate as a function of the solar zenith angle is predicted. Only the shape of the calculated solar zenith angle variation is used, the amplitude of it is scaled by an arbitrary parameter. The extended maximum likelihood fit to extract the solar neutrino signal is expanded to allow time-varying signals. The likelihood is then evaluated as a function of the average signal rates, the background rates and the scaling parameter which is called the “day/night amplitude”. The equivalent day/night asymmetry is calculated by multiplying the fit scaling parameter with the expected day/night asymmetry. In this manner the day/night asymmetry is measured more precisely statistically. Because the amplitude fit depends on the assumed shape of the day/night variation, it necessar-

ily depends on the oscillation parameters, although with very little dependence expected on the mixing angles (in or near the large mixing angle solutions and for θ_{13} values consistent with reactor neutrino measurements [8]).

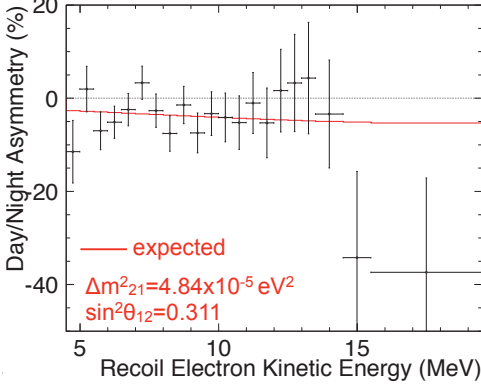


Fig. 17. SK combined energy dependence of the fitted day/night asymmetry (measured day/night amplitude times the expected asymmetry (red)) for $\Delta m_{21}^2 = 4.84 \times 10^{-5} \text{eV}^2$, $\sin^2 \theta_{12} = 0.311$ and $\sin^2 \theta_{13} = 0.025$. The error bars shown are statistical uncertainties only.

The day/night asymmetry coming from the SK-I to IV combined amplitude fit can be seen as a function of recoil electron kinetic energy in Fig.17, for $\Delta m_{21}^2 = 4.84 \times 10^{-5} \text{eV}^2$, $\sin^2 \theta_{12} = 0.311$ and $\sin^2 \theta_{13} = 0.025$. The day/night asymmetry in this figure is found by multiplying the fitted day/night amplitude from each energy bin, to the expected day/night asymmetry (red distribution) from the corresponding bin.

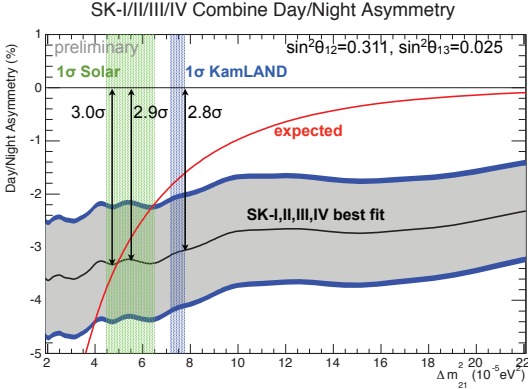


Fig. 18. Dependence of the measured day/night asymmetry (fitted day/night amplitude times the expected day/night asymmetry (red)) on Δm_{21}^2 (light gray band=stat. error, dark gray band=stat.+syst. error) for $\sin^2 \theta_{12} = 0.311$ and $\sin^2 \theta_{13} = 0.025$. Overlaid are the allowed ranges from solar neutrino data (green band) and KamLAND (blue band).

Fig.18 shows the Δm_{21}^2 dependence of the SK all phases combined day/night asymmetry for $\sin^2 \theta_{12} = 0.311$ and $\sin^2 \theta_{13} = 0.025$. Here the day/night asymmetry is also found by multiplying the fitted day/night amplitude by the expected day/night asymmetry (red curve). The point where the best fit crosses the expected curve represents the value of Δm_{21}^2 where the measured day/night asymmetry is equal to the expectation. Superimposed are the allowed ranges in Δm_{21}^2 from the global solar neutrino data fit (green) and from KamLAND (blue).

The amplitude fit shows no dependence on the values of θ_{12} (within the LMA region of the MSW plane) or θ_{13} .

We analyzed the SK-IV elastic scattering rate, the recoil electron spectral shape and the day/night variation to constrain the solar neutrino oscillation parameters. We then combined the SK-IV constraints with those of previous SK phases, as well as other solar neutrino experiments. The allowed contours of all solar neutrino data (as well as KamLAND's constraints) are shown in Fig.19 and 20. In Fig.19 the contours from the fit to all solar neutrino data are almost identical to the ones of the SK+SNO combined fit. In the right panel some tension between the solar neutrino and reactor anti-neutrino measurements of the solar Δm_{21}^2 is evident. This tension is mostly due to the SK day/night measurement. Even though the expected amplitude agrees well within 1σ with the fitted amplitude for any Δm_{21}^2 in either the KamLAND or the SK range, the SK data somewhat favor the shape of the variation predicted by values of Δm_{21}^2 that are smaller than KamLAND's. The best fit values are $\sin^2 \theta_{12} = 0.308 \pm 0.013$, $\Delta m_{21}^2 = 7.50_{-0.18}^{+0.19} \times 10^{-5} \text{eV}^2$, and $\sin^2 \theta_{13} = 0.027_{-0.014}^{+0.016}$. The significance of non-zero θ_{13} is about 2σ .

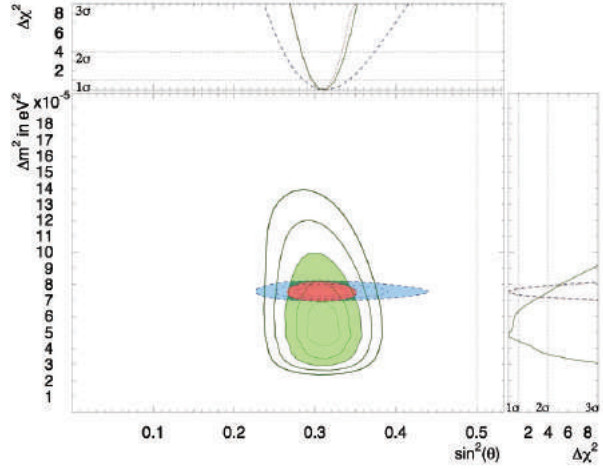


Fig. 19. Allowed contours of Δm_{21}^2 vs. $\sin^2 \theta_{12}$ from solar neutrino data (green) at 1, 2, 3, 4 and 5 σ and KamLAND data (blue) at the 1, 2 and 3 σ confidence levels. Also shown are the combined results in red. For comparison, the almost identical results of the SK+SNO combined fit are shown by the dashed dotted lines. θ_{13} is constrained by $\sin^2 \theta_{13} = 0.0242 \pm 0.0026$.

In summary, the analysis threshold was successfully lowered to 3.5 MeV kinetic recoil electron energy in SK-IV and by adding SK-IV data, $\sim 70,000$ solar neutrino interactions has been observed in $\sim 4,500$ days (1.5 solar activity cycles), by far the largest sample of solar neutrino events in the world. It turned out Super-K solar rate measurements are fully consistent with a constant solar neutrino flux emitted by the Sun. SK spectrum results slightly disfavor the MSW resonance curves, but are consistent with MSW prediction within $1 \sim 1.7\sigma$. SK data provide the first indication (at $2.8 \sim 3.0\sigma$) of terrestrial matter effects on ^8B solar neutrino oscillation. This is the

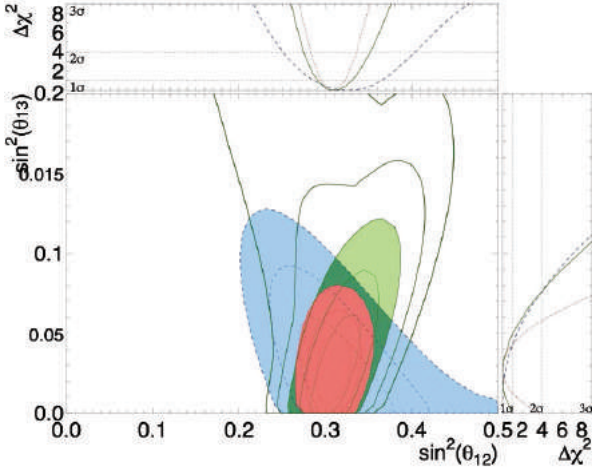


Fig. 20. Allowed contours of $\sin^2 \theta_{13}$ vs. $\sin^2 \theta_{12}$ from solar neutrino data (green) at 1, 2, 3, 4 and 5 σ and KamLAND measurements (blue) at the 1, 2 and 3 σ confidence levels. Also shown are the combined results in red.

first observation using a single detector and identical neutrino beams that matter affects neutrino oscillations [9]. These SK measurements strongly constrain neutrino oscillation parameters: SK uniquely selects the Large Mixing Angle MSW region by $> 3\sigma$, gives world's best constraint on Δm_{21}^2 using neutrinos, and significantly contributes to the measurement of θ_{12} .

Bibliography

- [1] J.Hosaka et al., Phys. Rev. D73, 112001 (2006).
- [2] Q.R.Ahmad et al., Phys. Rev. Lett. 87 071301 (2001).
- [3] S.P.Mikheyev and A.Y.Smirnov, Sov. Jour. Nucl. Phys. 42, 913 (1985); L.Wolfenstein, Phys. Rev. D17, 2369 (1978).
- [4] J.P.Cravens et al., Phys. Rev. D 78, 032002(2008).
- [5] K.Abe et al., Phys. Rev. D 83 052010 (2011).
- [6] http://solarscience.msfc.nasa.gov/greenwch/spot_num.txt
- [7] M.B.Smy et al., Phys. Rev. D. 69, 011104(R) (2004).
- [8] F.P.An et al., arXiv:1210.6327 (2012); J.K.Ahn et al., Phys.Rev.Lett. 108 191802 (2012); Y.Abe et al.,Phys.Rev. D86 052008 (2012).
- [9] A.Renshaw et al., Phys. Rev. Lett. 112, 091805 (2014).

Supernova neutrinos

In 1987, the observation of supernova 1987a by Kamiokande and IMB etc, opened the neutrino astronomy. This observation confirmed that the energy released by neutrinos is about

several $\times 10^{53}$ ergs. However, the core collapse supernova (ccSN) mechanism is not yet fully understood. Super-Kamiokande (SK) would be able to detect several thousand neutrino events if a ccSN happened near the center of our galaxy. Such an observation would enable us to investigate in detail the mechanics of the ccSN explosion.

On average, 1-2 ccSNe per century are expected in our galaxy and therefore we must be prepared for these events. An online program called SNWATCH searches for time clustered events [1]. Events with total energy greater than 7 MeV and vertex position within the 22.5-kton fiducial volume in SK are selected. Cosmic ray muons and their subsequent decay electron events are removed. For each selected event, a 20-second time window is opened backwards in time, and the number of selected events in the window, N_{clus} , is counted. A variable D that identifies the dimension of the vertex distribution is computed. It is an integer number from 0 to 3, corresponding to point-, line-, plane- and volume-like distributions, respectively.

When $N_{clus} \geq 60$ and $D = 3$ a prompt SN warning is generated including an automatic phone-calling and emails to experts. Then, the experts check whether it is a real supernova signal or not by looking at various plots which are uploaded to a secured site accessible from the Internet. These alarms are usually due to the accidental coincidence of two cosmic ray induced clusters. We have supernova drills several times per year. So far, no real supernova neutrino burst signal has been observed at SK.

In the drill, the SNWATCH conveners and the executive committee members meet via TV conference system, and discuss to make a decision for a prompt announcement (within 1 hour) to outside researchers and the press. We practice this drill as if a real supernova happened. We also have SK shift training by illuminating an LD in the SK detector a few times every month. SK shift members are notified by a dummy alarm that SNWATCH makes when the LD is illuminated. The shift members then call to the SNWATCH experts and give a report. The SK collaborators will be ready for the real supernovae through the drill and the training.

Another searches conducted at SK are those for neutrinos from Supernova Relic Neutrinos (SRNs). The SRN signal is the diffuse supernova neutrino background from all the core collapse supernovae in the past. This signal has never been detected, but it is expected to be detectable in the 16-30 MeV energy region, which is the gap between the energy ranges of solar neutrinos and atmospheric neutrinos. Our published result [2] utilizes SK-I, II and SK-III data with analysis energy threshold of 16 MeV. A maximum likelihood search was performed in multiple regions of the Cherenkov angle distribution to extract the most accurate flux limit. The obtained flux limit is between 2.7 and 3.0 $\bar{\nu} cm^{-2} s^{-1}$ (positron energy > 16 MeV), which in fact depends on the shape of the neutrino spectrum assumed. This result currently provides the world's best limit on SRN flux. (Figure 22).

In SK-IV, a new result of the SRN search using the neutron tagging technique was also published [3]. In this analysis, neutrons from SRN reactions ($\bar{\nu}_e, p \rightarrow e^+, n$) are captured on hydrogen. After a neutron is captured, a single 2.2 MeV gamma is emitted. Thus, by detecting the prompt positron

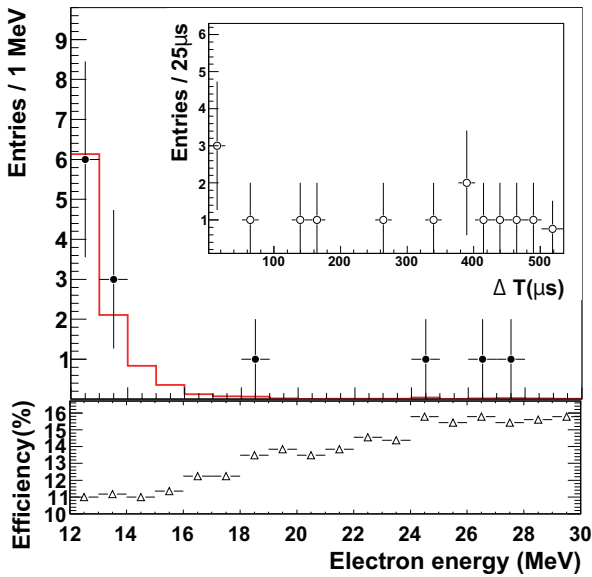


Fig. 21. Energy spectrum of prompt signals (points). The red histogram shows the expected accidental background. The plot embedded in the upper right shows the timing difference for the delayed candidates. The bottom figure shows the detection efficiency of SRN for each energy bin; the jumps at 18 MeV and 24 MeV are due to energy-dependent spallation cuts. Errors are statistical only.

R&D for the gadolinium project

As mentioned above, although at SK a few SRN events a year are expected, SRNs have not been detected yet because of the large backgrounds that constrain our search. The main goal of our research is to reduce these backgrounds and be able to detect SRNs. The observation of SRNs in general or neutrinos from distant supernovae in particular, would give us some information about the universe, for example the core collapse rate from SRNs, and about the neutrino itself too, for example its lifetime.

As shown in the previous section, the current SK detector can only detect positrons efficiently but not neutrons. In order to achieve a high detection efficiency for neutrons, it is proposed to add 0.2% of gadolinium (Gd) sulfate into SK. Since Gd has a neutron capture cross section of 49,000 barns (about 5 orders of magnitude larger than that of protons) and emits a gamma cascade of 8 MeV, neutrons could be easily detected at SK (in space, vertices within tens of cm and in time, with the neutron capture delayed about 20 μ sec).

EGADS (Evaluation Gadolinium's Action on Detector Systems) project was funded in 2009. The main motivation of EGADS is to show that by adding Gd, SK will be able to detect anti-neutrinos using the delayed coincidence technique, while keeping all its capabilities in the other analyses like solar and atmospheric neutrinos. Since then, a new hall near the SK detector has been excavated and a 200-ton tank with its ancillary equipment has been installed, see Fig.23, to mimic the conditions at SK. Of special importance is the selective water filtration system, that filters out water impurities while keeping the Gd in the water.

From January 2010 to July 2011 we circulated pure water through the 200-ton tank and proved that our water system

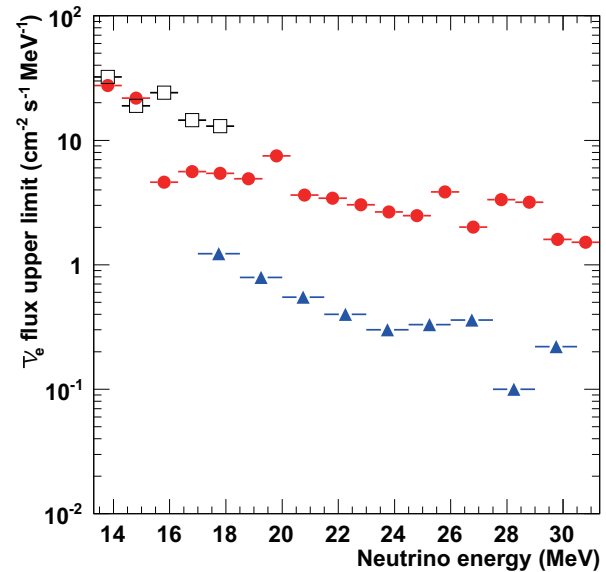


Fig. 22. Model-independent SRN 90% C.L. upper limits as a function of neutrino energy for SK-IV (solid circle). For comparison, both KamLAND result (open square) and previous SK result (solid triangle) are also shown.



Fig. 23. In the new cavern the 200-ton tank (a) with currently 240 photomultipliers installed, the Gd pre-mixing and pre-treatment 15-ton tank (b), the selective filtration system (d), Gd removal resins (c) for test and a device to measure the water transparency (e) have been installed.

is stable and achieves a high water quality. In 2013, from February 6th to April 20th, the 200-ton tank has been step-wise loaded with Gd until the final 0.2% concentration was reached. By measuring Gd concentration at some detector positions, we confirmed that the Gd sulfate quickly dissolves homogeneously in the 200-ton tank, and we can achieve and maintain a good water quality.

In summer 2013, we installed 240 photomultipliers and the data taking started from September without Gd.

After the water quality became good and stable, detector calibrations were performed. In April 2015, we finally achieved to make a final configuration with 0.2% $Gd_2(SO_4)_3$ concentration.

Figure 24 shows the time variation of Cherenkov light left after travelling 15 m in Gd loaded water. The blue band in the

figure shows typical values for SK-III and SK-IV. As shown in the figure, the transparency of 0.2% $\text{Gd}_2(\text{SO}_4)_3$ water is within the SK range. In addition to the good water transparency, no Gd loss has been detected since the EGADS detector reached the final concentration more than a year ago.

Detailed studies have evaluated the impact on current analyses at SK. These studies show that current analyses will be basically unharmed after adding Gd in SK and all other tests and studies conducted have shown no showstoppers. As a consequence, the SK collaboration decided in spring 2015 to approve the SuperK-Gd project. The project has been funded and the actual schedule is being determined together with the T2K collaboration.

For EGADS the next step will be to upgrade the electronics and become a detector with instant supernova detection capabilities.

T2K EXPERIMENT

[Spokesperson : Tsuyoshi Nakaya (Kyoto University)]

The Tokai-to-Kamioka long baseline neutrino oscillation (T2K) experiment [1] is a 295 km long-baseline neutrino oscillation experiment, employing a high intensity muon neutrino beam or antineutrino beam sent from the Japan Proton Accelerator Research Complex (J-PARC) in Tokai village to the Super-Kamiokande (SK) water Cherenkov detector in Kamioka. One of the primary goals of the experiment was to discover the appearance of the electron neutrino in the muon neutrino beam, which was accomplished in 2013 [2]. Since 2010, the data have been accumulated and both electron neutrino appearance and muon neutrino disappearance at SK have been studied to determine the oscillation parameters, θ_{13} , Δm_{32}^2 and θ_{23} , precisely. Recently, muon antineutrino beam data have been collected. By comparing the observations of two different beam modes between muon neutrino and antineutrino, T2K studies the CP (charge conjugation parity) symmetry in the lepton sector.

T2K is the first accelerator based long-baseline neutrino oscillation experiment to adopt an off-axis beam [3] technique. The beam is directed 2.5° away from the direction to Super-K, which creates the muon neutrino energy narrow with peaking around 0.6 GeV, corresponding to the oscillation maximum.

The T2K beam is composed primarily of muon neutrinos, which are produced from the decays of charged pions and kaons created in the interactions of 30 GeV protons from the J-PARC accelerator hitting a graphite target. We employ a series of three special magnets, so-called magnetic horn, driven by pulsed electric current to generate magnetic field to focus the particles produced in the target, and guide them to the Helium filled 96m long decay volume to generate neutrino beam. The selection of muon neutrino and antineutrino is realized by reversing the direction of the electric current fed to the magnetic horns.

The T2K accumulated neutrino data in the seven run periods is listed in Tab. 2. The total accumulated neutrino data

Table 2. T2K data taking periods and integrated numbers of protons on target (POT) after the event selection applied. References for main T2K results from each data update are also listed.

Run	Dates	$\times 10^{20}$ POT	
		ν	$\bar{\nu}$
1	Jan.2010 - Jun.2010	0.32	–
2	Nov.2010 - Mar.2011	1.11 [4, 5]	–
3	Mar.2012 - Jun.2012	1.58 [2, 6]	–
4	Oct.2012 - May.2013	3.56 [7, 8, 9]	–
5	May.2014 - Jun.2014	0.24	0.51
6	Oct.2014 - Jun.2015	0.10	3.51
7	Feb.2016 - May.2016	0.09	3.46

corresponds to 14.47×10^{20} protons on target (POT). Among of them, 7.00×10^{20} POT is in neutrino beam mode and 7.47×10^{20} POT is in antineutrino beam mode. The intensity of the proton has been continuously increased owing to efforts of the accelerator group in J-PARC and the beam power exceeds 400 kW during the Run 7 period.

The near neutrino (ND) is located 280 m from the T2K target consists of two detector complexes, one of them is on the beam axis and the other is off. The on-axis interactive neutrino grid (INGRID [10]), composed of the arrays of iron plate and scintillator layer, monitors the neutrino beam intensity, direction and profile. The off-axis detector (ND280) is situated along the same direction to SK and measures the neutrino beam flux, composition and energy spectrum prior to neutrino oscillations. ND280 provides various important information on the neutrino flux and neutrino-nucleus interactions and these inputs are used in the oscillation analyses to suppress the systematic uncertainties.

The far detector, SK [11], is a 50 kton water Cherenkov detector which uses timing information from the Global Positioning System (GPS) to record events, which coincide with the operation of the T2K beam cycle. All data within $\pm 500 \mu\text{s}$ of the beam arrival time at SK are recorded for the use in the later analysis.

The neutrino flux is calculated with a full Monte Carlo (MC) simulation considering the T2K beamline and measurements of the primary proton beam profile, the magnetic fields produced by the magnetic horns, and hadron production data from the NA61/SHINE measurements [12, 13]. Neutrino interactions are then simulated based on the flux predictions at both the ND280 and SK sites using NEUT [14]. Parametric model of neutrino interaction and fluxes are constrained with samples from ND measurements [15], and the systematic uncertainties of the model are largely reduced by this method.

As explained, various neutrino-nucleus interactions are studied and used as the inputs to the oscillation analyses. In 2015, some of the results from these studies were published. The ν_μ charged current (CC) quasi-elastic (QE) cross sections on carbon was evaluated at neutrino energies around 1 GeV using the on-axis INGRID detector. One-track and two-track samples of ν_μ CCQE scattering were selected in the Proton Module for the neutrino target with a 303 kg fiducial mass during 7.32×10^{20} POT in Run 2-4. The measured cross-sections on

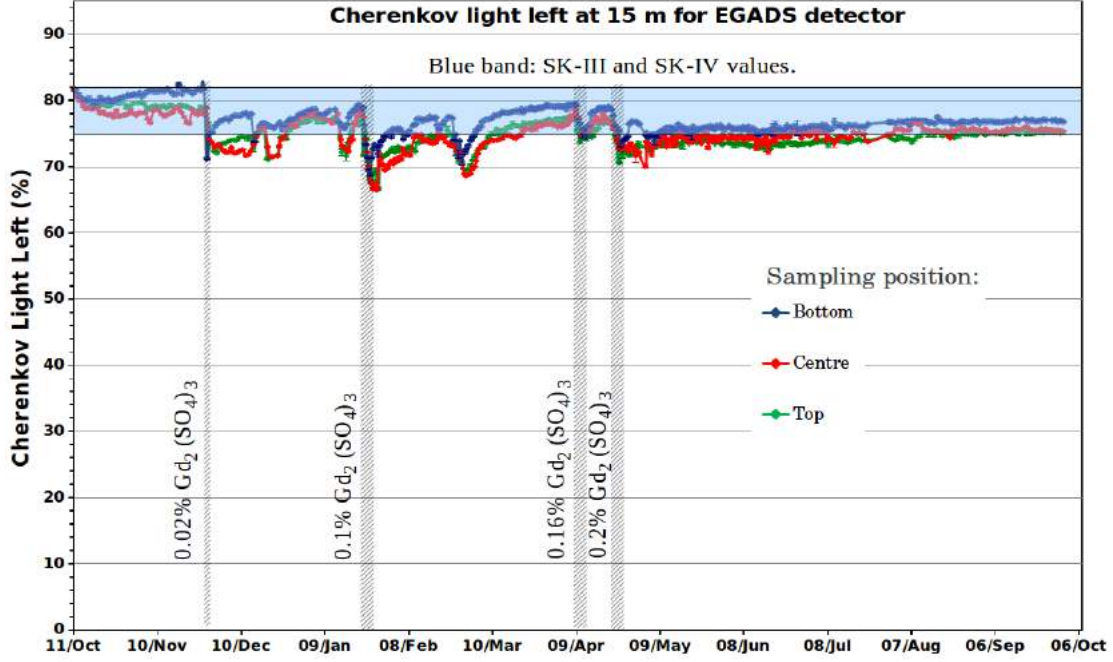


Fig. 24. Cherenkov light left at 15 m for Gd loaded water. The horizontal blue band are the typical values for SK-III and SK-IV. The vertical lines shows the injection date where we also indicate the concentration (% in mass) in the 200-ton tank.

carbon at mean neutrino energies of 1.94 GeV and 0.93 GeV are $(11.95 \pm 0.19(stat.) +1.82^{+1.47}_{-1.47}(sys.)) \times 10^{-39} \text{cm}^2/\text{neutron}$, and $(10.64 \pm 0.37(stat.) +2.03^{+1.65}_{-1.65}(sys.)) \times 10^{-39} \text{cm}^2/\text{neutron}$, respectively [16].

As well, by the off-axis ND280 detector, the same ν_μ CCQE cross section on a carbon target was evaluated to be $(0.83 \pm 0.12) \times 10^{-38} \text{cm}^2$ consistently [17]. It was obtained by the distribution of muon momentum and angle with respect to the incident neutrino beam with collecting 2.6×10^{20} POT. The axial mass, M_A^{QE} , of the dipole axial form factor was extracted to be $1.26^{+0.21}_{-0.18} \text{GeV}/c^2$ or $1.43^{+0.28}_{-0.22} \text{GeV}/c^2$, using the absolute or shape-only distribution in analyses, respectively.

The first measurement of the electron-neutrino charged-current interaction rate on water above 1.5 GeV was given by the π^0 detector composing the ND280 detector [18]. By comparing fillable 1900 kg fiducial water with air, and using 2.6×10^{20} POT (water) and 3.5×10^{20} POT (air), the ratio of the observed beam interaction rate to the predicted rate in the detector with water was measured to be $0.87 \pm 0.33(stat.) \pm 0.21(sys.)$. It is consistent with the nominal expectation using NEUT, within statistical and systematic uncertainties. The uncertainties are still large due to limited statistics.

In 2015, the first result using a combined analysis of ν_μ -disappearance and ν_e -appearance was accomplished, to advance our knowledge of the oscillation parameters $\sin^2\theta_{23}$, $\sin^2\theta_{13}$, $|\Delta m^2|$, the CP violation phase δ_{CP} , and the mass hierarchy [9]. Since T2K is insensitive to the solar oscillation parameters, values of $\sin^2\theta_{12} = 0.306$ and $\Delta m_{21}^2 = 7.5 \times 10^{-5} \text{eV}^2/c^4$ were taken from [19]. In order to study the CP violation, i.e. the study of the allowed or exclude regions of δ_{CP} , the θ_{13} value is constrained as $(\sin^2 2\theta_{13})_{reactor} = 0.095 \pm 0.01((\sin^2 \theta_{13})_{reactor}$

$= 0.0243 \pm 0.0026)$ [20], which is extracted from the weighted average of the results from three reactor experiments, Daya Bay, RENO, and Double Chooz.

As the ν_e -appearance channel, 28 events were selected in 6.57×10^{20} POT during Run 1-4. The selection criteria of the ν_e CC sample are defined as follows: (1) only one reconstructed Cherenkov ring, (2) e -like ring, (3) the visible energy, E_{vis} , is greater than 100 MeV, (4) no reconstructed Michel electron, (5) the reconstructed energy, E_V^{rec} , is less than 1.25 GeV, (6) background rejection applied with a π^0 hypothesis.

The selection criteria of the ν_μ CC candidate sample, which are used to study of ν_μ -disappearance channel, are defined as follows: (1) only one reconstructed Cherenkov ring, (2) μ -like ring, (3) the reconstructed momentum is greater than 200 MeV/c and (4) less than two reconstructed Michel electrons are applied, then 120 events remain.

The neutrino oscillation parameters were extracted using the measured momentum and direction of the charged lepton, and the reconstructed energy distribution of event samples. A $\Delta\chi^2$ function is defined to compare the observation with the expectation varied with systematic uncertainties. The profiled $\Delta\chi^2$ as a function of each oscillation parameter is calculated as shown in Fig. 25, In Fig. 26, the 68% and 90% confidence level (CL) regions for the two mass hierarchies constructed using $\Delta\chi^2$ with respect to the best-fit point, the one for the normal hierarchy, are presented.

In order to take into account the statistical fluctuations and the systematic uncertainties, an analysis using the Feldman and Cousins method was performed for the study of δ_{CP} . At 90% confidence level and including reactor measurements, the excluded region was obtained as $\delta_{CP} = [0.15, 0.83]\pi$ for

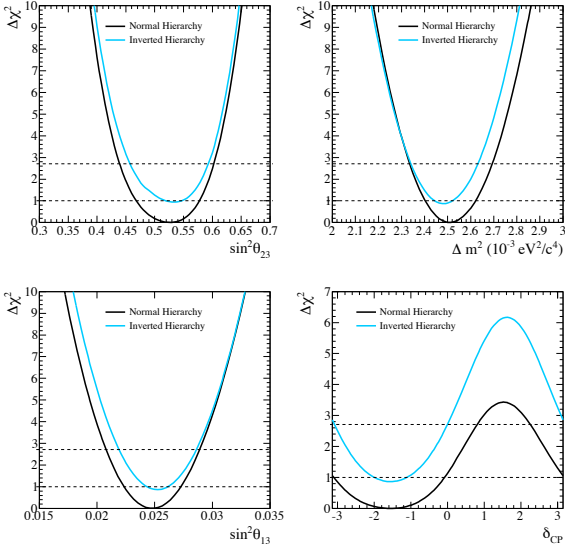


Fig. 25. Profiled $\Delta\chi^2$ for the joint 3-flavor oscillation analysis combined with the results from reactor experiments. The parameter $|\Delta m^2|$ represents Δm_{32}^2 or Δm_{13}^2 for normal and inverted mass hierarchy assumptions respectively. The horizontal lines show the critical $\Delta\chi^2$ values for one dimensional fits at the 68 % and 90 % CL ($\Delta\chi^2 = 1.00$ and 2.71 respectively).

normal hierarchy and $\delta_{CP} = [-0.08, 1.09]\pi$ for inverted hierarchy.

The most probable values and 68% 1D credible intervals for the other oscillation parameters were evaluated by Bayesian techniques and obtained to be $\sin^2 \theta_{23} = 0.528^{+0.055}_{-0.038}$ and $|\Delta m_{32}^2| = (2.51 \pm 0.11) \times 10^{-3} \text{ eV}^2/c^4$.

There is a study of upper bound on neutrino mass by relative arrival times of muon and electron neutrino candidate events at the T2K far detector as a function of neutrino energy. Though a sum of all neutrino masses is strictly constrained by measurements of the cosmological background radiation, less than $0.2 \text{ eV}/c^2$ (95% CL) [19], it depends on assumptions about the cosmological parameters. By means of the long baseline experiment of neutrinos, the 90% CL upper limit on the mixture of neutrino mass eigenstates represented in the data sample by 6.57×10^{20} POT is found to be $m_\nu^2 < 5.6 \text{ MeV}^2/c^4$ [23].

The T2K experiment has accumulated the data but it is less than 20% the total and thus, continues to collect more data with both neutrino and antineutrino beam modes. With an exposure of 7.8×10^{21} POT, it is expected to achieve 1- σ resolution of 0.050(0.054) on $\sin^2 \theta_{23}$ and $0.040(0.045) \times 10^{-3} \text{ eV}^2$ on Δm_{32}^2 , for 100%(50%) neutrino beam mode running assuming $\sin^2 \theta_{23} = 0.5$ and $\Delta m_{32}^2 = 2.4 \times 10^{-3} \text{ eV}^2$ [24]. T2K will have a sensitivity to the CP violating phase δ_{CP} at 90% CL as indicated in Fig. 27. In near future, more various knowledge on neutrinos is expected by the T2K experiment.

Bibliography

[1] K. Abe *et al.* [T2K Collaboration], Nucl. Instrum. Meth. A **659**, 106 (2011) [arXiv:1106.1238 [physics.ins-det]].

- [2] K. Abe *et al.* [T2K Collaboration], Phys. Rev. D **88**, 032002 (2013) [arXiv:1304.0841 [hep-ex]].
- [3] D. Beavis, A. Carroll, I. Chiang, *et al.*, Long Baseline Neutrino Oscillation Experiment at the AGS (Proposal E889), 1995. Physics Design Report, BNL 52459.
- [4] K. Abe *et al.* [T2K Collaboration], Phys. Rev. Lett. **107**, 041801 (2011) [arXiv:1106.2822 [hep-ex]].
- [5] K. Abe *et al.* [T2K Collaboration], Phys. Rev. D **85**, 031103 (2012) [arXiv:1201.1386 [hep-ex]].
- [6] K. Abe *et al.* [T2K Collaboration], Phys. Rev. Lett. **111**, 211803 (2013) [arXiv:1308.0465 [hep-ex]].
- [7] K. Abe *et al.* [T2K Collaboration], Phys. Rev. Lett. **112**, 061802 (2014) [arXiv:1311.4750 [hep-ex]].
- [8] K. Abe *et al.* [T2K Collaboration], Phys. Rev. Lett. **112**, 181801 (2014) [arXiv:1403.1532 [hep-ex]].
- [9] K. Abe *et al.* [T2K Collaboration], Phys. Rev. D **91**, 072010 (2015).
- [10] M. Otani, N. Nagai, D. Orme, A. Minamino, K. Nitta, O. Drapier, F. Moreau and M. Besnier *et al.*, Nucl. Instrum. Meth. A **623**, 368 (2010).
- [11] Y. Fukuda *et al.* (Super-Kamiokande Collaboration), Nucl. Instrum. Meth. A **501**, 418 (2003).
- [12] N. Abgrall *et al.* [NA61/SHINE Collaboration], Phys. Rev. C **84**, 034604 (2011) [arXiv:1102.0983 [hep-ex]].
- [13] N. Abgrall *et al.* [NA61/SHINE Collaboration], Phys. Rev. C **85**, 035210 (2012) [arXiv:1112.0150 [hep-ex]].
- [14] Y. Hayato, Nucl. Phys. (Proc. Suppl.) B **112**, 171 (2002).
- [15] K. Abe *et al.* [T2K Collaboration], Phys. Rev. D **89**, 092003 (2014) [arXiv:1403.2552 [hep-ex]].
- [16] K. Abe *et al.* [T2K Collaboration], Phys. Rev. D **91**, 112002 (2015).
- [17] K. Abe *et al.* [T2K Collaboration], Phys. Rev. D **92**, 112003 (2015).
- [18] K. Abe *et al.* [T2K Collaboration], Phys. Rev. D **91**, 112010 (2015).
- [19] J. Beringer *et al.* [Particle Data Group], Phys. Rev. D **86**, 010001 (2012).
- [20] J. Beringer *et al.* [Particle Data Group], http://pdg.lbl.gov/2013/pdg_2013.html.
- [21] K. Abe *et al.* [T2K Collaboration], Phys. Rev. D **91**, 051102(R) (2015).
- [22] C. Giunti *et al.*, Phys. Rev. D **86**, 113014 (2012).
- [23] K. Abe *et al.* [T2K Collaboration], Phys. Rev. D **93**, 012006, (2016).
- [24] K. Abe *et al.* [T2K Collaboration], Prog. Theor. Exp. Phys. **043C01** (2015).

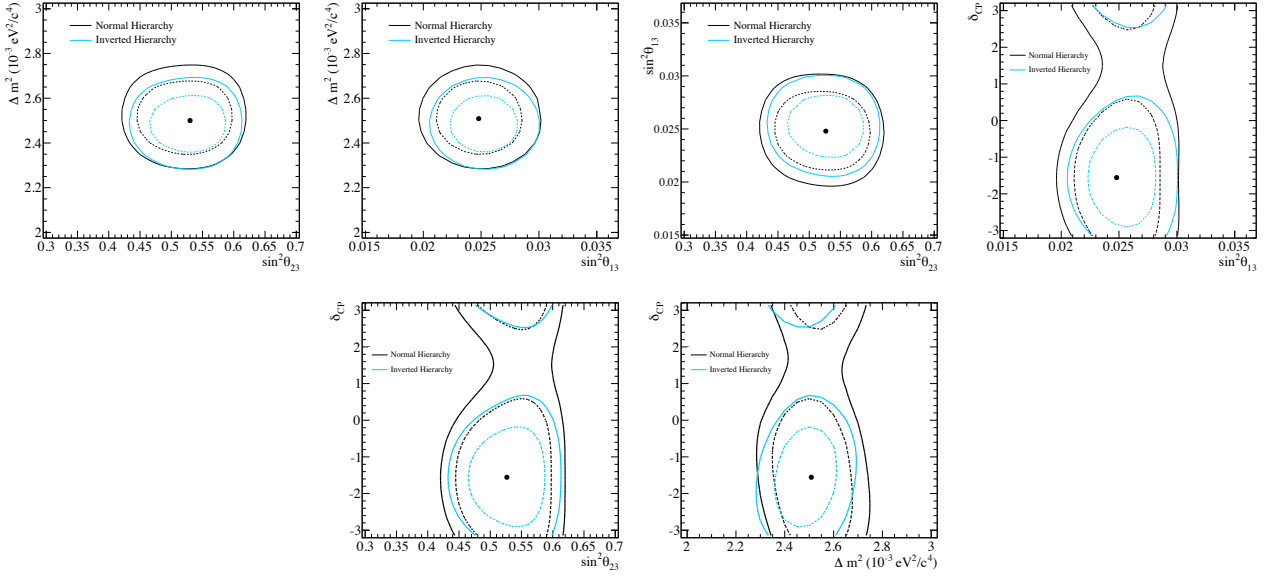


Fig. 26. 68% (dashed) and 90% (solid) CL regions from the analysis that includes results from reactor experiments with different mass hierarchy assumptions using $\Delta\chi^2$ with respect to the best-fit point, the one from the fit with normal hierarchy. The parameter $|\Delta m^2|$ represents Δm_{32}^2 or Δm_{13}^2 for normal and inverted mass hierarchy assumptions respectively.

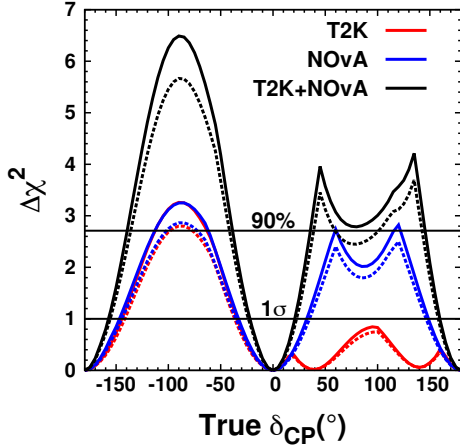


Fig. 27. The predicted sensitivity of $\Delta\chi^2$ for rejecting $\sin\delta_{CP} = 0$ hypothesis is drawn as a function of δ_{CP} in the red line. The blue curve is that of expectation in another experiment that recently began operation, NOvA (http://www-nova.fnal.gov/nova_cd2_review/tdr_oct.23/tdr.htm), and combined estimate of T2K+NOvA is shown in the black curve. In dashed curves, the normalization systematics are considered, while it is not included in the solid ones. The true value of $\sin^2\theta_{23} = 0.5$ and normal hierarchy of neutrino mass is assumed.

XMASS EXPERIMENT

[Spokesperson : Yoichiro Suzuki
(Kavli IPMU, the University of Tokyo)]

Introduction

The XMASS project is designed to detect dark matter, neutrinoless double beta decay, and ${}^7\text{Be}/pp$ solar neutrinos using highly-purified liquid xenon scintillator in an ultra-low radioactivity environment [1]. The advantages of using liquid xenon are a large amount of scintillation light yield, scalability of the size of the detector mass, an easy purification to reduce internal radioactive backgrounds, and a high atomic number ($Z = 54$) to shield radiations from outside of the detector. As the first stage of the XMASS project (XMASS-I), the detector with 835 kg of liquid xenon was constructed. Its construction started in April 2007 and completed in September 2010. After completion of the detector, commissioning data was taken from December 2010 to May 2012. We published results from a search for light weakly interacting massive particle (WIMP) dark matter [2] and a search for solar axions [3], both using 6.7 live days of data collected with the full 835 kg liquid xenon volume and with the lowest energy threshold of 0.3 keV. We also performed searches for inelastic WIMP-nucleon scattering on ${}^{129}\text{Xe}$ [4] and bosonic super-WIMPs [5], both using 165.9 live days of data with a restricted target mass of 41 kg at the central region of the detector. During the commissioning data-taking, we found that a majority of events at low energy originated from radioactive contamination in the aluminum seal of the photomultiplier tube (PMT) window. In order to reduce the backgrounds, detector refurbishment was conducted. The contaminated parts of PMTs were covered by copper rings and plates in order to stop scintillation lights and radiations caused by its contamination. PMTs were cleaned by acid and copper parts were electropolished in order to remove possible surface contamination. After a year of detector refurbishment, data-taking resumed in November 2013 and is continuing for more than two years till now.

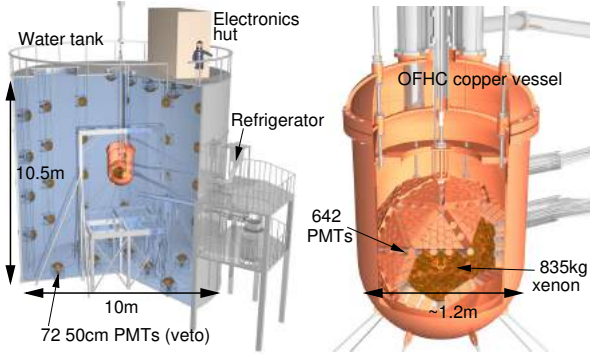


Fig. 28. Schematic drawing of the XMASS-I detector.

The XMASS-I detector

XMASS-I is a single phase liquid xenon scintillator detector located underground (2700 m water equivalent) at the Kamioka Observatory. Fig. 28 shows a schematic drawing of the XMASS-I detector. It contains 835 kg of liquid xenon in an active region. The volume is viewed by 630 hexagonal and 12 cylindrical Hamamatsu R10789 PMTs arranged on an 80 cm diameter pentakis-dodecahedron support structure. A total photocathode coverage of more than 62% is achieved. The spherical arrays of PMTs are arranged in a double wall vessel made of oxygen free high conductivity (OFHC) copper. The detector is calibrated regularly with a ^{57}Co source inserted along the central vertical axis of the detector. By the data taken with the ^{57}Co source at the center of the detector volume, the photoelectron yield was determined to be ~ 14 photoelectrons/keV. In order to shield the liquid xenon detector from external gammas, neutrons, and muon-induced backgrounds, the copper vessel was placed at the center of a $\phi 10\text{ m} \times 10.5\text{ m}$ cylindrical tank filled with pure water. The water tank is equipped with 72 Hamamatsu R3600 20-inch PMTs to provide both an active muon veto and passive shielding against these backgrounds. XMASS-I is the first direct detection dark matter experiment equipped with such an active water Cherenkov shield. The liquid xenon and water Cherenkov detectors are hence called an Inner Detector (ID) and an Outer Detector (OD), respectively. More details are described in Ref. [6].

Dark matter search by annual modulation [7]

The count rate of dark matter signal is expected to modulate annually due to the relative motion of the Earth around the Sun. The relative velocity of the Earth to the dark matter distribution becomes maximal in June and minimal in December. The amplitude of the modulation can be changed from positive (i.e. higher rate in June than in December) to negative at a cross-over energy and it is possible to observe this effect if the detector threshold is lower than that energy. The annual modulation would be a strong signature for dark matter.

We conducted a search for an annual modulation signal using 359.2 live days of data accumulated between November 2013 and March 2015. This analysis used the full 832 kg liquid xenon volume. Two different energy scales were used: keV_{ee} represents an electron equivalent energy, and keV_{nr} de-

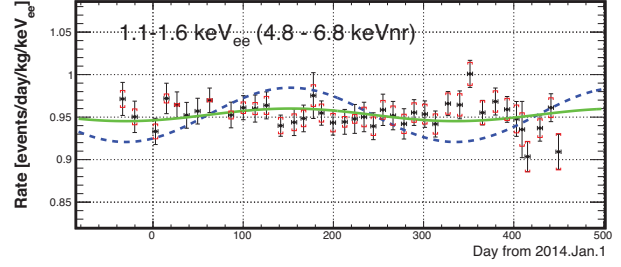


Fig. 29. Observed count rate as a function of time in the $1.1\text{--}1.6\text{ keV}_{\text{ee}}$ ($=4.8\text{--}6.8\text{ keV}_{\text{nr}}$) energy range. The error bars show the statistical uncertainty and the square brackets indicate the 1σ systematic error for each time bin. The solid and dashed curves indicate the expected count rates assuming the spin-independent WIMP-nucleon cross section of $2 \times 10^{-40}\text{ cm}^2$ for the 7 and 8 GeV/c^2 WIMPs, respectively.

notes the nuclear recoil energy. The energy threshold in this analysis was $1.1\text{ keV}_{\text{ee}}$ ($=4.8\text{ keV}_{\text{nr}}$), corresponding to ~ 8 photoelectrons.

To obtain the annual modulation amplitude from the data, the least squares method was used. The data set was divided into 40 time-bins with roughly 10 days of live time each. The data in each time-bin were further divided into energy-bins with a width of $0.5\text{ keV}_{\text{ee}}$. Fig. 29 shows the observed count rate as a function of time in the energy region between 1.1 and $1.6\text{ keV}_{\text{ee}}$ ($=4.8\text{--}6.8\text{ keV}_{\text{nr}}$). The expected count rates assuming the spin-independent WIMP-nucleon cross section of $2 \times 10^{-40}\text{ cm}^2$ for WIMP masses of 7 and 8 GeV/c^2 are also shown. This demonstrates the high sensitivity of XMASS to the annual modulation claimed by the DAMA/LIBRA experiment.

Two fitting methods were performed independently: the pull term method and the covariance matrix method to propagate the effects of the systematic errors. Both of them fit all energy- and time-bins simultaneously. We performed two analyses, one assuming WIMP interactions and the other independent of any specific dark matter model.

In the case of the WIMP analysis, the expected count rate in the i -th energy and j -th time bin is expressed as:

$$R_{i,j}^{\text{ex}} = \int_{t_j - \frac{1}{2}\Delta t_j}^{t_j + \frac{1}{2}\Delta t_j} \left(C_i + \sigma_{\chi N} \cdot A_i(m_\chi) \cos \frac{2\pi(t - t_0)}{T} \right) dt, \quad (1)$$

where C_i is the unmodulated count rate at i -th energy bin and $\sigma_{\chi N}$ is the WIMP-nucleon cross section. Since the WIMP mass m_χ determines the recoil energy spectrum, the expected modulation amplitudes become a function of the WIMP mass $A_i(m_\chi)$. t_j and Δt_j are the time-bin's center and width, respectively. The modulation period T is fixed to one year and the phase t_0 is fixed to 152.5 days (~ 2 nd of June) when the Earth's velocity relative to the dark matter distribution is expected to be maximal. C_i , $\sigma_{\chi N}$, and m_χ are the free parameters to be determined by the fit. Fig. 30 shows the 90% confidence level exclusion limit on the spin-independent WIMP-nucleon cross section obtained by the pull term method. The $\pm 1\sigma$ and $\pm 2\sigma$ bands represent the expected 90% confidence level exclusion sensitivity estimated using 10,000 dummy samples

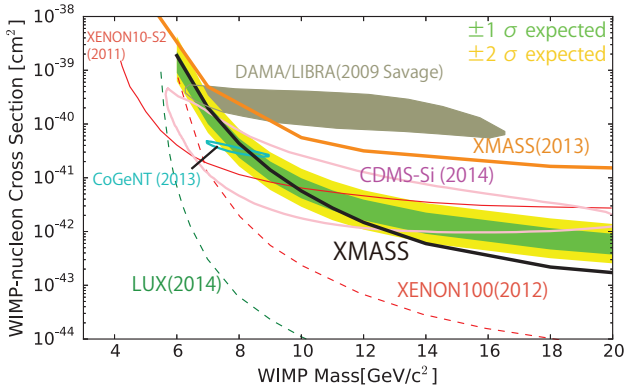


Fig. 30. Limits on the spin-independent WIMP-nucleon cross section as a function of WIMP mass. The solid curve shows the XMASS 90% confidence level exclusion limit from the annual modulation analysis. The $\pm 1\sigma$ and $\pm 2\sigma$ bands represent the expected 90% confidence level exclusion sensitivity.

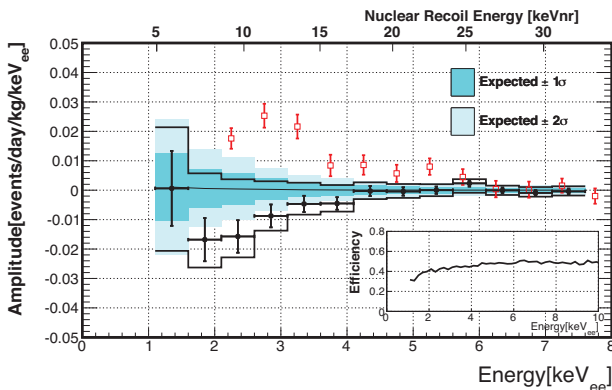


Fig. 31. Observed modulation amplitude as a function of energy for the model independent analysis (circle). The solid lines represent the XMASS 90% positive (negative) upper limits on the modulation amplitude. The $\pm 1\sigma$ and $\pm 2\sigma$ bands represent the expected sensitivity on the amplitude. The DAMA/LIBRA result (square) is also shown.

including systematic uncertainties. The upper limit of $4.3 \times 10^{-41} \text{ cm}^2$ at $8 \text{ GeV}/c^2$ was obtained. The difference between two fitting methods is less than 10%. The result excludes the DAMA/LIBRA allowed region for the WIMP masses higher than $8 \text{ GeV}/c^2$.

For the model independent analysis, the expected count rate is estimated as:

$$R_{i,j}^{\text{ex}} = \int_{t_j - \frac{1}{2}\Delta t_j}^{t_j + \frac{1}{2}\Delta t_j} \left(C_i + A_i \cos \frac{2\pi(t-t_0)}{T} \right) dt, \quad (2)$$

where the free parameters C_i and A_i are the unmodulated count rate and the modulation amplitude at i -th energy bin, respectively. In the fitting procedure, the energy range between 1.1 and $7.6 \text{ keV}_{\text{ee}}$ was used. The modulation period T and phase t_0 were again fixed to one year and 152.5 days, respectively. Fig. 31 shows the best fit amplitude as a function of energy after correcting for the efficiency obtained by the pull term method. The efficiency was evaluated from the simulation of

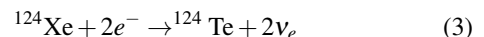
gamma-ray with a flat energy spectrum uniformly distributed in the sensitive volume. Both fitting methods are in good agreement. The $\pm 1\sigma$ and $\pm 2\sigma$ bands represent the expected sensitivity on the modulation amplitude derived from the same dummy samples mentioned above. This test gave a p -value of 0.014 (2.5σ) for the pull term method and of 0.068 (1.8σ) for the covariance matrix method. To be able to test any model of dark matter, we evaluated the constraints on the positive and negative amplitudes separately. The 90% confidence level upper limits on the positive and negative amplitudes a_{up} were calculated by the relations $\int_0^{a_{\text{up}}} G(a) da / \int_0^{\infty} G(a) da = 0.9$ and $\int_{a_{\text{up}}}^0 G(a) da / \int_{-\infty}^0 G(a) da = 0.9$, respectively, where $G(a)$ is the Gaussian distribution with the mean and sigma of the amplitude obtained from the fit. We obtained positive (negative) upper limit of 2.1 (-2.1) $\times 10^{-2}$ events/day/kg/keV $_{\text{ee}}$ in the energy range between 1.1 and $1.6 \text{ keV}_{\text{ee}}$, and the limits become stricter at higher energy.

We make direct comparisons with other experiments not by considering a specific dark matter model but amplitude count rate. DAMA/LIBRA obtained the modulation amplitude of $\sim 2 \times 10^{-2}$ events/day/kg/keV $_{\text{ee}}$ in the energy range between 2.0 and $3.5 \text{ keV}_{\text{ee}}$. The XENON100 experiment found no statistically significant modulation. Since XENON100 gave the best-fit parameters and uncertainties, we estimated a 90% confidence level upper limit of 3.7×10^{-3} events/day/kg/keV $_{\text{ee}}$ between 2.0 and $5.8 \text{ keV}_{\text{ee}}$ for their result. The XMASS experiment obtained the positive upper limits of $(1.7 - 3.7) \times 10^{-3}$ events/day/kg/keV $_{\text{ee}}$ in the same energy region and gave more stringent constraint.

Search for two-neutrino double electron capture [8]

Neutrinoless double beta decay and its inverse, neutrinoless double electron capture, are lepton number violating processes, and their existence is an evidence that neutrino is a Majorana particle. On the other hand, two-neutrino modes of double beta decay and double electron capture are allowed within the standard model of particle physics. Although two-neutrino double beta decay has been observed in more than ten isotopes, there exists only a few positive experimental results for two-neutrino double electron capture (2νECEC) so far: a geochemical measurement for ^{130}Ba with a half-life of $(2.2 \pm 0.5) \times 10^{21}$ years and a direct measurement for ^{78}Kr with a half-life of $(9.2_{-2.6}^{+5.5}(\text{stat}) \pm 1.3(\text{sys})) \times 10^{21}$ years. Any measurement of 2νECEC will provide a new reference for the calculation of nuclear matrix elements.

Natural xenon contains the double electron capture nuclei ^{124}Xe (0.095%) and ^{126}Xe (0.089%), as well as the double beta decay nuclei ^{136}Xe (8.9%) and ^{134}Xe (10.4%). The process of 2νECEC on ^{124}Xe is



with a Q -value of 2864 keV. In the case that two K -shell electron in the ^{124}Xe atom are captured simultaneously, the daughter atom of ^{124}Te is formed with two vacancies in the K -shell and de-excites by emitting atomic X -rays and/or Auger electrons. The total energy deposition in the detector is 63.6 keV, which is twice of the binding energy of a K -shell electron in a tellurium atom. Although ^{126}Xe can also undergo 2νECEC,

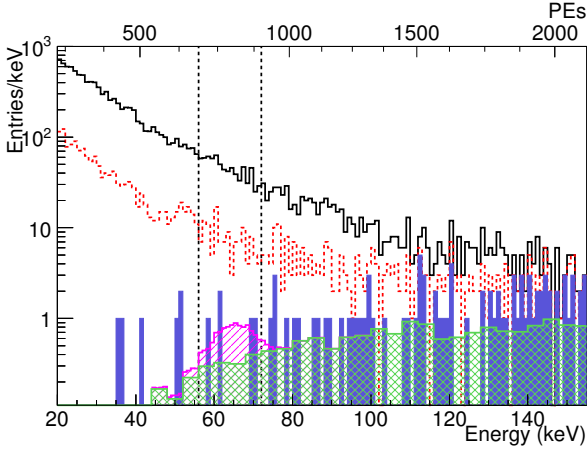


Fig. 32. Energy spectra of the observed events after each reduction step. From top to bottom, the observed energy spectrum after pre-selection and radius cut (solid), timing balance cut (dashed) and band-like pattern cut (filled). The vertical dashed lines indicate the 56-72 keV signal window. The expected ^{214}Pb background (cross-hatched) together with the signal expectation for the 90% confidence level upper limit (hatched) are also shown.

this reaction is expected to be much slower than that on ^{124}Xe since its Q -value of 920 keV is smaller. There exists a wide spread of calculated half-lives for $2\nu\text{ECEC}$ on ^{124}Xe : between 10^{20} and 10^{24} years.

We performed a search for $2\nu\text{ECEC}$ on ^{124}Xe using 165.9 live days of data collected between December 2010 and May 2012. This analysis used a restricted target volume within 15 cm from the center of the detector. The fiducial mass of natural xenon in that volume is 41 kg, containing 39 g of ^{124}Xe . The signal window is defined such that it contains 90% of the simulated signal with equal 5% tails to either side after all the above cuts are applied, resulting in a 56-72 keV window. From the simulation, the signal detection efficiency is estimated to be 59.7%.

Fig. 32 shows energy spectra of the observed events remaining after each reduction step. After all cuts, 5 events are left in the signal region. The main contribution to the remaining background in this energy region is the ^{222}Rn daughter ^{214}Pb in the detector. The expected number of background events in the signal region is 5.3 ± 0.5 events estimated from the observed rate of ^{214}Bi - ^{214}Po consecutive decays.

Fig. 33 shows the energy distribution of the observed events overlaid with the ^{214}Pb background simulation after all cuts except for the energy window cut. The energy spectrum in data is consistent with the expected ^{214}Pb background spectrum. Note that an excess in the highest energy bin is due to a gamma-ray from $^{131\text{m}}\text{Xe}$ in liquid xenon.

Since the observed data spectrum does not exceed the expected background in the signal region, a lower limit on the $2\nu\text{ECEC}$ half-life is derived using the Bayesian method. The conditional probability distribution for the decay rate is defined as follows:

$$P(\Gamma|n_{\text{obs}}) = \frac{\iiint\int \frac{e^{-(\Gamma\lambda\varepsilon+b)(1+\delta)} ((\Gamma\lambda\varepsilon+b)(1+\delta))^{n_{\text{obs}}}}{n_{\text{obs}}!}}{\times P(\Gamma)P(\lambda)P(\varepsilon)P(b)P(\delta)} d\lambda d\varepsilon db d\delta \quad (4)$$

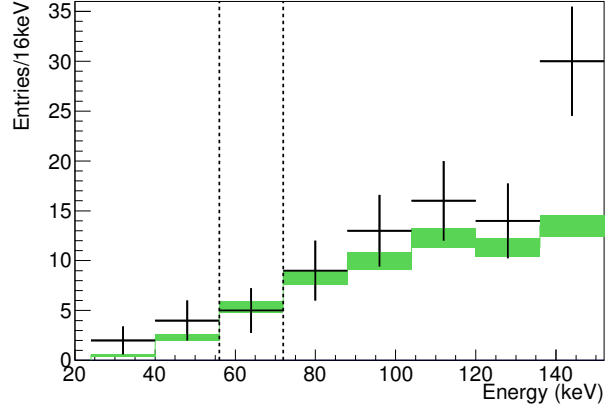


Fig. 33. Energy distribution of the observed events (+) overlaid with the ^{214}Pb background simulation (band) after all cuts except for the energy window cut. The vertical dashed lines indicate the 56-72 keV signal window.

where Γ is the decay rate, n_{obs} is the observed number of events, λ is the detector exposure including the abundance of ^{124}Xe , ε is the detection efficiency, b is the expected number of background events, and δ is a parameter representing the systematic uncertainty in the event selection which affects both signal and background. The decay rate prior probability $P(\Gamma)$ is 1 for $\Gamma \geq 0$ and otherwise 0. $P(\lambda)$, $P(\varepsilon)$, $P(b)$, and $P(\delta)$ are the prior probability distributions incorporating systematic uncertainties in the detector exposure, detection efficiency, background, and event selection, respectively. We calculate the 90% confidence level limit using the relation $\int_0^{\Gamma_{\text{limit}}} P(\Gamma|n_{\text{obs}}) d\Gamma / \int_0^{\infty} P(\Gamma|n_{\text{obs}}) d\Gamma = 0.9$ to obtain

$$T_{1/2}^{2\nu 2K}(^{124}\text{Xe}) = \frac{\ln 2}{\Gamma_{\text{limit}}} > 4.7 \times 10^{21} \text{ years}, \quad (5)$$

which provides the most stringent limit for ^{124}Xe . In addition, the fact that we do not observe significant excess above background allows us to give a lower limit on the half-life of $2\nu\text{ECEC}$ on ^{126}Xe in the same manner, and we obtain $T_{1/2}^{2\nu 2K}(^{126}\text{Xe}) > 4.3 \times 10^{21}$ years at 90% confidence level.

Detectability of galactic supernova neutrinos [9]

The coherent elastic neutrino-nucleus scattering (CEvNS) is a process in which a neutrino with an energy in the order of MeV interacts with all nucleons in a nucleus coherently,

$$\nu + \text{nucleus} \rightarrow \nu + \text{nucleus}, \quad (6)$$

resulting in a large cross section. However, it has not been observed yet, primarily because the only observable of this interaction is the recoiled nucleus with kinetic energy in the order of keV. The coherent scattering plays a crucial role at the final evolution of stars: it is believed to be the main mechanism for neutrinos to be trapped in the core of a supernova. The CEvNS process has been also proposed as a method to probe non-standard neutrino interactions with quarks, extra heavy neutral gauge bosons, and the neutron part of nuclear form

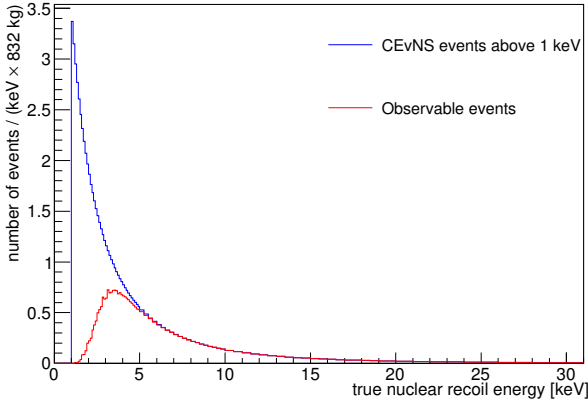


Fig. 34. Energy spectrum as a function of true xenon nuclear recoil energy. The upper and lower curve are the energy spectra with and without taking into account the detection efficiency, respectively. The upper line is calculated above 1 keV. The supernova model used here is the one from Nakazato *et al.* with $M_p = 20 M_\odot$, $Z = 0.02$ and $t_{\text{rev}} = 200$ ms. The distance of the supernova from the Earth is assumed to be 10 kpc.

factors. Therefore, the detection of the process would be of importance in both particle and astroparticle physics.

Among all available neutrino sources, galactic supernovae give the highest neutrino flux in the MeV range. It has been pointed out that experiments for direct dark matter search have the potential to detect galactic supernova neutrinos coherently scattered off nuclei. Among all existing experiments, large-volume liquid xenon dark matter detectors seem to be the most practical choice at this moment.

The possibility to detect galactic supernova neutrinos coherently scattered off xenon nuclei in the XMASS detector is calculated. The differential cross section of the coherent scattering as a function of neutrino energy E_ν and nuclear recoil energy E_{nr} is expressed as:

$$\frac{d\sigma}{dE_{\text{nr}}}(E_\nu, E_{\text{nr}}) = \frac{G_F^2 M}{2\pi} G_V^2 \left[1 + \left(1 - \frac{E_{\text{nr}}}{E_\nu} \right)^2 - \frac{M E_{\text{nr}}}{E_\nu^2} \right], \quad (7)$$

where G_F is the Fermi constant, M is target nuclear mass, and

$$G_V = \left[\left(\frac{1}{2} - 2 \sin^2 \theta_W \right) Z - \frac{1}{2} N \right] F(q^2). \quad (8)$$

The axial vector current, leading to a small incoherent contribution to the total neutral current cross section, is ignored. θ_W is the weak mixing angle ($\sin^2 \theta_W = 0.23$). Z and N are the numbers of protons and neutrons in the nucleus, respectively. $F(q^2)$ is the nuclear form factor.

Fig. 34 shows energy spectra as a function of true xenon nuclear recoil energy with and without taking into account the detection efficiency. The total number of observable events from different supernova models are listed in Table 3. Two distances are chosen for comparison, $d = 10$ kpc is roughly the distance from the center of the Milky Way to the Earth, $d = 196$ pc is the distance from Betelgeuse to the Earth. The number of observable events predicted by most of the Nakazato

Table 3. Number of observable supernova events in XMASS. The weakest Nakazato model is the one with $M_p = 20 M_\odot$, $Z = 0.02$ and $t_{\text{rev}} = 100$ ms. The brightest Nakazato model is the one with $M_p = 30 M_\odot$, $Z = 0.02$ and $t_{\text{rev}} = 300$ ms. The black-hole-forming model is the one with $M_p = 30 M_\odot$, $Z = 0.004$. Neutrino energy spectra used in the calculation are all integrated from core collapse till about 18 seconds later.

Supernova model	$d = 10$ kpc	$d = 196$ pc
Livermore	15.2	3.9×10^4
Nakazato (weakest)	3.5	0.9×10^4
Nakazato (brightest)	8.7	2.3×10^4
Nakazato (black hole)	21.1	5.5×10^4

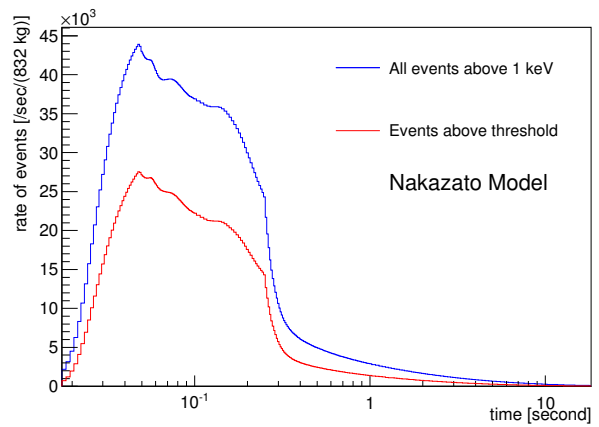


Fig. 35. Rate of CEvNS events in XMASS for a supernova 196 pc away from the Earth predicted by the Nakazato model with $M_p = 20 M_\odot$, $Z = 0.02$ and $t_{\text{rev}} = 200$ ms. The upper lines correspond to all the CEvNS events above 1 keV nuclear recoil energy predicted by models; the lower lines corresponds to all events that can be detected in XMASS.

models are significantly less than that predicted by the Livermore model. However, one Nakazato model, which forms a black-hole, predicts similar number of observable events as the Livermore model. This points out the possibility to detect failed supernovae with no optical signal. In case of a supernova as close as Betelgeuse, all the models predict a definitely possible observation.

Fig. 35 shows the rate of CEvNS events in XMASS in about 18 second for a supernova 196 pc away from the Earth predicted by the Nakazato model with $M_p = 20 M_\odot$, $Z = 0.02$ and $t_{\text{rev}} = 200$ ms, assuming without any DAQ loss. Given such a high rate, it is possible to study in detail the supernova explosion mechanism by examining the time evolution of the event rate, since the flux and energy of the neutrinos predicted by different models vary in different phases of the explosion. Possible optimization of XMASS electronic system is under investigation to cope with such a high event rate.

There are three detectors in the Kamioka Underground Observatory which are capable of detecting supernova neutrinos: Super-Kamiokande, KamLAND, and XMASS. They cover each other's dead time, are sensitive to different neutrino interactions and may provide comprehensive understanding of

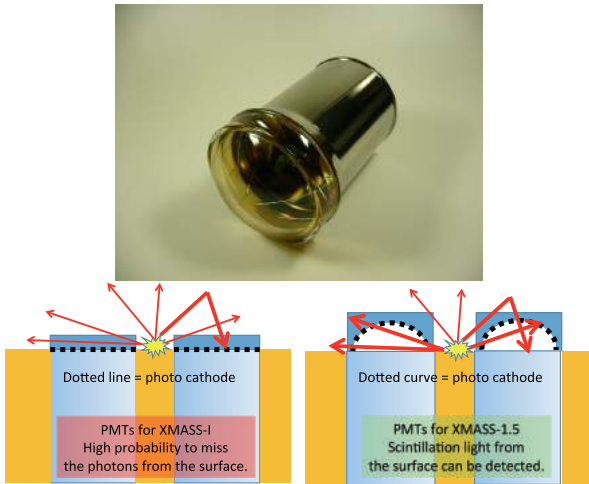


Fig. 36. Picture of a newly-developed 3-inch PMT for the next generation XMASS detector.

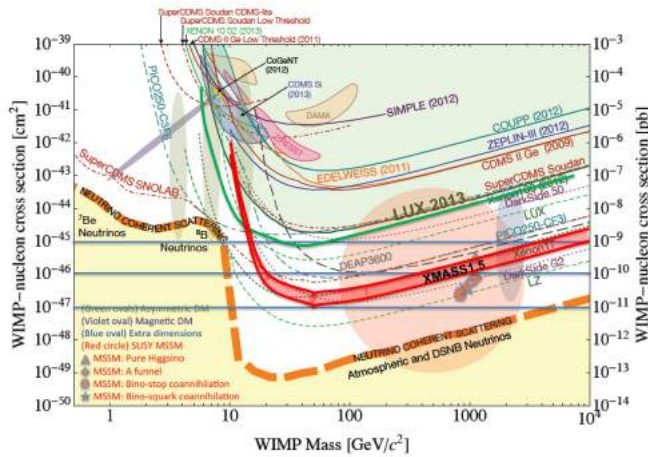


Fig. 37. Expected sensitivity on the spin-independent WIMP-nucleon scattering with XMASS-1.5.

the supernova neutrino burst in case of a simultaneous observation.

XMASS-1.5 and beyond

We are planning to build the next stage detector, XMASS-1.5, with total 6 tons of liquid xenon. Increasing the fiducial mass is indispensable to examine cross sections smaller than current constraints for standard WIMPs. The basic design of the detector is the same as the one for the XMASS-I detector but with an essential improvement of the discrimination between the surface background and the inner events. For this purpose, we have developed a new type of PMT which has a dome-shaped photocathode as shown in Fig. 36. The dome-shaped PMTs are more efficient for detecting scintillation photons originated at the inner surface of the detector than the flat-shaped PMTs used for the XMASS-I detector.

Fig. 37 shows the expected sensitivity to the spin-independent WIMP-nucleon cross section with the XMASS-1.5 detector. With XMASS-1.5, the sensitivity will reach $(1-3) \times 10^{-47} \text{ cm}^2$

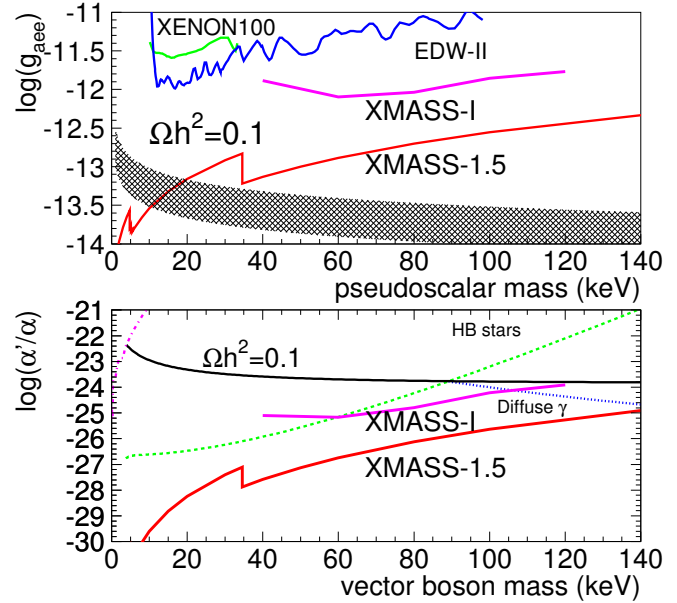


Fig. 38. Expected sensitivity on coupling constants between bosonic super-WIMPs and electrons with XMASS-1.5. The top and bottom panels are for pseudoscalar and vector bosons, respectively.

for $50 \text{ GeV}/c^2$ WIMPs assuming the fiducial mass of 3 tons. It is noteworthy that XMASS has a unique feature that it has a very low energy threshold as well as high sensitivity for other types of dark matter. The low energy threshold is essentially important for a low mass WIMP search and achieved by the high light yield as confirmed with the XMASS-I detector. The detector is sensitive to axion-like particles as well as bosonic super-WIMPs because the detector is designed to realize low background even without e/γ rejection. These unique features are particularly important to have a detector sensitive to a broad range of dark matter candidates. The expected sensitivity to bosonic super-WIMPs with the XMASS-1.5 detector is shown in Fig. 38. Furthermore, XMASS-1.5 is expected to be able to observe pp solar neutrino events at a rate of a few events per day. Beyond XMASS-1.5, XMASS-II with total 24 tons of liquid xenon is planned.

Bibliography

- [1] Y. Suzuki *et al.*, hep-ph/0008296.
- [2] K. Abe *et al.* (XMASS Collaboration), Phys. Lett. B **719** (2013) 78.
- [3] K. Abe *et al.* (XMASS Collaboration), Phys. Lett. B **724** (2013) 46.
- [4] H. Uchida *et al.* (XMASS Collaboration), Prog. Theor. Exp. Phys. (2014) 063C01.
- [5] K. Abe *et al.* (XMASS Collaboration), Phys. Rev. Lett. **113** (2014) 121301.

- [6] K. Abe *et al.* (XMASS Collaboration), Nucl. Instrum. Meth. A **716** (2013) 78.
- [7] K. Abe *et al.* (XMASS Collaboration), Phys. Lett. B **759** (2016) 272.
- [8] K. Abe *et al.* (XMASS Collaboration), Phys. Lett. B **759** (2016) 64.
- [9] K. Abe *et al.* (XMASS Collaboration), arXiv:1604.01218 [physics.ins-det].

HYPER-KAMIOKANDE

[Project Leader: Masato Shiozawa
(Kamioka Observatory, ICRR, The University of Tokyo)]

The Hyper-Kamiokande (Hyper-K) detector is proposed as a next generation underground water Cherenkov detector, which is designed based on the extremely successful Super-Kamiokande (Super-K) detector, but with an order of magnitude larger detector volume and upgraded photosensors. It will serve as a far detector of a long baseline neutrino oscillation experiment, having an enormous potential to discover leptonic CP violation in neutrino oscillations. Hyper-K will also have far better capabilities to search for proton decays and to observe atmospheric neutrinos, solar neutrinos, and neutrinos from other astronomical sources than those of predecessor experiments.

The Hyper-K project has been supported by both the high energy physics community and the cosmic-ray community, and the project was selected as one of top 27 important large research projects in the "Master Plan 2014" by the Science Council of Japan. Various R&D works as well as the physics potential studies had been done by members of the Hyper-K international working group, and since 2012 a series of open working group meetings to discuss them had been held semi-annually. In January 2015, the Hyper-K international proto-collaboration was established. The proto-collaboration consists of about 240 researchers from 13 countries. The first and second Hyper-K international proto-collaboration meetings were held in June 2015 and in January 2016, respectively.

One of major international R&D activities for Hyper-K is to develop new photosensors as alternatives to Hamamatsu R3600 50 cm PMTs, which have successfully been used in Super-K for 20 years. The new 50 cm PMT, R12860, jointly developed with Hamamatsu Photonics K.K., looks much like the Super-K PMT, but has improved photocathode and dynodes inside. The peak quantum efficiency in the new PMT is about 30%, 1.4 times higher than that of the Super-K PMT. In addition, the photoelectron collection efficiency is greatly improved by utilizing Box-and-Line type dynodes, instead of the Venetian-Blind type dynodes used inside the Super-K PMT. Consequently, the new Hyper-K PMT has twice higher single photon detection efficiency as shown in Fig. 39. Thanks to this dynode structure improvement, the timing and charge resolutions for single photoelectron signals of the new PMT (1.1 ns

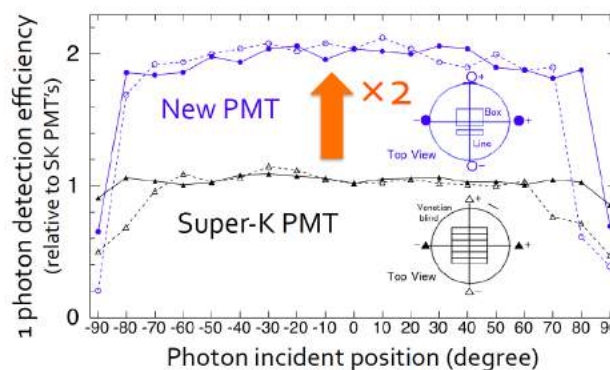


Fig. 39. Single photon detection efficiency of the Super-K PMT (black points) and the new Hyper-K PMT (blue points) as a function of photon incident position. The data points are normalized relative to the Super-K PMT's efficiency for photons incident on the center of the photocathode.

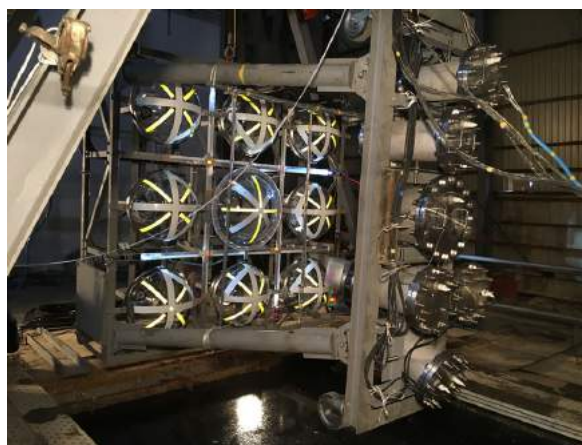


Fig. 40. The strength test setup of the PMT protective covers. The test was carried out in a deep vertical shaft located at Kami-Sunagawa town, Hokkaido. The events at a water depth of 60-80 m of an artificial implosion of the center bulb, with and without the protective cover, have been measured by using monitors such as pressure gauges and high-speed cameras.

and 35%, respectively) are also much higher than those of the Super-K PMT (2.1 ns and 53%, respectively).

Studies for improving the mechanical strength of the new 50 cm PMT have also been advanced in 2015. The hydrostatic pressure test of the glass bulbs has proved that their pressure tolerance was significantly correlated with the glass thickness especially in the neck part. The new PMT R12860 is eventually designed to have smoother curvature and larger thickness in the glass bulb shape, compared to the R3600 PMT. To evaluate the pressure tolerance of the R12860 PMT, fifty of the final design vacuum glass bulbs were pressurized up to the water pressure at a depth of 125 m, and none of them was broken.

To prevent a chain reaction of imploding PMTs caused by the unlikely event of a single PMT implosion, every PMT in the Hyper-K water tank will be housed in the shockwave prevention cover. The prototype cover consists of an acrylic front window and a stainless steel backside cover. To evaluate the performance of the prototype cover, a mock test simulating

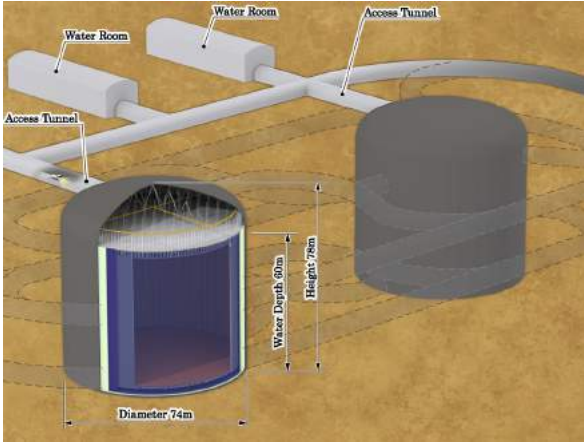


Fig. 41. A schematic view of the Hyper-K detector. The detector consists of two cylindrical tanks, which are filled with 516,000 tons of ultrapure water. The total fiducial mass is 374,000 tons, which is roughly 20 times as large as that of Super-K.

the event of a photosensor implosion in Hyper-K was carried out in a deep vertical shaft at Kami-Sunagawa town, Hokkaido from February to March 2016 (Fig. 40). It has been demonstrated that the peak amplitude of the pressure shockwave was significantly reduced outside the cover for the imploded glass bulb and thus could not cause a chain reaction.

In year 2015, the Hyper-K proro-collaboration has intensively worked for further optimizing the detector design. The successful development of the new ultrasensitive 50 cm PMT has made it possible to design the detector quite differently from its original design [1]. Adopting the new PMTs with twice higher photon detection efficiency greatly enhances the Hyper-K's sensitivity to low energy signals, such as a 2.2 MeV gamma from a neutron captured on a Hydrogen nucleus, resulting in far better performance on the signal detection and background rejection in various physics analyses. Consequently, the detector volume and hence the construction cost of Hyper-K can be significantly reduced from those in the original design, without degrading sensitivities in most of the important Hyper-K physics programs.

Fig. 41 shows the optimized design of the Hyper-K detector. The detector consists of two cylindrical water tanks, each with a height of 60 m and a diameter of 74 m. The tanks are filled with 516,000 metric tons of ultrapure water. The total fiducial mass is 374,000 tons, which is two thirds of that in the original design but still roughly 20 times as large as that of Super-K. The innermost main water volume of each tank will be viewed by 40,000 new 50cm PMTs, providing about 40% photocathode coverage on the inner detector wall, i.e. the same photocathode coverage as that in Super-K. To build the two huge tanks, a staged-construction scenario is being considered. Namely, the first tank will be constructed prior to the second one to start the Hyper-K experiment as quickly as possible, then second one will be constructed to further expand physics reaches of the experiment. In the estimation of Hyper-K physics sensitivities described below, it is assumed that the second tank will start its observation 6 years behind the first tank.

Fig. 42 shows the Hyper-K's 3σ discovery potential for

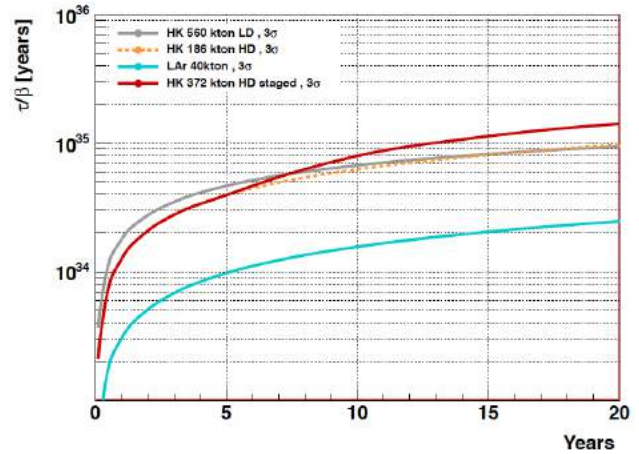


Fig. 42. The $p \rightarrow e^+ \pi^0$ discovery potential (3σ) as a function of running time of Hyper-K with a nominal staging scenario (red solid).

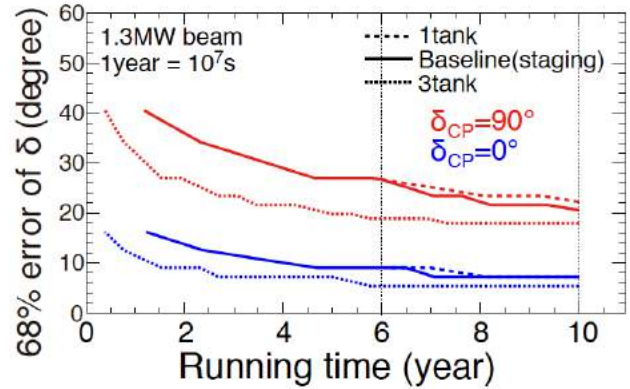


Fig. 43. The expected uncertainty (1σ) of the δ_{CP} measurement using the upgraded J-PARC neutrino beam as a function of running time of Hyper-K with a nominal staging scenario (thick solid). The blue (red) lines are for the case of true $\delta_{CP} = 0^\circ (90^\circ)$.

the proton decay mode $p \rightarrow e^+ \pi^0$ as a function of running time. If the proton lifetime is 1.7×10^{34} years, just beyond the current limit obtained by Super-K, its decay into $e^+ \pi^0$ will be seen at 3σ within one year of Hyper-K running, and its significance will reach 9σ in 10 years. Even if the proton lifetime is as long as 1×10^{35} years, the 3σ discovery for $p \rightarrow e^+ \pi^0$ will be made by about 15 years of Hyper-K observation. In the search for the decay mode $p \rightarrow \bar{\nu} K^+$, which is favored by supersymmetry grand unified theories, the 3σ discovery potential will reach $\tau/B = 2.5 \times 10^{34}$ years in 10 years of Hyper-K running (Note that the present limit obtained by Super-K is 0.7×10^{34} years at 90% C.L.). Even in the absence of proton decay signals, Hyper-K is expected to extend existing lifetime limits by more than an order of magnitude for a wide variety of proton decay modes including the two mentioned above.

Studies on the Hyper-K's sensitivity to the neutrino CP violation [2] have also been updated by considering the optimized detector design and the latest J-PARC beam power projection. As shown in Fig. 43, the CP violating phase δ_{CP} will be measured with 1σ error of $7^\circ (21^\circ)$ after 10 years if $\delta_{CP} = 0^\circ (90^\circ)$. The neutrino CP violation, $\sin \delta_{CP} \neq 0$, will be discovered with more than 3σ significance for 78% of the

possible values of δ_{CP} in 10 years of the beam neutrino measurement. The high statistics data sample of atmospheric neutrinos obtained by Hyper-K will also play an important role to grasp the full picture of neutrino oscillations. The neutrino mass hierarchy will be determined with 3σ significance in a few years of atmospheric neutrino observation by Hyper-K in combination with the beam neutrino measurement. As for the solar neutrino observation, the upturn in the solar neutrino energy spectrum, which is caused by the matter effect in the Sun, will be observed with 5σ significance in 10 years Hyper-K running. Hyper-K has also a great potential to discover the diffuse supernova neutrino background, often called the relic supernova neutrinos.

In January 2015, ICRR and KEK-IPNS signed a memorandum of understanding (MoU) for cooperation on the Hyper-K project. In accordance of the MoU, the Hyper-K Advisory Committee (HKAC) has been formed under the directors of ICRR and KEK-IPNS. The HKAC is composed of international members outside the Hyper-K collaboration, and its task is to advise on the scientific, technical and managerial strategy of the experiment with a view to further developing a highly effective neutrino program based in Japan. Under the HKAC, a subcommittee focusing on the Hyper-K cavern excavation and water tank construction has also been formed. The cavern/tank subcommittee consists of Japanese experts on geology engineering, civil engineering and architectural engineering. In winter 2015-2016, the first round of the HKAC and subcommittee meetings were held. In the meetings, the technical and scientific feasibility of the updated detector design and experimental strategy was assessed. Though the official report from the HKAC is still under preparation, the HKAC endorses Hyper-K as a very important experiment for the world-wide program of fundamental science, and encourages ICRR and KEK-IPNS to fully support it.

Bibliography

- [1] K. Abe *et al.*, “Letter of Intent: The Hyper-Kamiokande Experiment — Detector Design and Physics Potential —,” arXiv:1109.3262 [hep-ex].
- [2] K. Abe *et al.* [Hyper-Kamiokande Proto-Collaboration], “Physics potential of a long-baseline neutrino oscillation experiment using a J-PARC neutrino beam and Hyper-Kamiokande,” PTEP **2015**, 053C02 (2015) doi:10.1093/ptep/ptv061 [arXiv:1502.05199 [hep-ex]].

HIGH ENERGY COSMIC RAY DIVISION

Overview

There are three major experimental research activities in the High Energy Cosmic Ray Division, the study of high energy gamma rays and the development of the next generation gamma-ray telescopes by the Cherenkov Cosmic Gamma Ray group, the study of extremely high energy cosmic rays by the Telescope Array (TA) group, and the study of very high energy cosmic rays and gamma rays by the Tibet AS γ group.

Other activities, such as experiments utilizing the Akeno observatory, the Norikura observatory, the Mt. Chacaltaya observatory (jointly operated with Bolivia) are closely related to inter-university joint research programs. Also an all-sky high resolution air-shower detector (Ashra) is in partial operation on the Hawaii island. The High Energy Astrophysics group created in the fiscal year 2009 aims to explore various high energy astrophysical phenomena, through theoretical and observational approaches.

The CANGAROO telescopes had been in operation in South Australia since 1992, with a 3.8 m small telescope and then with four 10 m telescopes. The major scientific objective was the study of Very High Energy (VHE) gamma-ray sources in our galaxy in the southern hemisphere. The mission of these telescopes was completed and the CANGAROO observation site was closed in 2011.

For further development of VHE gamma-ray astronomy, the Cherenkov Cosmic Gamma Ray group is working on the design study and development of the next generation international ground-based gamma-ray observatory CTA which will offer an order of magnitude better sensitivity than currently running Cherenkov telescopes, three times better angular resolution, and wider energy coverage from 20 GeV to 100 TeV or higher.

At the Akeno observatory, a series of air shower arrays of increasing geometrical sizes were constructed and operated to observe extremely high energy cosmic rays (EHECRs). The Akeno Giant Air Shower Array (AGASA) was operated from 1991 to January 2004 and covered the ground area of 100 km² as the world largest air shower array. In 13 years of operation, AGASA observed a handful of cosmic rays exceeding the theoretical energy end of the extra-galactic cosmic rays (GZK cutoff) at 10²⁰ eV.

The Telescope Array (TA), a large plastic scintillator array with air fluorescence telescopes, has been constructed in Utah, USA, which succeeds AGASA and measures the EHECRs with an order of magnitude larger aperture than that of AGASA for the further study of EHECRs. The full-scale TA is accumulating data as the largest array viewing the northern sky and observed the energy spectrum with high statistics, which is in good agreement with the GZK suppression.

An air shower experiment aiming to search for celestial gamma-ray point sources started in 1990 with Chinese physicists at Yangbajing (Tibet, 4,300 m a.s.l.). This international collaboration is called the Tibet AS γ Collaboration. An ex-

tension of the air shower array was completed in 1995 and an emulsion chamber has been combined with this air shower array since 1996 to study the primary cosmic rays around the knee energy region. After successive extensions carried out in 1999, 2002 and 2003, the total area of the air shower array amounts to 37,000 m². The sun's shadow in cosmic rays affected by the solar magnetic field was observed for the first time in 1992, utilizing its good angular resolution at multi-TeV energy region.

The High Energy Astrophysics group is conducting theoretical researches on fundamental processes responsible for non-thermal particle acceleration in various astrophysical environments, including first-order diffusive shock acceleration, second-order stochastic acceleration in shock downstream regions, modification of shock structure by pick-up interstellar neutrals, as well as injection processes of suprathermal particles. In addition to these theoretical works, R/D studies for radio observations of pulsars and cosmic ray air showers are also being made.

Cherenkov Cosmic Gamma-Ray Group

CTA Project (Cherenkov Telescope Array)

CTA-Japan Consortium

[Spokespersons : M.Teshima and H.Kubo]

Collaboration list:

Institute for Cosmic Ray Research, The University of Tokyo, Chiba, Japan; Department of Physics, Aoyama Gakuin University, Tokyo, Japan; Department of Physics, Hiroshima University, Hiroshima, Japan; Hiroshima Astrophysical Science Center, Hiroshima University, Hiroshima, Japan; Faculty of Science, Ibaraki University, Ibaraki, Japan; Institute of Particle and Nuclear Studies, High Energy Accelerator Research Organization (KEK), Ibaraki, Japan; Department of Physics, Konan University, Hyogo, Japan; Faculty of Medical Engineering and Technology, Kitasato University, Kanagawa, Japan; Graduate School of Science and Technology, Kumamoto University, Kumamoto, Japan; Department of Physics, Kyoto University, Kyoto, Japan; Department of Applied Physics, University of Miyazaki, Miyazaki, Japan; Department of Physics, Nagoya University, Aichi, Japan; Solar-Terrestrial Environment Laboratory, Nagoya University, Aichi, Japan; Kobayashi-Maskawa Institute, Nagoya University, Aichi, Japan; Department of Earth and Space Science, Osaka University, Japan; Department of Physics, Kinki University, Osaka, Japan; Astrophysical Big Bang laboratory, RIKEN, Wako, Japan; Department of Physics, Rikkyo University, Tokyo, Japan; Department of Physics, Saitama University, Saitama, Japan; Institute of Space and Astronautical Science, JAXA, Kanagawa,

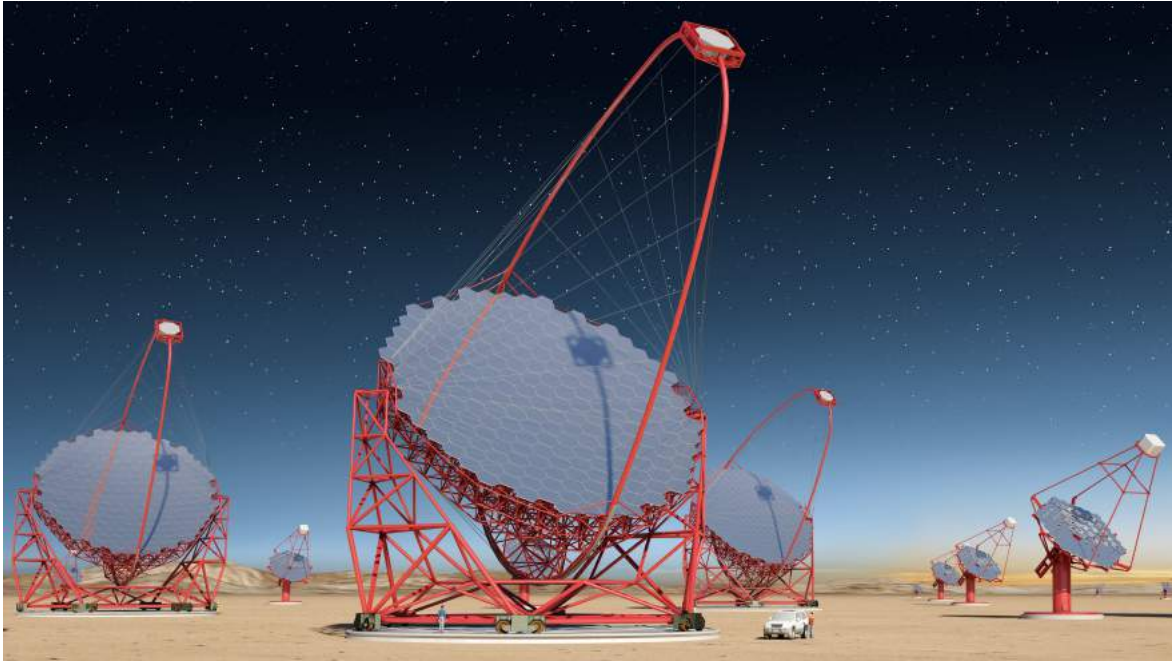


Fig. 1. Artist view of the CTA observatory. CTA consists of three types of telescopes, Large Size Telescopes (23m diameter), Mid Size Telescopes (12m) and Small Size Telescopes (4m), and covers the broad energy band from 20GeV to 100TeV.

Japan; Department of Physics, Tokai University, Kanagawa, Japan; Faculty of Integrated Arts and Sciences, The University of Tokushima; Department of Astronomy, The University of Tokyo, Tokyo, Japan; Department of Physics, The University of Tokyo, Tokyo, Japan; Faculty of Science and Engineering, Waseda University, Tokyo, Japan; Department of Physics, Yamagata University, Yamagata, Japan; Faculty of Management Information, Yamanashi Gakuin University, Yamanashi, Japan; Center for Cosmology and AstroParticle Physics, Ohio State University, Ohio, USA; Max-Planck-Institute for Physics, Munich, Germany [1].

CTA Project

During the past several years, Very High Energy (VHE) gamma-ray astronomy has made spectacular progress and has established itself as a vital branch of astrophysics. To advance this field even further, we propose the Cherenkov Telescope Array (CTA) [5], the next generation VHE gamma ray observatory, in the framework of a worldwide, international collaboration. CTA is the ultimate VHE gamma ray observatory, whose sensitivity and broad energy coverage will attain an order of magnitude improvement above those of current Imaging Atmospheric Cherenkov Telescopes (IACTs). By observing the highest energy photons known, CTA will clarify many aspects of the extreme Universe, including the origin of the highest energy cosmic rays in our Galaxy and beyond, the physics of energetic particle generation in neutron stars and black holes, as well as the star formation history of the Universe. CTA will also address critical issues in fundamental physics, such as the identity of dark matter particles and the nature of quantum gravity.

VHE gamma rays from 100GeV to 10TeV can be observed with ground-based IACTs. The history of VHE gamma ray as-

tronomy began with the discovery of VHE gamma rays from the Crab Nebula by the Whipple Observatory in 1989. To date, the current generation IACTs featuring new technologies, such as H.E.S.S., MAGIC, VERITAS, and CANGAROO, have discovered more than 100 Galactic and extragalactic sources of various types.

CTA is designed to achieve superior sensitivity and performance, utilizing established technologies and experience gained from the current IACTs. The project is presently in its preparatory phase, with international efforts from Japan, the US and EU. It will consist of several 10s of IACTs of three different sizes (Large Size Telescopes, Mid Size Telescopes, and Small Size Telescopes). With a factor of 10 increase in sensitivity ($1\text{m Crab} \sim 10^{-14} \text{erg s}^{-1} \text{cm}^{-2}$), together with a much broader energy coverage from 20GeV up to 100TeV, CTA will bring forth further dramatic advances for VHE gamma ray astronomy. The discovery of more than 1000 Galactic and extragalactic sources is anticipated with CTA.

CTA will allow us to explore numerous diverse topics in physics and astrophysics. The century-old question of the origin of cosmic rays is expected to be finally settled through detailed observations of supernova remnants and other Galactic objects along with the diffuse Galactic gamma ray emission, which will also shed light on the physics of the interstellar medium. Observing pulsars and associated pulsar wind nebulae will clarify physical processes in the vicinity of neutron stars and extreme magnetic fields. The physics of accretion onto supermassive black holes, the long-standing puzzle of the origin of ultrarelativistic jets emanating from them, as well as their cosmological evolution, will be addressed by extensive studies of active galactic nuclei (AGN). Through dedicated observing strategies, CTA will also elucidate many aspects of the mysterious nature of gamma ray bursts (GRBs), the most

energetic explosions in the Universe. Detailed studies of both AGNs and GRBs can also reveal the origin of the highest energy cosmic rays in the Universe, probe the cosmic history of star formation including the very first stars, as well as provide high precision tests of theories of quantum gravity. Finally, CTA will search for signatures from elementary particles constituting dark matter with the highest sensitivity yet. Realization of the rich scientific potential of CTA is very much feasible, thanks to the positive experience gained from the current IACTs.

The CTA-Japan consortium [1] is aiming at contributing in particular to the construction of the Large Size Telescopes (LSTs) and is involved in their development. The LST covers the low energy domain from 20GeV to 1000GeV and is especially important for studies of high redshift AGNs and GRBs. The diameter and area of the mirror are 23m and 400m², respectively, in order to achieve the lowest possible energy threshold of 20GeV. All optical elements/detectors require high specifications, for example, high reflectivity, high collection efficiency, high quantum efficiency and ultra fast digitization of signal, etc. For this purpose, CTA-Japan is developing high quantum efficiency photomultipliers, ultrafast readout electronics and high precision segmented mirrors. On the strength of their experience gained from construction of the MAGIC telescope, the Max-Planck-Institute for Physics in Munich is responsible for the design of the 23m diameter telescope structure, based on a carbon fiber tube space frame. The LSTs require very fast rotation (180 degrees/20seconds) for promptly observing GRBs. The first LST will be built in the CTA North, La Palma, Spain in 2016 and three more LSTs will be built during 2017 and 2018, then four more LSTs in the CTA South will be built in the ESO site in Paranal, Chile. The location of the LST array in the CTA North will overlap with MAGIC telescopes, which will allow us to operate CTA-LSTs and MAGIC telescopes together in the early phase of the construction.

The Cherenkov Cosmic Gamma Ray group is also operating the MAGIC Telescopes [9] on La Palma, Canary Islands. This facility is used not only for scientific observations but also for technological development toward the future observatory CTA.

Bibliography

- [1] CTA Consortium website: <http://www.cta-observatory.jp/> and <http://www.cta-observatory.org/>.
- [2] The Cherenkov Telescope Array potential for the study of young supernova remnants, *Astropart. Phys.* 62 (2015) 152-164.
- [3] Introducing the CTA concept, The CTA Consortium, *Astropart. Phys.* 43 (2013) 3-18.
- [4] Gamma-ray burst science in the era of the Cherenkov Telescope Array, S. Inoue et al., *Astropart. Phys.* 43 (2013) 252-275.
- [5] Design Concepts for The Cherenkov Telescope Array,

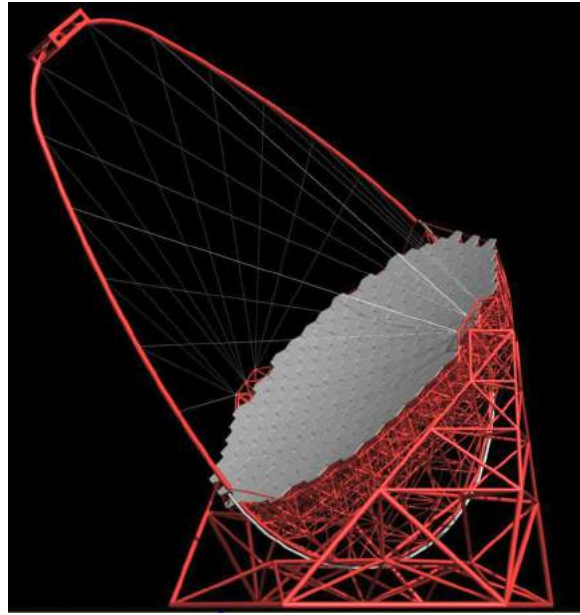


Fig. 2. Large Size Telescope (23m diameter) designed by Max-Planck-Institute for Physics. CTA Japan is contributing to the design and prototyping of the imaging camera at the focal plane, ultrafast readout electronics, and high precision segmented mirrors.



Fig. 3. Camera cluster for the Large Size Telescope (LST) developed by CTA-Japan. This cluster consists of seven high quantum efficiency photomultipliers (R11920-100), CW High Voltages, pre-amplifier, Slow Control Board, DRS4 Ultra fast waveform recording system and Trigger. The LST camera can be assembled with 265 of these clusters, cooling plates and camera housing.



Fig. 4. The high precision segmented mirrors for the Large Size Telescope (LST) developed by CTA-Japan in cooperation with Sanko Co.LTD. The mirror is made of a 60mm thick aluminum honeycomb sandwiched by 3mm thin glass on both sides. A surface protection coat consisting of the materials SiO₂ and HfO₂ is applied to enhance the reflectivity and to elongate the lifetime.



Fig. 5. MAGIC Stereo System with two Cherenkov telescopes of 17m diameters, so far achieved the threshold energy of 25GeV. It locates near the mountain top of the Roque de los Muchachos on the Canary Island of La Palma. Two telescopes are located with the distance of 85 meters.

The CTA Consortium, *Exper. Astron.* 32 (2011) 193-316.

- [6] Status of Very High Energy Gamma Ray Astronomy and Future Prospects, M. Teshima, *The Astronomical Herald*, 104 (2011) 333-342.
- [7] Design Study of a CTA Large Size Telescope, Proc. of ICRC2012 at Beijing China, M. Teshima, arXiv:1111.2183.
- [8] Introducing the CTA Concept, B. Acharya et al., *Astroparticle Physics*, 34 (2013) 3.
- [9] MAGIC Collaboration website: <http://magic.mppmu.mpg.de/>.

MAGIC

The MAGIC Collaboration has built in 2002 / 2003 a first large atmospheric imaging Cherenkov telescope, MAGIC-I, with a mirror surface of 236 sq.m. and equipped with photomultiplier tubes of optimal efficiency. In 2009, a second telescope of essentially the same characteristics was added; MAGIC-II was installed at a distance of 85m from MAGIC-I. With the accent of these instruments on large mirror surface and best light collection, cosmic gamma-rays at an energy threshold lower than any existing or planned terrestrial gamma-ray telescope have become accessible. So far achieved has been a threshold of 25 GeV. The Japanese group has joined the MAGIC collaboration since 2010, and contributed to the operation, observations and data analysis. The MAGIC telescopes are upgraded with new cameras, electronics and partially new mirrors in 2012, and are now operated with an unprecedented sensitivity by an international collaboration of 17 institutes from 8 countries.

The recent highlights from MAGIC are, 1) the successful observation of pulsed gamma ray signal from the Crab pulsar up to TeV regime [1], 2) the discoveries of the most distant blazars 3S 0218 + 35 with the redshift of 0.944 [2] and PKS 1441 + 25 with the redshift of 0.939 [3], 3) the observation of the very fast flare of 1min time scale from the blazar inside Perseus cluster, IC310 [4]. These results brought new questions on the pulsar emission mechanism, the EBL energy density, and gamma ray emission mechanism from the super-massive blackholes or vicinity of them.



Fig. 6. Akeno atmospheric Cherenkov telescope equipped with an R & D system of 32 pixel imaging camera.

Bibliography

- [1] Phase-resolved energy spectra of the Crab pulsar in the range of 50-400 GeV measured with the MAGIC telescopes, the MAGIC Collaboration, Aleksić et al. *A&A* 540 (2012) A69.
- [2] ATEL 6349.
- [3] ATEL 7416.
- [4] Black hole lightning due to particle acceleration at sub-horizon scales, the MAGIC collaboration, *Science* 346 (2014) 1080-1084.

Other Activities

As a test bench for domestic R & D activities of future ground-based gamma-ray observatory projects, a used atmospheric Cherenkov telescope of a 3 m diameter was obtained and placed at the Akeno Observatory in November 2010. This telescope (Akeno telescope, hereafter) is currently the only atmospheric Cherenkov telescope located in Japan [1]. In the fiscal year 2015, noise resistance of the R & D imaging camera system installed to the Akeno telescope in 2014 (Figure 6) was improved significantly, aiming to detect atmospheric Cherenkov light events with a self-triggering system. The telescope was also utilized for some other R & D studies, such as a test of a central CCD camera system for CTA Large-Sized Telescopes and a test observation using radio antennas attached at the focus of the telescope in order to search for forward radio emission coincident with extensive air showers.

We also started preparing another system to detect optical pulses from the Crab pulsar with the Akeno telescope, using a PMT near the center of the imaging camera described above. The goal of this R & D is to carry out simultaneous observations with the 34 m radio antenna in Kashima, Japan. Radio pulses from the Crab pulsar inevitably pass through the Crab Nebula plasma and the effect there in the acceleration site is possibly seen as fluctuation of the dispersion measure (DM). The role of the optical observations with the Akeno telescope is to give a good timing reference to the DM measurement. We expect to get new insight on the acceleration site of the Crab Nebula with this new approach [2].

Bibliography

- [1] M. Ohishi et al., Proc. of 33rd Internat. Cosmic Ray Conf. (Rio de Janeiro), 587 (2013).
- [2] T. Yoshikoshi et al., Proc. of 34th Internat. Cosmic Ray Conf. (The Hague), 887 (2015).

TA: Telescope Array Experiment

[Spokespersons: H. Sagawa¹, G. B.Thomson²]

1 : ICRR, The Univ. of Tokyo, Kashiwa, Chiba, Japan

2 : Dept. of Physics, University of Utah, Salt Lake City, UT, USA

Collaborating Institutions:

Chiba Univ., Chiba, Japan; Chubu Univ., Kasugai, Japan; Earthquake Research Institute, Univ. of Tokyo, Tokyo, Japan; Ehime Univ., Matsuyama, Japan; Ewha W. Univ., Seoul, Korea; Hiroshima City Univ., Hiroshima, Japan; Hanyang Univ., Seoul, Korea; ICRR, Univ. of Tokyo, Kashiwa, Japan; INR, Moscow, Russia; IPMU, Univ. of Tokyo, Kashiwa, Japan; Kanagawa Univ., Yokohama, Japan; KEK/ IPNS, Tsukuba, Japan; Kinki Univ., Higashi-Osaka, Japan; Kochi Univ., Kochi, Japan; Kyushu Univ., Fukuoka, Japan; Moscow M.V. Lomonosov State Univ., Moscow, Russia; Nat. Inst. of Rad. Sci., Chiba, Japan; Osaka City Univ., Osaka, Japan; RIKEN, Wako, Japan; Ritsumeikan Univ., Kusatsu, Japan; Rutgers Univ., Piscataway, NJ, USA; Saitama Univ., Saitama, Japan; Shinshu Univ., Nagano, Japan; Sungkyunkwan Univ., Suwon, Korea; Tokyo City Univ., Tokyo, Japan; Tokyo Inst. of Tech., Tokyo, Japan; Tokyo Univ. of Science, Noda, Japan; ULB, Brussels, Belgium; UNIST, Ulsan, Korea; Univ. of Utah, Salt Lake City, USA; Univ. of Yamanashi, Kofu, Japan; Waseda Univ., Tokyo, Japan; Yonsei Univ., Seoul, Korea

Overview and Status of TA and TALE

TA

The Telescope Array (TA) is the largest Ultra-High-Energy Cosmic-Ray (UHECR) observatory in the Northern Hemisphere, located in the West Desert in Utah, USA (latitude 39.3° N, longitude 112.9° W, altitude ~1400 m) [1]. TA is designed to observe extensive air showers (EAS) induced by UHECRs with energies from about 10^{18} to $10^{20.5}$ eV, and measures the energy spectrum, mass composition, and arrival direction distribution of UHECRs, and searches for ultra-high-energy photon and neutrino primaries. The aim of these measurements is to explore the origin, propagation and interaction of UHECRs. The TA detector will consist of an air shower surface detector (SD) array of plastic scintillation counters to measure the lateral distribution of secondary particles on the ground, and fluorescence detectors (FDs) to measure the longitudinal development of the EAS in the atmosphere. The SD array consists of 507 counters each with an area of 3 m², which were

deployed on a square grid with 1.2-km spacing between each, covering an area of approximately 700 km². Three FD stations are located at the periphery, looking inward over the SD array. The Middle Drum (MD) FD site is located to the north of the SD array, and is instrumented with 14 refurbished telescopes that were used at the High-Resolution Fly's Eye (HiRes) [2]. The Black Rock Mesa (BRM) and Long Ridge (LR) FD sites are located to the southeast and southwest of the SD array, respectively. They are each instrumented with 12 new telescopes. The TA detector is operated by an international collaboration of researchers from Japan, the USA, Korea, Russia, and Belgium. Hybrid observations using both SDs and FDs commenced in March 2008.

TALE

The TA Low Energy Extension (TALE) enables detailed studies of the energy spectrum and composition from about 10^{16} eV upwards. Previous experiments reported the second knee in the cosmic-ray spectrum around the 10^{17} -eV decade. The energy scales of these detectors differed by about a factor of two, so the energy at which this spectral break occurred was quite uncertain. There is a possibility that the transition from galactic cosmic rays to extragalactic cosmic rays occurs in this energy region. Thus we expect to observe the transition from heavy to light composition. A 14-TeV center-of-mass collision at the Large Hadron Collider (LHC) corresponds to a proton of about 10^{17} eV colliding with another proton at rest. The cosmic-ray data observed by the TALE could be compared with the air shower Monte Carlo (MC) simulation tuned by the results of the LHC experiments.

The TALE detector is located north of the TA site. Ten additional TALE FDs view 31°–59° in elevation angle, and have been operational using refurbished HiRes-II telescopes. The TALE infill SD array consists of approximately 100 plastic scintillation counters each with an area of 3 m². These counters have graded spacings, ranging from 400 m near the FD to 600 m further away, which merge into the TA SD array with 1200-m spacing at its northwestern corner. The TALE FD operation was commenced in the spring of 2013. The 35 TALE surface detectors were deployed at that time, and 16 surface detectors are running.

Energy Spectrum

The energy spectrum for four years of the TA SD data with zenith angles less than 45 degrees has been published [3]. Here, we update the energy spectrum using the SD data for seven years of observations from May 2008 to May 2015 with an exposure of 6300 km² sr yr [4]. The MC data were generated by a CORSIKA air shower simulation with the QGSJET-II-03 hadronic interaction model. A GEANT4 simulation was used for the detector simulation. We use a lookup table of the charge density S_{800} at a distance of 800 m from the shower core and zenith angle θ with primary energy E from the MC study for the first estimation of the cosmic-ray energy.

The energy scale uncertainty in the SD MC simulation can be large, mainly due to the modeling of hadronic interactions. The energy scale uncertainty is experimentally controlled by the FD, because the energy measurement is calorimetric. We

correct SD energy scale to FD energy scale using events detected by both the FD and SD. The observed differences between the FD and SD events are well described by a simple proportionality relationship, where the SD energy must be reduced by 27% to agree with the FD energy.

The resulting cosmic-ray flux multiplied by E^3 is shown together with a broken power-law fit in Figure 7. We found the two breaks at $10^{18.70 \pm 0.02}$ eV and $10^{19.78 \pm 0.04}$ eV. These are consistent with the ankle and the GZK suppression [5, 6], respectively. We observed 44 events above the suppression, whereas a linear extrapolation of the power law below the break predicts 99.3 events above the break. This result provides evidence for the flux suppression with a statistical significance of $\sim 6\sigma$. The Auger spectrum after energy-scale shift by +8.5% agrees with the TA spectrum below $10^{19.4}$ eV, whereas the suppression points differ between the two spectra.

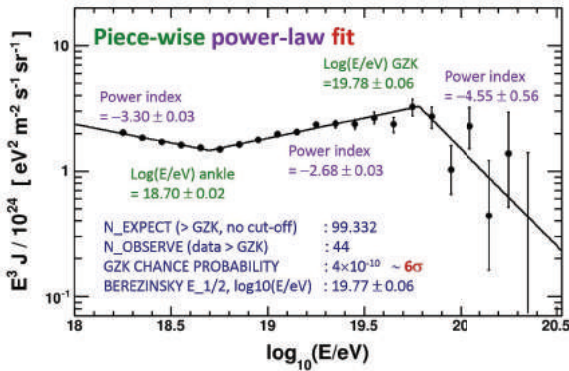


Fig. 7. The preliminary cosmic-ray flux multiplied by E^3 using seven years of the TA surface-detector data [4]. The solid line shows the fit of the TA data to a broken power law.

Figure 8 shows the energy spectrum using the TALE FD data [7] together with the TA monocular FD data [8] and SD data [9]. In the fluorescence detection observation, Cherenkov light produced in the air shower was considered to be a contamination to the fluorescence signal and events that had high fractions of Cherenkov light in the signals were discarded. The spectrum of events with energies above $10^{16.5}$ eV that are selected to dominate by scintillation light is shown by red filled circles. For the lower energies, the TALE FD is also sensitive to Cherenkov light. Low energy cosmic rays in the PeV energy range are detectable by the TALE as Cherenkov events. Using these events, we measured the energy spectrum of cosmic rays with energies from $10^{15.6}$ eV to $10^{17.4}$ eV as shown by red open squares. We see two clear breaks at around $10^{16.34}$ eV and $10^{17.3}$ eV.

Mass Composition

The dependence of shower maximum depth, X_{\max} , on the primary energy is used to determine the mass composition. The HiRes result was consistent with proton-dominated composition for $E > 10^{18}$ eV [10], whereas the Auger result was compatible with mixed composition [11].

The X_{\max} result using the events observed with the MD FD and SDs (hybrid events) from May 2008 through May 2013 has been presented [12]. In this analysis, an updated version

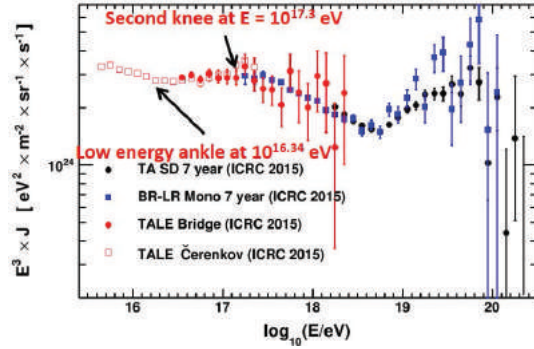


Fig. 8. The preliminary energy spectra using the TALE telescope data [7] together with the TA monocular FD (blue filled squares) [8] and TA SD (black filled circles) energy spectra [9]. The TALE spectra using Cherenkov-light dominant analysis and fluorescence-light dominant analysis are denoted by red open squares and red filled circles, respectively.

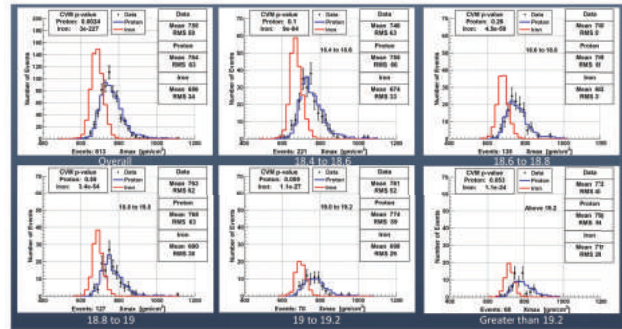


Fig. 9. The reconstructed X_{\max} distributions for the TA MD hybrid data (points) with QGSJET II-03 MC simulation for six energy regions (all, $\log_{10}E = 18.4-18.6, 18.6-18.8, 18.8-19.0, \text{ and } 19.0-19.2$ and > 19.2 from top-left to bottom-right panels [14]. The blue and red histograms are the proton and iron predictions, respectively.

of the pattern recognition analysis (PRA) method, which selects events that have a clear rise and fall in shower profile signal, is used.

Using an updated version of the PRA method [13], a result of X_{\max} using the MD hybrid events in the seven year period is presented [14]. The distribution of reconstructed X_{\max} for the TA data is in agreement with the distribution of the QGSJET II-03 proton model in each energy range as shown in Figure 9. Here the X_{\max} values include reconstruction and acceptance bias both for the TA data and MC simulation. The evolution of the average X_{\max} with energy for the TA hybrid data is shown with the MC simulation in the energy range of $10^{18.4}$ to $10^{19.8}$ eV in Figure 10. The TA MD hybrid X_{\max} result is in agreement with light composition.

We performed the X_{\max} analysis using the hybrid data with the BRM FD or LR FD [15] and the analysis using the stereoscopic FD data (BRM FD and LR FD, LR FD and MD FD or MD FD and BRM FD) [16]. Their results are consistent with light composition.

Proton air cross section

The value of σ_{p-air}^{inel} using K-factor method is determined. This method infers the attenuation length and the cross sec-

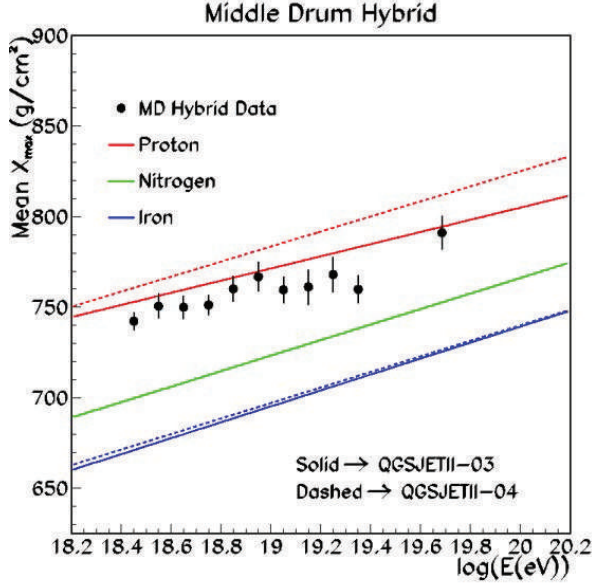


Fig. 10. The average reconstructed X_{\max} (black points) as a function of energy for the TA MD hybrid data [14]. The red lines are the pure proton predictions with two interaction models: QGSJET II-03 (solid line), and QGSJET II-04 (dashed line). The green and blue lines show the nitrogen and iron predictions, respectively.

tion from the exponential tail of the X_{\max} distribution. This assumes that the tail of the X_{\max} distribution is comprised of the most lighter particles (protons). The tail of the X_{\max} distribution is fit to the exponential $\exp(-X_{\max}/\Lambda_m)$, where Λ_m is the attenuation length. Λ_m is proportional to the interaction length λ_{p-air} : $\Lambda_m = K\lambda_{p-air} = K(14.45m_p)/\sigma_{p-air}^{inel}$. Here K is a constant. The MD hybrid events collected between May of 2008 and May of 2013 was used in this analysis [17]. The Λ_m value is found to be (50.47 ± 6.26) g/cm² from the fit to the tail between 790 and 1000 g/cm² of X_{\max} distribution of MD hybrid events with energy between $10^{18.3}$ and $10^{19.3}$ eV, of which average energy is $10^{18.68}$ eV. The result of the proton-air cross section (σ_{p-air}^{inel}) is $567.0 \pm 70.5^{+29}_{-25}$ mb, and is shown together with the results from other experiments in Figure 11. Ultimately the value of σ_{p-p} is determined from σ_{p-air}^{inel} using Glauber theory and BHS QCD inspired fit [18, 19]. The value of σ_{p-p}^{tot} was determined to be 170^{+48}_{-44} (stat.) $^{+19}_{-17}$ (sys.) mb. This result is shown in Figure 12 compared to previous results from cosmic ray experiments.

Anisotropy in Arrival Directions of UHECRs

We have published an analysis of UHECRs for correlations with Active Galactic Nuclei (AGNs), as well as for autocorrelations and correlations with the Large-Scale Structure (LSS) for a 40-month TA data set [20]. Here, we update the anisotropy results using the full seven years of the TA data with zenith angles below 55° and a more relaxed border cut than the cut used for the measurement of the energy spectrum. The data set contains 2996 events with $E > 10^{19}$ eV, 210 events with $E > 4 \times 10^{19}$ eV, and 83 events with $E > 5.7 \times 10^{19}$ eV for the LSS correlations. There are 53 events with $E > 5.7 \times 10^{19}$ eV for zenith angles below 45° for AGN correlations [21].

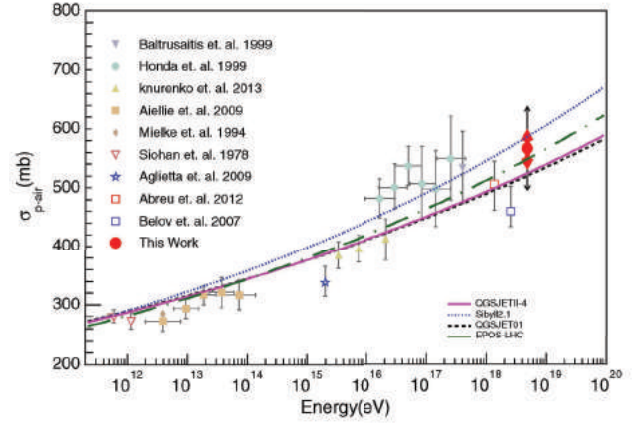


Fig. 11. The proton-air cross section of this work including the statistical and systematic error bars in comparison to other experimental results [17].

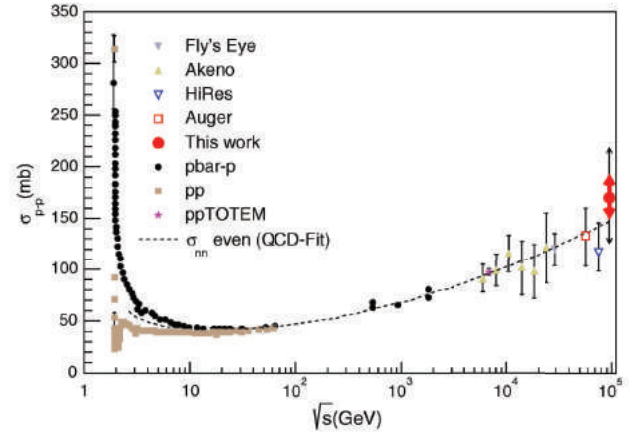


Fig. 12. The proton-proton cross section of this work including the statistical and systematic error bars in comparison to other experimental results [17].

Correlations with AGNs

The Auger Collaboration reported correlations between the arrival directions of UHECRs with $E > 5.7 \times 10^{19}$ eV and the positions of nearby AGNs from the Véron 2006 catalog with $0 < z \leq 0.018$ in 2007 [22]. The number of correlating events for angular separations of less than 3.1° was 8 out of 13, whereas 2.7 events were expected to correlate by chance for an isotropic distribution. The hypothesis of isotropy was rejected with at least a 99 % confidence level. The Auger analysis has been updated, and it was found that the number of correlating events was 41 out of 146 above 5.3×10^{19} eV, which corresponds to about 28.1% of events, which was 2 standard deviation above an isotropic expectation [23].

We searched for AGN correlations using the same requirements as Auger, and found 24 correlating events (37.5%) out of 64 total events with $E > 5.7 \times 10^{19}$ eV. The number of random coincidences expected for this total number of events is 15.5. Using a binomial distribution with a single-event correlation probability of $p_{iso} = 0.24$, the probability of this excess occurring by chance is 1.2%, assuming an isotropic distribution.

Correlations with LSS

We use galaxies at distances of 5 to 250 Mpc and with Ks magnitudes of less than 12.5 in the 2MASS Galaxy Redshift Catalog (XSCz) [24]. This catalog provides the most accurate information about the three-dimensional distribution of galaxies. We assume that UHECRs are protons, and that the effects of galactic and extragalactic magnetic fields on each arrival direction can be approximated by a Gaussian probability density function with an angular resolution (called a smearing angle) of θ , which is treated as a free parameter. The data with $E > 5.7 \times 10^{19}$ eV is compatible with the LSS model, of which p -value is about 10%, and is incompatible with the isotropy model, of which p -value is about a few 0.1% at above a smearing angle of 6° .

Hotspot for highest-energy cosmic rays

We have searched for intermediate-scale anisotropy of cosmic-ray events with energy greater than 5.7×10^{19} eV using five years of the TA SD data [25]. Here we use the event selection somewhat looser than the above analyses in order to increase the number of events with maintaining reasonable energy and angular resolution. By the looser cuts, of which major change is abolishing the cut of the SD array edge, we obtain 109 cosmic-ray events for seven years of TA SD data. Figure 13 (a) shows a sky map in equatorial coordinates of these events. A cluster of events that we call a ‘‘hotspot’’ appears in this map centered near right ascension $\sim 150^\circ$ and declination $\sim 40^\circ$, with a diameter of $\sim 30^\circ$ to 40° . In order to estimate the significance of this hotspot, we use oversampling with circles 20° in radius. Figure 13 (b) shows a pre-trial significance map of the cosmic-ray events with energies greater than 5.7×10^{19} eV using seven years of the TA SD data. The maximum excess in our Field-of-View (FoV) appears as a hotspot centered at right ascension of 148.4° and declination of 44.5° with a statistical significance of 5.07σ (the number of observed events = 24, and the number of events expected in an isotropic cosmic-ray sky = 6.88). The probability of such a hotspot appearing by chance in an isotropic cosmic-ray sky is estimated to be 3.7×10^{-4} (3.4σ) [26].

Search for EeV protons of Galactic origin

The EeV cosmic rays are thought to have a light, probably protonic, composition. To study their origin one can search for anisotropy in their arrival directions. Galactic cosmic rays of this type should be seen mostly along the galactic plane, and there should be a shortage of events coming from directions near the galactic anticenter. Guided by models of the galactic magnetic field that indicate that the enhancement along the galactic plane should have a standard deviation of $20^\circ - 35^\circ$ in galactic latitude, and the deficit in the galactic anticenter direction should have a standard deviation of about 50° , we use the data of the TA experiment to search for these effects [27]. Neither an enhancement along the galactic plane nor a deficit in the galactic anticenter direction is found. An upper limit on the fraction of EeV cosmic rays of galactic origin at 0.9% at 90% confidence level.

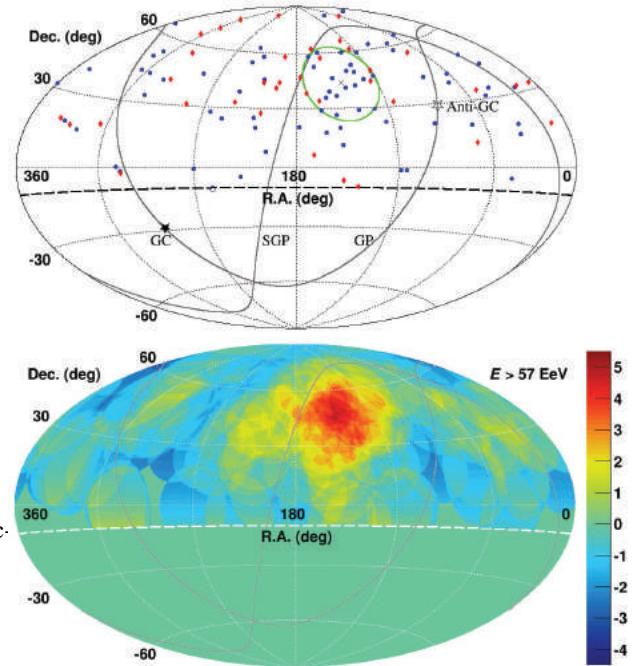


Fig. 13. Aitoff projection of the UHECR maps in the equatorial coordinates [26]. The solid curves indicate the galactic plane (GP) and supergalactic plane (SGP). The TA FoV is defined as the region above the declination of -10° (the dashed curve). (a) The points show the directions of the UHECRs with $E > 5.7 \times 10^{19}$ eV observed by the TA SD array, and the closed and open stars indicate the Galactic center (GC) and the anti-Galactic center (Anti-GC), respectively. The line labelled SGP is the supergalactic plane, and the line labelled GP is the galactic plane. (b) Significance map using oversampling with circles 20° in radius. Color scale denotes significance value.

Prospects

We describe the status of joint studies by the TA and Auger collaborations, the TA extension plans and R&D of future detectors.

TA and Auger Joint Studies

The TA and Auger collaborations began a program of joint studies in order to understand the differences of the TA and Auger results for the energy spectra, X_{\max} , and arrival directions. The following progress reports were presented at the International Cosmic Ray Conference 2015 (ICRC2015).

- The TA and Auger anisotropy working group and the IceCube-TA-Auger anisotropy working group
 - A large-scale anisotropy result with full sky coverage using the TA and Auger data above 1×10^{19} eV was published by developing a method to combine the two data sets [28].
 - Search for a correlation between the UHECRs measured by the TA and the Auger and the neutrino candidate events from IceCube was reported at ICRC2015 [29].
- High energy composition working group
 - The energy evolution of the mean of X_{\max} as measured by the Telescope Array and Pierre Auger Collaborations

was compared. The X_{\max} analysis of ad hoc data that is compatible with the Auger composition model via TA reconstruction is being studied in order to know how well the TA detector distinguishes between the Auger mixed composition and protonic composition. [30].

- TA muon project and Auger surface detector at the TA site
 - The number of muons observed in the Auger data is 1.8 times that of QGSJET II-03 simulation assuming proton primaries at 10^{19} eV. In order to make direct comparisons between the SD detection techniques used by Auger and TA, we deployed a water Cherenkov tank of the Auger South design in addition to that of the Auger North design [31] at the TA Central Laser Facility, where the TA muon detector project consisting of scintillators with concrete blocks and the detector with a lead sheet sandwiched between two scintillator plates is also ongoing [32]. We took data of single muon signals from Auger SD for calibration purpose and observed signals from Auger SD that coincided with the air-shower events observed by the TA surface detectors.
- FAST (the Fluorescence detector Array of Single-pixel Telescopes)
 - A Fluorescence detector Array of Single-pixel Telescopes (FAST) was proposed for large area and low-cost detection of ultra-high energy cosmic rays for the next generation of UHECR experiments [33]. The test of the FAST prototype was performed in 2014, and a full-scale FAST prototype is under development.

TA Low Energy Extension

We saw two clear breaks at around $10^{16.3}$ eV and $10^{17.3}$ eV in the energy spectrum measured with the TALE FD as shown in Figure 8. It is of importance to measure X_{\max} precisely adding timing information of surface detectors near the shower core on the ground. Therefore we proposed to complete the TALE surface detectors by adding remaining surface detectors. The proposal of adding remaining SDs in the TALE SD array was applied for the Japan Society for the Promotion of Science through Grants-in-Aids for Scientific Research on Scientific Research (S) (PI: S. Ogio of Osaka City University) and was approved in Japan in May of 2015. It will be in effect over a period of five years between Japanese Fiscal Year (JFY) 2015 and JFY 2019 [34].

We are also proposing the observation of cosmic rays with energies further down to approximately 10^{15} eV. The detector is called the Non-Imaging Cherenkov (NICHE) array [35]. The plan is to install an array of simple Cherenkov counters of PMTs each three inches in diameter on the ground looking upwards, deployed with 100-, 200-, and 400-meter spacings within the TALE infill array. We use counter timing to reconstruct the shower geometry, counter pulse heights to reconstruct the shower energy, and counter signal widths to reconstruct X_{\max} . The part of the NICHE with 15 PMTs that we call jNICHE has been approved in Japan in 2014 and supported by the Japan Society for the Promotion of Science through Grants-in-Aids for Young Scientists (A) (PI: Y. Tsunesada of

Osaka City University) . It is being constructed. The full NICHE will be proposed to the NSF in the USA.

TAx4 project

The TA confirmed the flux suppression consistent with the GZK cutoff at $10^{19.78}$ eV in the energy spectrum. The TA found evidence for intermediate-scale anisotropy of the highest-energy cosmic rays ($E > 5.7 \times 10^{19}$ eV). The TA X_{\max} result is consistent with light composition above $10^{18.2}$ eV. If the proton GZK cutoff exists, the sources of the highest-energy cosmic rays are expected to be restricted to nearby objects. If their sources are related to nearby matter distribution that is very anisotropic, we expect to observe anisotropy of the arrival directions of the highest-energy cosmic rays assuming their rectilinear propagation in the galactic and extragalactic magnetic fields. With enhanced statistics, we expect to observe the structure of that hotspot along with other possible excesses, point sources along with the correlations with extreme phenomena in the nearby universe. Based on this picture, we proposed to quadruple the area of the TA SD aperture. We plan to install additional 500 counters of the current TA SD design, which will be deployed on a square grid with wider, 2.08-km spacing between each [36]. Including the existing TA SD array, we will extend the aperture of the surface detector array in total to approximately 3,000 km². The new array would need two FD stations overlooking it to increase the number of hybrid events for the confirmation of the energy scale and the measurement of X_{\max} . These FDs will be formed using additional refurbished HiRes telescopes. The proposal of the FD part of TAx4 was also submitted to the National Science Foundation in 2015. This TA extension, which we call TAx4, will greatly accelerate the pace at which we will reach the goals. The layout of TAx4 is shown in Figure 14.

The proposal of the SD part of TAx4 was applied for the Japan Society for the Promotion of Science through Grants-in-Aids for Scientific Research on Specially Promoted Research (PI: H. Sagawa of ICRR), and was approved in Japan in April of 2015. It will be in effect over a period of five years between April 2015 and March 2020. Assuming the observation for the additional TAx4 SD array after about three-year construction and five years of the current TA data, we expect to have obtained in total the equivalent of 19 years TA SD exposures by adding seven years of the TA data that have already been recorded. We expect to obtain about 300 cosmic rays with energies greater than 5.7×10^{19} eV. After five years, the recorded data will clarify anisotropy of arrival directions of highest-energy cosmic rays, which can be originated from the matter structure or extreme phenomena in the nearby universe, with a significance greater than 5σ if the correlation continues at the current level. In JFY2015, 100 scintillator counters were assembled in Japan.

R&D for JEM-EUSO

The JEM-EUSO is a new type of observatory that will utilize very large volumes of the earth's atmosphere as a detector of the highest-energy cosmic rays in the Universe. It will be mounted to the International Space Station (ISS) at an altitude of approximately 400 km. The light sensor is a very

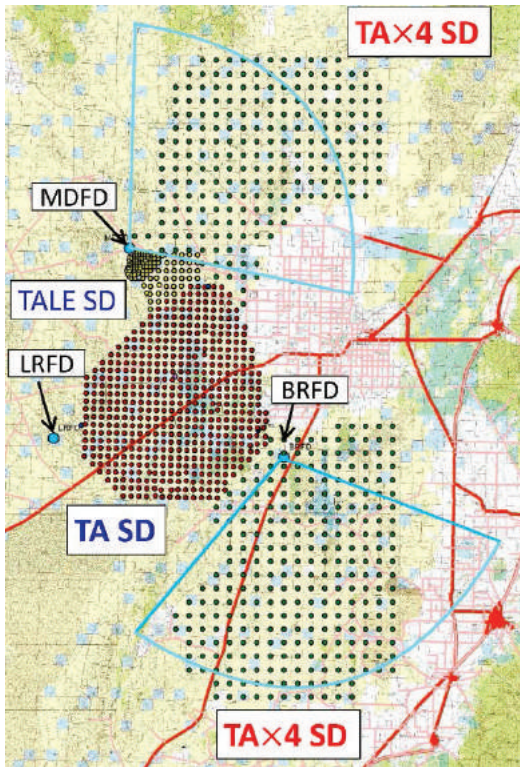


Fig. 14. The layout of the proposed Tax4 [36]. The array of 507 SDs (red filled circles on the left) is the current TA SD array. There are three TA FD stations (MD to the north, LR to the west, and BRM to the east of the TA array). The array of surface detectors to the north of the TA SD array is the TALE SD array. Additional two sub-arrays of 500 surface detectors in total (green filled circles) for Tax4 are located to the northeast and southeast of the TA SD array. Additional two FD stations with refurbished HiRes telescopes for the Tax4 are located at the MD and BRM FD sites and view to the northeast and southeast as denoted by the fans in light blue.

wide-field, very fast, and large telescope, and observes brief UV flashes in the earth's atmosphere caused by the highest-energy cosmic rays. The goal of JEM-EUSO year time exposure is one order of magnitude of Auger. The K-EUSO program, which is the Russian mission of the UHECR observatory using JEM-EUSO technology, is currently evaluated. In ICRR, we set up the calibration system of Multi-Anode PMTs (MAPMT) which will be used at the focal surface detector of JEM-EUSO [37]. We calibrated MAPMTs for the EUSO prototype test at the TA site (EUSO-TA), which was resumed in February, 2015. The first cosmic-ray data was recorded by EUSO-TA in May of 2015.

Summary

The TA confirmed the flux suppression above $10^{19.78}$ eV, which is consistent with the GZK suppression expected for protons, with a statistical significance of $\sim 6\sigma$ and the ankle at $10^{18.70}$ eV. The preliminary X_{\max} measurement above $10^{18.2}$ eV is consistent with light composition. We found an indication of a cluster of cosmic rays with energy greater than 5.7×10^{19} eV by oversampling using 20° -radius circles. Its significance appearing in an isotropic cosmic-ray sky is 3.7×10^{-4} (3.4σ). Analyses of these highest-energy cosmic-ray arrival directions for correlations with AGNs, and correlations with

the LSS proton model show a hint of anisotropy at a level of 2σ to 3σ .

The TA results suggest that anisotropy of arrival directions of highest-energy cosmic rays could be related to the matter distribution or extreme phenomena in the nearby universe. Therefore we propose the Tax4, which will quadruple the TA SD aperture and will add two FD stations. After five years, the Tax4 is expected to have obtained in total the equivalent to 19 years of TA SD data and 16.3 years of TA hybrid data by adding seven years of the TA data taken before the Tax4. The signal at a level of 3σ in the current anisotropy studies is expected to result in an observation at more than 5σ . And we will have more events for the measurement of energy spectrum and X_{\max} at around or above the cutoff.

The TA, TALE, and the proposed Tax4 and NICHE will provide important measurements of the spectrum, composition, and anisotropy from the knee region up to the highest-energy region of over five to six decades (10^{15} eV to 10^{21} eV) in energy.

The prototype test of the JEM-EUSO that will be the observation of extreme-energy cosmic rays in the space has been performed at the BRM FD site. The calibration test of JEM-EUSO MAPMTs for the EUSO-TA was performed in ICRR, and the test at the TA site is being performed.

Bibliography

- [1] K. Kawai *et al.*, J. Phys. Soc. Jpn. Suppl. A 78 (2009) 108.
- [2] G. Thomson *et al.*, Nucl. Phys. B 36 (2004) 28.
- [3] T. Abu-Zayyad *et al.*, Astrophys. J. Lett. 768 (2013) L1 (5pp).
- [4] C.H.H. Jui *et al.*, International Cosmic Ray Conference (ICRC) 2015 #1375 (2015).
- [5] K. Greisen, Phys. Rev. Lett. 16 (1966) 748-750.
- [6] G.T. Zatsepin and V.A. Kuz'min, JETP Lett. 4 (1966) 78-80.
- [7] T. Abu-Zayyad *et al.*, ICRC2015 #1185(2015).
- [8] T. Fujii *et al.*, ICRC2015 #714 (2015).
- [9] D. Ivanov *et al.*, ICRC2015 #847 (2015).
- [10] R.U. Abbasi *et al.*, Phys. Rev. Lett. 104 (2010) 161101.
- [11] A. Aab *et al.*, Astrophys. J. 794 (2014) 172 (15pp).
- [12] R.U. Abbasi *et al.*, Astropart. Phys. 64 (2015) 49-62.
- [13] J.P. Lundquist *et al.*, ICRC2015 #1332 (2015).
- [14] J.P. Lundquist *et al.*, ICRC2015 #1330 (2015).
- [15] D. Ikeda and W. Hanlon *et al.*, ICRC2015 #906 (2015).
- [16] T. Stroman *et al.*, ICRC2015 #905 (2015).
- [17] R.U. Abbasi *et al.*, Phys. Rev. D92 (2015) 032007.
- [18] M.M. Block, Phys. Rev. D84 (2011) 091501.

- [19] M.M. Block, F. Halzen, and T. Stanev. *Phys. Rev D* 62 (2000) 077501.
- [20] T. Abu-Zayyad *et al.*, *Astrophys. J.* 757 (2012) 26 (11pp).
- [21] P. Tinyakov *et al.*, *ICRC2015 #765* (2015).
- [22] J. Abraham *et al.*, *Science* 318 (2007) 939; J. Abraham *et al.*, *Astropart. Phys.* 29 (2008) 188-204.
- [23] A. Aab *et al.*, *Astrophys. J.* 804 (2015) 15.
- [24] T. Jarrett, arXiv:astro-ph/0405069.
- [25] R.U. Abbasi *et al.*, *Astrophys. J. Lett.* 790 (2014) 21.
- [26] K. Kawata *et al.*, *ICRC2015 #414* (2015).
- [27] D. Ivanov *et al.*, *ICRC2015 #858* (2015).
- [28] A. Aab *et al.*, *Astrophys. J.* 794 (2014) 172.
- [29] A. Christov *et al.*, *ICRC2015 #734* (2015).
- [30] M. Unger for the Pierre Auger Collaboration and the Telescope Array Collaboration, *ICRC2015*.
- [31] R. Takeishi *et al.*, *ICRC2015 #1054* (2015).
- [32] T. Nonaka *et al.*, *ICRC2015 #1018* (2015).
- [33] T. Fujii *et al.*, *ICRC2015 #738* (2015).
- [34] S. Ogio *et al.*, *ICRC2015 #859* (2015).
- [35] D. Bergman *et al.*, *ICRC2015 #837* (2015).
- [36] H. Sagawa *et al.*, *ICRC2015, #1022* (2015).
- [37] M. Casolino *et al.* *Proc. of 2014 Conference on Ultra High Energy Cosmic Rays (UHECR2014)*.

Tibet AS γ Project

[Spokespersons : M. Takita]

ICRR, The Univ. of Tokyo, Kashiwa, Chiba 277-8582

Experiment

The Tibet air shower experiment has been successfully operated at Yangbajing (90°31' E, 30°06' N; 4300 m above sea level) in Tibet, China since 1990. It has continuously made a wide field-of-view (approximately 2 steradian) observation of cosmic rays and gamma rays in the northern sky.

The Tibet I array was constructed in 1990 and it was gradually upgraded to the Tibet II by 1994 which consisted of 185 fast-timing (FT) scintillation counters placed on a 15 m square grid covering 36,900 m², and 36 density (D) counters around the FT-counter array. Each counter has a plastic scintillator plate of 0.5 m² in area and 3 cm in thickness. All the FT counters are equipped with a fast-timing 2-inch-in-diameter

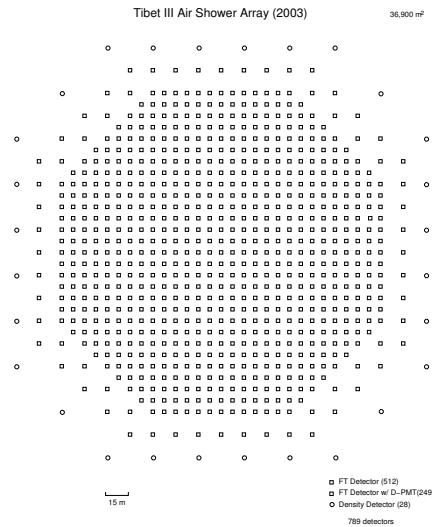


Fig. 15. Schematic view of Tibet III.

photomultiplier tube (FT-PMT), and 52 out of 185 FT counters are also equipped with a wide dynamic range 1.5-inch-in-diameter PMT (D-PMT) by which we measure up to 500 particles which saturates FT-PMT output, and all the D-counters have a D-PMT. A 0.5 cm thick lead plate is put on the top of each counter in order to increase the counter sensitivity by converting gamma rays into electron-positron pairs in an electromagnetic shower. The mode energy of the triggered events in Tibet II is 10 TeV.

In 1996, we added 77 FT counters with a 7.5 m lattice interval to a 5,200 m² area inside the northern part of the Tibet II array. We called this high-density array Tibet HD. The mode energy of the triggered events in Tibet HD is a few TeV.

In the late fall of 1999, the array was further upgraded by adding 235 FT-counters so as to enlarge the high-density area from 5,200 m² to 22,050 m², and we call this array and further upgraded one Tibet III. In 2002, all of the 36,900 m² area was covered by the high-density array by adding 200 FT-counters more. Finally we set up 56 FT-counters around the 36,900 m² high density array and equipped 8 D-counters with FT-PMT in 2003. At present, the Tibet air shower array consists of 761 FT-counters (249 of which have a D-PMT) and 28 D-counters as in Fig. 15.

The performance of the Tibet air shower array has been well examined by observing the Moon's shadow (approximately 0.5 degrees in diameter) in cosmic rays. The deficit map of cosmic rays around the Moon demonstrates the angular resolution to be around 0.9° at a few TeV for the Tibet III array. The pointing error is estimated to be better than $\sim 0.01^\circ$, as shown in Fig. 16, by displacement of the shadow center from the apparent center in the north-south direction, as the east-west component of the geomagnetic field is very small at the experimental site. On the other hand, the shadow center displacement in the east-west direction due to the geomagnetic field enables us to spectroscopically estimate the energy scale uncertainty at $\pm 12\%$ level, as shown in Fig. 17. Thus, the Tibet air shower experiment introduces a new method for

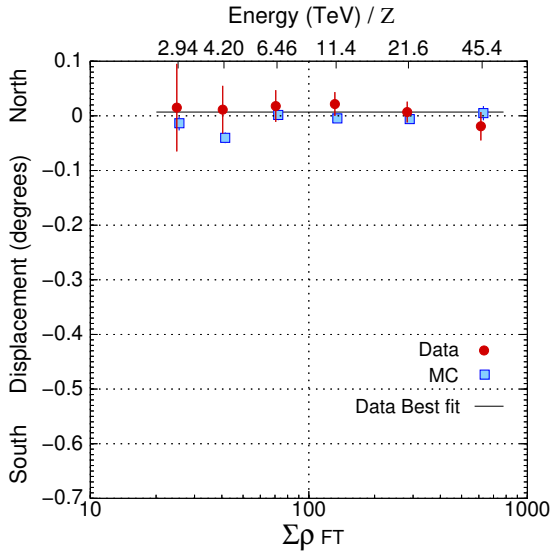


Fig. 16. From [1]. The Moon's shadow center displacement from the apparent position in the north-south direction as a function of energy, observed by Tibet III.

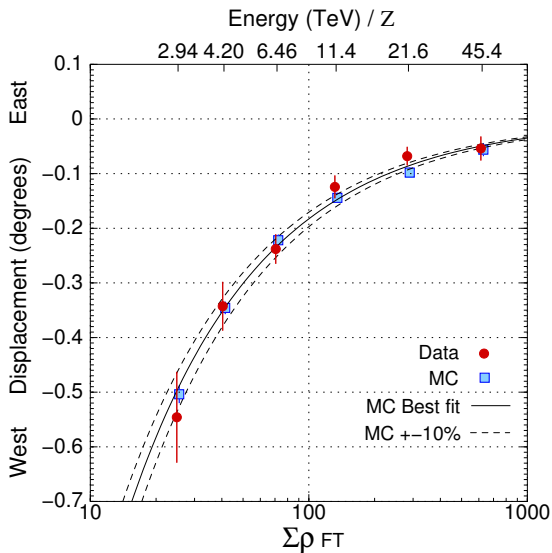


Fig. 17. From [1]. The Moon's shadow center displacement from the apparent position in the east-west direction as a function of energy, observed by Tibet III.

energy scale calibration other than the conventional estimation by the difference between the measured cosmic-ray flux by an air shower experiment and the higher-energy extrapolation of cosmic-ray flux measured by direct measurements by balloon-borne or satellite experiments.

Physics Results

Our current research theme is classified into 4 categories:

- (1) TeV celestial gamma-ray point/diffuse sources,
- (2) Chemical composition and energy spectrum of primary cosmic rays in the knee energy region,
- (3) Cosmic-ray anisotropy in the multi-TeV region with high

precision,

- (4) Global 3-dimensional structure of the solar and interplanetary magnetic fields by observing the Sun's shadow in cosmic rays.

We will introduce a part of the results obtained in this fiscal year.

We constructed a new hybrid detector system in 2014 to measure the chemical components of primary cosmic rays around the knee energy region in a wide energy range. It is composed of air shower core detectors (YAC-II: Yangbajing Air-shower Core detectors-II) to detect high-energy electromagnetic core component, Tibet-III and a large underground water Cherenkov muon detectors (MD). A detailed Monte Carlo (MC) simulation is done in order to study the performance of the hybrid experiment by means of CORSICA (version 6.204), where two hadronic interaction models, QGSJET01c and SIBYLL2.1, are employed. We assume three primary cosmic ray models, i.e., helium-poor, helium-rich and Gaisser's fit composition models, around the knee energy region. The detector responses are properly taken into account by means of GEANT4 (version 9.5) in the simulation to reflect the real detector configurations. The generated MC events are reconstructed by the same procedures as the real data analysis. The energy is estimated by lateral density fitting (LDF) method assuming modified NKG function. We employ the artificial neural network (ANN) method and the random forest (RF) method to select the light component (proton, helium) among primary cosmic rays. We evaluate possible systematic uncertainties of the proton and helium energy spectra arising at each step of the analysis, including dependence of the MC simulation on the hadronic interaction models and the chemical composition models of primary cosmic rays, and the difference in particle identification methods. We estimate the systematic uncertainty in the fluxes in the new hybrid experiment to be less than 30 % in total. Our MC simulation shows that the new hybrid experiment is useful to study the chemical component, especially when we measure proton and helium energy spectra of primary cosmic rays in the energy range between 50 TeV to 10 PeV which overlaps direct-observation data from balloon-borne/satellite experiments and indirect-observation data from ground-based experiments. The new hybrid experiment is very promising to find out the individual knee position of the power-law indices of the proton and helium components. It is very important to experimentally verify the standard cosmic-ray acceleration mechanism by shock waves in the vicinity of a supernova remnant, as it predicts that the knee position of an atom is proportional to its atomic number.

Another result is related to high-energy gamma rays from the Crab nebula.

Gamma rays at TeV energies from the Crab Nebula were first detected by the Whipple collaboration in 1989. Since the detection, the energy spectrum of the Crab Nebula has been measured by many imaging air Cherenkov telescopes as well as air shower arrays; the Tibet AS γ collaboration was the first air shower array which detected gamma rays from the Crab Nebula at multi-TeV energies. The Crab Nebula is now commonly used as a standard candle for gamma-ray experiments.

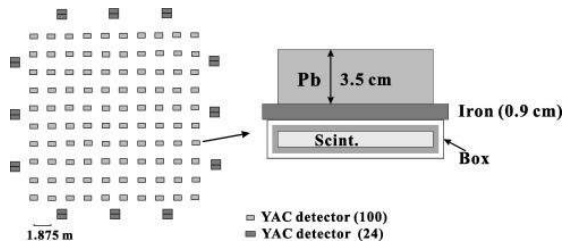


Fig. 18. From Ref. [2]. Schematic view of YAC-II array (left) and a YAC detector structure (right). The YAC-II array consists of 124 detectors. The inner 100 scintillator units are arranged as an array (10×10 grid). Each detector has an area of $50 \text{ cm} \times 80 \text{ cm}$ and it is placed with 1.875 m interval. The outer 24 units of the sizes of $50 \text{ cm} \times 100 \text{ cm}$ are arranged around the inner array and they are used to reject non core events whose shower cores are far from the YAC-II array. Each detector consists of lead plates with a thickness of 3.5 cm above the scintillator to convert high energy electrons and γ into electromagnetic showers

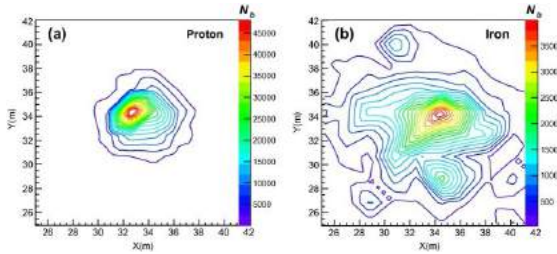


Fig. 19. From Ref. [2]. Contour map of typical high-energy core events of proton origin (a) and iron origin (b) simulated for the YAC-II array. Some parameters about primary nuclei are as follows: Proton, $E_0 = 2.02 \times 10^5 \text{ TeV}$, zenith angle = 23.5° , $N_e = 1.81 \times 10^6$; Iron, $E_0 = 3.43 \times 10^5 \text{ TeV}$, zenith angle = 34.4° , $N_e = 1.63 \times 10^6$. Proton-induced event (a) looks more like concentric circles, while iron-induced event (b) shows very irregular structure. In addition, the top burst size N_b^{top} among fired YAC detectors by proton event is greater by about one order of magnitude than that of iron event in spite of their close accompanied air-shower sizes N_e .

The energy spectrum is reproduced with a mechanism based on the synchrotron self-Compton (SSC) emission of high energy electrons. None of the experiments has detected gamma rays above 100 TeV from the Crab Nebula, and the best upper limits have been given by the CASA-MIA experiment. The observation of the energy spectrum of the Crab Nebula around 100 TeV with higher sensitivity is very important in order to confirm the leptonic origin of the Crab's TeV gamma-ray emission. Therefore, a search is made for gamma rays above $\sim 100 \text{ TeV}$ from the Crab Nebula, using the Tibet air shower (AS) array combined with a 100 m^2 muon detector (MD).

The 100 m^2 MD was constructed 90 m southwest of the center of the existing Tibet AS array in 2007. It is made up of two waterproof concrete cells set up 2.6 m underground (the thickness of the soil and the concrete ceiling is 2.25 m and 0.35 m, respectively). The density of the soil and the concrete cells is measured to be 2.1 g/cm^3 and 2.41 g/cm^3 , respectively. Each detector cell, 7.15 m wide \times 7.15 m long \times 1.5 m deep in size, is filled with water and equipped with three downward-facing 20-inch-in-diameter PMTs on the ceiling. We record the charge and timing information of each PMT, when a trigger signal is issued by the surface AS array. Neither water purifier nor water circulation system has been

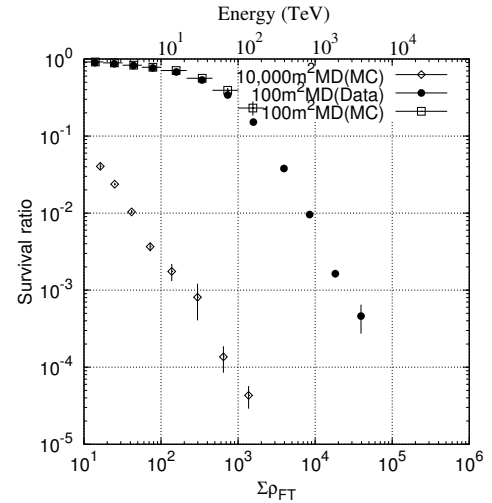


Fig. 20. From Ref. [3] (references therein). Fraction of the number of background cosmic rays that survive the N_μ -based event selection, as a function of $\Sigma \rho_{FT}$. Open diamonds represent the fraction obtained by our detailed MC simulation for the full-scale ($10,000 \text{ m}^2$) MD, while closed circles indicate the fraction calculated from the experimental data of the 100 m^2 MD. Open squares show the fraction by MC simulation for the 100 m^2 MD.

installed; the water temperature is cold and stable enough at $5^\circ\text{C} - 10^\circ\text{C}$ at the depth of 2.6 m underground, so that bacteria proliferate barely and water does not freeze. The data collected by the 100 m^2 MD from 2008 March to 2010 February (438 live days) are used in this analysis. We find that our MC simulation is in good agreement with the experimental data, for example, as demonstrated in Fig. 20.

Using the data collected by the 100 m^2 MD from March 2008 to February 2010 (438 live days), we search for continuous gamma-ray emission from the Crab Nebula above 100 TeV. No significant excess is found, and the most stringent upper limit is obtained above 140 TeV, as shown in Fig. 21, even with the small 100 m^2 MD.

Other Activities

The emulsion-pouring facilities can meet the demands for making any kind of nuclear emulsion plates which are used for cosmic ray or accelerator experiments. The thermostatic emulsion-processing facilities are operated in order to develop nuclear emulsion plates or X-ray films. Using these facilities, it is also possible to make and develop emulsion pelticle in 600-micron thickness each. In this way, these facilities have been open to all the qualified scientists who want to carry out joint research programs successfully. Of recent, however, the shrinking demand for the facilities let us decide that we should suspend calls for joint research programs to utilize the emulsion-pouring facilities, starting from 2012.

Ongoing Plans

(1) Chemical composition of primary cosmic rays making the knee in the all-particle energy spectrum

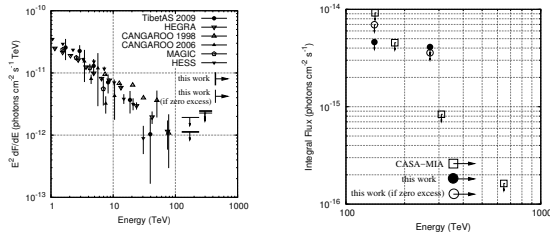


Fig. 21. From Ref. [3] (references therein). (a) Upper limits on the Crab Nebula's differential flux at the 90% confidence level obtained by this work (thick solid lines with downward arrows). The upper limits obtained by this work assuming zero excess counts are drawn by thin solid lines with downward arrows. The flux points measured by our previous work (closed circles) as well as by HEGRA (open inverse triangles), CANGAROO (filled and open triangles), MAGIC (open pentagons), and H.E.S.S. (filled inverse triangles) are also shown. (b) Upper limits on the Crab Nebula's integral flux at the 90% confidence level obtained by this work (filled circles with downward arrows), along with the upper limits at the 90% confidence level by CASA-MIA (open squares with downward arrows). The upper limits obtained by this work assuming zero excess counts are drawn by open circles with downward arrows.



Fig. 22. YAC2 set up at Yangbajing.

We have measured the energy spectra of primary cosmic-ray protons, helium, all particles around the knee energy region. The main component responsible for making the knee structure in the all particle energy spectrum is heavier nuclei than helium. The next step is to identify the chemical component making the knee in the all particle energy spectrum. We have a plan to install an Yangbajing Air shower Core detector array (YAC) around the center of Tibet III to distinguish the chemical component making the knee. We completed construction of YAC2 (~ 100 detectors over $\sim 160\text{m}^2$ in area), as is shown in Fig. 22, and started data-taking in March 2013. YAC2 aims at mainly studying the energy spectra of proton and helium components in the knee energy region.

(2) Gamma-ray astronomy in the 100 TeV region

We have a plan[4] to construct a large ($\sim 10,000\text{m}^2 \times 1.5\text{m}$ deep) underground ($\sim 2.5\text{m}$ soil+concrete overburden) water Cherenkov muon detector array (Tibet MD) around an ex-

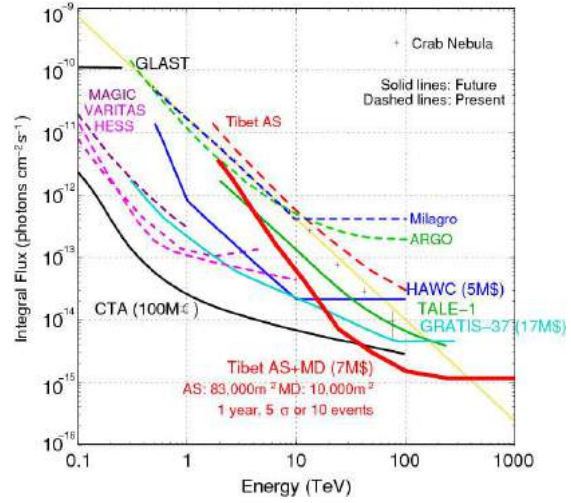


Fig. 23. Tibet AS + MD (red curve) integral flux sensitivity (5σ or 10 events/1yr) for a point source.

tended version (Tibet AS, $\sim 83,000\text{m}^2$) of Tibet III. By Tibet AS + MD, we aim at background-free detection of celestial point-source gamma rays in the 100 TeV region (10 TeV – 1000 TeV) with world-best sensitivity and at locating the origins of cosmic rays accelerated up to the knee energy region in the northern sky. The measurement of cut off energies in the energy spectra of such gamma rays in the 100 TeV region may contribute significantly to understanding of the cosmic-ray acceleration limit at SNRs. Search for extremely diffuse gamma-ray sources by Tibet AS + MD, for example, from the galactic plane or from the Cygnus region may be very intriguing as well. Above 100 TeV, the angular resolution of Tibet AS with 2-steradian wide field of view is 0.2° and the hadron rejection power of Tibet MD is 1/10000.

In addition to unknown point-like sources, we expect to detect established sources in the 100 TeV region: TeV J2032+4130, HESS J1837-069, Crab, MGRO J2019+37, MGRO J1908+06, Milagro candidate sources, Mrk421, Mrk501 are sufficiently detectable and Cas A, HESS J1834-087, LS I+63 303, IC443 and M87 are marginal.

Furthermore, our integral flux sensitivity to diffuse gamma rays will be the world-best as well. The diffuse gamma rays from the Cygnus region reported by the Milagro group and also diffuse gamma-rays from the galactic plane will be clearly detected. Diffuse gamma-rays of extragalactic origin may be an interesting target as well.

In 2007, a prototype 100-m^2 underground water Cherenkov muon detector was successfully constructed in Tibet to demonstrate the technical feasibility, cost estimate, validity of our Monte Carlo simulation. Data analyses demonstrate that our MC simulation reproduces real data quite reasonably.

In March 2013, construction of 5/12 of the full-scale MD, as is shown in Fig. 24, was successfully completed and data-taking started. We have accumulated approximately two-year data. One of the detector cell filled with water is demonstrated in Fig. 25.

Development of Monte Carlo simulation is under way for comparison with real data. Various analysis tools are also ex-

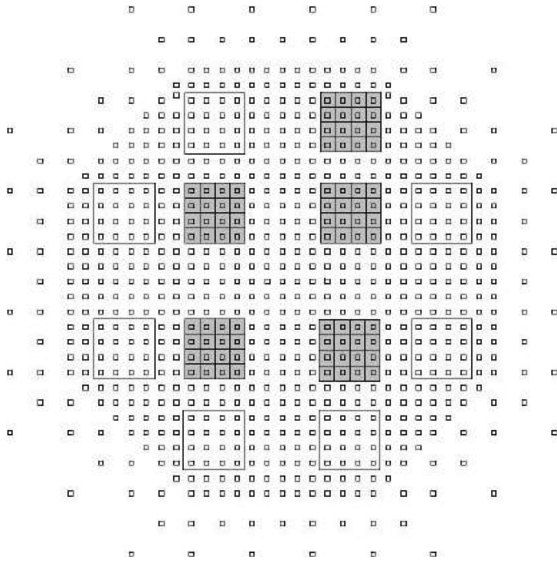


Fig. 24. The 5 shaded squares represent the constructed 5 MD pools.



Fig. 25. PMTs mounted in a MD cell filled with water.

tensively being developed. According to the simulation, the sensitivity of the current configuration (Tibe AS + one-third scale MD) is demonstrated in Fig. 26.

Bibliography

Papers in refereed journals

- [1] “Multi-TeV Gamma-Ray Observation from the Crab Nebula Using the Tibet-III Air Shower Array Finely Tuned by the Cosmic-Ray Moon’s Shadow”, M. Amenomori *et al.*, *Astrophysical Journal*, **692**, 61-72 (2009).
- [2] “Performance of the Tibet hybrid experiment (YAC-II + Tibet-III + MD) to measure the energy spectra of the light primary cosmic rays at energies 50 - 10,000 TeV”, J. Huanget *al.*, *Astroparticle Physics*, **66**, 18-30 (2015).
- [3] “SEARCH FOR GAMMA RAYS ABOVE 100 TeV FROM THE CRAB NEBULA WITH THE TIBET AIR SHOWER ARRAY AND THE 100m² MUON DETEC-

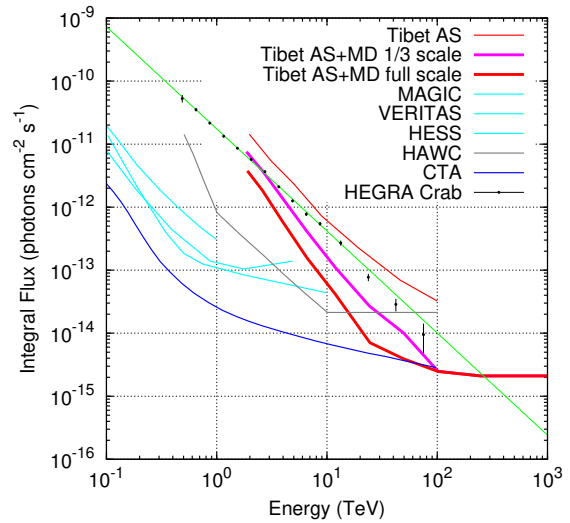


Fig. 26. Sensitivity to point-like gamma-ray sources with the current configuration (Tibet AS + one-third scale MD) by pink curve.

TOR”, M. Amenomori *et al.*, *THE ASTROPHYSICAL JOURNAL*, **813**, 98-1-5 (2015).

- [4] “Exploration of a 100 TeV gamma-ray northern sky using the Tibet air-shower array combined with an underground water-Cherenkov muon-detector array”, T.K. Sako *et al.*, *Astroparticle Physics*, **32**, 177-184 (2009).

The Tibet AS γ Collaboration

M. Amenomori,¹ X. J. Bi,² D. Chen,³ T. L. Chen,⁴ W. Y. Chen,² S. W. Cui,⁵ Danzengluobu,⁴ L. K. Ding,² C. F. Feng,⁶ Zhaoyang Feng,² Z. Y. Feng,⁷ Q. B. Gou,² Y. Q. Guo,² H. H. He,² Z. T. He,⁵ K. Hibino,⁸ N. Hotta,⁹ Haibing Hu,⁴ H. B. Hu,² J. Huang,² H. Y. Jia,⁷ L. Jiang,² F. Kajino,¹⁰ K. Kasahara,¹¹ Y. Katayose,¹² C. Kato,¹³ K. Kawata,¹⁴ M. Kozai,¹³ Labaciren,⁴ G. M. Le,¹⁵ A. F. Li,^{16,6,2} H. J. Li,⁴ W. J. Li,^{2,7} C. Liu,² J. S. Liu,² M. Y. Liu,⁴ H. Lu,² X. R. Meng,⁴ T. Miyazaki,¹³ K. Mizutani,^{11,17} K. Munakata,¹³ T. Nakajima,¹³ Y. Nakamura,¹³ H. Nanjo,¹ M. Nishizawa,¹⁸ T. Niwa,¹³ M. Ohnishi,¹⁴ I. Ohta,¹⁹ S. Ozawa,¹¹ X. L. Qian,^{6,2} X. B. Qu,² T. Saito,²⁰ T. Y. Saito,²¹ M. Sakata,¹⁰ T. K. Sako,¹⁴ J. Shao,^{2,6} M. Shibata,¹² A. Shiomi,²² T. Shirai,⁸ H. Sugimoto,²³ M. Takita,¹⁴ Y. H. Tan,² N. Tateyama,⁸ S. Torii,¹¹ H. Tsuchiya,²⁴ S. Udo,⁸ H. Wang,² H. R. Wu,² L. Xue,⁶ Y. Yamamoto,¹⁰ K. Yamauchi,¹² Z. Yang,² S. Yasue,²⁵ A. F. Yuan,⁴ T. Yuda,¹⁴ L. M. Zhai,² H. M. Zhang,² J. L. Zhang,² X. Y. Zhang,⁶ Y. Zhang,² Yi Zhang,² Ying Zhang,² Zhaxisangzhu,⁴ X. X. Zhou⁷

¹Department of Physics, Hirosaki University, Hirosaki 036-8561, Japan

²Key Laboratory of Particle Astrophysics, Institute of High Energy Physics, Chinese Academy of Sciences, Beijing 100049, China

³National Astronomical Observatories, Chinese Academy of Sciences, Beijing 100012, China

⁴Department of Mathematics and Physics, Tibet University, Lhasa 850000, China

⁵Department of Physics, Hebei Normal University, Shijiazhuang

050016, China

⁶Department of Physics, Shandong University, Jinan 250100, China

⁷Institute of Modern Physics, SouthWest Jiaotong University, Chengdu 610031, China

⁸Faculty of Engineering, Kanagawa University, Yokohama 221-8686, Japan

⁹Faculty of Education, Utsunomiya University, Utsunomiya 321-8505, Japan

¹⁰Department of Physics, Konan University, Kobe 658-8501, Japan

¹¹Research Institute for Science and Engineering, Waseda University, Tokyo 169-8555, Japan

¹²Faculty of Engineering, Yokohama National University, Yokohama 240-8501, Japan

¹³Department of Physics, Shinshu University, Matsumoto 390-8621, Japan

¹⁴Institute for Cosmic Ray Research, University of Tokyo, Kashiwa 277-8582, Japan

¹⁵National Center for Space Weather, China Meteorological Administration, Beijing 100081, China

¹⁶School of Information Science and Engineering, Shandong Agriculture University, Taian 271018, China

¹⁷Saitama University, Saitama 338-8570, Japan

¹⁸National Institute of Informatics, Tokyo 101-8430, Japan

¹⁹Sakushin Gakuin University, Utsunomiya 321-3295, Japan

²⁰Tokyo Metropolitan College of Industrial Technology, Tokyo 116-8523, Japan

²¹Max-Planck-Institut für Physik, München D-80805, Deutschland

²²College of Industrial Technology, Nihon University, Narashino 275-8576, Japan

²³Shonan Institute of Technology, Fujisawa 251-8511, Japan

²⁴Japan Atomic Energy Agency, Tokai-mura 319-1195, Japan

²⁵School of General Education, Shinshu University, Matsumoto 390-8621, Japan

High Energy Astrophysics Group

[Spokesperson: K. Asano]

ICRR, Univ. of Tokyo, Kashiwa, Chiba 277-8582

Overview

Since its creation in December 2009, the high energy astrophysics group has been making theoretical and observational studies of violent astrophysical phenomena in which nonthermal cosmic ray particles are being accelerated. In April 2013, new members, a research associate and a JPSP fellow, joined the group, who have been contributing to extend the group activity significantly. Targets of the group's study include high energy astrophysical objects such as supernova remnants/pulsar magnetospheres, giant flares and repeating bursts of magnetars, a giant galactic explosion called 'Fermi bubble', neutron star merger events, fast radio bursts (FRBs), jets from active galactic nuclei (AGN), as well as mysterious gamma ray bursts (GRBs). Research works on the origin of ultra high

energy cosmic rays (UHECRs) are also within the coverage of the group.

Research topics: 1. Stochastic Acceleration in Relativistic Jets

The wide-band photon spectra of AGN jets are usually explained by synchrotron radiation (from radio to X-ray) and inverse Compton scattering (gamma-ray) by non-thermal electrons. Such high-energy electrons have been supposed to be accelerated via shocks in jets. To reproduce complex feature of photon spectra by such models, however, we need to assume broken power-law spectra for electrons at injection into the emission region. The break energies and power-law indices of the electron spectra seem to be determined ad hoc. There is no convective model to explain such breaks in the electron spectra. Furthermore, the maximum energy of electrons is far below the most optimistic prediction of the shock acceleration theory, which successfully agrees with observed electron spectra in young supernova remnants.

Alternatively, we have considered a stochastic acceleration model, which is so called the 2nd order Fermi acceleration. In this process, electrons are scattered with turbulences, and gain energy stochastically. This acceleration mechanism can produce harder electron spectra than the spectra the shock acceleration yields. Our model has greatly succeeded to explain the curved spectra of blazars, such as Mrk 421. In this year, we adopt our model to the very short and bright flare of 3C 279 detected with Fermi-Large Area Telescope in 2013 December. Our time-dependent simulation shows that the very hard spectrum and asymmetric light curve are successfully reproduced by changing only the magnetic field from the value in the steady period (see Figure 27). The maximum energy of electrons drastically grows with the decrease of the magnetic field, which yields a hard photon spectrum as observed. Rapid cooling due to the inverse-Compton scattering with the external photons reproduces the decaying feature of the light curve.

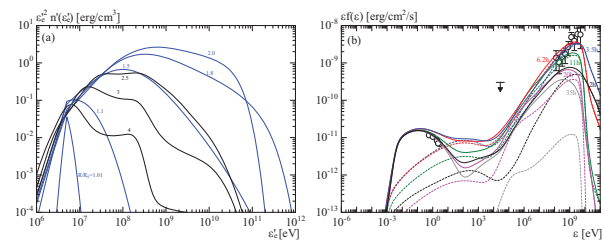


Fig. 27. (a) Evolution of the electron energy distribution with increasing distance R in the blazar 3C 279 flare model. (b) Photon spectrum for the most intense flare in 2013. The solid lines are the model spectra at observation times of 2 (black), 3.5 (blue), 6.2 (red), 11 (green), 20 (purple), and 35 (gray) hours.

We also develop our model to resolve the problem in the low-energy photon spectrum of GRBs. The low-energy portion (typically below 100 keV) of the GRB spectra is too hard to be explained by the conventional synchrotron radiation. The strong magnetic field leads to a soft photon spectrum emitted by cooled electrons, which contradicts the observed spectra. Our discussion reveals that the balance between the ac-

celeration and synchrotron cooling yields a narrow energy-distribution similar to the Maxwellian distribution. The synchrotron spectrum becomes consistent with the observed hard photon index for the low-energy region. On the other hand, the narrow electron energy distribution contradicts the power-law spectrum for the high-energy region. We consider an evolution of the electron energy distribution to solve this problem. The turbulence and magnetic field induced by a certain hydrodynamical instability gradually decay. According to this evolution, the typical synchrotron photon energy also decreases with time. The time-integrated spectrum forms the power-law shape for the high-energy region. We discuss the required evolutions of the turbulence and magnetic field to produce a typical spectral shape.

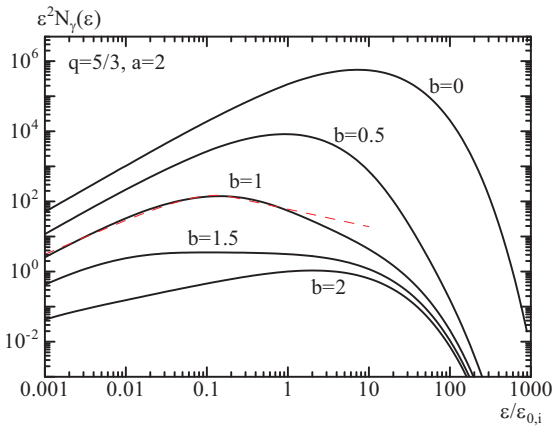


Fig. 28. Gamma-ray burst model spectra based on the evolving turbulence acceleration. While the results depend on the evolution parameters a and b of the turbulence, several reasonable parameter sets agree with the typical spectral shape (red dashed line).

Research topics: 2. Spectra of Giant Radio Pulses from the Crab Pulsar

Pulsar radio emission cannot be explained by a simple sum of emission from accelerated particles in the pulsar magnetosphere, and may be attributed to a coherent process such as the bunching mechanism of plasma or maser process. Many theoretical models have been proposed, but the question how the radio emission is produced has not been solved yet. From several pulsars, sporadic intense radio pulses that are much brighter than the normal pulse flux, called giant radio pulses (GRPs) are observed.

Radio observation of GRPs from the Crab pulsar has been our major subject since the birth of our group in 2009. Our group has developed the analysis method of the large set of the radio data to probe the unknown mechanism of the radio emission in close collaboration with radio astronomers in Japan. Based on a campaign of multi-frequency observations of the Crab pulsar from P (325MHz) to X (8GHz) bands, we study the broadband GRP spectrum. In our observation, 3194 and 272 GRPs occurring at the main pulse and the interpulse phases, respectively are detected. A few GRPs detected at both 0.3 and 8.4 GHz are the most wide-band samples ever reported (see Figure 29).

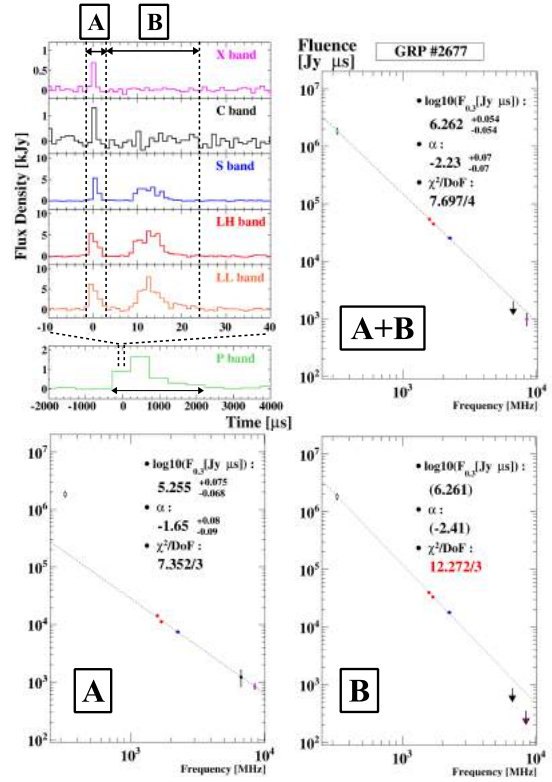


Fig. 29. The spectra of the Crab giant radio pulse (upper-right) #2677, which occurred at 01:32:49-51 UTC on September 7, 2014. The spectra for time intervals A and B defined in the upper-left light curve are shown in the bottom panels. The data point at P band is excluded for the fits for the time intervals A and B, respectively.

We dedispersed the data in each band, and calibrated the fluence by reference sources such as Cas A, Cyg A, and so on. In the frequency range from 0.3 to 2.2 GHz, we find that about 70% or more of the GRP spectra are consistent with single power-laws and the spectral indices of them are distributed from -4 to -1 , while the previous studies claimed that GRP spectra tend to show bended shape at 0.6–2.2 GHz. We also find that a significant number of GRPs have so hard spectral index (~ -1) that the fluence at 0.3 GHz is below the detection limit (“dim-hard” GRPs). Stacking light curves of such dim-hard GRPs at 0.3 GHz, we detect consistent enhancement compared to the off-GRP light curve. Our samples show correlations between the fluences and the spectral hardness, which indicates that more energetic GRPs tend to show softer spectra. In order to probe the intrinsic distributions of the fluences and indices, we simulate multi-frequency observations of single power-law GRPs with the Monte Carlo method. Our simulations succeed in reproducing the observed properties, and show that the typical spectral index of GRPs is as hard as -1 , differently from the previous studies.

Our comprehensive studies on the GRP spectra are summarised and will be published in 2016. Those are useful materials to verify the GRP model of another sporadic phenomenon, fast radio burst, which is extragalactic radio transient with a few millisecond duration.

Research topics: 3. Radial profile of the radio– γ emission in pulsar wind nebulae

Pulsar wind Nebulae (PWNe) are extended sources around a rotation powered pulsar. They show a very broad band spectrum from radio to gamma-rays and imply the existence of very high energy non-thermal electrons and positrons. The central pulsar releases its rotational energy as the pulsar wind, which is a highly relativistic magnetic and particle outflow, and plays a role of the energy source of the PWN. The strong termination shock, which is formed by the interaction between the pulsar wind and outer supernova remnant (or interstellar medium), has been supposed to produce the non-thermal electrons and positrons, and then they emit the synchrotron and inverse Compton radiation. Based on this picture, Kennel & Coroniti (1984, hereafter KC84) constructed a steady-state and 1D magnetohydrodynamic model of PWNe. However, the KC84 model disagrees with the observed radial profile of the X-ray spectral index in 3C 58. The X-ray spectral index profile in the model is much softer, and the X-ray nebula size becomes more compact than the observations.

We revisit the spherical steady outflow model of pulsar wind nebulae, motivated by the discrepancy in the spatial extents in X-ray observations. The volume-integrated photon spectrum and its radial profile are simultaneously discussed. The parameter dependence, especially on the shock radius and magnetization parameter, for the photon spectrum (see Figure 30) and surface brightness profile is complicated. To enlarge the X-ray size of the nebula as large as observed, a smaller magnetization or larger shock radius is preferable. We apply the model to the sources 3C 58 and G21.5-0.9, but the constraint from the photon spectrum leads to a smaller size of the X-ray nebula than observed. However, the discrepancy is not as prominent as the previous studies. If we can neglect the radio/optical component, whose origin may be different from the pulsar wind material, there are parameter sets that can reproduce both the spectrum and X-ray profile. However, those models imply very short advection time compared to the PWN age. Our detailed discussion clarifies the limit of application of the spherical steady outflow model, and provide clues to its improvement.

Research topics: 4. Time and Space Dependent Stochastic Acceleration Model for the Fermi Bubbles

This year we have published the study on the Fermi bubbles (FBs), which are gamma-ray structure of bilobal giant bubbles extending above and below the Galactic disk. There the microwave bubbles also exist in the same region, so-called the WMAP haze. These huge structures may suggest past large-scaled activities in the Galactic Center, such as active galactic nucleus jet activity or wind driven by supernovae. The gamma-ray spectra of the FBs are harder than the ambient diffuse spectrum of the Galactic halo, and the surface brightness profiles show a sharp rise at the bubble edges. The intensity inside the FBs is almost constant, which requires inhomogeneous gamma-ray emissivity inside the FBs. If the volume emissivity is constant, the surface brightness should show a bump-like profile with gradually rising edges as a result of the projection effect. On the other hand, a localized emissivity at the shock fronts should yield limb-brightened

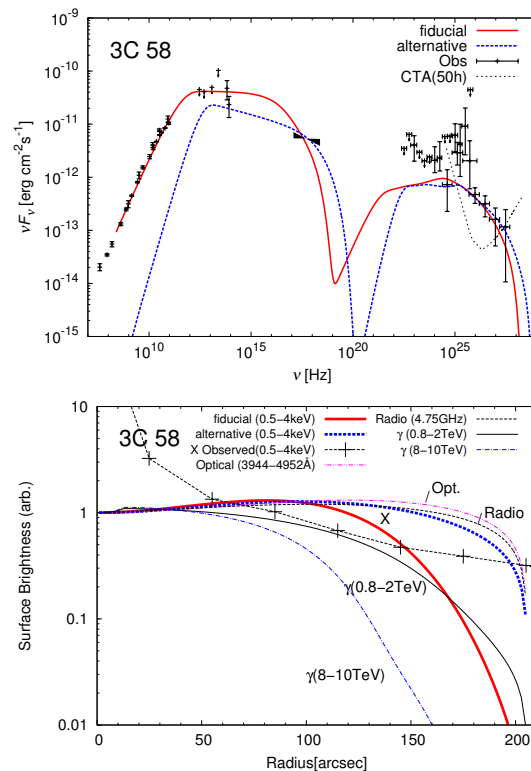


Fig. 30. Entire photon spectra (upper) and radial profiles of the surface brightness in various frequencies (lower) for pulsar wind nebula 3C 58. While the red solid lines represent the fiducial models, the blue dashed line represent the alternative models, in which the radio/IR data are disregarded.

profiles. Significantly thick shells are therefore preferable for the emission regions.

The short cooling timescale for electrons requires continuous acceleration in the downstream to secure a large volume of the emission region. We test the stochastic acceleration model for the FBs focusing on the effects of the time-dependence and escape from the acceleration regions. Turbulence is excited just behind the shock front via Kelvin–Helmholtz, Rayleigh–Taylor, or Richtmyer–Meshkov instabilities, and plasma particles are continuously accelerated by the interaction with the turbulence. The turbulence gradually decays as it goes away from the shock fronts. Adopting a phenomenological model for the stochastic acceleration, we explicitly solve the temporal evolution of the particle energy distribution in the turbulence. Our results show that the spatial distribution of high-energy particles is different from those for a steady solution, which was assumed in the previous studies. We also show that the contribution of electrons that escaped from the acceleration regions significantly softens the photon spectrum. The photon spectrum and surface brightness profile are reproduced by our models (see Figure 31). If the escape efficiency is very high, the radio flux from the escaped low-energy electrons can be comparable to that of the WMAP haze. We also demonstrate hadronic models with the stochastic acceleration, but they are unlikely in the viewpoint of the energy budget.

Research topics: 5. Photon cooling by induced Compton

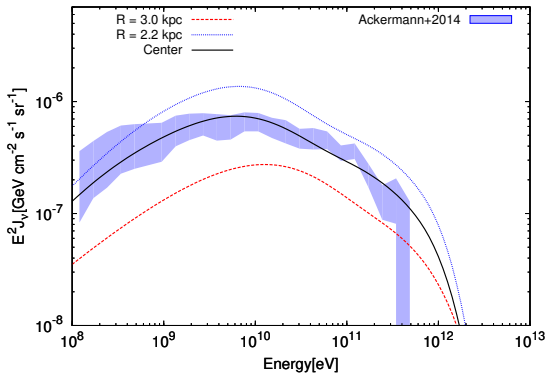


Fig. 31. Gamma-ray photon spectra of the Fermi bubbles in our model.

scattering

Our study on the induced Compton scattering (ICS) is published this year. ICS is an interaction between intense electromagnetic radiation and plasmas, where ICS transfers the energy from photons to plasma. Although ICS is important for laser plasma interactions in laboratory experiments and for radio emission from pulsars propagating in pulsar wind plasmas, the detail of the photon cooling process has not been understood. The problem is that, when ICS dominates, the evolution of photon spectra is described as a nonlinear convection equation, which makes the photon spectra multi-valued. We propose a new approach to treat the evolution of photon spectra affected by ICS. Starting from the higher-order Kompaneets equation, we find a new equation that resolves the unphysical behavior of photon spectra. In addition, we find the steady-state analytic solution, which is linearly stable. We also successfully simulate the evolution of photon spectra without artificial viscosity. We find that photons rapidly lose their energy by ICS with continuously forming solitary structures in frequency space (see Figure 32). The solitary structures have the same logarithmic width characterized by an electron temperature. The energy transfer from photons to plasma is more effective for a broader spectrum of photons such as that expected in astrophysical situations.

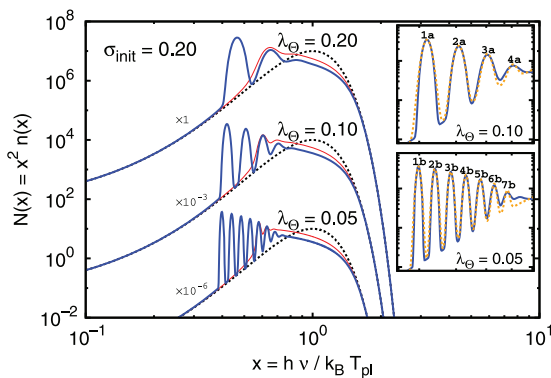


Fig. 32. The evolution of the photon spectra due to the photon cooling by induced Compton scattering.

Research topics: 6. CALET project

We have joined CALET, CALorimetric Electron Telescope, which is a mission for the Japanese Experiment Module-Exposed Facility (JEM-EF) on the International Space Station. The CALET mission aims at revealing unsolved problems in high energy phenomena of the Universe by carrying out accurate measurements of high energy spectra of electrons, gamma-rays and nuclei. HTV5 equipped with CALET was successfully launched by the H-IIB at 8:50:49 p.m. on August 19 2015 (JST) from the Tanegashima Space Center, and CALET is observing cosmic rays without apparent problems.

Major scientific objectives are to search nearby cosmic ray sources and dark matter signatures by carrying out accurate measurements of cosmic ray electrons in 1 GeV - 20 TeV and gamma-rays in 4 GeV - 10 TeV. Since proton background is very large, high proton rejection power is mandatory for high energy electron and gamma-ray measurements. CALET has an imaging and deep calorimeter with 30 radiation length for electromagnetic particles, which provides high proton rejection and excellent energy resolution.

Our team is successfully operating the observation. Some of our group joins to calibration task for one of the instruments on CALET, gamma-ray burst monitor (CGBM), which already detected several GRBs. The calibrated spectra of those GRBs will be published in near future. One of the most exciting events during the first year observation is the detection of the first gravitational-wave GW151226 by LIGO. The main instrument of CALET observes gamma-rays with a field of view of ~ 2 sr. The CGBM views ~ 3 sr and $\sim 2\pi$ sr of the sky in the 7 keV-1 MeV and the 40 keV-20 MeV bands, respectively, by using two different scintillator-based instruments. We set upper-limits of the gamma-ray fluxes for GW151226, which is significantly dimmer than usual short GRBs.

Bibliography

Papers in refereed journals

1. Kakuwa, J., Toma, K., Asano, K., Kusunose, M., & Takahara, F. "Synchrotron Self-Compton Emission by Relativistic Electrons under Stochastic Acceleration: Application to Mrk 421 and Mrk 501", *Mon. Not. R. Astron. Soc.*, 449, 551-558 (2015).
2. Tanaka, S. J., Asano, K., & Terasawa, T. "Avalanche Photon Cooling by Induced Compton Scattering: Higher-Order Kompaneets Equation", *Prog. Theor. Exp. Phys.*, 2015, 073E01(14pp) (2015).
3. Asano, K., & Hayashida, M. "The Most Intensive Gamma-Ray Flare of Quasar 3C 279 with the Second-Order Fermi Acceleration", *Astrophys. J.*, 808, L18(5pp) (2015).
4. Asano, K., & Murase, K. "Gamma-Ray Bursts as Multi-energy Neutrino Sources", *Adv. Astron.*, 2015, 568516(10pp) (2015).
5. Adams Jr. J. H., et al. "Special Issue on the JEM-EUSO Mission", *Exp. Astron.*, 40, 3-326 (2015).
6. Asano, K., & Terasawa, T. "Stochastic Acceleration Model of Gamma-Ray Burst with Decaying Turbulence", *Mon. Not. R. Astron. Soc.*, 454, 2242-2248 (2015).

7. Sasaki, K., Asano, K., & Terasawa, T. “Time-Dependent Stochastic Acceleration Model for the Fermi Bubbles”, *Astrophys. J.*, 814, 93(9pp) (2015).

Thesis

8. Mikami, R., “Simultaneous multi-wavelength observation of giant radio pulses from the Crab pulsar”, Doctor thesis, Department of Physics, University of Tokyo, March 2016.
9. Ishizaki, W., “Spatial Profile of the Emission from Pulsar Wind Nebulae”, Master thesis (in Japanese), Department of Physics, University of Tokyo, March 2016.
10. Hiroshima, N., “Time Variability Analysis of the Crab Nebula Based on Giant Radio Pulse Observations”, Master thesis (in Japanese), Department of Physics, University of Tokyo, March 2016.

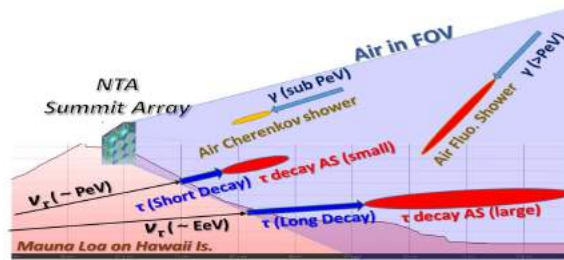


Fig. 33. Imaging ν_τ and γ air-showers.



Fig. 34. Ashra-1 light collector (left), photo-electric lens imaging tube fabricated in 2016 (center) and photoelectric image pipeline (right).

Other Activities

Ashra NTA

[Spokesperson: Makoto Sasaki]

ICRR, Univ. of Tokyo, Kashiwa, Chiba 277-8582

Pevatron Identification with PeV ν s and γ s

IceCube reported the detection of PeV scale astrophysical neutrinos (ν s). The origin (Pevatron) has not been revealed yet [1]. ν production is closely related to that of gamma-rays (γ s) in reactions: $p + \gamma \rightarrow \Delta^+ \rightarrow \pi^0 + p$, $\pi^+ + n$; $p + \text{nucleus} \rightarrow \pi^{\pm,0} + X$. Independently, HESS also reported deep γ observations with arcminute angular resolution of the region surrounding the supermassive black hole Sgr A* at the Galactic Center [2]. The observation of the hard power-law γ spectra indicates a candidate of Pevatron. Combined detection of PeV ν s and γ s from an accelerator provides indispensable identification of the location and the physics mechanism. Such a “multi-particle” paradigm [6] can be performed uniquely by NTA with a single detector system [7]. The photopion ($p\gamma$) reaction is typically the main ν generation process. Extragalactic sources like jets and cores of active galactic nuclei (AGN) [3] and γ -ray burst (GRB) jets [4] have been widely studied. Galactic sources like starburst galaxies (SBGs) and hypernovae may emit ν flux mainly through the hadronuclear (pp) reaction [5].

Imaging ν_τ and γ Air-showers

The Earth-skimming tau ν (ES- ν_τ) technique [8] enjoys a large target mass by detecting air-showers (ASs) produced by τ decays in the air. The τ s, produced by ν_τ s that interact with the Earth matter, traverse, and emerge out of a mountain or the ground decaying and generating ASs. This method has a good detection sensitivity for ν s originating from hadron acceleration in astronomical objects in the PeV-EeV region. Additional advantages are perfect shielding of cosmic ray secondaries, precise arrival direction determination, and negligible

background from atmospheric ν s [9]. The Ashra detector can efficiently image AS Cherenkov (CE) and fluorescence (FL) light generated from ES- ν_τ and γ ASs in the effective volume of air in the field of view (FOV) (Figure 33). The unique point is the resolution better than 0.1° yielding strong hadron rejection as selecting γ s both with FL and CE light.

From Ashra-1 to Ashra NTA

Ashra Phase I (Ashra-1) [10] was developed with very high resolution CE and FL light images of ν_τ and γ ASs for “multi-particle” astronomy [6]. The Ashra-1 light collector (LC) as the detector unit (Figure 34) achieves the total resolution of ~ 3 arcminutes covering 42° FOV. The key feature is the use of electrostatic rather than optical lenses to generate convergent beams with the 20 inch Photoelectric Lens Imaging tube (PLI) [11] (Figure 34) which is the world’s largest image intensifier, demagnifying to 1 inch at focal surface, enabling high resolution over a wide FOV [12]. The following trigger readout Photoelectric Image Pipeline (PIP) [13] can image and read out three independent phenomena on different time scales, i.e. AS CE emission (ns), AS FL (μ s), and starlight (s), without sacrificing the S/N ratios. The demonstration phase has been operated since 2008 at the Mauna Loa Observation Site at 3300 m asl. on Hawaii Island. With alert for GRB081203A given by SWIFT satellite, Ashra-1 succeeded in the first search for PeV-EeV ν_τ s originating from a GRB [14] with the ES- ν_τ technique setting stringent fluence limits. Based on Ashra-1 performance, we have planned a new extension, i.g. Ashra Neutrino Telescope Array (NTA), which is an AS imaging ν and γ observation system for the aim/scientific goal [7]: *Clear Discovery and Identification of Nonthermal Hadronic Processes in the Universe, be it Galactic, Extragalactic, or Cosmogenic*. A Letter of Intent for NTA published in 2013 [7]. In 2014, a preliminary workshop (VHEPA2014) was held at Kashiwa campus of the University of Tokyo to discuss the design of the project and plans with interested colleagues. After a workshop in Taipei and an informal meeting to discuss post-IceCube new detector project at the 34th International Cosmic Ray Conference in The Hague in 2015, we held a workshop as VHEPA2016 at University

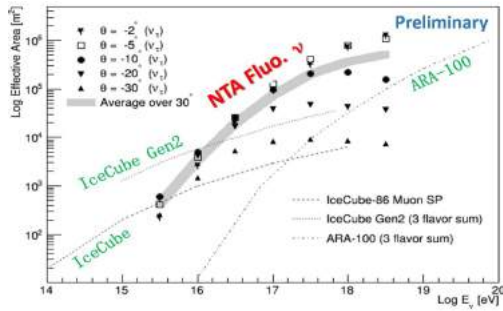


Fig. 35. Effective area for ES- ν_τ s as changing the energies with NTA in comparison with those for all flavor ν s with IceCube, IceCube Gen2, and ARA.

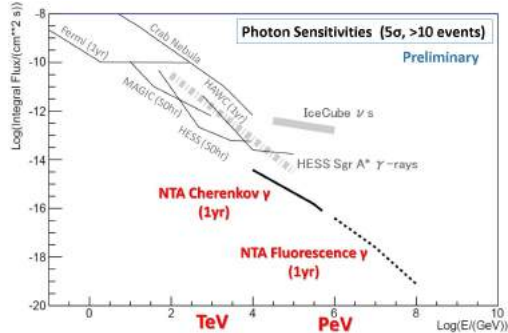


Fig. 36. Integral flux sensitivity limits (5σ or more than 10 events) for γ s versus the energies with NTA (1yr observation) and other detectors.

of Hawaii Manoa in January, 2016 to discuss more detailed physics and NTA potential performance, funding requests in each country. We have set up an International Promotion Working Group (IPWG), for reconfirming the basic design of NTA after discussions, editing and publishing White Paper in 2016 and Technical Design Report early in 2017. From the detailed studies with three stages for the simulation: (1) $\nu_\tau \rightarrow \tau$ conversion in the earth; (2) τ shower development; (3) detector performance, we evaluate the reconstructed arrival direction of τ AS axes to be within 0.1° of the original direction of the PeV-scale ES- ν_τ s [7, 9]. We have optimized the layout of the NTA stations, mainly enhancing the detection sensitivity for ES- ν_τ s around 1 PeV where IceCube found the significance of astronomical ν s. Four NTA stations are to be deployed on Mauna Loa at 3000 - 3500 m asl (NTA Summit Array), watching the air volume surrounding Mauna Loa including the surface of Mauna Loa, the largest volcano, to efficiently detect CE and FL light generated from τ ASs with both short and long decay lengths and γ ASs (Figure 33). The accurate reconstruction of AS images with very fine resolution is a very powerful technique not only in the determination of point sources of PeV ν_τ s but also FL observation for γ ASs above PeV with the large effective area (Figure 33). Figure 35 shows effective detection areas for FL ASs induced by ES- ν_τ s on average over the different elevation angles of the arrival direction between 0° and -30° , compared with those for all flavor ν s with IceCube, IceCube Gen2, and ARA. NTA achieves the effective area similar with that of IceCube at 3 PeV and 10-100 times larger than it above 30 PeV. The sensitivity for ES- ν_τ s with observing CE light is under study, which may enhance more the discovery potential around PeV or lower energy region. Figure 36 shows the integral flux sensitivity limits for γ s with NTA for one year observation i.e.

700 hours exposure time comparing with those of other detectors. The power of NTA is to survey ν_τ source objects with the best-yet sensitivity in the detection solid angle for ν_τ s defined as $-30^\circ < \theta_{\text{elev}} < 0^\circ$ and $0^\circ < \phi_{\text{azi}} < 360^\circ$, and for $3 \text{ PeV} < E_{\nu_\tau} < 30 \text{ EeV}$. In the case of γ s, NTA will survey AS CE (FL) light induced by γ s of which arrival direction angle below 30 degree in elevation angle (in all half-sky) for the energies between 10 TeV (1 PeV) and several 100 TeV (100 PeV). The unique combination among CE and FL observations for both ES- ν_τ s and γ with NTA will truly identify Pevatron(s) and open up new types of search for γ in wide energy range, e.g. γ s beyond the cutoff around PeV due to the cosmic photon background, break of Lorentz invariance, indications of extra dimension, and so on.

Bibliography

- [1] M. Aartsen *et al.*, PRL **113**, 101101 (2014).
- [2] HESS Collaboration, Nature **531**, 476 (2016).
- [3] W. Essey *et al.*, PRL **104** 141102 (2010).
- [4] K. Murase and K. Ioka, PRL **111** 121102 (2013).
- [5] A. Loeb and E. Waxman, J. Cosm. Astropart. Phys. **5**, 3 (2006).
- [6] M. Sasaki, ICRR2000 Sat. Sympo., 109 (2000).
- [7] M. Sasaki and G. Hou, arXiv:1408.6244 (2014).
- [8] M. Sasaki, *et al.*, Astropart. Phys. **19**, 37 (2003).
- [9] Y. Asaoka and M. Sasaki, Astropart. Phys. **41**, 7 (2013).
- [10] M. Sasaki, Prog. Theo. Phys. Suppl. **151**, 192 (2003).
- [11] Y. Asaoka and M. Sasaki, NIMA **647**, 34 (2011).
- [12] M. Sasaki, *et al.*, NIMA **492**, 49 (2002).
- [13] M. Sasaki *et al.*, NIMA **501**, 359 (2003).
- [14] Y. Aita *et al.*, ApJ Lett. **736**, L12 (2011).

γ I Project

γ I Consortium

[Spokesperson : R.Enomoto]

Collaboration list:

Institute for Cosmic Ray Research, The University of Tokyo, Chiba, Japan; Ibaraki University, Ibaraki, Japan; Faculty of Medical Engineering and Technology, Kitasato University, Kanagawa, Japan; National Cancer Center, East, Chiba, Japan; Fuji Electric Co, Tokyo, Japan;

γ I Project

γ I is a gamma-ray imager for especially sub-MeV gamma-rays.

This device uses Compton scatterings in order to identify the gamma-ray's incident direction (i.e., "Compton Camera"). Last year we had developed a low-cost-high-sensitivity camera whose field of view (FOV) was $1\text{sr}(\text{forward}) + 1\text{sr}(\text{backward})$ [1].

This year, we have developed wider FOV cameras, such as panorama, and/or all-sky view. The previous detector had 8 CsI(Tl) counters (3.5cm cube) as the first layer and 8 more as the second layer, each layer was separated 40cm. The new detector has 4 plus 2 counters, separated in 10cm. The configuration, however, is different, the counters in the first layer are located on the horizontal half-circle with radius of 10cm, with a separation angle of 45 degrees. Those in the second layer are located at the horizontal center of circle, separated $\pm 4\text{cm}$ vertically as shown in Fig.37 (left). This detector has

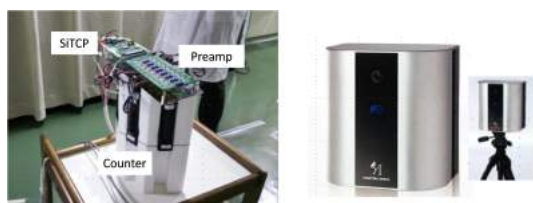


Fig. 37. A photograph of prototype (left) and "γI evolution", Fuji Electric Co (right).



Fig. 38. The result of the fieldwork at Fukushima.

a good uniformity in the all horizontal directions with vertical FOV within ± 30 degree. This detector is going to be produced by Fuji Electric Co. as "γI evolution". Its photograph is shown in Fig.37 (right). "γI evolution" has twice larger sensitivity compared to "old type (8x8)", due to the shorter counter separation of 10cm, however, the angular resolution is 14 degree (enough for many usages) while that of 8x8 was 3.5 degree. As shown in Fig.37 (right), the detector became compact, lighter and now we can put it on a tripod.

A fieldwork was carried out in Fukushima and the results are shown in Fig.38. The "hot" areas where the dose-rates are greater than $0.23 \mu\text{Sv/h}$ are shown in red. The numbers in the figure are the dose-rate ($\mu\text{Sv/h}$) measured by the NaI(Tl) surveymeter. The panorama view of gamma-ray image is obtained just only in-one-shot. With an improvement of the software, the FOV was improved from panorama to all-sky within 20% [2].

The other usage of this detector is introduced as follows. Fig.39 is a shot in a Hospital. The National Cancer Center, East Hospital has a facility of PET, i.e., positron emission tomography. A PET judges whether a tumor is malignant or benign. The radio isotope of ^{18}F made by a cycrotron with $^{18}\text{O}(n,p)^{18}\text{F}$ reaction was replaced with one of "OH" of glucose in the "so-called HOT-CELL" in the figure. The image indicates leaks of gamma rays from the "HOT-CELL". The gamma ray energy is 511 keV, which is an annihilation gamma ray of positron.

Those results opened new applications in many places. We are aiming at those applications and also measurements at Universe of anti-

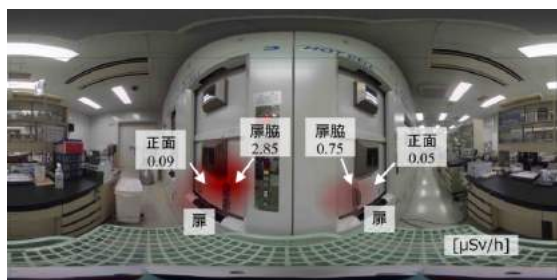


Fig. 39. Result at National Cancer Center.

matter using this technology. The summary of panorama and all-sky monitor will be submitted for publication soon[2].

Bibliography

- [1] M.Kagaya et al., Nucl. Instrum. Meth., A804 (2015) 25-32.
- [2] T.Watanabe et al., to be submitted to Nucl. Instrum. Meth. A.

ASTROPHYSICS AND GRAVITY DIVISION

Overview

Astrophysics and Gravity Division consists of Gravitational Wave Group, The Observational Cosmology Group, Primary Cosmic Ray Group and Theory Group.

The Gravitational Wave Group conducts experimental research of gravitational wave with researchers of gravitational wave experiment and theory in Japan. The main items are the construction of the large scale cryogenic interferometer(KAGRA) at Kamioka underground and the operation of CLIO. For this purpose, Gravitational Wave Project Office (GWPO) was established at the beginning of the fiscal year of 2011 to assist the construction of KAGRA gravitational wave telescope. The main office is located at Kamioka since 2014.

The Observational Cosmology Group studies the cosmic history based on deep multi-wavelength observations in collaboration with worldwide researchers. This group has started a new optical deep survey project with the wide-field imager of Hyper Suprime-Cam mounted on the Subaru telescope.

Theory Group conducts both theoretical study of the Universe and astroparticle physics.

Gravitational Wave Group

KAGRA Project Status

[Spokesperson : Seiji KAWAMURA]

ICRR, The Univ. of Tokyo, Hida, Gifu 506-1205

Overview including commissioning and iKAGRA run

KAGRA, Large-scale Cryogenic Gravitational wave Telescope, aims at detecting gravitational waves and developing gravitational wave astronomy, which was established by the recent first detection of gravitational waves by LIGO. KAGRA employs a 3 km L-shaped laser interferometer with a cryogenic mirror system placed underground at Kamioka. The KAGRA development is divided into two stages: the initial KAGRA (iKAGRA) and baseline KAGRA (bKAGRA). The iKAGRA detector is a simple Michelson interferometer with a 2-Watt laser, room-temperature mirrors, and a simple seismic isolation system. We completed the iKAGRA detector with a test run in March 2016. Then we proceed to bKAGRA. The bKAGRA detector will employ a Resonant Sideband Extraction (RSE) interferometer with 180-Watt laser, cryogenic Sapphire mirrors, and an advanced Seismic Attenuation System (SAS). The bKAGRA detector should attain the sensitivity high enough for the detection of gravitational waves with the help of the high power laser and RSE interferometer to reduce the quantum noise, the cryogenic Sapphire mirrors to reduce the thermal noise, and the SAS to reduce the seismic noise. We plan to operate the cryogenic 3 km Michelson interferometer by the end of March 2018, and then install other necessary bKAGRA subsystems to attain the target sensitivity.

Figure 1 shows the estimated ultimate sensitivity limits of KAGRA, where incoherent sum of the fundamental noise sources is assumed. The observation range for an inspiral and merger of neutron star binary with the ultimate sensitivity limit of KAGRA is about

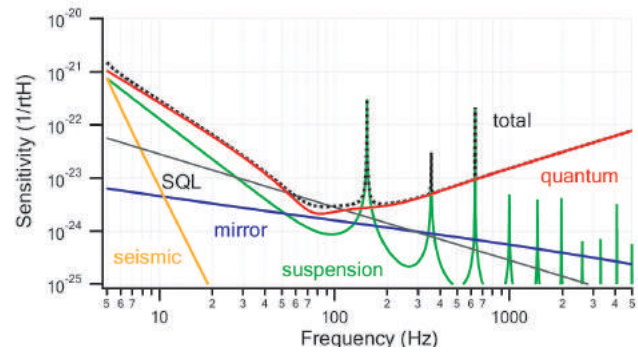


Fig. 1. Ultimate sensitivity limit of KAGRA.

173Mpc with the same definition of the observation range as LIGO and Virgo.

In FY 2015 we installed many subsystems necessary for iKAGRA, including the connecting beam tubes, gate valves, input mode cleaner, input mode-matching telescope, power recycling folding mirrors, beam splitter, two end mirrors, suspension systems, other optics, optical levers, beam dumpers, analog electronics, digital control system, etc. Then we successfully locked the input mode cleaner, aligned the 3 km Michelson interferometer, and locked the interferometer.

Then we performed a test run between Mar. 25 and Mar. 31, 2016. (The second test run was conducted in April 2016, but it will be reported in the annual report next year.) The input power to the beam splitter was 220 mW. The duty factor of the Michelson interferometer was 85.2 %, and that of the input mode cleaner was 94.4 %. The total lock time was 129.5 hours, and the longest lock was 3.6 hours. The typical strain sensitivity of the detector was $3 \times 10^{-15} \text{ Hz}^{-1/2}$ at 100 Hz, which corresponds to a neutron star binary inspiral range of 0.77 pc.

The interferometer was locked to the mid-fringe with a unity gain frequency of 8 Hz. All the suspended mirrors were controlled with the optical lever systems. The finesse and mode matching ratio of the pre-mode cleaner was 197 and 75 %, respectively. The finesse and mode matching ratio of the input mode cleaner was 540 and 86.2 %, respectively. The input mode cleaner mirrors, beam splitter, and end mirrors had Type-C suspension systems, while the power recycling folding mirror 3 had a Type-Bp' suspension system. The beam splitter, end mirrors, and power recycling folding mirror 3 were not in the vacuum because of insufficient commissioning time. The 80 Hz and 135 Hz monochromatic signals were applied to the control loop for the calibration of the interferometer. The interferometer lock was lost mainly because of the tidal drift of the mirrors. The noise spectrum was fluctuated by one order of magnitude. The sensitivity was limited mainly by intensity noise of laser light above 100 Hz.

The scimon shift we took during the test run was the following. Each day was divided into three shift: 1:00 to 9:00, 9:00 to 17:00, and 17:00 to 1:00. In each shift slot one expert from ICRR, NAOJ, and KEK and two researchers from other universities/institutes were allocated. These scimons registered what happened as well as unusual events that they noticed during the shift. The scimon shift worked pretty smoothly.



Fig. 2. Entrance of the KAGRA tunnel.



Fig. 4. Cryostat for the cryogenic mirror and the shaft for the vibration isolation system.



Fig. 3. Vacuum chambers in the central area.



Fig. 5. Slope to the 2nd floor.

All the data that was taken during the test run was stored and transferred to ICRR Kashiwa and Osaka City University in real time. The delayed mirroring of raw data was performed by Academia Sinica, Taiwan. KISTI, Korea was also copying the data. The transfer time from the KAGRA site to surface, ICRR Kashiwa, and Osaka City University was 0.3 sec, 2.5 sec, and 3 sec, respectively. The data management system worked very well.

The photos of KAGRA taken in FY 2015 are shown (Fig. 2 - Fig. 9).

We also enhanced the international collaborations with the Einstein Telescope (ET) project, LIGO, Virgo, Korean and other Asian groups mainly based on the JSPS core-to-core program.

The rapidly progressing status of KAGRA were presented in many international conferences. Many papers about the progress of KAGRA were also published [1], [2], [3], [4], [5], [6], [7], [8], [9], [10], [11]. We also presented activities on our web-page.[12]

Bibliography

- [1] "Gravitational waves: Classification, methods of detection, sensitivities and sources", Kazuaki Kuroda, Wei-Tou Ni and Wei-Ping Pan, *Int. J. Mod. Phys. D* **24**, 1530031 (2015)
- [2] "Ground-based Gravitational-wave detectors", Kazuaki Kuroda, *Int. J. Mod. Phys. D* **24**, 1530032 (2015)
- [3] "Realistic loss estimation due to mirror surfaces in a 10 meters-long high finesse Fabry-Perot filter-cavity", Nicolas Straniero, Jerome Degallaix, Raffaele Flaminio, Laurent Pinard, and Gianpietro Cagnoli, *Opt. Express* **23**, 21455 (2015)
- [4] "Gravitational wave astronomy: the current status", David Blair, Li Ju, ChunNong Zhao, LinQing Wen, Qi Chu, Qi Fang, RongGen Cai, JiangRui Gao, XueChun Lin, Dong Liu, Ling-An Wu, ZongHong Zhu, David H. Reitze, Koji Arai, Fan Zhang, Raffaele Flaminio, XingJiang Zhu, George Hobbs, Richard N. Manchester, Ryan M. Shannon, Carlo Baccigalupi, Wei Gao, Peng Xu, Xing Bian, ZhouJian Cao, ZiJing Chang, Peng Dong, XueFei Gong, and ShuangLin Huang, *Sci. China Phys. Mech. Astron.* **58**, 120402 (2015)
- [5] "5mg Suspended Mirror Driven by Measurement-Induced Backaction", N. Matsumoto, K. Komori, Y. Michimura, G. Hayase, Y. Aso and K. Tsubono, *Phys. Rev. A* **9**, 33825 (2015)
- [6] "Performance test of pipe-shaped radiation shields for cryogenic interferometric gravitational-wave detectors", Y. Sakaibara, N. Kimura, A. Akutsu, T. Suzuki and K. Kuroda, *Class. Quantum Grav.* **32**, 155011 (2015)
- [7] "An experiment to distinguish between diffusive and specular surfaces for thermal radiation in cryogenic gravitational-wave"



Fig. 6. 3-km beam tube in the Y-arm tunnel.

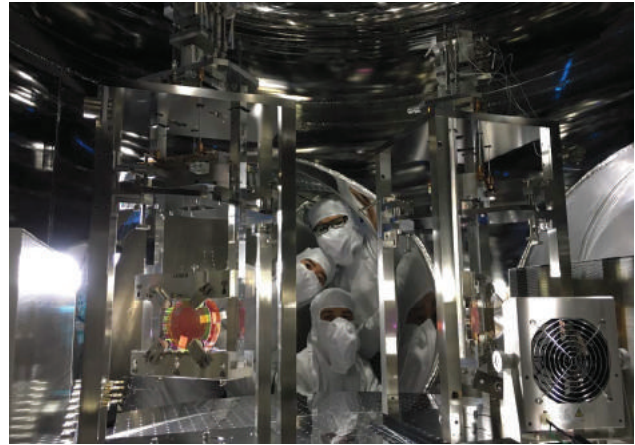


Fig. 8. Mirrors and suspension systems of the input mode cleaner.

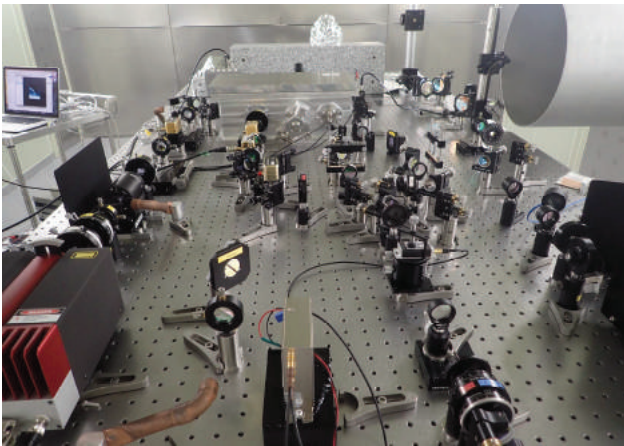


Fig. 7. Pre-stabilized laser for iKAGRA.

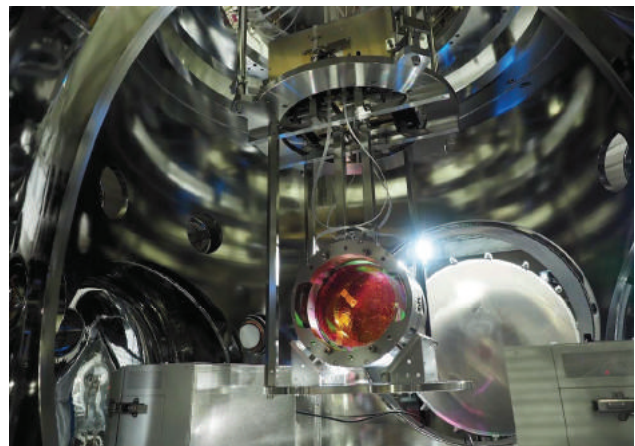


Fig. 9. Power recycling folding mirror and its suspension system.

- detectors”, Y. Sakaibara, N. Kimura, T. Suzuki, K. Yamamoto, C. Tokoku, T. Uchiyama and K. Kuroda, *Prog. Theor. Exp. Phys.*, 073F01 (2015)
- [8] ”The effect of crystal orientation on the cryogenic strength of hydroxide catalysis bonded sapphire”, K. Haughian, R. Douglas, A. A. van Veggel, J. Hough, A. Khalaidovski, S. Rowan, T. Suzuki and K. Yamamoto, *Class. Quantum Grav.* **32**, 75013 (2015)
- [9] ”Mechanical loss in state-of-the-art amorphous optical coatings”, Massimo Granata, Emeline Saracco, Nazario Morgado, Alix Cajgfinger, Gianpietro Cagnoli, Jerome Degallaix, Vincent Dolique, Daniele Forest, Janyce Franc, Christophe Michel, Laurent Pinard, and Raffaele Flaminio, *Rhys. Rev. D.* **93**, 12007 (2016)
- [10] ”Characterization of the room temperature payload prototype for the cryogenic interferometric gravitational wave detector KAGR”, Fabian Erasmo Pena Arellano, Takanori Sekiguchi, Yoshinori Fujii, Ryutarō Takahashi, Mark Barton, Naoatsu Hirata, Ayaka Shoda, Joris van Heijningen, Raffaele Flaminio, Riccardo DeSalvo, Koki Okutumi, Tomotada Akutsu, Yoichi Aso, Hideharu Ishizaki, Takashi Uchiyama, Osamu Miyakawa, Masahiro Kamiizumi, Akiteru Takamori, Ettore Majorana, Jo van den Brand, and Alessandro Bertolini, *Rev. Sci. Instrum.* **87**, 34501 (2016)

- [11] ”New method to measure the angular antispring effect in a Fabry-Perot cavity with remote excitation using radiation pressure”, Koji Nagano, Yutaro Enomoto, Masayuki Nakano, Akira Furusawa, and Seiji Kawamura, *Phys. Lett. A* **380**, 983 (2016)
- [12] <http://gwcenter.icrr.u-tokyo.ac.jp/en/>

Vacuum system for KAGRA

[Spokesperson : Takashi UCHIYAMA]

ICRR, The Univ. of Tokyo, Hida, Gifu 506-1205

The vacuum sub-group of the KAGRA project has been designed and fabricated two vacuum chambers those are the OMMT (Output Mode Matching Telescope) chamber and the OMC (Output Mode Cleaner) chamber in 2015. Both chambers have already placed in the KAGRA center experiment room. The OMMT chamber is made of SUS304 and dimensions are diameter of 1200 mm, height of 2500 mm, and weight of 1500 kg. The OMC chamber is made of SUS304 and dimensions are diameter of 1500 mm, height of 2500 mm, and weight of 2400 kg.

Cryogenic payload

[Spokesperson : Kazuhiro YAMAMOTO]

ICRR, The Univ. of Tokyo, Kashiwa, Chiba 277-8582

Outlines A key feature of KAGRA is the operation of the interferometer which consists of mirrors made from sapphire at cryogenic temperature. These mirrors are suspended by sapphire fibers (sapphire suspension). They are a part of cryogenic payloads which is functions to control mirror position and direction, for vibration isolation and so on.

The cryogenic payload is developed by ICRR and KEK. Here, the activities of members of ICRR in fiscal year 2015 are focused. Prototype of cryogenic payload was assembled at KEK and the properties were investigated. Based on this experiment, the design was revised and first cryogenic payload for KAGRA was delivered. As components of cryogenic payload, tilt adjustment system and sensors and actuators to control mirrors are being developed. Sapphire parts for two sapphire suspensions for KAGRA were delivered. We confirmed quality of delivered items has no serious problems. We are proceeding with preparing of assembly jig for prototype sapphire suspension under collaboration with INFN Perugia. Simpler one fiber prototype was constructed and we checked it can survive after 15 times thermal cycles. Coating mechanical loss is being measured to evaluate thermal noise of KAGRA. In the following, the details of these items and an international collaboration (ELiTES) are explained.

Cryogenic payload The cooled sapphire mirror is at the bottom of the cryogenic payload. This payload is in the radiation shield for cooling and suspended from the Type A vibration isolation system in vacuum but at room temperature. The cryocoolers and payload are connected by heat links made from pure aluminum for cooling. The payload is necessary to control the position and angle of the mirror (otherwise, the interference of the light can never be realized), and for the vibration isolation (especially, the vibration via heat links) and so on.

Prototype of cryogenic payload was manufactured (It must be note that a sapphire mirror and fibers are replaced by dummy ones made from metal in this prototype). A member of ICRR (Takahiro Miyamoto) and KEK collaborators assembled (Fig. 10) and tested prototype. Based on these lessons, we revised design drawing. First payload for KAGRA was delivered on the end of March 2016. Test of this payload is in progress.

Mirror angle adjustment systems and sensors to observe positions and angles of components of the cryogenic payload must work at cryogenic temperature. Takahiro Miyamoto is testing candidates as follows. The angle adjustment system which consists of motor and weight was developed. He measured dynamic range (adjustable maximum angle) at room temperature and it is enough large for our purpose (3 mrad). Combination of Light Emitting Diode and Photo Detector is a candidate as sensor for control. Efficiency of LED and PD at cryogenic temperature was measured. Although this combination works at low temperature, strong temperature dependence of efficiency was observed. We must investigate LED-PD sensor taking temperature dependence into account. Coil magnet actuators will be used to control mirror and other masses in cryogenic payload. The measured efficiency of coil magnet actuator was consistent with our expectation.

Sapphire lop-eared suspension The cooled mirror is suspended by four sapphire fibers. We call this system sapphire lop-eared suspension (Fig. 11). This sapphire suspension consists of a mirror, fibers with nail heads, ears for connection between fibers and a mirror, blade springs to compensate the length differences between four fibers. All of them are made from sapphire. Two joint techniques are

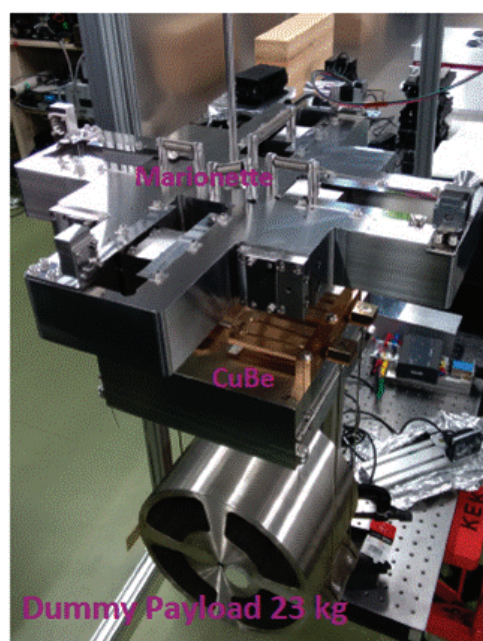


Fig. 10. Assembled prototype of KAGRA cryogenic payload

adopted. Between the ears and mirror, Hydroxide Catalysis Bonding is applied. This technique is also adopted in Advanced LIGO and Advanced Virgo. On the nail heads of the fibers, indium is applied for joint with the ear or blade spring. When fibers are broken, heat is applied to melt indium (melting point is 157 degree Celsius) and the broken fibers are removed. Our paper about indium bonding was published (G. Hofmann *et al.*, Classical and Quantum Gravity 32(2015)245013).

Now we proceed with procurement of sapphire parts except for mirrors. In fiscal year 2015, we purchase sapphire parts for two sapphire suspensions (Fig. 12). After procurement, we investigated quality of delivered products with support or cooperation of other institute. For example, in order to measure geometrical shape of sapphire ears and flatness of surface of ears for Hydroxide Catalysis Bonding, we asked Kazuhiro Enami (KEK) and Akitoshi Ueda (NAOJ), respectively. Fortunately, no serious problem was found. In fiscal year 2016, we order sapphire items for other two suspensions.

We proceed with investigation of prototype sapphire suspension. The sapphire parts for prototype suspension have already been prepared. We (especially, Kieran Craig) are preparing jig to assembly. Helios Vocca (INFN Perugia) joined KAGRA collaboration and supports development of assembly jig based on Advanced Virgo expertise.

We have manufactured simpler prototype, one fiber prototype (Fig. 13). Only one sapphire fiber suspends a sapphire mass whose weight is a quarter of that of a KAGRA mirror. We need not to take care of balance between fibers during assembly. The stress in suspension is comparable with that in actual sapphire suspension. As like actual suspension, Hydroxide Catalysis Bonding and indium bonding are adopted in this one fiber prototype. We (mainly, Hiroki Tanaka) conducted cooling test. So far, we repeated 15 thermal cycles and one fiber prototype survives.

Coating mechanical loss Thermal noise caused by mechanical loss of reflective coating is one of the fundamental sensitivity limits of interferometric gravitational wave detector. This is one of the

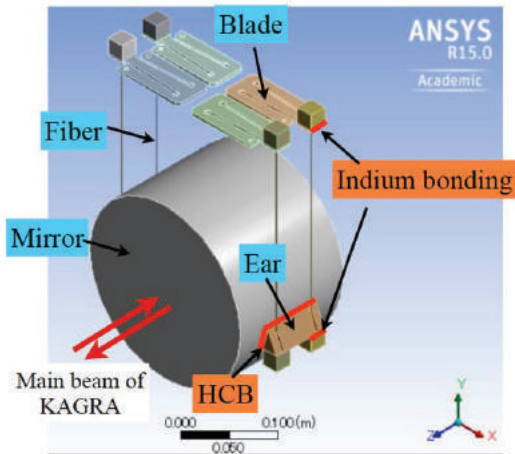


Fig. 11. KAGRA sapphire suspension



Fig. 12. Delivered sapphire fibers for KAGRA sapphire suspension

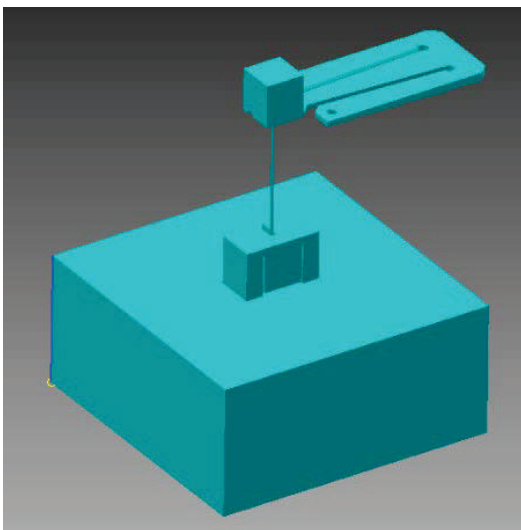


Fig. 13. One fiber prototype to investigate sapphire suspension

hottest topics in development of future gravitational wave detectors. In order to evaluate this thermal noise, mechanical loss must be measured (at cryogenic temperature in the case of KAGRA). Now we are investigating dissipation in coating by LMA Lyon which provides coating for Advanced LIGO and Virgo. We sent sapphire disks to LMA and they came back after coating procedure. Now the measurement is in progress with Junko Katayama and Kieran Craig.

ELiTES ELiTES (ET-LCGT interferometric Telescope Exchange of Scientists) is a European grant (European 7th Framework Programme Marie Curie action between Mar. 2012 and Feb. 2016) for the collaboration between KAGRA and Einstein Telescope (European future project). This grant supports people in Europe to visit Japan for KAGRA. In 2015, 8 visitors (from Germany, U.K., Italy, and France) stayed at ICRR. A part of them helped and supported cryogenic experiments for sapphire, reflective coating and so on. The period of ELiTES is extended (February 2017). One of the main results in fiscal year 2015 of ELiTES is our paper about indium bonding (G. Hofmann *et al.*, *Classical and Quantum Gravity* 32(2015)245013).

Master theses Two Master theses by Takahiro Miyamoto (*Development of cryo-payload for the gravitational wave telescope KAGRA*) and Hiroki Tanaka (*Study of thermal noise of sapphire suspension system for the gravitational wave telescope KAGRA*) were accepted.

Integrated DAQ/control system using real time computers and analog electronic

[Spokesperson : Osamu MIYAKAWA]

ICRR, The Univ. of Tokyo, Hida, Gifu 506-1205

A real time control system for the KAGRA interferometer started working in the mine. The system is being used for all of aspects in the installation, commissioning and observation.

After finishing the tunnel construction and the next following experimental setup in the mine, we installed 6 field racks in the laboratory area to control subsystems such as mode cleaner suspensions, input optics, vibration isolation systems for power recycling mirror, beamsplitter and both end mirrors. Each field rack consists of IO chassis with several ADC/DAC cards, anti alias/anti image filters, coil drivers, servo electronics and so on. We are trying to avoid noise of AC 60 Hz and computers from the laboratory area. DC power of +/-24 V for the IO chassis and +/-18 V for the circuits are provided from a 100 m away isolated frontal room through thick cables. IO chassis working as a front-end in the laboratory area are also connected through 100 m scale optical fiber cables to the computers in the isolated room.

Main control signals of Michelson interferometer of iKAGRA are fed-back to each end mirror differentially. Transmissions of controls signal to 3 km away of the end area have been realized by the Reflective Memory technology that is a very low latency network but only the small amount of data for the control can be transmitted. The control bandwidth has reached about 100 Hz during the observation.

This control system has another important function as a data acquisition system (DAQ). All the important data related to interferometer controls are stored into redundant data storages, typically with 16384 Hz, 2048 Hz and 16 Hz. Amount of data during the iKAGRA observation was about 150 GB/day. All the data were stored into local 20 TB×2 storages in the mine temporarily, then transmitted out to a 200 TB storage and moved to a 100 TB storage at Kashiwa campus. Many environmental signals are also stored through EPICS database. EPICS is a good signal database being developed in high

energy physics projects but the speed is limited around 64Hz. It is not enough fast as a real time control for the interferometer but good to record many slow status channels of the interferometer like switches, gains and so on. As a good example of use of EPICS in KAGRA, more than 20 of temperature and humidity sensors have been installed in many locations in the mine, and the data are being recorded through the EPICS database into the main storage. Additionally 10 or more CCD cameras and many pico motors have been setup and used through the EPICS interface.



Fig. 14. A remote control room in the outside building at Higashimozumi, Kamioka. Real time iKAGRA sensitivity is shown in the middle top large screen.

Human activities in the mine may be a cause of noise of the interferometer during observations, so almost of the functions of KAGRA can be remotely controlled. The remote control room (See Fig.14) at 7 km away from the center of KAGRA has been designed to control, monitor, and analyze KAGRA or data from KAGRA. The room worked pretty well as a good location to gather people and communicate each other during the commissioning and observation in order to operate KAGRA. All the fast and slow realtime/past data can be easily monitored and analyzed in the control room using many access tools like Dataviewer (digital oscilloscope), DTT (FFT tool), MEDM (EPICS graphical user interface) and StripTool (long term data recorder for EPICS signal). The tools can be seen on the monitors in Fig.14 with many kinds of graphs.

Basic functions of the control system has been tested through the iKAGRA commissioning and observation. It will be upgraded during the next two years toward bKAGRA.

Core Optics for KAGRA

[Spokesperson : Eiichi HIROSE]

ICRR, The Univ. of Tokyo, Kashiwa, Chiba, 277-8582

The mirror sub-group of the KAGRA project is in charge of core optics such as the test mass mirrors, the beamsplitter, the recycling cavity mirrors, the mode cleaner mirrors, and so on. We design and fabricate them to satisfy the interferometer's requirements, and some of the optics have been finished and installed with the suspension systems for the room-temperature pilot interferometer, iKAGRA. For the cryogenic-temperature interferometer, bKAGRA, we need four ultra-low loss sapphire test mass mirrors for two Fabry-Perot cavities in which only a power loss of 100 ppm, per round trip is allowed. In order to achieve it, figure error and micro roughness over 140 mm,

clear aperture need to be less than 0.5 nm, and 0.16 nm in RMS, respectively. We have demonstrated not only the above but also the other requirements are technologically satisfied doing both a test polish and a test coating. Currently, the real sapphire mirrors are being fabricated, and all the core optics are to be completed next year.

Observational Cosmology Group

[Spokesperson : Yoshiaki Ono]

ICRR, The Univ. of Tokyo, Kashiwa, Chiba 277-8582

Morphologies of $\sim 190,000$ Galaxies at $z = 0 - 10$ Revealed with HST Legacy Data I. Size Evolution [1]

We present the redshift evolution of the galaxy effective radius r_e obtained from the *Hubble Space Telescope* (HST) samples of $\sim 190,000$ galaxies at $z = 0 - 10$. Our HST samples consist of 176,152 photo- z galaxies at $z = 0 - 6$ from the 3D-HST+CANDELS catalog and 10,454 Lyman break galaxies (LBGs) at $z = 4 - 10$ identified in the CANDELS, HUDF09, HUDF12, and HFF parallel fields, providing the largest data set to date for galaxy size evolution studies. We derive r_e with the *same* technique over the wide redshift range of $z = 0 - 10$, evaluating the optical-to-UV morphological K correction and the selection bias of photo- z galaxies+LBGs as well as the cosmological surface brightness dimming effect. We find that r_e values at a given luminosity significantly decrease toward high z , regardless of statistics choices (e.g., $r_e \propto (1+z)^{-1.10 \pm 0.06}$ for median). For star-forming galaxies, there is no evolution of the power-law slope of the size-luminosity relation and the median Sérsic index ($n \sim 1.5$). Moreover, the r_e distribution is well represented by log-normal functions whose standard deviation $\sigma_{\ln r_e}$ does not show significant evolution within the range of $\sigma_{\ln r_e} \sim 0.45 - 0.75$. We calculate the stellar-to-halo size ratio from our r_e measurements and the dark-matter halo masses estimated from the abundance matching study, and obtain a nearly constant value of $r_e/r_{\text{vir}} = 1.0 - 3.5\%$ at $z = 0 - 8$. The combination of the r_e -distribution shape+standard deviation, the constant r_e/r_{vir} , and $n \sim 1.5$ suggests a picture in which typical high- z star-forming galaxies have disk-like stellar components in a sense of dynamics and morphology over cosmic time of $z \sim 0 - 6$. If high- z star-forming galaxies are truly dominated by disks, the r_e/r_{vir} value and the disk formation model indicate that the specific angular momentum of the disk normalized by the host halo is $j_d/m_d \simeq 0.5 - 1$. These are statistical results for major stellar components of galaxies, and the detailed study of clumpy sub-components is presented in the paper II.

Bibliography

- [1] Shibuya, T., Ouchi, M., & Harikane, Y. 2015, The Astrophysical Journal Supplement Series, 219, 15

ALMA Census of Faint 1.2 mm Sources Down to ~ 0.02 mJy: Extragalactic Background Light and Dust-Poor High- z Galaxies [2]

In collaboration with the members of National Astronomical Observatory of Japan.

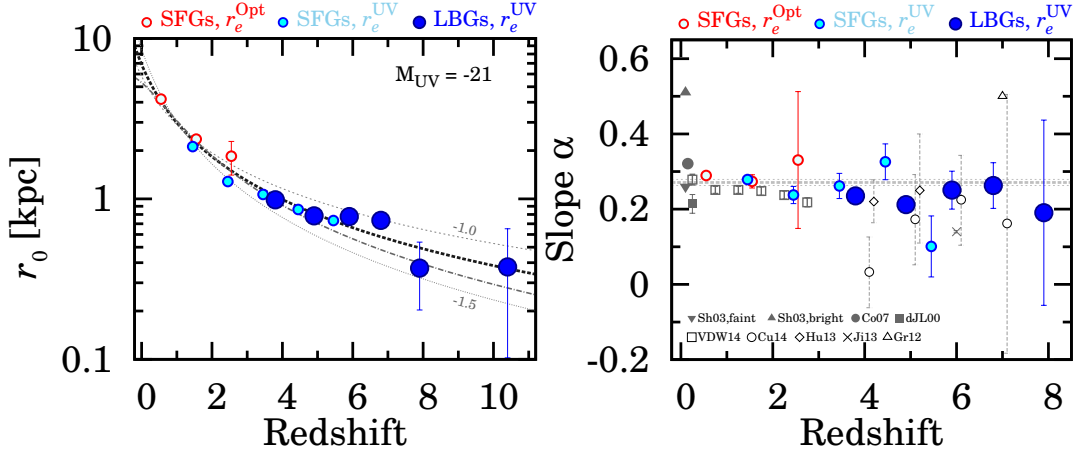


Fig. 15. Results of power-law fits for the r_e - M_{UV} relation. The red, cyan, and blue filled circles indicate estimates of r_0 and α based on r_e^{Opt} and r_e^{UV} for the star-forming galaxies (SFGs) and r_e^{UV} for the LBGs, respectively. (Left) Effective radius r_0 at $L_{\text{UV}} = 1 L_{z=3}^*$ corresponding to $M_{\text{UV}} = -21$. The thin dashed, dotted and thick dashed lines show the best-fit curves with $(1+z)^{-1}$, $(1+z)^{-1.5}$, and $(1+z)^{\beta_z}$, respectively. The dot-dashed line indicates the fit of $r_e \propto H(z)^{\beta_H}$. The best-fit β_z and β_H values are -1.20 ± 0.04 and -0.97 ± 0.04 , respectively. (Right) Slope α of $r_e \propto L_{\text{UV}}^\alpha$ as a function of redshift. The thick dashed and thin gray lines denote the weighted-average value with a 1σ error, $\alpha = 0.27 \pm 0.01$. The open symbols show α for the SFGs or the LBGs in the literature. The gray filled symbols represent the results for local spiral and/or disk galaxies. This figure is reproduced by permission of the AAS.

We present statistics of 133 faint 1.2 mm continuum sources detected in about 120 deep ALMA pointing data that include all the archival deep data available by 2015 June. We derive number counts of 1.2 mm continuum sources down to 0.02 mJy partly with the assistance of gravitational lensing, and find that the total integrated 1.2 mm flux of the securely identified sources is $22.9_{-5.6}^{+6.7}$ Jy deg^{-2} that corresponds to $104_{-25}^{+31}\%$ of the extragalactic background light (EBL) measured by COBE observations. These results suggest that the major 1.2 mm EBL contributors are sources with 0.02 mJy, and that very faint 1.2 mm sources with $\lesssim 0.02$ mJy contribute negligibly to the EBL with the possible flattening and/or truncation of number counts in this very faint flux regime. To understand the physical origin of our faint ALMA sources, we measure the galaxy bias b_g by the counts-in-cells technique, and place a stringent upper limit of $b_g < 3.5$ that is not similar to b_g values of massive distant red galaxies and submillimeter galaxies but comparable to those of UV-bright star-forming BzK galaxies (sBzKs) and Lyman break galaxies (LBGs). Moreover, in the optical and near-infrared (NIR) deep fields, we identify optical-NIR counterparts for 59% of our faint ALMA sources, the majority of which have luminosities, colors, and the IRX- β relation the same as sBzKs and LBGs. We thus conclude that about a half of our faint ALMA sources are dust-poor high- z galaxies as known as sBzKs and LBGs in optical studies, and that these faint ALMA sources are not miniature (U)LIRGs simply scaled down with the infrared brightness.

Bibliography

- [2] Fujimoto, S., Ouchi, M., Ono, Y., Shibuya, T., Ishigaki, M., Nagai, H., & Momose, R. 2016, The Astrophysical Journal Supplement Series, 222, 1

An extremely dense group of massive galaxies at the centre of the protocluster at $z = 3.09$ in the SSA22 field [3]

In collaboration with the members of Tohoku University, Ehime University, National Astronomical Observatory of Japan, and European Southern Observatory.

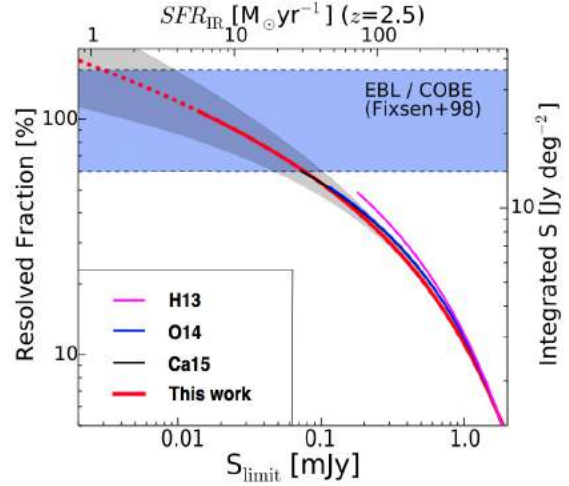


Fig. 16. Fraction of resolved EBL at 1.2 mm as a function of the detection limit, S_{limit} . The red line and the gray shade indicate the best estimate from our study and the associated errors, respectively. The magenta, blue, and black lines present the estimates from the previous ALMA studies. The blue shade denotes the IR EBL measurements from COBE. The right axis represents the absolute values of the integrated flux densities, $\int_{S_{\text{limit}}}^\infty S \phi(S) dS$, which correspond to the resolved EBL fraction. The top axis ticks IR star-formation rates SFR_{IR} corresponding to the 1.2 mm flux for the case that a source resides at $z = 2.5$. This figure is reproduced by permission of the AAS.

We report the discovery of an extremely dense group of massive galaxies at the center of the protocluster at $z = 3.09$ in the SSA22 field from near-infrared spectroscopy conducted with MOIRCS on the Subaru Telescope. The newly discovered group comprises seven galaxies confirmed at $z_{\text{spec}} \approx 3.09$ within 180 kpc, including five massive objects with the stellar masses larger than $10^{10.5} M_\odot$ and is associated with a bright submillimeter source SSA22-AzTEC14. The dynamical mass of the group estimated from the line-of-sight velocity dispersion of the members is $M_{\text{dyn}} \sim 1.6 \pm 0.3 \times 10^{13} M_\odot$. Such a dense group is expected to be very rare at high redshift, as

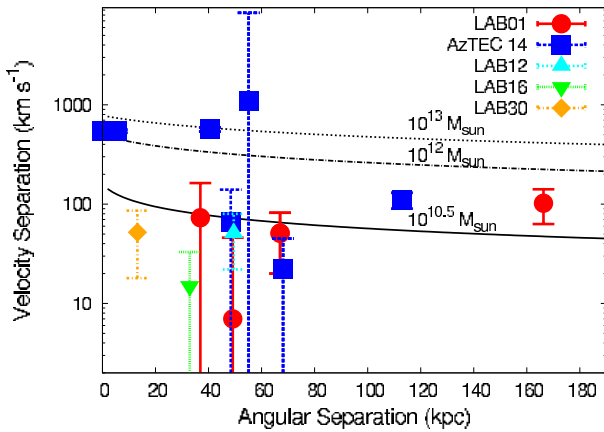


Fig. 17. Line-of-sight velocity and spatial distributions of the group members. The blue squares, the red circles, the cyan triangle, the green reversed triangle and the orange diamond show angular spatial separations and line-of-sight velocity offsets of the counterparts from the central counterparts of the AzTEC14 group, LAB01, LAB12, LAB16 and LAB30, respectively. The solid, dashed-dotted and dotted curves indicate the escape velocities from the objects with $M_{\text{halo}} = 10^{10.5}$, 10^{12} and $10^{13} M_{\odot}$, respectively, calculated assuming the Navarro-Frenk-White mass profile. We assume the concentration parameter $c = 5$ for the halo with $M_{\text{halo}} = 10^{13} M_{\odot}$, and $c = 4.5$ for the halos with $M_{\text{halo}} = 10^{10.5}$ and $10^{12} M_{\odot}$ predicted in the literature. This figure is reproduced by permission of the RAS.

we have found only a few comparable systems in large-volume cosmological simulations. Such rare groups in simulations are hosted in collapsed halos with $M_{\text{vir}} = 10^{13.4} - 10^{14.0} M_{\odot}$ and evolve into the brightest cluster galaxies (BCGs) of the most massive clusters at present. The observed AzTEC14 group at $z = 3.09$ is therefore very likely to be a proto-BCG in the multiple merger phase. The observed total stellar mass of the group is $5.8_{-2.0}^{+5.1} \times 10^{11} M_{\odot}$, which suggests that over half the stellar mass of its descendant had been formed by $z = 3$. Moreover, we have identified over two members for each of the four Ly α blobs (LABs) using our new spectroscopic data. This verifies our previous argument that many of the LABs in the SSA22 protocluster associated with multiple developed stellar components.

Bibliography

- [3] Kubo, M., Yamada, T., Ichikawa, T., Kajisawa, M., Matsuda, Y., Tanaka, I., & Umehata, H. 2016, Monthly Notices of the Royal Astronomical Society, 455, 3333–3344

A Close Comparison between Observed and Modeled Ly α Lines for ~ 2.2 Lyman Alpha Emitters [4]

In collaboration with the members of The University of Tokyo, Geneva Observatory, The French National Centre for Scientific Research, and Observatories of the Carnegie Institution of Washington.

We present the results of a Ly α profile analysis of 12 Ly α emitters (LAEs) at $z \sim 2.2$ with high-resolution Ly α spectra. We find that all 12 objects have a Ly α profile with the main peak redward of the systemic redshift defined by nebular lines, and five have a weak, secondary peak blueward of the systemic redshift (blue bump). The average velocity offset of the red main peak (the blue bump, if any) with respect to the systemic redshift is $\Delta v_{\text{Ly}\alpha, r} = 174 \pm 19 \text{ km s}^{-1}$ ($\Delta v_{\text{Ly}\alpha, b} = -316 \pm 45 \text{ km s}^{-1}$), which is smaller than (comparable

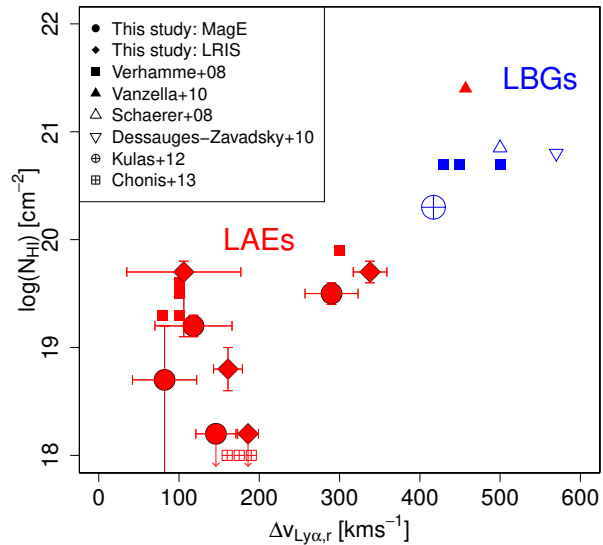


Fig. 18. $\log(N_{\text{HI}})$ plotted against $\Delta v_{\text{Ly}\alpha, r}$. Red (blue) symbols correspond to objects with $\text{EW}(\text{Ly}\alpha)_{\text{photo}}$ larger (smaller) than 30 \AA . The filled circles and diamonds are the non-blue-bump LAEs obtained by MagE and LIRS, respectively. The filled squares show $z \sim 3$ objects in the literature. The filled triangle denotes a $z = 5.56$ [NIV emitter with $\text{EW}(\text{Ly}\alpha) = 89 \text{ \AA}$]. The open triangle is a lensed LBG with Ly α absorption, cB58, while the inverted triangle is a lensed LBG with Ly α absorption, “the 8 o’clock arc”. In addition, the objects studied in the literature are plotted as a circle and three squares with a cross inside, respectively. For the purpose of display, three LAEs in the literature, which have similar $\Delta v_{\text{Ly}\alpha, r}$ and $\log(N_{\text{HI}})$ values of 175 km s^{-1} and 18 cm^{-2} , are shifted toward the x -axis. We stress that all the data points and error bars are obtained assuming uniform expanding shells. The positions and/or error bars of data points in the figure can be significantly changed if we consider other models. This figure is reproduced by permission of the AAS.

to) that of Lyman-break galaxies (LBGs). The outflow velocities inferred from metal absorption lines in three individual and one stacked spectra are comparable to those of LBGs. The uniform expanding shell model constructed by Verhamme et al. reproduces not only the Ly α profiles but also other observed quantities, including the outflow velocity and the FWHM of nebular lines for the non-blue-bump objects. On the other hand, the model predicts too high FWHMs of nebular lines for the blue bump objects, although this discrepancy may disappear if we introduce additional Ly α photons produced by gravitational cooling. We show that the small $\Delta v_{\text{Ly}\alpha, r}$ values of our sample can be explained by low neutral hydrogen column densities of $\log(N_{\text{HI}}) = 18.9 \text{ cm}^{-2}$ on average. This value is more than one order of magnitude lower than those of LBGs but is consistent with recent findings that LAEs have high ionization parameters and low HI gas masses. This result suggests that low N_{HI} values, giving reduced numbers of resonant scattering of Ly α photons, are the key to the strong Ly α emission of LAEs.

Bibliography

- [4] Hashimoto, T., Verhamme, A., Ouchi, M., Shimasaku, K., Schaerer, D., Nakajima, K., Shibuya, T., Rauch, M., Ono, Y., & Goto, R. 2015, The Astrophysical Journal, 812, 157

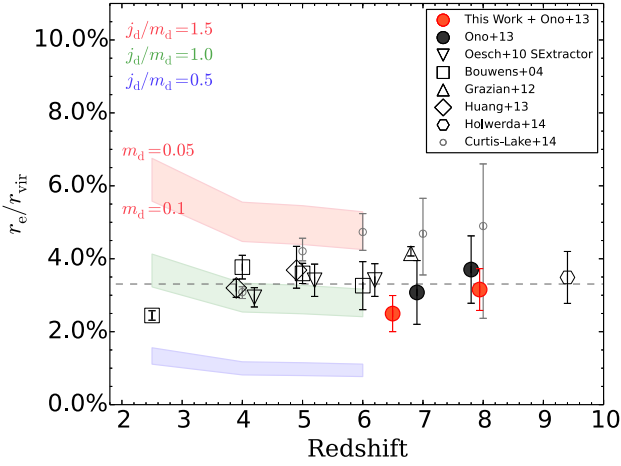


Fig. 19. Redshift evolution of the half-light radius to virial radius. The error bars show the 1σ standard error of the half-light radius. The shaded bands are predictions from the model by Mo et al. changing the j_d/m_d and m_d within the range of 0.05–0.1. The red, green, and blue bands correspond to $j_d/m_d = 1.5, 1.0, 0.5$. The upper edge of each band corresponds to $m_d = 0.05$ and the lower to $m_d = 0.1$. This figure is reproduced by permission of the AAS.

The sizes of $z \sim 6-8$ lensed galaxies from the Hubble Frontier Fields Abell 2744 data [5]

In collaboration with the members of The University of Tokyo.

We investigate the sizes of $z \sim 6-8$ dropout galaxies using the complete data of the Abell 2744 cluster and parallel fields in the Hubble Frontier Fields program. By directly fitting light profiles of observed galaxies with lensing-distorted Sérsic profiles on the image plane with the `glafic` software, we accurately measure intrinsic sizes of 31 $z \sim 6-7$ and 8 $z \sim 8$ galaxies, including those as faint as $M_{UV} \simeq -16.6$. We find that half-light radii r_e positively correlates with UV luminosity at each redshift, although the correlation is not very tight. The largest ($r_e > 0.8$ kpc) galaxies are mostly red in UV color while the smallest ($r_e < 0.08$ kpc) ones tend to be blue. We also find that galaxies with multiple cores tend to be brighter. Combined with previous results at $2.5 \lesssim z \lesssim 12$, our result confirms that the average r_e of bright ($(0.3-1)L_{z=3}^*$) galaxies scales as $r_e \propto (1+z)^{-m}$ with $m = 1.24 \pm 0.1$. We find that the ratio of r_e to virial radius is virtually constant at $3.3 \pm 0.1\%$ over a wide redshift range, where the virial radii of hosting dark matter halos are derived based on the abundance matching. This constant ratio is consistent with the disk formation model by Mo et al. with $j_d \sim m_d$, where j_d and m_d are the fractions of the angular momentum and mass within halos confined in the disks. A comparison with various types of local galaxies indicates that our galaxies are most similar to circumnuclear star-forming regions of barred galaxies in the sense that a sizable amount of stars are forming in a very small area.

Bibliography

[5] Kawamata, R., Ishigaki, M., Shimasaku, K., Oguri, M., & Ouchi, M. 2015, *The Astrophysical Journal*, 804, 103

Statistical Properties of Diffuse Ly α Halos around Star-forming Galaxies at $z \sim 2$ [6]

In collaboration with the members of National Astronomical Observatory of Japan, Geneva Observatory, The University of Tokyo, Mahidol University, and The University of Tsukuba.

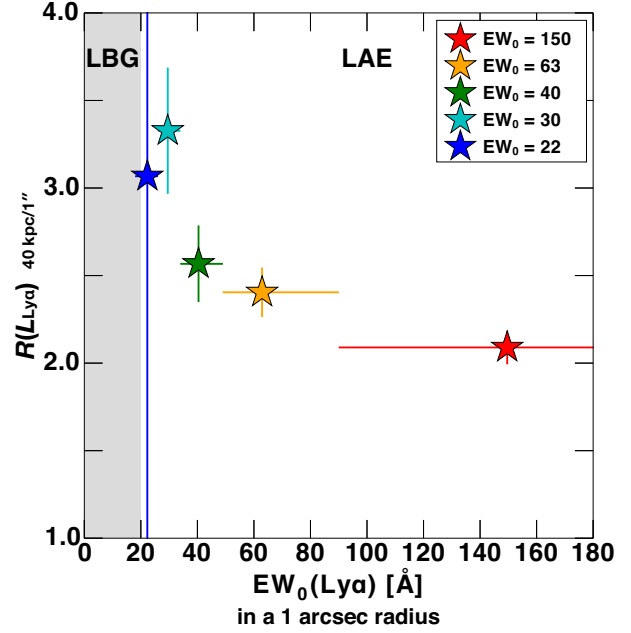


Fig. 20. Ly α luminosity within $r = 40$ kpc that is normalized by the one within $r = 1$ arcsec. These normalized Ly α luminosities are shown as a function of EW_0 defined in a $r = 1$ arcsec area. The EW_0 range of a subsample is shown as error bars in the x -axis. This figure is reproduced by permission of the RAS.

We present statistical properties of diffuse Ly α halos (LAHs) around high- z star-forming galaxies with large Subaru samples of Ly α emitters (LAEs) at $z = 2.2$. We make subsamples defined by the physical quantities of LAEs' central Ly α luminosities, UV magnitudes, Ly α equivalent widths, and UV slopes, and investigate LAHs' radial surface brightness (SB) profiles and scale lengths r_n as a function of these physical quantities. We find that there exist prominent LAHs around LAEs with faint Ly α luminosities, bright UV luminosities, and small Ly α equivalent widths in cumulative radial Ly α SB profiles. We confirm this trend with the anti-correlation between r_n and Ly α luminosities (equivalent widths) based on the Spearman's rank correlation coefficient that is $\rho = -0.9 (-0.7)$ corresponding to the 96% (93%) confidence level, although the correlation between r_n and UV magnitudes is not clearly found in the rank correlation coefficient. Our results suggest that LAEs with properties similar to typical Lyman-break galaxies (with faint Ly α luminosities and small equivalent widths) possess more prominent LAHs. We investigate scenarios for the major physical origins of LAHs with our results. Because we find relatively small Ly α equivalent widths up to 77\AA in LAHs that include LAEs' central components, these results suggest that the cold stream scenario is not preferred. There remain two possible scenarios of Ly α scattering in circum-galactic medium and satellite galaxies that cannot be tested with our observational data.

Bibliography

[6] Momose, R., Ouchi, M., Nakajima, K., Ono, Y., Shibuya, T., Shimasaku, K., Yuma, S., Mori, M., & Umemura, M. 2016, *Monthly Notices of the Royal Astronomical Society*, 457, 2318–2330

Theory Group

Overview

The theory group is active in phenomenology in elementary particle physics focusing on particle phenomenology, and astroparticle physics focusing on particle cosmology. In particle physics, the main topics are theoretical studies of dark matter, inflation and extensions of the standard model. In astroparticle physics, the main topics are theoretical studies of inflation, thermal history of the early universe, dark matter, baryogenesis and big-bang nucleosynthesis.

In June, the ATLAS collaboration reported a resonance of around 2 TeV in the di-jet mass spectrum with the 8 TeV data corrected in 2012. Around the same time, the Large Hadron Collider Run II started data taking at a center-of-mass energy of 13 TeV. Many theoretical interpretations of the excess have been proposed, but the 13 TeV LHC has not met the excess yet. In December, the ATLAS and the CMS collaborations reported another excess around 750 GeV in the di-photon resonance search. If it is a true signal, it may change the whole picture of particle phenomenology. A huge number of papers about the excess have been published, but still we need more data to conclude. In February, the LIGO and VIRGO collaborations announced the detection of gravitational waves of two around 30 solar mass black holes merging about 1.3 billion light-years away. Though they are aimed at astronomical targets, they opened up an entirely new window on the Universe and the future programs, such as eLISA and DECIGO, will certainly give important information about the early stage of the Universe.

The supersymmetric (SUSY) extension of the standard model (SM) in the particle physics is considered to be one of the most promising models beyond the standard model. It solves the naturalness problem for the Higgs boson mass term in the standard model, and it is also compatible with the grand unified theories (GUTs). Our group has been studying phenomenological and cosmological aspects of the SUSY models.

Recent cosmological observations including the Planck data determine precisely the mean densities of matter and baryon in the Universe, and existence of non-baryonic dark matter is established. Weakly interacting massive particles (WIMPs) are considered to be good candidates of the dark matter. They act as the cold dark matter in the structure formation of the universe. Our group has been studying model building for dark matter and detectability in direct and indirect search experiments.

For understanding of the early universe, a role of the elementary particle physics is crucial. Recent progress in the particle physics such as grand unification theories and supersymmetry leads us to a more deeper insight into the fundamental aspects of the early universe. In the inflationary universe, the quantum fluctuations of the scalar field which drives the inflation become the density fluctuations and lead to formation of the structure observed in the present universe. On the other hand cosmology and astrophysics are used to test new theories in particle physics. Such particle cosmology is one of main subjects of our group.

Big Bang Nucleosynthesis (BBN) is one of the most important subjects in modern cosmology. Predicted abundances of the light elements are very sensitive to the cosmological scenario. On the other hand, physics beyond the standard model predicts the new particles which would have existed at the BBN epoch. Such particles may spoil the success of BBN, which leads to constraints on the new particles and the particle physics models.

The grand unified theories predict that our universe undergoes several vacuum phase transitions. In the course of phase transitions topological defects (monopoles, cosmic strings and domain walls) are generally produced depending on symmetries of the vacua. Our group has studied evolution of various topological defects.

Particle Phenomenology

[Spokesperson : M. Ibe]

ICRR, The Univ. of Tokyo, Kashiwa, Chiba 277-8582

Extensions of the Standard Model

• Seminatual SUSY from the E_7 non linear sigma model

In collaboration with the members of ICRR, Kavli IPMU and INFN.

We present a new focus point supersymmetry breaking scenario based on the supersymmetric E_7 non-linear sigma model. In this non-linear sigma model, squarks and sleptons are identified with (pseudo) Nambu-Goldstone bosons. Their masses are generated only radiatively through gauge and yukawa interactions, and they are much smaller than the gravitino and gaugino masses at a high energy scale. On the other hand, Higgs doublets belong to matter multiplets and hence may have unsuppressed supersymmetry-breaking soft masses. We consider their masses to be equal to the gravitino mass at the high energy scale, assuming the minimal Kahler potential for Higgs doublets. We show that the fine-tuning measure of the electroweak symmetry breaking scale is reduced significantly to $\Delta = 30-70$, if the ratio of the gravitino mass to the gaugino mass is around $5/4$. Also, the prospects of the discovery/exclusion of supersymmetric particles at the Large Hadron Collider and dark matter direct detection experiments are discussed [1].

• Indirect Probe of Electroweak-Interacting Particles at Future Lepton Colliders

In collaboration with the members of ICRR, Kavli IPMU, Calcutta University and DESY.

Various types of electroweak-interacting particles, which have non-trivial charges under the $SU(2)_L \times U(1)_Y$ gauge symmetry, appear in extensions of the Standard Model (SM). These particles are good targets of future lepton colliders, such as the International Linear Collider (ILC) and the Compact Linear Collider (CLIC). An advantage of the experiments is, that even if their beam energy is below the threshold of the production of new particles, quantum effects of the new particles can be detected through high precision measurements. We estimate the capability of future lepton colliders to probe electroweak-interacting particles through quantum effects, with particular focus on wino, Higgsino and so-called minimal dark matter. We find that a particle whose mass is greater than the beam energy by 100-1000 GeV is detectable by measuring di-fermion production cross sections with $O(0.1)\%$ accuracy [2].

• A Model of Visible QCD Axion

In collaboration with the members of ICRR and Kavli IPMU.

We pursue a class of visible axion models where the axion mass is enhanced by strong dynamics in a mirrored copy of the Standard Model in the line of the idea put forward by Rubakov. In particular, we examine the consistency of the models with laboratory, astrophysical, and cosmological constraints. As a result, viable parameter regions are found, where the mass of the axion is of $O(100)$ MeV or above while the Peccei-Quinn breaking scale is at around 10^{3-5} GeV [3].

• Muon $g - 2$ in Focus Point SUSY

In collaboration with the members of ICRR, Kavli IPMU and INFN.

We point out that the anomaly of the muon $g - 2$ can be easily explained in a focus point supersymmetry scenario, which realizes the semi-natural supersymmetry. Among known focus point supersymmetry scenarios, we find that a model based on Higgs-gaugino mediation works with a mild fine-tuning $\Delta = 40 - 80$. We propose two new focus point supersymmetry scenarios where the anomaly of the muon $g - 2$ is also explained. These scenarios are variants of the widely known focus point supersymmetry based on gravity mediation with universal scalar masses [4].

• Peccei-Quinn Symmetry from Dynamical Supersymmetry Breaking

In collaboration with the members of ICRR and Kavli IPMU.

The proximity of the Peccei-Quinn scale to the scale of supersymmetry breaking in models of pure gravity mediation hints at a common dynamical origin of these two scales. To demonstrate how to make such a connection manifest, we embed the Peccei-Quinn mechanism into the vector-like model of dynamical supersymmetry breaking a la IYIT. Here, we rely on the anomaly-free discrete Z_{4R} symmetry required in models of pure gravity mediation to solve the μ problem to protect the Peccei-Quinn symmetry from the dangerous effect of higher-dimensional operators. This results in a rich phenomenology featuring a QCD axion with a decay constant of $O(10^{10})$ GeV and mixed WIMP/axion dark matter. In addition, exactly five pairs of extra $\mathbf{5}$ and $\bar{\mathbf{5}}$ matter multiplets, directly coupled to the supersymmetry breaking sector and with masses close to the gravitino mass, $m_{3/2} \sim 100$ TeV, are needed to cancel the Z_{4R} anomalies [5].

• Cosmological Selection of Multi-TeV Supersymmetry

In collaboration with the members of ICRR and Kavli IPMU.

We discuss a possible answer to the fundamental question of why nature would actually prefer low-scale supersymmetry, but end up with a supersymmetry scale that is not completely natural. This question is inevitable if we postulate that low-energy supersymmetry is indeed realized in nature, despite the null observation of superparticles below a TeV at the Large Hadron Collider. We find that superparticle masses in the multi-TeV range can, in fact, be reconciled with the concept of naturalness by means of a cosmological selection effect—a selection effect based on the assumption of an exact discrete R -symmetry that is spontaneously broken by gaugino condensation in a pure supersymmetric Yang-Mills theory. In such theories, the dynamical scale of the Yang-Mills gauge interactions is required to be higher than the inflationary Hubble scale, in order to avoid the formation of domain walls. This results in a lower limit on the superparticle masses and leads us to conclude that, according to the idea of naturalness, the most probable range of superparticle masses is potentially located at the multi-TeV, if the inflationary Hubble rate is of $O(10^{14})$ GeV. Our argument can be partially tested by future measurements of the tensor fraction in the Cosmic Microwave Background fluctuations [6].

• Diboson Resonance as a Portal to Hidden Strong Dynamics

In collaboration with the members of ICRR and Kavli IPMU.

We propose a new explanation for excess events observed in the search for a high-mass resonance decaying into dibosons by the ATLAS experiment. The resonance is identified as a composite spin-0

particle that couples to the Standard Model gauge bosons via dimension-5 operators. The excess events can be explained if the dimension-5 operators are suppressed by a mass scale of $O(1 - 10)$ TeV. We also construct a model of hidden strong gauge dynamics which realizes the spin-0 particle as its lightest composite state, with appropriate couplings to Standard Model gauge bosons [7].

• Cosmologically safe QCD axion models

In collaboration with the members of ICRR, IPMU, and Tohoku University.

We propose QCD axion models that avoid the cosmological domain wall problem and/or isocurvature problem. In Ref. [8], we introduce a global $SU(3)_f$ family symmetry to which we embed the unwanted PQ discrete symmetry. The spontaneous breaking of $SU(3)_f$ and PQ symmetry predicts eight NG bosons as well as axion, all of which contribute to dark radiation in the Universe. In Refs. [9, 10, 12], we provide QCD axion models where the Peccei-Quinn symmetry is badly broken by a larger amount in the past than in the present, in order to avoid the axion isocurvature problem. In Ref. [11], we propose a simple QCD axion model without any fine-tunings by considering an extra dimension [8, 9, 10, 11, 12].

• Cosmological Problems of the String Axion Alleviated by High Scale SUSY of $m_{3/2} \simeq 10 - 100$ TeV

In collaboration with the members of ICRR, Kavli IPMU and INFN.

The string axion may provide the most attractive solution to the strong CP problem in QCD. However, the axion energy density easily exceeds the dark matter density in the present universe due to a large decay constant around 10^{16} GeV, unless the initial value of the axion field is finely tuned. We show that this problem is alleviated if and only if the SUSY particle mass scale is 10-100 TeV, since the decay of saxion can produce a large enough amount of entropy after the QCD phase transition, not disturbing the BBN prediction. The saxion decay also produces a large number of the lightest SUSY particles (LSPs). As a consequence, R -parity needs to be violated to avoid the overproduction of the LSPs. The saxion field can be stabilized with relatively simple Kähler potentials, not inducing a too large axion dark radiation. Despite the large entropy production, the observed baryon number is explained by the Affleck-Dine mechanism. Furthermore, the constraint from isocurvature perturbations is relaxed, and the Hubble constant during inflation can be as large as several $\times 10^{10}$ GeV [13].

• Mass-Splitting between Haves and Have-Nots

In collaboration with the members of ICRR.

We revisit the long-standing problem of supersymmetric grand unified theory (GUT), the doublet-triplet splitting problem. We discuss whether symmetry which controls the μ term in the minimal supersymmetric standard model is compatible with GUT. We find that the symmetry must be broken at the GUT scale. A similar argument also shows that the R symmetry, which is important for low energy supersymmetry, must be broken down to a Z_{2R} symmetry at the GUT scale. We propose a new prescription to achieve the doublet-triplet splitting by symmetry. There, the symmetry which controls the μ term is spontaneously broken at the GUT scale by order parameters which are charged under other symmetries. Bilinear terms of triplet Higgses are *charged* under the other symmetries, while those of doublet Higgses are *not*. Then triplet Higgses directly couple to the order

parameters and hence obtain GUT scale masses, while doublet Higgses obtain suppressed masses. The broken R symmetry can be also effectively preserved by a similar prescription. As a demonstration, we construct an $SU(5) \times SU(5)$ GUT model. We also comment on unification of yukawa couplings [14].

• Revisiting Scalar Quark Hidden Sector in Light of 750-GeV Diphoton Resonance

In collaboration with the members of ICRR, Kavli IPMU, and Taiwan National Central University

We revisit the model of a CP-even singlet scalar resonance proposed in arXiv:1507.02483, where the resonance appears as the lightest composite state made of scalar quarks participating in hidden strong dynamics. We show that the model can consistently explain the excess of diphoton events with an invariant mass around 750 GeV reported by both the ATLAS and CMS experiments. We also discuss the nature of the charged composite states in the TeV range which accompany to the neutral scalar. Due to inseparability of the dynamical scale and the mass of the resonance, the model also predicts signatures associated with the hidden dynamics such as leptons, jets along with multiple photons at future collider experiments. We also associate the TeV-scale dynamics behind the resonance with an explanation of dark matter [15].

• Why three generations?

In collaboration with the members of ICRR, Kavli IPMU, and UCLA

We discuss an anthropic explanation of why there exist three generations of fermions. If one assumes that the right-handed neutrino sector is responsible for both the matter-antimatter asymmetry and the dark matter, then anthropic selection favors three or more families of fermions. For successful leptogenesis, at least two right-handed neutrinos are needed, while the third right-handed neutrino is invoked to play the role of dark matter. The number of the right-handed neutrinos is tied to the number of generations by the anomaly constraints of the $U(1)_{B-L}$ gauge symmetry. Combining anthropic arguments with observational constraints, we obtain predictions for the X-ray observations, as well as for neutrinoless double-beta decay [16].

• 750 GeV diphoton resonance in a visible heavy QCD axion model

In collaboration with the members of ICRR, Kavli IPMU, and Taiwan National Central University

In this paper, we revisit a visible heavy QCD axion model in light of the recent reports on the 750 GeV diphoton resonance by the ATLAS and CMS experiments. In this model, the axion is made heavy with the help of the mirror copied sector of the Standard Model while the successful Peccei-Quinn mechanism is kept intact. We identify the 750 GeV resonance as the scalar boson associated with spontaneous breaking of the Peccei-Quinn symmetry which mainly decays into a pair of the axions. We find that the mixings between the axion and η and η' play important roles in its decays and the resultant branching ratio into two photons. The axion decay length can be suitable for explaining the diphoton excess by the di-axion production when its decay constant $f_a = 1$ TeV. We also find that our model allows multiple sets of the extra fermions without causing the domain wall problem, which is advantageous to explain the diphoton signal [17].

Bibliography

- [1] K. Harigaya, T. T. Yanagida and N. Yokozaki, PTEP **2015**, no. 8, 083B03 (2015) doi:10.1093/ptep/ptv106 [arXiv:1504.02266 [hep-ph]].
- [2] K. Harigaya, K. Ichikawa, A. Kundu, S. Matsumoto and S. Shirai, JHEP **1509**, 105 (2015) doi:10.1007/JHEP09(2015)105 [arXiv:1504.03402 [hep-ph]].
- [3] H. Fukuda, K. Harigaya, M. Ibe and T. T. Yanagida, Phys. Rev. D **92**, no. 1, 015021 (2015) doi:10.1103/PhysRevD.92.015021 [arXiv:1504.06084 [hep-ph]].
- [4] K. Harigaya, T. T. Yanagida and N. Yokozaki, Phys. Rev. D **92**, no. 3, 035011 (2015) doi:10.1103/PhysRevD.92.035011 [arXiv:1505.01987 [hep-ph]].
- [5] K. Harigaya, M. Ibe, K. Schmitz and T. T. Yanagida, Phys. Rev. D **92**, no. 7, 075003 (2015) doi:10.1103/PhysRevD.92.075003 [arXiv:1505.07388 [hep-ph]].
- [6] K. Harigaya, M. Ibe, K. Schmitz and T. T. Yanagida, Phys. Lett. B **749**, 298 (2015) doi:10.1016/j.physletb.2015.07.073 [arXiv:1506.00426 [hep-ph]].
- [7] C. W. Chiang, H. Fukuda, K. Harigaya, M. Ibe and T. T. Yanagida, JHEP **1511**, 015 (2015) doi:10.1007/JHEP11(2015)015 [arXiv:1507.02483 [hep-ph]].
- [8] M. Kawasaki, M. Yamada and T. T. Yanagida, Phys. Rev. D **91**, no. 12, 125018 (2015) doi:10.1103/PhysRevD.91.125018 [arXiv:1504.04126 [hep-ph]].
- [9] M. Kawasaki, M. Yamada and T. T. Yanagida, Phys. Lett. B **750**, 12 (2015) doi:10.1016/j.physletb.2015.08.043 [arXiv:1506.05214 [hep-ph]].
- [10] F. Takahashi and M. Yamada, JCAP **1510**, no. 10, 010 (2015) doi:10.1088/1475-7516/2015/10/010 [arXiv:1507.06387 [hep-ph]].
- [11] M. Yamada, T. T. Yanagida and K. Yonekura, Phys. Rev. Lett. **116**, no. 5, 051801 (2016) doi:10.1103/PhysRevLett.116.051801 [arXiv:1510.06504 [hep-ph]].
- [12] M. Kawasaki, F. Takahashi and M. Yamada, Phys. Lett. B **753**, 677 (2016) doi:10.1016/j.physletb.2015.12.075 [arXiv:1511.05030 [hep-ph]].
- [13] M. Kawasaki, T. T. Yanagida and N. Yokozaki, Phys. Lett. B **753**, 389 (2016) doi:10.1016/j.physletb.2015.12.043 [arXiv:1510.04171 [hep-ph]].
- [14] K. Harigaya, M. Ibe and M. Suzuki, JHEP **1509**, 155 (2015) doi:10.1007/JHEP09(2015)155 [arXiv:1505.05024 [hep-ph]].
- [15] C. W. Chiang, M. Ibe and T. T. Yanagida, JHEP **1605**, 084 (2016) doi:10.1007/JHEP05(2016)084 [arXiv:1512.08895 [hep-ph]].
- [16] M. Ibe, A. Kusenko and T. T. Yanagida, Phys. Lett. B **758**, 365 (2016) doi:10.1016/j.physletb.2016.05.025 [arXiv:1602.03003 [hep-ph]].
- [17] C. W. Chiang, H. Fukuda, M. Ibe and T. T. Yanagida, Phys. Rev. D **93**, no. 9, 095016 (2016) doi:10.1103/PhysRevD.93.095016 [arXiv:1602.07909 [hep-ph]].

Particle Cosmology

[Spokesperson : M. Kawasaki]

ICRR, The Univ. of Tokyo, Kashiwa, Chiba 277-8582

Inflation and Thermal History in the early Universe

• Revisiting the Minimal Chaotic Inflation Model

In collaboration with the members of ICRR and Kavli IPMU.

We point out that the prediction of the minimal chaotic inflation model is altered if a scalar field takes a large field value close to the Planck scale during inflation due to a negative Hubble induced mass. In particular, we show that the inflaton potential is effectively flattened at a large inflaton field value in the presence of such a scalar field. The scalar field may be identified with the standard model Higgs field or super partners of standard model fermions. With such Hubble-induced flattening, we find that the minimal chaotic inflation model, especially the model with a quadratic potential, is consistent with recent observations of the cosmic microwave background fluctuation without modifying the inflation model itself [1].

• Dynamics of Peccei-Quinn Breaking Field after Inflation and Axion Isocurvature Perturbations

In collaboration with the members of ICRR and Kavli IPMU.

The Peccei-Quinn mechanism suffers from the problem of the isocurvature perturbations. The isocurvature perturbations are suppressed if the Peccei-Quinn breaking scale is large during inflation. The oscillation of the Peccei-Quinn breaking field after inflation, however, leads to the formation of domain walls due to the parametric resonance effect. We discuss the evolution of the Peccei-Quinn breaking field after inflation in detail, and propose a model where the parametric resonance is ineffective and hence domain walls are not formed. We also discuss consistency of our model with supersymmetric theory [2].

• High-scale SUSY from an R-invariant New Inflation in the Landscape

In collaboration with the members of ICRR, IPMU, and INFN.

We provide an anthropic reason that the supersymmetry breaking scale is much higher than the electroweak scale as indicated by the null result of collider experiments and observed 125 GeV Higgs boson. We focus on a new inflation model as a typical low-scale inflation model that may be expected in the string landscape. In this model, the R-symmetry is broken at the minimum of the inflaton potential and its breaking scale is related to the reheating temperature. Once we admit that the anthropic principle requires thermal leptogenesis, we obtain a lower bound on gravitino mass, which is related to R-symmetry breaking scale. This scenario and resulting gravitino mass predict the consistent amplitude of density perturbations [3].

• The two-field regime of natural inflation

In collaboration with the members of Universiteit Leiden and Tohoku University.

The simplest two-field completion of natural inflation has a regime in which both fields are active and in which its predictions are within the Planck $1-\sigma$ confidence contour. We show this for the original model of natural inflation, in which inflation is achieved through the explicit breaking of a U(1) symmetry. We consider the case in which the mass coming from explicit breaking of this symmetry is comparable to that from spontaneous breaking, which we show is consistent with a hierarchy between the corresponding energy scales. While both masses are comparable when the observable modes left the horizon, the mass hierarchy is restored in the last e-foldings of

inflation, rendering the predictions consistent with the isocurvature bounds. For completeness, we also study the predictions for the case in which there is a large hierarchy of masses and an initial period of inflation driven by the (heavy) radial field [4].

• Thermalization Process after Inflation and Effective Potential of Scalar Field

In collaboration with the members of IPMU.

We investigate the thermalization process of the Universe after inflation to determine the evolution of the effective temperature. The time scale of thermalization is found to be so long that it delays the evolution of the effective temperature, and the resulting maximal temperature of the Universe can be significantly lower than the one obtained in the literature [5].

• Constraints on the neutrino parameters by future cosmological 21cm line and precise CMB polarization observations

In collaboration with the members of KEK.

Observations of the 21 cm line radiation coming from the epoch of reionization have a great capacity to study the cosmological growth of the Universe. Besides, CMB polarization produced by gravitational lensing has a large amount of information about the growth of matter fluctuations at late time. In this paper, we investigate their sensitivities to the impact of neutrino property on the growth of density fluctuations, such as the total neutrino mass, the effective number of neutrino species (extra radiation), and the neutrino mass hierarchy. We show that by combining a precise CMB polarization observation such as Simons Array with a 21 cm line observation such as Square kilometer Array (SKA) phase 1 and a baryon acoustic oscillation observation (Dark Energy Spectroscopic Instrument:DESI) we can measure effects of non-zero neutrino mass on the growth of density fluctuation if the total neutrino mass is larger than 0.1 eV. Additionally, the combinations can strongly improve errors of the bounds on the effective number of neutrino species $\sigma(N_\nu) \sim 0.06 - 0.09$ at 95 % C.L.. Finally, by using SKA phase 2, we can determine the neutrino mass hierarchy at 95 % C.L. if the total neutrino mass is similar to or smaller than 0.1 eV [6].

Bibliography

- [1] K. Harigaya, M. Ibe, M. Kawasaki and T. T. Yanagida, *Phys. Lett. B* **756**, 113 (2016) doi:10.1016/j.physletb.2016.03.001 [arXiv:1506.05250 [hep-ph]].
- [2] K. Harigaya, M. Ibe, M. Kawasaki and T. T. Yanagida, *JCAP* **1511**, no. 11, 003 (2015) doi:10.1088/1475-7516/2015/11/003 [arXiv:1507.00119 [hep-ph]].
- [3] M. Kawasaki, M. Yamada, T. T. Yanagida and N. Yokozaki, *Phys. Rev. D* **93**, no. 5, 055022 (2016) doi:10.1103/PhysRevD.93.055022 [arXiv:1512.04259 [hep-ph]].
- [4] A. Achúcarro, V. Atal, M. Kawasaki and F. Takahashi, *JCAP* **1512**, no. 12, 044 (2015) doi:10.1088/1475-7516/2015/12/044 [arXiv:1510.08775 [astro-ph.CO]].
- [5] K. Mukaida and M. Yamada, *JCAP* **1602**, no. 02, 003 (2016) doi:10.1088/1475-7516/2016/02/003 [arXiv:1506.07661 [hep-ph]].
- [6] Y. Oyama, K. Kohri and M. Hazumi, *JCAP* **1602**, no. 02, 008 (2016) doi:10.1088/1475-7516/2016/02/008 [arXiv:1510.03806 [astro-ph.CO]].

Dark Matter, Baryogenesis, Big-Bang nucleosynthesis

• Adiabatic Invariance of Oscillations/I-balls

In collaboration with the members of ICRR and Tohoku Univ.

Real scalar fields are known to fragment into spatially localized and long-lived solitons called oscillons or I-balls. We prove the adiabatic invariance of the oscillons/I-balls for a potential that allows periodic motion even in the presence of non-negligible spatial gradient energy. We show that such potential is uniquely determined to be the quadratic one with a logarithmic correction, for which the oscillons/I-balls are absolutely stable. For slightly different forms of the scalar potential dominated by the quadratic one, the oscillons/I-balls are only quasi-stable, because the adiabatic charge is only approximately conserved. We check the conservation of the adiabatic charge of the I-balls in numerical simulation by slowly varying the coefficient of logarithmic corrections. This unambiguously shows that the longevity of oscillons/I-balls is due to the adiabatic invariance [1].

• Spontaneous Baryogenesis from Asymmetric Inflaton

In collaboration with the members of Tohoku University.

We propose a variant scenario of spontaneous baryogenesis from asymmetric inflaton based on current-current interactions between the inflaton and matter fields with a non-zero B-L charge. When the inflaton starts to oscillate around the minimum after inflation, it may lead to excitation of a CP-odd component, which induces an effective chemical potential for the B-L number through the current-current interactions. We study concrete inflation models and show that the spontaneous baryogenesis scenario can be naturally implemented in the chaotic inflation in supergravity [2].

• Affleck-Dine baryogenesis and inflation

We investigate the backreaction of the Affleck-Dine leptogenesis to inflaton dynamics in the F-term hybrid and chaotic inflation models in supergravity. We determine the lightest neutrino mass in both models so that the predictions of spectral index, tensor-to-scalar ratio, and baryon abundance are consistent with observations. We also propose a new scenario of Affleck-Dine baryogenesis where a flat direction in the MSSM generates B-L asymmetry just after the end of inflation. The resulting amount of baryon asymmetry is independent of low-energy supersymmetric models but is dependent on inflation models [3, 4].

• Can massive primordial black holes be produced in mild waterfall hybrid inflation?

In collaboration with the members of ICRR and Kavli IPMU

We studied the possibility whether the massive primordial black holes (PBHs) surviving today can be produced in hybrid inflation. Though it is of great interest since such PBHs can be the candidate for dark matter or seeds of the supermassive black holes in galaxies, there have not been quantitatively complete works yet because of the non-perturbative behavior around the critical point of hybrid inflation. Therefore, combining the stochastic and δN formalism, we numerically calculated the curvature perturbations in a non-perturbative way and found, without any specific assumption of the types of hybrid inflation, PBHs are rather overproduced when the waterfall phase of hybrid inflation continues so long that the PBH

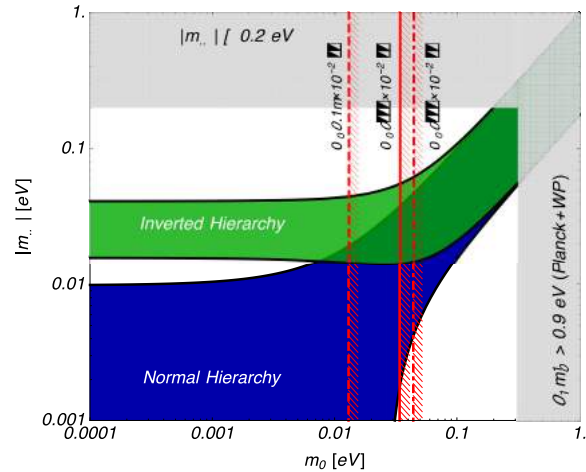


Fig. 21. The effective mass of the neutrinoless double beta decay, $|m_{ee}|$ is shown as a function of the lightest neutrino mass m_0 , where the gray regions are excluded by current observations. The red lines show upper limits on m_0 for successful leptogenesis.

scale is well enlarged and the corresponding PBH mass becomes sizeable enough [5].

• Spontaneous thermal Leptogenesis via Majoron oscillation

In collaboration with the members of ICRR.

A novel model of spontaneous leptogenesis is investigated, where leptogenesis takes place in the thermal equilibrium due to a background Nambu-Goldstone field in motion. In particular, we identify the Nambu-Goldstone field to be the Majoron which associates with spontaneous breakdown of (discrete) B-L symmetry. In this scenario sufficient lepton number asymmetry is generated in a primordial thermal bath without having CP-violating out-of-equilibrium decay of the heavy right-handed Majorana neutrinos. To obtain the observed baryon asymmetry, the neutrino masses are predicted in certain ranges, which can be translated into the effective mass of the neutrinoless double beta decay [6].

• Wino Dark Matter in light of the AMS-02 2015 Data

In collaboration with the members of ICRR. The AMS-02 collaboration has recently reported the antiproton to proton ratio with improved accuracy. In view of uncertainties of the production and the propagation of the cosmic rays, the observed ratio is still consistent with the secondary astrophysical antiproton to proton ratio. However, it is nonetheless enticing to examine whether the observed spectrum can be explained by a strongly motivated dark matter, the wino dark matter. As we will show, we find that the antiproton flux from the wino annihilation can explain the observed spectrum well for its mass range 2.5-3 TeV. The fit to data becomes particularly well compared to the case without the annihilation for the thermal wino dark matter case with a mass about 3 TeV. The ratio is predicted to be quickly decreased at the energy several hundreds of GeV, if this possibility is true, and it will be confirmed or ruled out in near future when the AMS-02 experiment accumulates enough data at this higher energy region [7]

- **Charged Q-balls in gauge mediated SUSY breaking models**

In collaboration with the members of ICRR.

It is known that after Affleck-Dine baryogenesis, spatial inhomogeneities of Affleck-Dine field grow into non-topological solitons called Q-balls. In gauge mediated SUSY breaking models, sufficiently large Q-balls with baryon charge are stable while Q-balls with lepton charge can always decay into leptons. For a Q-ball that carries nonzero B and L charges, the difference between the baryonic component and the leptonic component in decay rate may induce nonzero electric charge on the Q-ball. This implies that charged Q-ball, also called gauged Q-ball, may emerge in our universe. In this paper, we investigate two complex scalar fields, a baryonic scalar field and a leptonic one, in an Abelian gauge theory. We find stable solutions of gauged Q-balls for different baryon and lepton charges. Those solutions shows that a Coulomb potential arises and the Q-ball becomes electrically charged as expected. It is energetically favored that some amount of leptonic component decays, but there is an upper bound on its amount due to the Coulomb force. The baryonic decay also becomes possible by virtue of electrical repulsion and we find the condition to suppress it so that the charged Q-balls can survive in the universe [8].

- **Axino dark matter and baryon number asymmetry production by the Q-ball decay in gauge mediation**

In collaboration with the members of ICRR and Kanagawa University.

We investigate the Q-ball decay into the axino dark matter in the gauge-mediated supersymmetry breaking. In our scenario, the Q ball decays mainly into nucleons and partially into axinos to account respectively for the baryon asymmetry and the dark matter of the universe. The Q ball decays well before the big bang nucleosynthesis so that it is not affected by the decay. We show the region of the parameters which realizes this scenario [9].

- **Can thermal inflation be consistent with baryogenesis in gauge-mediated SUSY breaking models?**

In collaboration with the members of ICRR.

Thermal inflation is an attractive idea to dilute cosmic density of unwanted particles such as moduli fields which cause cosmological difficulties. However, it also dilutes preexisting baryon asymmetry and some viable baryogenesis is necessary for a cosmologically consistent scenario. We investigate whether the Affleck-Dine mechanism can produce baryon asymmetry enough to survive after the dilution in gauge-mediated SUSY breaking models. Flat directions except for LH_u flat direction cannot provide such huge baryon number because of Q-ball formation. We show that although the LH_u flat direction is special in terms of having μ -term which prevents Q-ball formation, it cannot explain the observed baryon asymmetry either [10].

- **Cosmology with a Heavy Polonyi Field**

In collaboration with the members of ICRR and UC Berkeley.

We consider a cosmologically consistent scenario with a heavy Polonyi field. The Polonyi field with a mass of $\mathcal{O}(100)$ TeV decays before the Big-Bang Nucleosynthesis (BBN) and avoids the severe constraint from the BBN. However, the abundance of the Lightest

Supersymmetric Particle (LSP) produced from the decay often exceeds the observed dark matter density. In our scenario, the dark matter density is obtained by the LSP abundance with an aid of entropy production, and baryon asymmetry is generated by the Affleck-Dine mechanism. We show that the observed baryon-to-dark matter ratio of $\mathcal{O}(0.1-1)$ is naturally explained in sequestering models with a QCD axion [11].

- **Dark matter annihilation and decay from non-spherical dark halos in the Galactic dwarf satellites**

In collaboration with the members of ICRR and Kavli IPMU

The dwarf spheroidal (dSph) galaxies in the Milky Way are the primary targets for the indirect searches for particle dark matter. In order to set robust constraints on candidates of dark matter particle, understanding of the dark halo structure of these systems is of substantial importance. In this paper, we first evaluate the astrophysical factor for dark matter annihilation and decay in 24 dSphs with taking into account non-spherical dark halo, using generalized axisymmetric mass models based on axisymmetric Jeans equations. First, from fitting analysis of the most recent kinematic data available, our axisymmetric mass models are so much better fit than previous spherical ones, thus our work should be the most realistic and reliable estimator for astrophysical factors. Second, we find that among analyzed dSphs, Triangulum 2 and Ursa Major II ultra faint dwarf galaxies are the most promising but large uncertain targets for dark matter annihilation while Draco classical dSph is the most robust and detectable target for dark matter decay. It is also found that non-sphericity of luminous and dark components has influence on the estimate of astrophysical factors, even though these factors largely depend on the sample size, the prior range of parameters and spatial extent of dark halo. Moreover, owing to these effects, the constraints on dark matter annihilation cross section are more conservative than those of previous spherical works. These results are important for optimizing and designing dark matter searches in current and future multi-messenger observations by space and ground-based telescopes [12].

- **Revisiting Big-Bang Nucleosynthesis Constraints on Dark-Matter Annihilation**

In collaboration with the members of KEK and University of Tokyo

We study the effects of dark-matter annihilation during the epoch of big-bang nucleosynthesis on the primordial abundances of light elements. We improve the calculation of the light-element abundances by taking into account the effects of anti-nucleons emitted by the annihilation of dark matter and the interconversion reactions of neutron and proton at inelastic scatterings of energetic nucleons. Comparing the theoretical prediction of the primordial light-element abundances with the latest observational constraints, we derive upper bounds on the dark-matter pair-annihilation cross section. Implication to some of particle-physics models are also discussed [13].

- **CMB Constraint on Dark Matter Annihilation after Planck 2015**

In collaboration with the members of IBS and University of Tokyo

We update the constraint on the dark matter annihilation cross section by using the recent measurements of the CMB anisotropy by the Planck satellite. We fully calculate the cascade of dark matter annihilation products and their effects on ionization, heating and excitation of the hydrogen, hence do not rely on any assumption on the energy fractions that cause these effects [14].

Bibliography

- [1] M. Kawasaki, F. Takahashi and N. Takeda, Phys. Rev. D **92**, no. 10, 105024 (2015) doi:10.1103/PhysRevD.92.105024 [arXiv:1508.01028 [hep-th]].
- [2] F. Takahashi and M. Yamada, Phys. Lett. B **756**, 216 (2016) doi:10.1016/j.physletb.2016.03.020 [arXiv:1510.07822 [hep-ph]].
- [3] M. Yamada, Phys. Lett. B **754**, 208 (2016) doi:10.1016/j.physletb.2015.12.080 [arXiv:1510.08514 [hep-ph]].
- [4] M. Yamada, Phys. Rev. D **93**, no. 8, 083516 (2016) doi:10.1103/PhysRevD.93.083516 [arXiv:1511.05974 [hep-ph]].
- [5] M. Kawasaki and Y. Tada, arXiv:1512.03515 [astro-ph.CO].
- [6] M. Ibe and K. Kaneta, Phys. Rev. D **92**, no. 3, 035019 (2015) doi:10.1103/PhysRevD.92.035019 [arXiv:1504.04125 [hep-ph]].
- [7] M. Ibe, S. Matsumoto, S. Shirai and T. T. Yanagida, Phys. Rev. D **91**, no. 11, 111701 (2015) doi:10.1103/PhysRevD.91.111701 [arXiv:1504.05554 [hep-ph]].
- [8] J. P. Hong, M. Kawasaki and M. Yamada, Phys. Rev. D **92**, no. 6, 063521 (2015) doi:10.1103/PhysRevD.92.063521 [arXiv:1505.02594 [hep-ph]].
- [9] S. Kasuya, E. Kawakami and M. Kawasaki, JCAP **1603**, no. 03, 011 (2016) doi:10.1088/1475-7516/2016/03/011 [arXiv:1511.05655 [hep-ph]].
- [10] T. Hayakawa, M. Kawasaki and M. Yamada, Phys. Rev. D **93**, no. 6, 063529 (2016) doi:10.1103/PhysRevD.93.063529 [arXiv:1508.03409 [hep-ph]].
- [11] K. Harigaya, T. Hayakawa, M. Kawasaki and M. Yamada, JCAP **1606**, no. 06, 015 (2016) doi:10.1088/1475-7516/2016/06/015 [arXiv:1601.02140 [hep-ph]].
- [12] K. Hayashi, K. Ichikawa, S. Matsumoto, M. Ibe, M. N. Ishigaki and H. Sugai, arXiv:1603.08046 [astro-ph.GA].
- [13] M. Kawasaki, K. Kohri, T. Moroi and Y. Takaesu, Phys. Lett. B **751**, 246 (2015) doi:10.1016/j.physletb.2015.10.048 [arXiv:1509.03665 [hep-ph]].
- [14] M. Kawasaki, K. Nakayama and T. Sekiguchi, Phys. Lett. B **756**, 212 (2016) doi:10.1016/j.physletb.2016.03.005 [arXiv:1512.08015 [astro-ph.CO]].

Gravitational waves

• Gravitational wave signals from short-lived topological defects in the MSSM

In collaboration with the members of IPMU, UC riverside.

We investigate the dynamics of flat directions with and without higher dimensional superpotentials in supersymmetric theories and show that topological defects, such as cosmic strings and domain walls, may form at the end of inflation and disappear at the beginning of oscillation of the flat direction. We numerically calculate their gravitational signals and find that the observation of gravitational signals would give us information of supersymmetric scale, the reheating temperature of the Universe, and higher dimensional operators (see Fig. 22) [1].

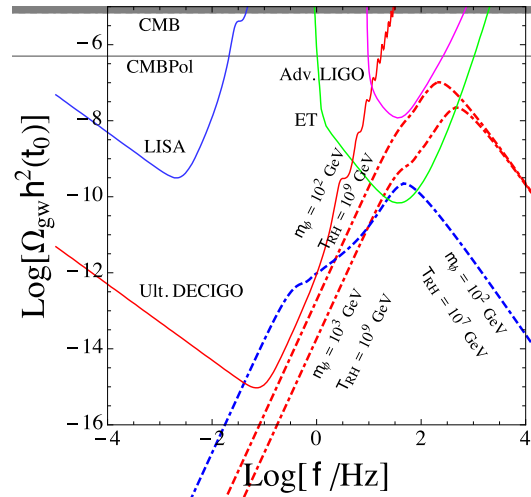


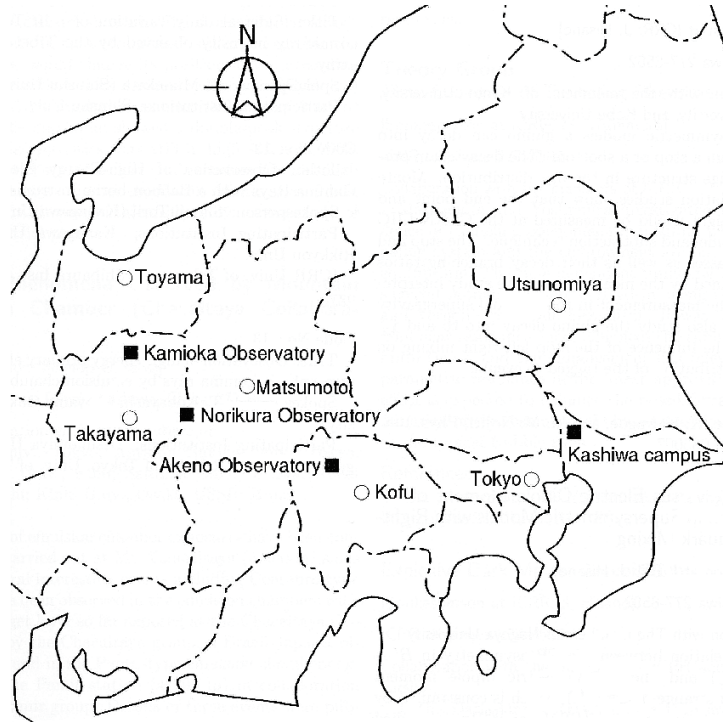
Fig. 22. GW spectra generated by cosmic strings (dash and dot-dashed curves) and sensitivities of planned interferometric detectors (solid curves).

Bibliography

- [1] A. Kamada and M. Yamada, JCAP **1510**, no. 10, 021 (2015) doi:10.1088/1475-7516/2015/10/021 [arXiv:1505.01167 [hep-ph]].

OBSERVATORIES and A RESEARCH CENTER

Location of the Institute and the Observatories in Japan



Norikura Observatory

Location: Norikuradake, Nyukawa-cho, Takayama-shi, Gifu Prefecture 506-2100
 N 36°06', E 137°33', 2770 m a.s.l.
 Telephone (Fax): 050-3730-3809
 Telephone (satellite): 090-7721-5674
 Telephone (car): 090-7408-6224

Akeno Observatory

Location: 5259 Asao, Akeno-machi, Hokuto-shi, Yamanashi Prefecture 408-0201
 N 35°47', E 138°30', 900 m a.s.l.
 Telephone / Fax: +551-25-2301 / +551-25-2303

Kamioka Observatory

Location: 456 Higashi-mozumi, Kamioka-cho, Hida-shi, Gifu Prefecture 506-1205
 N 36°25'26", E 137°19'11", 357.5 m a.s.l.
 Telephone / Fax: +578-85-2116 / +578-85-2121

Research Center for Cosmic Neutrinos

Location: 5-1-5 Kashiwanoha, Kashiwa, Chiba Prefecture 277-8582
 Telephone / Fax: +4-7136-3138 / +4-7136-3115

NORIKURA OBSERVATORY

Introduction

Norikura Observatory (36.10°N and 137.55°E) was founded in 1953 and attached to ICRR in 1976. It is located at 2770 m above sea level, and is the highest altitude manned laboratory in Japan. Experimental facilities of the laboratory are made available to all the qualified scientists in the field of cosmic ray research and associated subjects. The AC electric power is generated by the dynamo and supplied throughout the observatory. In 1996, two dynamos of 70 KVA each were replaced with the new ones. The observatory can be accessed easily by car and public bus in summer (July-September). The 50th anniversary of Norikura Observatory was celebrated in 2003.



Fig. 1. Norikura Observatory.

The feasibility of the automatic operation of Norikura Observatory during winter period has been tested since winter 2004 in order to study the possibilities to reduce maintenance and labor costs without seriously damaging to the use of researches. A long-distance (~40km) wireless LAN system (11M bps) was set up in 2003. Two new easy-to-handle and easy-to-maintain dynamos of 115 KVA each were installed in 2004 as well. The unmanned operation of Norikura Observatory has been mostly successful in winter, during which the battery backed-up solar panels and/or wind power generators kept supplying the electricity to the wireless LAN and on-going cosmic-ray experiments. The 60th anniversary of Norikura Observatory was celebrated in 2013.

Present major scientific interests of the laboratory is focused on the modulation of high energy cosmic rays in the interplanetary space associated with the solar activity and the generation of energetic particles by the solar flares, both of which require long-term monitoring. This research has been carried out by the group of universities, where ICRR provides them with laboratory facility. A part of the facility has been open for the environmental study at high altitude such as aerosol-related mechanism in the atmosphere, observation of total ozone and UV solar radiation, for botanical study in the high-altitude environment, etc.



Fig. 2. A dynamo of 115KV.

Cosmic Ray Physics

A neutron monitor has been continuously operated to study the correlation of solar activities and cosmic ray flux for a long time. It is the only active one in Japan now. The neutron monitor data are open to researchers worldwide as a world observation network point (WDC). In addition, space weather observation is actively made by a 25 m² muon hodoscope at Norikura Observatory[1], [2], [3], [4], [5], [6], [7], [8], [9].

The anisotropy observed with the global muon detector network (GMDN) provides us with a unique information of the spatial gradient of the GCR density which reflects the large-scale magnetic structure in the heliosphere. The solar cycle variation of the gradient gives an important information on the GCR transport in the heliosphere, while the short-term variation of the gradient enables us to deduce the large-scale geometry of the magnetic flux rope and the interplanetary coronal mass ejection (ICME). Real-time monitoring of the precursor anisotropy which has often been observed at the Earth preceding the arrival of the ICME accompanied by a strong shock may provide us with useful tools for forecasting the space weather with a long lead time. By using a self-supporting power system utilizing the solar panels and batteries, we keep a 25 m² muon hodoscope running at the Mt. Norikura Cosmic Ray Observatory as an important component detector of the GMDN. The total power consumption of this detector has been suppressed as low as 36 Watt by replacing all amplifier boards with those using CMOS ICs and by introducing a new recording system using the FPGA. This new system, in which the observation has been automatically carried out by a PC connected with the internet, also enabled us to monitor the data on the real-time basis for the space weather study.

The Sun is the nearest site to the Earth capable of accelerating particles up to high energies. When the Sun becomes active, flares are frequently observed on its surface. The flare accelerates the proton and ion to high energy and they are detected on the Earth soon after the flare. Among the particles generated by the flare, high energy neutrons provide the most direct information about the acceleration mechanism as they come straight from the flare position to the Earth without deflected by the magnetic field.

Observation of solar neutron has been conducted at the Norikura Observatory since 1990. Neutron is used to clarify the acceleration mechanism of high energy particles in association with solar flares, because the neutron is not reflected by the interplanetary magnetic field. The 64m^2 solar neutron telescope was constructed in 1996, which is one of 7 solar neutron telescopes deployed at different longitudes to make up a network of 24 hour observation of solar neutrons. The Norikura 64m^2 solar neutron telescope has been operated by solar batteries and windmills since 2004.

This collaborative work has started since fiscal 2007 succeeding to the previous project titled ‘Observation of solar neutrons by using a new method.’ Although solar cycle 24 has started since 2008, the solar activity has continued to be inactive, and no new solar neutron event has been detected by the network since 2006. The last solar neutron event was on September 7, 2005. This event is unique because it indicates ions were accelerated or trapped at the acceleration region longer than electrons. The summary of 11 solar neutron events detected until 2005 shows that it may not be probable that a very efficient acceleration such as the shock acceleration works for ions at solar flares. This is given by deriving the energy spectrum of neutrons at the solar surface for each solar neutron event with a power law. Power law indices obtained span from 3 to 7. The energy spectrum of the original ions is softer than that of neutron. Therefore an efficient acceleration has not been detected by the observation of solar neutrons so far. This work continues in solar cycle 24 to accumulate more events to obtain definite results related with particle acceleration at the solar surface.

Another effort aiming at observation of highest-energy solar cosmic rays started at the Norikura Observatory. The Sun is an accelerator of protons and electrons in the universe. In association with large solar flares, protons and electrons are accelerated into high energies. It is known that protons are accelerated over 50 GeV in the largest solar flares[24]. These high energy particles produce the Ground Level Enhancement (GLE).

In order to understand the acceleration mechanism of protons, we have prepared several solar neutron telescopes at the high altitude laboratories in the world. They are located at Gornergrat (3,135m), Mt. Aragats in Armenia (3,200m), Tibet (4,200m), Mauna-Kea in Hawaii (4,200m), Mt. Chacaltaya in Bolivia (5,250m), and at Mt. Sierra Negra in Mexico (4,900m). We have constructed a solar neutron telescopes at Mt. Norikura Cosmic Ray Observatory (2,770m) in 1990 and operated it until 2004[21]. However due to the lack of power supply during the winter time since 2005, the first solar neutron telescope (36m^2) has not been operated.

From 2008 to 2009, we have decided to make a new solar neutron telescope to utilize the large amount of the plastic scintillator (0.5m^3), as shown in Fig.3, left at the observatory.

The new solar neutron telescope with use of the recycled plastic scintillator consists of main target where neutrons are converted into protons and of the anti-counters surrounding the target. The signals of neutrons converted into protons are observed by using one photomultiplier from bottom side to reduce the electric power. Furthermore a lead plate with the thickness of 1cm is located over the target and the lead plate is sandwiched by two layers of the plastic scintillator to identify gamma-rays from neutrons.

The new solar neutron telescope has a function to reject charged particles with an efficiency of 90%. Therefore the new solar neutron telescope has capability of 1/3 of the 64m^2 large solar neutron telescope located at the same place. We are waiting large solar flares over our detectors.



Fig. 3. 0.5-m^2 plastic scintillation counter for a new neutron telescope.

In addition to the long-term cosmic-ray observations mentioned above, various kinds of short-dated experiments are carried out every year taking an advantage of the high altitude of the observatory.

High-energy radiations from thunderstorms have been observed by flight measurement, high-mountain observations and ground-based measurement. There are two types of those radiations associated with thunderstorms. One is short-duration radiations with duration of 1 ms or less. The other is long-duration emissions lasting for a few seconds to a few minutes, or a few tens of minutes on rare occasions. It is believed that both emissions originate from electrons accelerated in strong electric fields formed in lightning and thunderclouds. However, compared with the former, the latter has remained less understood due to lack of a large sample of observations.

To investigate production mechanism of long-duration emissions and the relevant electron acceleration, we installed at Norikura Cosmic-ray Observatory a radiation detection system and environmental sensors to measure light and electric fields during 2008–2010. The radiation system consists of a spherical NaI scintillator and a thin plastic scintillator that is placed just above the NaI counter. During the period, the system detected one long-duration bursts as well as five short-duration events.

Fig. 4 (top) shows the long-duration event observed during thunderstorms on 2008 September 20th [25]. The event lasted for 90 sec. Fig.4 (bottom) represents an observed photon spectrum extending from 10 keV to 10 MeV. This indicates that electrons can be accelerated to at least 10 MeV in a quasi-stable thundercloud electric field. In addition, we compared the observed spectrum with model ones, and concluded that a gamma-ray source is located 60 m–130 m (at 90% confidence level) apart from our detector. Given these results, the observed emission was found to consist of not only gamma rays but also electrons. This was the first simultaneous observation of gamma rays and electrons in long-duration bursts.

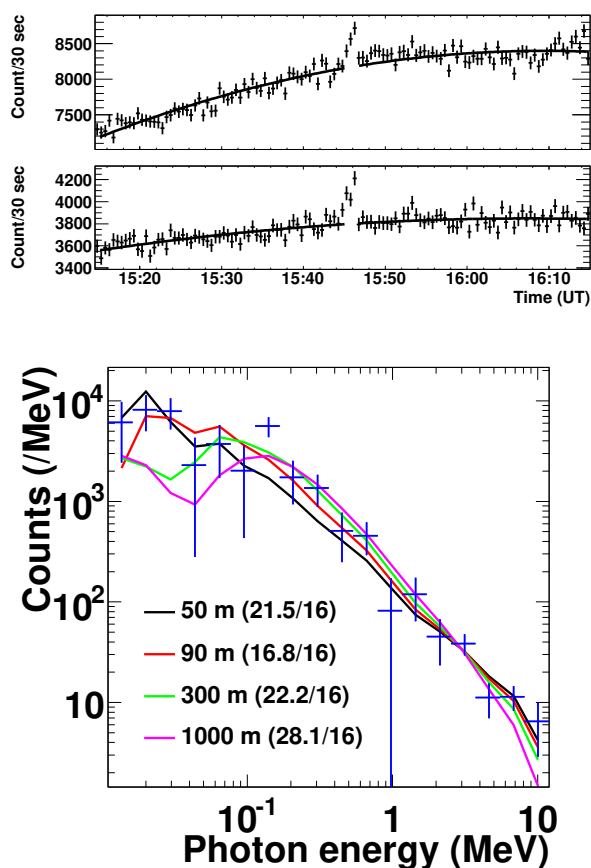


Fig. 4. (Top) Count rates per 30 sec observed by the >10 keV NaI scintillator (upper) and >100 keV plastic one (lower). (Bottom) The photon spectrum observed by the NaI scintillator.

Observation of night sky background is carried out at Mt. Norikura for basic study of ultra high energy cosmic-ray physics.

The JEM-EUSO mission is going on in order to study ultra high energy cosmic rays (UHECRs), especially above 10^{20} eV. A 2.5m telescope with 60° FoV will be attached to the International Space Station in 2017 and detect fluorescence in near UV band from extensive air showers induced by UHECRs. Observation of UHECRs from a satellite orbit has not been done yet, so that the knowledge of background light intensity is important to realize the observation. We have measured it from a balloon altitude, but the opportunity is limited. We started the background measurement at Mt. Norikura. Two 1 inch multi-anode photomultipliers (MAPMTs) developed for EUSO was used with UV filters. The center wavelengths of the filters were 337, 350, 358, 370, 380, 391, 400nm with 10nm band width. In addition BG3 filter was used to detect light in wider range from 330nm to 430nm. The MAPMTs were collimated to 7° FoV. The data was taken with the photon counting method.

We have observed several nights for three years. The intensity at zenith was almost constant at 600-800 photons/ns \sim sr m 2 for BG3 filter. The spectral intensity was about 1.5-2 times larger than those measured at La Palma and Namibia. The estimated portion of star light and zodiacal light was $\sim 30\%$ and artificial light and nightglow at upper atmosphere may be the main components at Mt. Norikura.

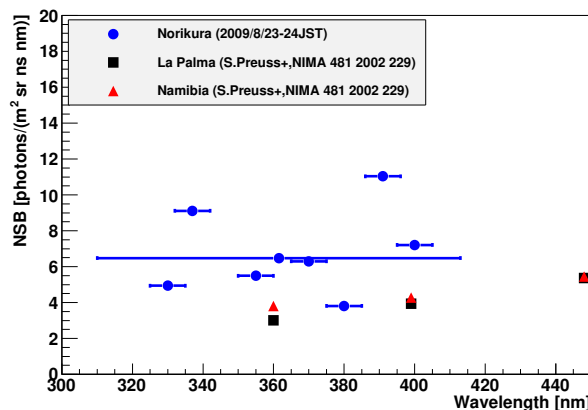


Fig. 5. Spectrum of night sky background measured at Mt. Norikura compared with those at La Palma and Namibia.

Environmental Study

One of the interesting topics is atmospheric environment especially relating with atmospheric aerosol particles and water soluble gases. The cosmic ray observatory at Mt. Norikura provides us very unique opportunity for the observations of atmosphere at free-tropospheric conditions with its high altitude, AC power supply at the site, accommodation facility, and easy accessibility. From year 2000 to 2007, we conducted continuous monitoring (mostly mid-May to mid-October) of meteorological parameters, number-size distribution of aerosols, aerosol chemical composition, ozone and radon concentrations, and column amount of aerosols from sky radiometer and ceilometers. We also collected rain, fog, water-condensed aerosol samples. These samples combined with other observed parameters were used in publications in the following subjects [26, 27, 28]:

- (1) Polluted air pumping effects over central Japanese Alps in summer
- (2) Seasonal variation of aerosol chemistry in free troposphere
- (3) Vertical profiles of aerosols and clouds near the top of the atmospheric boundary layer.

Ceilometer (lidar with small output energy) was installed in summer 2002, and was operated in 6 summer seasons. The aerosol and cloud profiles near the top of the atmospheric boundary layer have been observed. Some events of Asian dust were detected.

Observations of total ozone and UV solar radiation with Brewer spectrophotometer on the Norikura mountains are also made [29, 30, 31].

Aerological Observatory started "Observations of total ozone and UV solar radiation with Brewer spectrophotometer at Norikura mountains" as a joint project with Institute for Cosmic Ray Research (ICRR), University of Tokyo at the Norikura Observatory of ICRR (Brewer site: 36.11 N, 137.56 E, 2,772 m a.s.l.), locating at the Northern Japanese Alps in every summer seasons from 2009 (Ito *et al.*: 2011). Purpose of this study is based on the concept of developing Regional Brewer Calibration Centre in Asia and study of total ozone, total sulfur oxide and global/diffuse UV included solar radiation on the high mountains. Observation results by using Brewer spectrophotometers and other instruments for the observation period of three summer seasons of recent three years between 2009 to 2011 are summarized as follows;

- (1) Daily means of ds O $_3$ (total ozone) at Norikura for the obser-

vation periods were approx. 280 to 290 m atm-cm and were running on the lower values of approx. -3 to -6% compared to the value at Tsukuba (36.06 N, 140.13 E, 39 m a.s.l.) at almost same latitude. Day-to-day variations at Norikura were also small against Tsukuba. On the other hand, daily mean of ds SO₂ (total sulfur oxide) values were not recognized at Norikura.

(2) Absolute calibration of Brewers for ds O₃ and ds SO₂ observations could be carried out within the range of air mass from 7.928 (maximum) to 1.028 (minimum) at Norikura in the clear day. O₃ and SO₂ Extra-Terrestrial Coefficients (=ETC) of Brewers could be produced as about 10 samples satisfying the condition of " $R^2 > 0.9997$ " by the calibrations. As an example of the calibration in 2011, the average of O₃ ETC of Brewers was identical within 1% to the currently used coefficient.

(3) In comparison to the data acquired at Tsukuba, the average of daily total GL_{UV} (global UV, e.g. CIE) for the observation periods indicated the intensities of approx. +23 % in 2009 to -6 % in 2011. The low intensity in 2011 was due to the bad weather on the Norikura Mountain. In the case of clear days, the GL_{UV} at Norikura indicated high intensities of approx. +35 to +52 % against the values at Tsukuba. On the other hand, the GL_{UV} increased in the short wavelength range at Norikura against the average at Tsukuba. The altitudinal increasing rate of GL_{UV} in the clear day indicated the calculated amounts of approx. +13 to +18 % per 1,000 m.

This joint project had been clarifying the low total O₃, high UV in clear day, low turbidity and etc. at Norikura against the value at Tsukuba. Those environmental conditions are useful for the inter-comparison and the absolute calibrations with Brewers. The continuous observations with Brewers and other instrument are very important for the clarification of the seasonal variation and the coefficient trends.

Botanical Study

Effects of snow cover on pine shrub *Pinus pumila* in the alpine region of Mt. Norikura

High mountainous habit is one of the most severe habits for plant life and sometimes dwarf shrubs cannot survive. In the alpine regions of Japan, the dwarf shrub *Pinus pumila* (Japanese name : Haimatsu) forms communities together with small alpine plants, whereas dwarf shrubs occur only in the transition zone between the alpine region and the subalpine forest in Europe and North America. This characteristic of alpine vegetation is considered to be owing to winter heavy snow in the alpine regions of Japan. The purpose of this study is to elucidate how snow cover protects Haimatsu from winter environmental stresses in the alpine region of Mt. Norikura.

Study site

Tree height of Haimatsu and snow depth differ greatly as a result of slight difference in topography. Two site of the study area were selected. (i) site P (wind-protected) and (ii) site E (wind-exposed). At site P, mean tree height was 1.1 m. There was a lot of snow accumulation and Haimatsu was almost entirely covered with snow during the winter. Needle browning and death occurred rarely. At site E, mean tree height was 0.4 m. Snow accumulation was minimal, and Haimatsu was not entirely covered with snow. Needle browning and death was observed frequently.

Winter needle death in Haimatsu[32]

At site E, the browning and death of needles of Haimatsu occurred mainly in early spring at the point where the shoot protrudes from the snowpack. They are thought to be caused by excessive wa-

ter loss due to mechanical damage to the cuticle and/or to a thinner cuticle. However, needle browning and death in Haimatsu were not related to mechanical damage of the cuticle but might be due to changes in the quality and structure of the cuticle wax and resultant increase in water loss from needle cells.

Photosynthetic capacity in Haimatsu[33]

At site E, needles of Haimatsu had lower biomass, nitrogen, Rubisco (enzyme) and cell wall per unit area, and had higher photosynthetic capacity and shorter needle life-span than Haimatsu at site P. These results suggest that Haimatsu at wind-exposed site produces needles at low cost with high productivity to compensate for a short leaf life-span which may be imposed by wind stress when needles appear above the snow surface in winter.

Bibliography

- [1] K. Munakata, S. Yasue, C. Kato, J. Kota, M. Tokumaru, M. Kojima, A. A. Darwish, T. Kuwabara and J. W. Bieber, "On the cross-field diffusion of galactic cosmic rays into the magnetic flux rope of a CME", *Advances in Geosciences*, 2, 115-124, eds. W. H. Ip and M. Duldig (World Scientific Publishing Co., USA), (2006).
- [2] T. Kuwabara, J. W. Bieber, J. Clem, P. Evenson, R. Pyle, K. Munakata, S. Yasue, C. Kato, S. Akahane, M. Koyama, Z. Fujii, M. L. Duldig, J. E. Humble, M. R. Silva, N. B. Trivedi, W. D. Gonzalez and N. J. Schuch, "Real-time cosmic ray monitoring system for space weather", *Space Weather*, 4, S08001-1 10, (2006).
- [3] M. R. Da Silva, A. Dal Lago, E. Echer, A. de Lucas, W. D. Gonzalez, N. J. Schuch, K. Munakata, L. E. A. Vieira, and F. L. Guarnieri, "Muon and neutron observations in connection with the corotating interaction regions", *Adv. Space Res.*, 40, pp348-352, (2007).
- [4] Y. Okazaki, A. Fushishita, T. Narumi, C. Kato, S. Yasue, T. Kuwabara, J. W. Bieber, P. Evenson, M. R. Da Silva, A. Dal Lago, N. J. Schuch, Z. Fujii, M. L. Duldig, J. E. Humble, I. Sabbah, J. Kóta and K. Munakata, "Drift effects and the cosmic ray density gradient in a solar rotation period: First observation with the Global Muon Detector Network (GMDN)", *Astrophys. J.*, 681, 693-707, (2008).
- [5] T. Kuwabara, J. W. Bieber, P. Evenson, K. Munakata, S. Yasue, C. Kato, A. Fushishita, M. Tokumaru, M. L. Duldig, J. E. Humble, M. R. Silva, A. Dal Lago, and N. J. Schuch, "Determination of ICME Geometry and Orientation from Ground Based Observations of Galactic Cosmic Rays", *J. Geophys. Res.*, 114, A05109-1 10, doi:10.1029/2008JA013717, (2009).
- [6] A. Fushishita, T. Kuwabara, C. Kato, S. Yasue, J. W. Bieber, P. Evenson, M. R. Da Silva, A. Dal Lago, N. J. Schuch, M. Tokumaru, M. L. Duldig, J. E. Humble, I. Sabbah, H. K. Al Jassar, M. M. Sharma, and K. Munakata, "Precursors of the Forbush Decrease on 2006 December 14 observed with the Global Muon Detector Network (GMDN)", *Astrophys. J.*, 715, 1239-1247, (2010).
- [7] A. Fushishita, Y. Okazaki, T. Narumi, C. Kato, S. Yasue, T. Kuwabara, J. W. Bieber, P. Evenson, M. R. Da Silva, A. Dal Lago, N. J. Schuch, M. Tokumaru, M. L. Duldig, J. E. Humble, I. Sabbah, J. Kóta, and K. Munakata, "Drift effects and the average features of cosmic ray density gradient in CIRs during successive two solar minimum periods", *Advances in Geosciences*, eds. W. H. Ip and M. Duldig (World Scientific Publishing Co., USA), 21, 199-210, (2010).

- [8] M. Tokumaru, M. Kojima, K. Fujiki, K. Munakata, T. Kuwabara and K. Marubashi, "Relation between loop-shaped interplanetary disturbances and the magnetic flux rope", *Advances in Geosciences*, eds. W. H. Ip and M. Duldig (World Scientific Publishing Co., USA), 21, 21-32, (2010).
- [9] M. Rockenbach, A. Dal Lago, W. D. Gonzalez, K. Munakata, C. Kato, T. Kuwabara, J. W. Bieber, N. J. Schuch, M. L. Duldig, J. E. Humble, H. K. Al Jassar, M. M. Sharma, and I. Sabbah, "Geomagnetic Storms Precursors Observed from 2001 to 2007 with the Global Muon Detector Network GMDN", *Geophys. Res. Lett.*, 38, L16108-1 4, doi:10.1029/2011GL048556, (2011).
- [10] "Solar neutron events of October-November 2003", Watanabe, K. *et al.*, *Astrophys. J.*, **636**, 1135–1144, 2006.
- [11] "Solar neutron events in association with large solar flares in November 2003", Watanabe, K. *et al.*, *Adv. Space Res.*, **38**, 425–430, 2006.
- [12] "Long-lived solar neutron emission in comparison with electron-produced radiation in the 2005 September 7 solar flare", Sako, T. *et al.*, *Astrophys. J.*, **651**, L69–L72, 2006.
- [13] "Highly significant detection of solar neutrons on 2005 September 7", Watanabe, K. *et al.*, *Adv. Space Res.*, **39**, 1462–1466, 2007.
- [14] "A solar neutron telescope in Tibet and its capability examined by the 1998 November 28th event", Muraki, Y. *et al.*, *Astroparticle Phys.*, **28**, 119–131, 2007.
- [15] "Simultaneous detection of high-energy solar neutrons and protons at Chacaltaya observatory on April 15, 2001", Muraki, Y. *et al.*, in Proc. 30th Int. Cosmic Ray Conf, Merida, **1**, 25–28, 2007.
- [16] "Search for solar neutrons associated with series of X-class flares during the declining period of solar cycle 23", Matsubara, Y. *et al.*, in Proc. 30th Int. Cosmic Ray Conf, Merida, **1**, 29–32, 2007.
- [17] "Ion acceleration and neutral emission mechanisms for 2005 September 7 flare", Watanabe, K. *et al.*, in Proc. 30th Int. Cosmic Ray Conf, Merida, **1**, 45–48, 2007.
- [18] "Emission profile of solar neutrons obtained from the ground-based observations for the 7 September 2005 event", Sako, T. *et al.*, in Proc. 30th Int. Cosmic Ray Conf, Merida, **1**, 53–56, 2007.
- [19] "Energy spectrum for the solar neutron event of September 7 2005, derived from the SNT at Sierra Negra", Gonzalez, L. X. *et al.*, in Proc. 30th Int. Cosmic Ray Conf, Merida, **1**, 57–60, 2007.
- [20] "Status of the world-wide network of solar neutron telescopes in solar cycle 24", Matsubara, Y. *et al.*, in Proc. 31st Int. Cosmic Ray Conf, Lodz, **1**, On Conference homepage, 2009.
- [21] "Detection of high-energy solar neutrons and protons by ground level detectors on April 15, 2001", Muraki, Y. *et al.*, *Astropart. Phys.*, **29**, 229–242, 2008.
- [22] "Solar neutron events as a tool to study particle acceleration at the Sun", Valdes-Galicia, J. F. *et al.*, *Adv. Space Res.*, **43**, 565–572, 2009.
- [23] "Physics of ion acceleration in the solar flare on 2005 September 7 determines γ -ray and neutron production", Watanabe, K. *et al.*, *Adv. Space Res.*, **44**, 789–793, 2009.
- [24] "Observation of solar neutrons associated with the large flare on 1991 June 4", Muraki, Y. *et al.*, *ApJ*, **400**, L75-L78, 1992.
- [25] "Observation of an energetic radiation burst from mountain-top thunderclouds", H. Tsuchiya *et al.*, *Phys. Rev. Lett.* **102**, 255003 (2009), Citation Index:13.
- [26] Nishita, C., K. Osada, K. Matsunaga, Y. Iwasaka, e, J. *Geophys. Res.*, **113**, D06202, doi:10.1029/2007JD009302, 2008.
"Nucleation mode particles in up-slope valley winds at Mt. Norikura, Japan: implications for the vertical extent of new particle formation events in the lower troposphere", Nishita, C., K. Osada, K. Matsunaga, Y. Iwasaka, J. *Geophys. Res.*, **113**, D06202, doi:10.1029/2007JD009302, 2008.
- [27] "Temporal variation of water-soluble ions of free tropospheric aerosol particles over central Japan", Osada, K., Kido, M., Nishita, C., Matsunaga, K., Iwasaka, Y., Nagatani, M., Nakada, H., *Tellus*, **59B**, 742-754, 2007.
- [28] "Number-size distributions of free tropospheric aerosol particles at Mt. Norikura, Japan: effects of precipitation and air-mass transportation pathways", Nishita, C., K. Osada, K. Matsunaga, Y. Iwasaka, J. *Geophys. Res.*, 112, doi:10.1029/2006JD007969, 2007.
- [29] "Observations of total ozone and UV solar radiation with Brewer spectrophotometers on the Norikura mountains in 2009.", Ito, M., M. Takano, H. Oguri, M. Takita, H. Shimodaira and H. Ishitsuka, *Jour. of the Aerological Observatory*, **69**, 41-54 2011.
- [30] "Observations of total ozone and UV solar radiation with Brewer spectrophotometers on the Norikura mountains, Northern Japanese Alps, from 2009.", Ito, M., S. Shimizu, Y. Noto, T. Shimamura, M. Takano, M. Takita, H. Shimodaira and H. Ishitsuka, The 13th WMO Biennial Brewer Workshop, Beijing, China in 2011, 2011.
- [31] "Total ozone and UV solar radiation with Brewer spectrophotometers at Norikura of Northern Japanese Alps, in recent three years.", Ito, M., S. Shimizu, Y. Noto, T. Shimamura, M. Takita, H. Shimodaira and H. Ishitsuka, *Jour. of the Aerological Observatory*, **70**, in contribution.
- [32] "Needle browning and death in *Pinus pumila* in the alpine region of central Japan were not related to mechanical damage of cuticle and cuticle thickness.", Nakamoto A., Ikeda T., Maruta E., *Can. J. For. Res.* 42, 167-178 (2012).
- [33] "Needle traits of an evergreen, coniferous shrub growing at wind-exposed and protected sites in a mountain region: does *Pinus pumila* produce needles with greater mass per area under wind-stress conditions?", Nagano S., Nakano T., Hikosaka K and Maruta E., *Plant Biology* 11(Suppl.1), 94-100, (2009).

AKENO OBSERVATORY

Introduction

The Akeno Observatory is situated in Akeno of Hokuto-city, 20 km northwest of Kofu and 130 km west of metropolitan Tokyo. The location is at the longitude of 138.5°E and the latitude of 35.8°N . The altitude is ~ 900 m above sea level. It was established in 1977 as a research center for air shower studies in the very high energy region, and it has been administered by the ICRR as a facility of joint-university-use.

Akeno Air Shower Experiments

The Akeno Air Shower Experiment started in 1979 with an array covering 1 km^2 area (the 1 km^2 array, see Fig.1). The array was enlarged to 20 km^2 in 1984 and was gradually expanded to Akeno Giant Air Shower Array (AGASA) of approximately 100 km^2 area by 1990. The AGASA was built



Fig. 1. Aerial View of Akeno Observatory and 1 km^2 Array Area

to detect Ultra-High Energy Cosmic Rays (UHECRs) in the energy range of 10^{20} eV.

One of the distinctive features of Akeno experiments is that the measurements were made over five decades of energies well covering 10^{15} eV - 10^{20} eV by using both the surface detector for electromagnetic component, and the shielded detector for muon component (Fig.2). The wide energy coverage was accomplished by the arrays of scintillation detectors of various inter-detector spacings from 3 m to 1 km and with different triggering conditions. This feature of Akeno air shower measurement is well demonstrated in Fig.3, in which the spectra from Akeno 1 km^2 array for $10^{14.5}$ eV - $10^{18.8}$ eV¹ and AGASA for $10^{18.5}$ eV - $10^{20.3}$ eV² are plotted.

*1 M. Nagano et al., J. Phys. **G10**, 1295 (1984); M. Nagano et al., J. Phys. **G18**, 423 (1992).

*2 M. Takeda et al., Astropart. Phys. **19**, 447 (2003).



Fig. 2. One of the muon detector housings with concrete shielding.

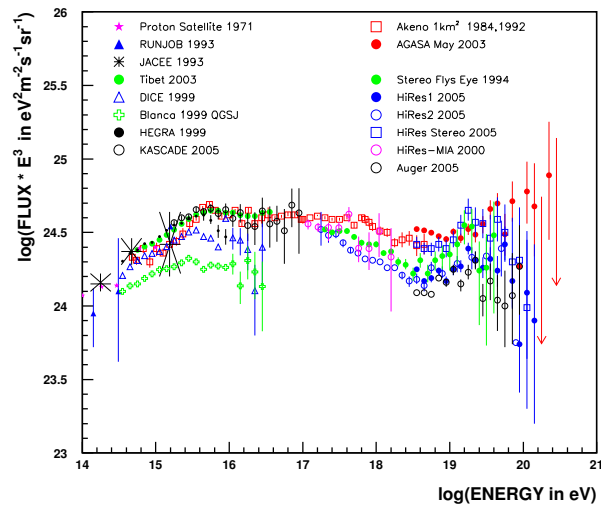


Fig. 3. Akeno energy spectrum measurements for 10^{15} eV - 10^{20} eV.

AGASA

The AGASA was composed of 111 surface detectors, each with plastic scintillator of 2.2 m^2 area and 5 cm thickness. The counters were deployed with ~ 1 km spacing covering the ground area of about 100 km^2 in the suburban area of Akeno, outside of the observatory campus. All counters were connected with optical fibers for the timing measurement and digital data transfer to the observatory. The AGASA served as the largest air shower array in the world since its commissioning in 1990 until it stopped data taking in January 2004, when the construction of the succeeding experiment, Telescope Array (TA), started in Utah. It was dismantled in 2007 together with other Akeno air shower arrays.

An exposure of $5.8 \times 10^{16}\text{ m}^2\text{ s sr}$ above 10^{19} eV was

accumulated by AGASA in 13 years of operation. Extensive air showers with zenith angles smaller than 45° and with core locations inside the array area were used for the analysis. The AGASA reported an extension of the energy spectrum beyond the predicted Greisen-Zatsepin-Kuzmin (GZK) cutoff in 1998³ and a total of eleven UHECR events were observed above 10^{20} eV by 2003.

Measurement of UHECRs

Since the AGASA measurement in 1998, High Resolution Fly's Eye (HiRes)⁴, Pierre Auger Observatory (PAO)⁵, and Telescope Array (TA)⁶ measured the energy spectra of UHECRs with higher statistics.

The HiRes observed the UHECR using the fluorescence telescope. The PAO and TA measure the spectrum using the surface array consisting of either water tanks (PAO) or plastic scintillators (TA), but the energy scale of the array is determined by the fluorescence telescope using a subset of events observed by the fluorescence telescope and surface array at the same time. The adoption of the energy scale by the fluorescence telescopes is based on its small dependence on the air shower simulation.

The energy spectra above 10^{18} eV by AGASA and other experiments are compiled and compared by the working group represented by UHECR experiments in the UHECR-2012 symposium held at CERN for Feb. 13th - 16th, 2012⁷. The result is plotted in Fig.4 with the energy scale of each experiment adjusted to a reference energy, which is set halfway between the PAO and TA/HiRes. Following factors were applied for the energy scale; $\times 1.10$ for PAO, $\times 0.91$ for TA and HiRes, $\times 0.65$ for AGASA and $\times 0.56$ for Yakutsk.

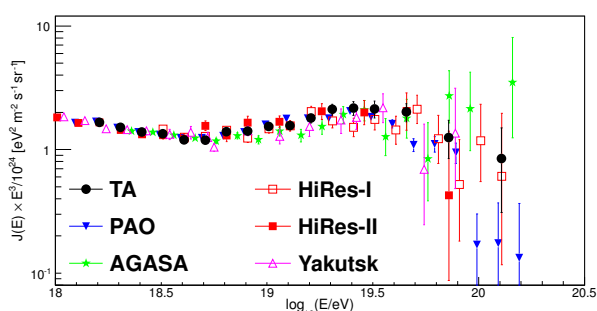


Fig. 4. Recent compilation of UHECR energy spectra. The energy scale of each experiment is adjusted as described in the text.

As seen in Fig.4, the overall agreement between experiments is good, and a “dip” structure was seen around $10^{18.7}$ eV by all experiments. The HiRes, PAO and TA confirmed a strong flux suppression above approximately $10^{19.7}$ eV. Although the AGASA spectrum does not demonstrate the cutoff structure, the number of events above 10^{20} eV became only two after the energy rescaling, making the claim of the extended spectrum statistically insignificant. The estimate of

systematic uncertainty of the energy measurement is approximately 20% for all the experiments, and rescalings for the TA/HiRes and PAO are within this limit. Rescaling of the surface array energy, $\times 0.65$ for AGASA and $\times 0.56$ for Yakutsk, indicates that there exist larger systematic uncertainties than originally estimated by running the air shower simulation. This difference of energy scale obtained by the surface array and by the fluorescence telescope remains as a basic question in the understanding of the air shower phenomena.

Recent Research Activities

The study of UHECRs by AGASA in Akeno was succeeded by the Telescope Array (TA) experiment in Utah, USA since 2008. After the cessation of AGASA, the Akeno Observatory has been used for small scale cosmic ray experiments, astrophysical observations and as a test and maintenance facility of TA by the ICRR and university researchers. Fig.5 shows a recent photograph of the main site of the Akeno Observatory.



Fig. 5. The main site of the Akeno Observatory. There are the movable tent for a small atmospheric Cherenkov telescope, the large experimental hall, the research building and the lodging facility from the left.

Research and development for the Telescope Array observation in Utah by the TA collaboration

All the fluorescence imaging cameras and a part of the surface detectors of TA were assembled in the Akeno Observatory by the TA collaboration team. The detectors were tested in Akeno and shipped to the Utah observation site for the installation. All the unit mirrors of the TA fluorescence telescope were tested in Akeno and the atmospheric monitoring lidar of TA using YAG laser was developed in Akeno. In JFY 2015, the R&D of the surface detectors were performed in the large experimental hall of the Akeno Observatory for the TAx4 project that quadruples the TA surface detector array in Utah.

Research activities in JFY 2015 (April 2015 - March 2016) are described in the following.

Observation by the multi-color imager for transients, survey and monstrous explosions (MITSuME) by N. Kawai (Tokyo Institute of Technology) et al.

One of the three MITSuME robotic telescopes was installed in the Akeno Observatory in 2003 (Fig. 6). The telescope has

*3 M. Takeda et al., Phys. Rev. Lett. **81**, 1163 (1998).

*4 R.U. Abbasi et al., Phys. Rev. Lett. **100**, 101101 (2008).

*5 J. Abraham et al., Phys. Lett. **B685**, 239 (2010).

*6 T. Abu-Zayyad et al., Astrophys. J. **768**, L1 (2013).

*7 <http://indico.cern.ch/conferenceDisplay.py?confId=152124>

an aperture of 50 cm, an FOV of $28' \times 28'$ and is equipped with a tricolor CCD camera capable of $g'R_C I_C$ -bands photometry (g' :400~550 nm, R_C :570~730 nm, I_C :730~850 nm). It is operated remotely from the Tokyo Tech at the Ookayama Campus using dedicated ADSL connections. Upon receiving a GRB alert from Swift or Fermi satellite, it quickly directs the telescope ($9^\circ/s$ maneuverability) toward the GRB direction, and makes a prompt observation of the GRB and its afterglow.

In JFY 2015, 63 GRBs were observed, and seven GRBs were identified as visible objects. The observations of several objects were performed by the MITSuME telescope in Akeno in cooperation with small- and medium-sized telescopes that belong to Japanese universities or NAOJ in or outside Japan as part of "Optical and Infrared Synergetic Telescopes for Education and Research".



Fig. 6. The dome in which the MITSuME telescope was installed in Akeno.

Observation of galactic cosmic rays by large area muon telescope by A. Oshima (Chubu University) et al.

Four layers of proportional counter telescopes, each with 25 m² area, were installed in three muon houses in Akeno (Fig.2) and have been continuously measuring the cosmic ray muons since 2003. The mode energy of the primary cosmic rays is approximately 2.5 GeV corresponding to 2m thick concrete ceiling of the muon house and the latitude of the Akeno Observatory. The measurement in Akeno is combined with a simultaneous measurement by the GRAPES-3 experiment at Ooty in India, and the modulation effects of galactic cosmic rays by the solar activity such as the Forbush decrease and its precursor have been continuously monitored⁸. In JFY 2015, individual proportional counters were checked to identify bad ones for repair. The networks at two of three muon stations were changed from ADSL service to wireless internet, and stable connections to the outside were established.

Research and development for a small atmospheric Cherenkov telescope at the Akeno Observatory by T. Yoshikoshi (ICRR) et al.

A small alt-azimuth telescope is being setup in Akeno for prototype tests with atmospheric Cherenkov observations of

gamma rays⁹. This telescope is the only atmospheric Cherenkov telescope from air showers induced by TeV gamma rays in Japan. In JFY 2015, after the check of the source of the noise in the trigger circuit of the data acquisition system, the noise was reduced by addition high pass filter. And the time resolution of the data acquisition system was improved. In addition, the test of the Central CCD camera for the CTA LST and the test observation of forward radio radiation from air showers were performed using the telescope in Akeno.

A part of the large experimental hall was used for the research on ultra-low frequency anti-vibration system, the assembly of anti-vibration system for PRG3 mirror before the installation in KAGRA, and temporary storage of the KAGRA, Large-scale Cryogenic Gravitational Wave Telescope Project.

Other tests using facilities or detectors in the Akeno Observatory were also performed.

*⁸ T. Nonaka et al, Proc. of the 29th ICRC, **1**, 363-366 (2005).

*⁹ M. Ohishi et al., 33rd ICRC, (Rio de Janeiro), **9**, in press (2013).

KAMIOKA OBSERVATORY

Kamioka observatory is located at 1000 m underground (2700 m water equivalent) in the Kamioka Mine, Gifu prefecture, about 200 km west of Tokyo. The observatory was established in 1995 in order to operate Super-Kamiokande experiment (SK). The underground laboratories are located under Mt. Ikeno-yama and accessible to the experimental site through a 1.7 km horizontal tunnel. The observatory also has surface research buildings and a dormitory located at the distance of 15 minutes drive from the entrance of the underground laboratories.

The Super-Kamiokande experiment had discovered neutrino oscillations through the observations of atmospheric and solar neutrinos (see the section for Neutrino and Astroparticle Division). The atmospheric neutrino oscillation was confirmed by the long baseline neutrino oscillation experiment, K2K, using accelerator neutrino beam, which was conducted between 1999 and 2004. A new long baseline neutrino oscillation experiment (the T2K experiment) using a high intensity beam, 50 times of the K2K neutrino beam, by the J-PARC proton accelerator has started in 2009. In 2011, the experiment has observed 6 ν_e appearance events indicating non-zero θ_{13} which was as yet determined the last neutrino oscillation parameter. Since then, the collaboration accumulated more electron neutrino appearance events and strengthen the discovery of non-zero θ_{13} . Since 2014, anti-neutrino beam data also has been taken in order to search for CP violation.

The low cosmic ray flux and low seismic noise environment in the underground site enables us to conduct various researches. There is a 100 m long laser interferometer, which is a proto-type of the 3 km gravitational wave antenna (KAGRA). Using the low radioactive background environment in the Kamioka Mine, a dark matter experiment, called XMASS is operated in Lab-C. The XMASS group constructed a 800kg liquid xenon detector and started data taking from 2010. The detector has been improved and searches for dark matter interactions and rare phenomena in liquid xenon have been conducted in the last few years. The R&D study of a tracking type detector for dark matter detection led by the Kobe University group (the NEWAGE experiment) has also been performed in Lab-B. A double beta decay experiment using ^{48}Ca (the CANDLES experiment) led by the Osaka University group has been running in Lab-D. The study to improve the neutrino detection sensitivity by adding gadolinium to Super-Kamiokande (called SK-Gd project) has been performed at Lab-E. A 200 ton test tank dedicated for the R&D study of the SK-Gd project was constructed and a feasibility study has been performed. In order to support those experiments and also related R&D works, the Observatory is equipped with low background Germanium detector in Lab-1 and Lab-A, ICP-MS and so on to measure extremely low radioactive backgrounds.

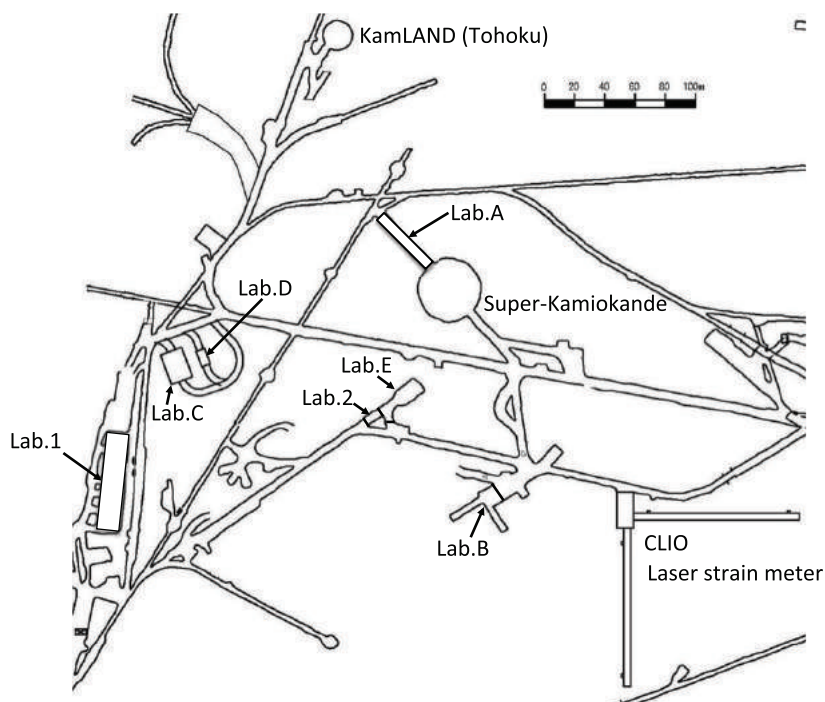


Fig. 1. Kamioka Underground Observatory.

RESEARCH CENTER FOR COSMIC NEUTRINOS

The Research Center for Cosmic Neutrinos (RCCN) was established in April, 1999. The main mission of this center is to promote researches related to neutrinos based on data from various observations and experiments, and we have provided the occasion to discuss theoretical ideas and experimental results on neutrino physics. Members of this center have been involved in the Super-Kamiokande and T2K experiments, and contributing precise measurements of neutrino oscillations. Also we have been involved in the future project, Hyper-Kamiokande, and worked on the calculation of the atmospheric neutrino flux to have better predictions of the neutrino flux.

RCCN, together with the computer committee of ICRR, is in charge of operating the central computer system in ICRR. The computer facility has high performance to analyze huge amount of data, and has been operated without any serious trouble since it was upgraded in 2014. Since 2004, RCCN has been accepted inter-university programs related to activities in the low-background underground facility also. In FY2015, We accepted 5 programs related to these facilities.

RCCN has been organizing domestic neutrino-related workshop since it was established. On February 20, 2016, we hosted one neutrino workshop on Atmospheric Neutrinos in commemoration of Nobel Prize award by Prof. Kajita. Forty physicists participated in this meeting. We have also contributed holding public lectures. Since JFY2009, ICRR and the Kavli Institute for the Physics and Mathematics of the Universe (Kavli-IPMU) have co-sponsored two public lectures each year. The public lecture held in Spring is co-organized by RCCN and the Public Relation Office of ICRR. The Spring public lecture in FY2015 was held on April 18, 2015. Two scientists lectured on the latest cosmology and the gravitational wave detection experiment.

APPENDICES

A. ICRR Workshops and Ceremonies

B. ICRR Seminars

C. List of Publications

- (a) **Papers Published in Journals**
- (b) **Conference Papers**
- (c) **ICRR Report**

D. Doctoral Theses

E. Public Relations

- (a) **ICRR News**
- (b) **Public Lectures**
- (c) **Visitors**

F. Inter-University Research Activities

G. List of Committee Members

- (a) **Board of Councillors**
- (b) **Advisory Committee**
- (c) **User's Committee**

H. List of Personnel

A. ICRR Workshops and Ceremonies

TeV Particle Astrophysics(TeVPA) 2015

Date: October 26-30, 2015

Place: Kashiwa-no-ha Conference Center

Outline: This 5-day conference aimed to provide the stage for the most recent advances in the booming field of Astroparticle Physics, bringing leading members of the scientific communities that are contributing to its success.

Participants: 169 participants.

Celebration party for Professor Takaaki Kajita's Nobel Prize in Physics

Date: November 14, 2015

Place: ANA Crowne Plaza Hotel Toyama, Japan

Outline: This party was held for the celebration of Professor Takaaki Kajita's Nobel Prize and for the gratitude for people concerned with Super-Kamiokande and local community, and organized by Super-Kamiokande collaboration.

Participants: 315 participants.

The extreme Universe viewed in very-high-energy gamma rays 2015

Date: January 13-14, 2015

Place: Media Hall, Kashiwa Library, the University of Tokyo

Outline: Including the report of JSPS Specially Promoted Research "study of the Extreme Universe with High Energy Gamma Rays," this workshop widely invited the talks on high-energy astrophysics, and provided the place of discussions about various topics.

Participants: 68 participants.

B. ICRR Seminars

1. May 7, 2015: Sadakazu Haino (Institute of Physics, Academia Sinica), "The new results from Alpha Magnetic Spectrometer (AMS) "
2. May 27, 2015: Roger Wendell (ICRR), " Antineutrino Results from T2K "
3. Jul 29, 2015: Yoshihiko Oyama (ICRR), " Constraints on the neutrino mass by future precise CMB polarization and 21cm line observations "
4. Aug 6, 2015: Tomohiro Abe (KEK), " Spin-1 particle and the ATLAS Diboson excess "
5. Aug 18, 2015: K.S. Cheng (The University of Hong Kong), " Possible high energy phenomena related to the stellar capture by the galactic supermassive black holes "
6. Sep 16, 2015: Tanguy Pierog (Karlsruhe Institute of Technology, Institute for Nuclear Physics), " Recent results from Auger and KASKADE-Grande, and introduction to the CORSIKA air shower simulation code "
7. Oct 28, 2015: Dijana Dominis Prester (University of Rijeka), " Gravitational lensing effect in observational astrophysics"
8. Nov 25, 2015: Masaki Fukushima (ICRR), " Ultra-high energy cosmic rays: status and prospects in 2015"
9. Dec 2, 2015: Michal Ostrowski (Jagiellonian University), " Selected scientific topics studied in high, medium and low frequency electromagnetic waves "
10. Dec 9, 2015: Yosui Akaike (Waseda University), " CALET: direct cosmic ray measurements on the International Space Station. "
11. Jan 13, 2016: Toshinori Matsui (Toyama University), " Gravitational waves as a probe of extended scalar sectors with the first order electroweak phase transition "
12. Feb 8, 2016: Pravata Mohanty (Tata Institute), " Cosmic Ray Studies with GRAPES-3 Experiment "
13. Feb 22, 2016: Hiroaki Yamamoto (LIGO), " Observation of Gravitational Waves from a Binary Black Hole Merger (in Japanese) "
14. Feb 24, 2016: Kouichi Hirotani (Academia Sinica Institute for Astronomy & Astrophysics, Taiwan), " Energetic Gamma Radiation from Rapidly Rotating Black Holes "
15. Mar 16, 2016: Carlos Delgado (CIEMAT, Madrid and ICRR), " A review of AMS-02 and its results after nearly 5 years of operation. "
16. Mar 23, 2016: Toshio Terasawa (ICRR), " Study of Cosmic Nonthermal/Transient Phenomena (in Japanese) "

C. List of Publications

(a) Papers Published in Journals

1. "Search for Neutrinos from Annihilation of Captured Low-Mass Dark Matter Particles in the Sun by Super-Kamiokande", K. Choi et al. (Super-Kamiokande Collaboration), *Phys. Rev. Lett.* **114**, 141301.
2. "Search for n - \bar{n} oscillation in Super-Kamiokande", K. Abe et al. (The Super-Kamiokande Collaboration), *Phys. Rev. D* **91**, 072006 (2015).
3. "Search for Nucleon and DiNucleon Decays with an Invisible Particle and a Charged Lepton in the Final State at the Super-Kamiokande Experiment", V. Takhistov et al. (The Super-Kamiokande Collaboration), *Phys. Rev. Lett.* **115**, 121803.
4. "First measurement of radioactive isotope production through cosmic-ray muon spallation in Super-Kamiokande IV", Y. Zhang et al. (Super-Kamiokande Collaboration), *Phys. Rev. D* **93**, 012004 (2016).

5. "Measurement of the $\nu \mu$ charged-current quasielastic cross section on carbon with the ND280 detector at T2K", K. Abe et al. (T2K Collaboration), *Phys. Rev. D* **92**, 112003 (2015).
6. "Neutrino oscillation physics potential of the T2K experiment", K. Abe et al. (T2K Collaboration), *Prog. Theor. Exp. Phys.* (2015) **043C01**.
7. "Measurements of neutrino oscillation in appearance and disappearance channels by the T2K experiment with $6.6E20$ protons on target", K. Abe et al. (T2K Collaboration), *Phys. Rev. D* **91**, 072010.
8. "Measurement of the $\nu \mu$ charged current quasielastic cross section on carbon with the T2K on-axis neutrino beam", K. Abe et al. (The T2K Collaboration), *Phys. Rev. D* **91**, 112002.
9. "Measurement of the electron neutrino charged-current interaction rate on water with the T2K ND280 π^0 detector", K. Abe et al. (T2K Collaboration), *Phys. Rev. D* **91**, 112010.
10. "Upper bound on neutrino mass based on T2K neutrino timing measurements", K. Abe et al. (T2K Collaboration), *Phys. Rev. D* **93**, 012006.
11. "Search for dinucleon decay into pions at Super-Kamiokande", J. Gustafson et al. (Super-Kamiokande Collaboration), *Phys. Rev. D* **91**, 072009.
12. "Direction-sensitive dark matter search with gaseous tracking detector NEWAGE-0.3b", Kiseki Nakamura, Kentaro Miuchi, Toru Tanimori, Hidetoshi Kubo, Atsushi Takada, Joseph D. Parker, Tetsuya Mizumoto, Yoshitaka Mizumura, Hironobu Nishimura, Hiroyuki Sekiya, Atsushi Takeda, Tatsuya Sawano, Yoshihiro Matsuoka, Shotaro Komura, Yushiro Yamaguchi and Takashi Hashimoto, *Prog. Theor. Exp. Phys.* (2015) **043F01**.
13. "Recent progress and future prospects with atmospheric neutrinos", Roger Wendell and Kimihiro Okumura, *New J. Phys.* **17** (2015) 025006.
14. "Evaluation of Photo Multiplier Tube candidates for the Cherenkov Telescope Array", R. Mirzoyan, D. Müller, Y. Hanabata, J. Hose, U. Menzel, D. Nakajima, M. Takahashi, M. Teshima, T. Toyama, T. Yamamoto, *NUCL INSTRUM METH A*.
15. "MAGIC detection of short-term variability of the high-peaked BL Lac object 1ES 0806+524", J. Aleksić et al., *Mon.Not.Roy.Astron.Soc.* **451**(2015),no1, 739-750.
16. "Evaluation of the basic properties of the novel 1.5 in. size PMTs from Hamamatsu Photonics and Electron Tubes Enterprises", T. Toyama, Y. Hanabata, J. Hose, U. Menzel, R. Mirzoyan, D. Nakajima, M. Takahashi, M. Teshima, T. Yamamoto, *NUCL INSTRUM METH A*, Volume **787**, 1 July 2015, Pages 280-283.
17. "Very high-energy γ -ray observations of novae and dwarf novae with the MAGIC telescopes", M. L. Ahnen et al., *Astronomy and Astrophysics*, **582**, A67.
18. "FIRST NuSTAR OBSERVATIONS OF MRK 501 WITHIN A RADIO TO TeV MULTI-INSTRUMENT CAMPAIGN", A. Furniss et al., *Astrophysical Journal*, **812**, 65.
19. "VERY HIGH ENERGY γ -RAYS FROM THE UNIVERSE'S MIDDLE AGE: DETECTION OF THE $z = 0.940$ BLAZAR PKS 1441+25 WITH MAGIC", M. L. Ahnen et al., *Astrophysical Journal Letters*, **815**, no2, L23.
20. "The major upgrade of the MAGIC telescopes, Part I: The hardware improvements and the commissioning of the system", J. Aleksić et al., *Astroparticle Physics*, **72**, 1 p61-75.
21. "Development of a low-cost-high-sensitivity Compton camera using CsI(Tl) scintillators(γ I)", M.Kagaya, H.Katagiri, R.Enomoto, et al., *NIM A* **804**(2015) 25-32.
22. "Study of Ultra-High Energy Cosmic Ray composition using Telescope Array's Middle Drum detector and surface array in hybrid mode", R.U. Abbasi et al. (TA collaboration), *Astroparticle Physics* **64** (2015) 49-62.
23. "A NORTHERN SKY SURVEY FOR POINT-LIKE SOURCES OF EeV NEUTRAL PARTICLES WITH THE TELESCOPE ARRAY EXPERIMENT", R.U. Abbasi et al. (Telescope Array Collaboration), *The Astrophysical Journal*, **804**:133 (11pp), 2015.
24. "Measurement of the proton-air cross section with Telescope Array's Middle Drum detector and surface array in hybrid mode", R.U. Abbasi et al. (Telescope Array Collaboration), *Physical Review D* **92**, 032007 (2015).

25. "Simulations of Ultra High Energy Cosmic Rays Propagation", O.E. Kalashev and E. Kido, *Journal of Experimental and Theoretical Physics*, 2015, Vol. **120**, No. 5, pp. 790-797.
26. "SEARCH FOR GAMMA RAYS ABOVE 100 TeV FROM THE CRAB NEBULA WITH THE TIBET AIR SHOWER ARRAY AND THE 100 m^2 MUON DETECTOR", M. Amenomori, X. J. Bi, D. Chen, T. L. Chen, W. Y. Chen, S. W. Cui, Danzengluobu, L. K. Ding, C. F. Feng, Zhaoyang Feng, 2015 *APJ*, **813**, 98.
27. "Performance of the Tibet hybrid experiment (YAC-II + Tibet-III + MD) to measure the energy spectra of the light primary cosmic rays at energies 50 - 10,000 TeV", J. Huang et al., *Astroparticle Physics* **66** (2015) 18-30.
28. "Sensitivity of YAC to measure the light-component spectrum of primary cosmic rays at the knee energies", L M Zhai et al., *J. Phys. G: Nucl. Part. Phys.* **42** (2015) 045201 (14pp).
29. "Avalanche Photon Cooling by Induced Compton Scattering: Higher-Order Kompaneets Equation", Shuta J. Tanaka, Katsuaki Asano, Toshio Terasawa, *PTEP* (2015) **073E01**.
30. "Stochastic Acceleration Model of Gamma-Ray Burst with Decaying Turbulence", Katsuaki Asano, and Toshio Terasawa, *Mon.Not.Roy.Astron.Soc.* **454** (2015) no.2, 2242-2248.
31. "Time-Dependent Stochastic Acceleration Model for the Fermi Bubbles", Kento Sasaki, Katsuaki Asano and Toshio Terasawa, 2015 *APJ*, **814**, 93.
32. "The Most Intensive Gamma-Ray Flare of Quasar 3C 279 with the Second-Order Fermi Acceleration", Katsuaki Asano and Masaaki Hayashida, *Astrophys.J.* **808** (2015) no.1, L18.
33. "The inauguration ceremony of the KAGRA facility", Keiko Kokeyama and Masatake Ohashi, *AAPPS Bulletin*, Vol. **26** No. 1, pp. 32,.
34. "New method to measure the angular antispring effect in a Fabry-Perot cavity with remote excitation using radiation pressure", Koji Nagano, Yutaro Enomoto, Masayuki Nakano, Akira Furusawa, Seiji Kawamura, *Phys. Lett. A* **380**, 983-988, 2016.
35. "Morphologies of $\sim 190,000$ Galaxies at $z=0-10$ Revealed with HST Legacy Data I. Size Evolution", Takatoshi Shibuya, Masami Ouchi, Yuichi Harikane, *APJS*, 2015, **219**.15(20pp).
36. "A Case Comparison between Observed and modeled Ly α Lines for $z\sim 2.2$ Lyman Alpha Emitters", Takuya Hashimoto, Anne Verhamme, Masami Ouchi, Kazuhiro Shimasaku, Daniel Schaerer, Kimihiko Nakajima, Takatoshi Shibuya, Michael Rauch, Yoshiaki Ono, Ryosuke Goto, *Astrophys.J.* **812** (2015) no.2, 157.
37. "Physical conditions of the interstellar medium in star-forming galaxies at $z\sim 1.5$ ", Masao Hayashi, Chun Ly, Kazuhiro Shimasaku, Kentaro Motohara, Matthew A. Malkan, Tohru Nagao, Nobunari Kashikawa, Ryosuke Goto, Yoshiaki Naito, *Publ Astron Soc Jpn* (October 2015) **67** (5): 80.
38. "Thirty Meter Telescope Detailed Science Case: 2015", TMT International Science Development Teams & TMT Science Advisory Committee, *Research in Astronomy and Astrophysics*, Vol. **15**, No.12.
39. "Deep rest-frame far-UV spectroscopy of the giant Lyman-alpha emitter 'Himiko'", J. Zabl, H. U. Nørgaard-Nielsen, J. P. U. Fynbo, P. Laursen, M. Ouchi, P. Kjærgaard, *MNRAS* (August 01, 2015) **451** (2): 2050-2070.
40. "ALMA Census of Faint 1.2 mm Sources Down to ~ 0.01 mJy: Extragalactic Background Light and Dust-Poor High- z Galaxies", Seiji Fujimoto, Masami Ouchi, Yoshiaki Ono, Takatoshi Shibuya, Masafumi Ishigaki, Rieko Momose, *The Astrophysical Journal Supplement Series*, Volume **222**, Number 1.
41. "The Subaru-XMM-Newton Deep Survey (SXDS) VIII.: Multi-wavelength Identification, Optical/NIR Spectroscopic Properties, and Photometric Redshifts of X-ray Sources", M. Akiyama, et al., *Publ Astron Soc Jpn* (October 2015) **67** (5): 82.
42. "Evolution of Star Formation in the UKIDSS Ultra Deep Survey Field - II. Star Formation as a Function of Stellar Mass Between $z=1.46$ and $z=0.63$ ", Alyssa B. Drake, Chris Simpson, Ivan K. Baldry, Phil A. James, Chris A. Collins, Masami Ouchi, Suraphong Yuma, James S. Dunlop, Daniel J. B. Smith, *Mon.Not.Roy.Astron.Soc.* **454** (2015) no.2, 2015-2025.
43. "Statistical Properties of Diffuse Lyman-alpha Halos around Star-forming Galaxies at $z\sim 2$ ", Rieko Momose, Masami Ouchi, Kimihiko Nakajima, Yoshiaki Ono, Takatoshi Shibuya, Kazuhiro Shimasaku, Suraphong Yuma, Masao Mori, Masayuki Umemura, *MNRAS* (April 11, 2016) **457** (3): 2318-2330.

44. "An extremely dense group of massive galaxies at the centre of the protocluster at $z = 3.09$ in the SSA22 field", M. Kubo, T. Yamada, T. Ichikawa, M. Kajisawa, Y. Matsuda, I. Tanaka, H. Umehata, *MNRAS*, **455**, 3333-3344 (2016).
45. "Precise Strong Lensing Mass Modeling of Four Hubble Frontier Fields Clusters and a Sample of Magnified High-Redshift Galaxies", Ryota Kawamata, Masamune Oguri, Masafumi Ishigaki, Kazuhiro Shimasaku, Masami Ouchi, 2016 *ApJ* **819** 114.
46. "ALMA Deep Field in SSA22: A concentration of dusty starbursts in a $z=3.09$ protocluster core", H. Umehata, Y. Tamura, K. Kohno, R. J. Ivison, D. M. Alexander, J. Geach, B. Hatsukade, D. H. Hughes, S. Ikarashi, Y. Kato, T. Izumi, R. Kawabe, M. Kubo, M. Lee, B. Lehmer, R. Makiya, Y. Matsuda, K. Nakanishi, T. Saito, I. Smail, T. Yamada, Y. Yamaguchi, M. Yun, 2015 *ApJ* **815** L8 .
47. "Morphologies of $\sim 190,000$ Galaxies at $z=0-10$ Revealed with HST Legacy Data II. Evolution of Clumpy Galaxies", Takatoshi Shibuya, Masami Ouchi, Mariko Kubo, Yuichi Harikane, 2015 *ApJS* **219** 15 .
48. "Physical Properties of Spectroscopically Confirmed Galaxies at $z \geq 6$. III. Stellar Populations from SED Modeling with Secure $L\alpha$ Emission and Redshifts", Jiang, Linhua; Finlator, Kristian; Cohen, Seth H.; Egami, Eiichi; Windhorst, Rogier A.; Fan, Xiaohui; Davé, Romeel; Kashikawa, Nobunari; Mechtley, Matthew; Ouchi, Masami; and 2 coauthors, *The Astrophysical Journal*, Volume **816**, Issue 1, article id. 16, 18 pp. (2016).
49. "On the Diffuse $Ly\alpha$ Halo around $Ly\alpha$ Emitting Galaxies", Lake, Ethan; Zheng, Zheng; Cen, Renyue; Sadoun, Raphael; Momose, Rieko; Ouchi, Masami, *The Astrophysical Journal*, Volume **806**, Issue 1, article id. 46, 10 pp. (2015).
50. "The Sizes of $z \sim 6-8$ Lensed Galaxies from the Hubble Frontier Fields Abell 2744 Data", Kawamata, Ryota; Ishigaki, Masafumi; Shimasaku, Kazuhiro; Oguri, Masamune; Ouchi, Masami, *The Astrophysical Journal*, Volume **804**, Issue 2, article id. 103, 13 pp. (2015).
51. "Large-scale environment of $z \sim 5.7$ C IV absorption systems -II. Spectroscopy of Lyman α emitters", Díaz, C. Gonzalo; Ryan-Weber, Emma V.; Cooke, Jeff; Koyama, Yusei; Ouchi, Masami, *Monthly Notices of the Royal Astronomical Society*, Volume **448**, Issue 2, p.1240-1270.
52. "Seminatural SUSY from E7 Nonlinear Sigma Model", Keisuke Harigaya, Tsutomu T. Yanagida, Norimi Yokozaki, *Theor. Exp. Phys.* 2015, **083B03**.
53. "Indirect Probe of Electroweak-Interacting Particles at Future Lepton Colliders", Keisuke Harigaya, Koji Ichikawa, Anirban Kundu, Shigeki Matsumoto, Satoshi Shirai, *JHEP***09**(2015)105.
54. "Spontaneous thermal Leptogenesis via Majoron oscillation", Masahiro Ibe and Kunio Kaneta, *Phys. Rev. D* **92**, 035019.
55. "Observable dark radiation from cosmologically safe QCD axion", Masahiro Kawasaki, Masaki Yamada, and Tsutomu T. Yanagida, *Phys. Rev. D* **91**, 125018 (2015).
56. "A Model of Visible QCD Axion", Hajime Fukuda, Keisuke Harigaya, Masahiro Ibe, Tsutomu T. Yanagida, *Phys. Rev. D* **92**, 015021 (2015).
57. "Hamiltonian analysis of non-projectable Horava-Lifshitz gravity with U(1) symmetry", Shinji Mukohyama, Ryo Namba, Rio Saitou, Yota Watanabe, *Phys. Rev. D* **92**, 024005 (2015).
58. "Muon $g-2$ in Focus Point SUSY", Keisuke Harigaya, Tsutomu T. Yanagida, and Norimi Yokozaki, *Phys. Rev. D* **92**, 035011.
59. "Charged Q-balls in gauge mediated SUSY breaking models", Jeong-Pyong Hong, Masahiro Kawasaki, and Masaki Yamada, *PhysRevD*.**92**.063521.
60. "Mass-Splitting between Haves and Have-Nots", Keisuke Harigaya, Masahiro Ibe, Motoo Suzuki, *JHEP***09**(2015)155.
61. "Inflationary baryogenesis with large tensor mode", Naoyuki Takeda, *Phys. Lett. B* **746** (2015) 368-371.
62. "A general method for the construction of stable Galileon models consistent with the Planck data results", Rio Saitou, Emilio Elizalde, *JCAP***09**(2015)001.
63. "Peccei-Quinn Symmetry from Dynamical Supersymmetry Breaking", Keisuke Harigaya, Masahiro Ibe, Kai Schmitz, Tsutomu T. Yanagida, *Phys. Rev. D* **92**, 075003.
64. "Cosmological Selection of Multi-TeV Supersymmetry", Keisuke Harigaya, Masahiro Ibe, Kai Schmitz, Tsutomu T. Yanagida, *Phys.Lett. B***749** (2015)298-303.

65. "Cosmologically safe QCD axion as a present from extra dimension", Masahiro Kawasaki, Masaki Yamada and Tsutomu T. Yanagida, Phys.Lett. **B750**(2015)12-16.
66. "Revisiting the Minimal Chaotic Inflation Model", Keisuke Harigaya, Masahiro Ibe, Masahiro Kawasaki and Tsutomu T. Yanagida, Phys.Lett..B.
67. "Thermalization Process after Inflation and Effective Potential of Scalar Field", Kyohei Mukaida and Masaki Yamada, JCAP**02**(2016)003.
68. "Dynamics of Peccei-Quinn Breaking Field after Inflation and Axion Isocurvature Perturbations", Keisuke Harigaya, Masahiro Ibe, Masahiro Kawasaki and Tsutomu T. Yanagida, JCAP**11**(2015)003.
69. "Diboson Resonance as a Portal to Hidden Strong Dynamics", Cheng-Wei Chiang, Hajime Fukuda, Keisuke Harigaya, Masahiro Ibe, Tsutomu T. Yanagida, JHEP**11**(2015)015.
70. "Derivative-dependent metric transformation and physical degrees of freedom", Guillem Dom'enech, Shinji Mukohyama, Ryo Namba, Atsushi Naruko, Rio Saitou and Yota Watanabe, Phys. Rev. D **92**, 084027 (2015).
71. "Adiabatic Invariance of Oscillons/I-balls", Masahiro Kawasaki, Fuminobu Takahashi and Naoyuki Takeda, Phys. Rev. D **92**, 105024.
72. "Revisiting Big-Bang Nucleosynthesis Constraints on Dark-Matter Annihilation", Masahiro Kawasaki, Kazunori Kohri, Takeo Moroi, and Yoshitaro Takaes, Phys.Lett.**B751**(2015)246-250.
73. "Strongly broken Peccei-Quinn symmetry in the early Universe", Fuminobu Takahashi and Masaki Yamada, JCAP**10**(2015)010 .
74. "Constraints on the neutrino parameters by future cosmological 21cm line and precise CMB polarization observations", Yoshihiko Oyama, Kazunori Kohri, Masashi Hazumi, JCAP**02**(2016)008.
75. "Cosmologically safe QCD axion without fine-tuning", Masaki Yamada, Tsutomu T. Yanagida, and Kazuya Yonekura, Phys. Rev. Lett. **116**, 051801.
76. "Affleck-Dine leptogenesis and its backreaction to inflaton dynamics", Masaki Yamada, Phys.Lett.**B754**(2016)208-213.
77. "The two-field regime of natural inflation", Ana Achucarro, Vicente Atal, Masahiro Kawasaki and Fuminobu Takahashi, JCAP**12**(2015)044.
78. "Suppressing the QCD Axion Abundance by Hidden Monopoles", Masahiro Kawasaki, Fuminobu Takahashi and Masaki Yamada, Phys.Lett.**B753**(2016)677-681.
79. "Axino dark matter and baryon number asymmetry production by the Q-ball decay in gauge mediation", Shinta Kasuya, Etsuko Kawakami and Masahiro Kawasaki, JCAP**03**(2016)011.
80. "CMB Constraint on Dark Matter Annihilation after Planck 2015", Masahiro Kawasaki, Kazunori Nakayama and Toyokazu Sekiguchi, Physics letters B (2016).
81. "ATLAS on-Z Excess via gluino-Higgsino-singlino decay chains in the NMSSM ", Keisuke Harigaya, Masahiro Ibe, Teppei Kitahara, JHEP **1601** (2016) 030.
82. "Solution to the baryon-dark-matter coincidence problem in the constrained minimal supersymmetric model with a 126-GeV Higgs boson", Ayuki Kamada, Masahiro Kawasaki, and Masaki Yamada, Phys. Rev. D **91**, 081301(R).

(b) Conference Papers

1. "Recent Progress in the Development of Photomultiplier Tubes", S. Nakayama, Proceedings for International Conference on New Photo-detectors (PhotoDet2015), 6-9 July 2015, Moscow, Troitsk, Russia.
2. "XMASS 1.5, the next step of the XMASS experiment", K. Ichimura, PoS(ICRC2015)1223, July 30 - August 6, 2015, The Hague, The Netherlands.
3. "XMASS detector calibration using a neutron source", K. Ichimura, LIDINE (Light Detection In Noble Elements) 2015.
4. "Using ^{220}Rn to calibrate liquid noble gas detectors", M.Kobayashi, Proceedings of the XIV International Conference on Topics in Astroparticle and Underground Physics (TAUP2015).

5. "Results from the fiducial volume analysis of the XMASS-RFB dark matter data", A. Takeda for the XMASS collaboration, Proceedings of "34th International Cosmic Ray Conference (ICRC2015)".
6. "XMASS MC simulation", K. Abe on behalf of XMASS collaboration, Journal of Instrumentation, Volume 11, February 2016.
7. "Results from the annual modulation analysis of the XMASS-I dark matter data,"K. Hiraide, Proceedings of the 34th International Cosmic Ray Conference (ICRC2015), PoS ICRC2015 (2015) 1198.
8. "XMASS experiment", Masaki Yamashita for the XMASS collaboration, 12th Conference on the Intersections of Particle and Nuclear Physics in Vail, CO (CIPANP2015), May 19-24 in US.
9. "Results from the fiducial volume analysis of the XMASS-RFB dark matter data", A. Takeda, 34th International Cosmic Ray Conference (ICRC2015), The Hague, Netherlands, July 30-August 6, 2015.
10. "The data acquisition system of the XMASS experiment," K. Hiraide, Proceedings of the 21st International Conference on Computing in High Energy and Nuclear Physics (CHEP2015), J. Phys. Conf. Ser. 664 (2015) 082018.
11. "Atmospheric neutrino oscillation and mass hierarchy determination in Super-Kamiokande", K. Okumura, Physics Procedia 61 (2015) 619-626.
12. "Nucleon decay search in Super-Kamiokande (poster session)", Makoto Miura, 34th International Cosmic Ray Conference (ICRC2015).
13. "Quest for the lowest-energy neutrinos in Super-Kamiokande", Hiroyuki Sekiya, Proceedings of the 5th International Workshop in Low Radioactivity Techniques AIP Conf. Proc. 1672, 080001 (2015).
14. "Recent Results from Super-Kamiokande", M Nakahata for the Super-Kamiokande collaboration, Proceedings of XVI International Workshop on Neutrino Telescopes, 2-6 March 2015, Venice, Italy.
15. "Solar neutrino results from Super Kamiokande", Yuuki Nakano for the Super Kamiokande Collaboration, 34th International Cosmic Ray Conference (ICRC2015), The Hague, Netherlands, July 30-August 6, 2015.
16. "Recent results from the Telescope Array - studies of ultra-high energy cosmic rays and the prospect -", H. Sagawa (Telescope Array Collaboration), PHOTON 2015: International Conference on the Structure and the Interactions of the Photon including the 21th International Workshop on Photon-Photon Collisions and the International Workshop on High Energy Photon Colliders, Russia, 15 - 19 June, 2015.
17. "Summary of Results from the Telescope Array Experiment", C.C.H. Jui (Telescope Array Collaboration), ICRC 2015: 34th International Cosmic Ray Conference, Netherlands, July 30 - August 6, 2015.
18. "Telescope Array extension: TAx4", H. Sagawa (Telescope Array Collaboration), ICRC 2015: 34th International Cosmic Ray Conference, Netherlands, July 30 - August 6, 2015.
19. "Telescope Array measurement of UHECR composition from stereoscopic fluorescence detection", T. Stroman and Y. Tameda (Telescope Array Collaboration), ICRC 2015: 34th International Cosmic Ray Conference, Netherlands, July 30 - August 6, 2015.
20. "Telescope Array search for photons and neutrinos with the surface detector data", G.I. Rubtsov, M. Fukushima, D. Ivanov, M.S. Piskunov, B. Stokes, G. Thomson, S.V. Troitsky (Telescope Array Collaboration), ICRC 2015: 34th International Cosmic Ray Conference, Netherlands, July 30 - August 6, 2015.
21. "Telescope Array Radar (TARA): First Measurement of EAS Radar Cross-section Upper Limit", I. Myers, J. Belz (Telescope Array Collaboration), ICRC 2015: 34th International Cosmic Ray Conference, Netherlands, July 30 - August 6, 2015.
22. "Measurement of the Proton-Air Cross Section with Telescope Array's Middle Drum Detector and Surface Array in Hybrid Mode.", R. Abbasi, J. Belz (Telescope Array Collaboration), ICRC 2015: 34th International Cosmic Ray Conference, Netherlands, July 30 - August 6, 2015.
23. "Interpretation of the energy spectrum observed with the Telescope Array surface detectors", E. Kido, O.E. Kalashev (Telescope Array Collaboration), ICRC 2015: 34th International Cosmic Ray Conference, Netherlands, July 30 - August 6, 2015.

24. "Study of UHECR Composition Using Telescope Array's Middle Drum Detector and Surface Array in Hybrid Mode", J.P. Lundquist (Telescope Array Collaboration), ICRC 2015: 34th International Cosmic Ray Conference, Netherlands, July 30 - August 6, 2015.
25. "Energy Spectrum and Mass Composition of Ultra-High Energy Cosmic Rays Measured with the Telescope Array Fluorescence Detector Using a Monocular Analysis", T. Fujii (Telescope Array Collaboration), ICRC 2015: 34th International Cosmic Ray Conference, Netherlands, July 30 - August 6, 2015.
26. "The distribution of shower longitudinal profile widths as measured by Telescope Array in stereo mode", D.R. Bergman and T.A. Stroman (Telescope Array Collaboration), ICRC 2015: 34th International Cosmic Ray Conference, Netherlands, July 30 - August 6, 2015.
27. "Search for UHE Photons with the Telescope Array Hybrid Detector", K. Yamazaki (Telescope Array Collaboration), ICRC 2015: 34th International Cosmic Ray Conference, Netherlands, July 30 - August 6, 2015.
28. "Cosmic Rays Energy Spectrum observed by the TALE detector using Cerenkov light", T. AbuZayyad (Telescope Array Collaboration), ICRC 2015: 34th International Cosmic Ray Conference, Netherlands, July 30 - August 6, 2015.
29. "Anisotropy search in the Ultra High Energy Cosmic Ray Spectrum in the Northern Hemisphere using the Telescope Array surface detector", T. Nonaka, R. Cady, M. Fukushima, D. Ivanov, K. Kawata, E. Kido, J.N. Matthews, S. Nagataki, T. Okuda, H. Sagawa, N. Sakurai, B.T. Stokes, M. Takeda and A. Taketa (Telescope Array Collaboration), ICRC 2015: 34th International Cosmic Ray Conference, Netherlands, July 30 - August 6, 2015.
30. "Energy Spectrum and Mass Composition of Ultra-High Energy Cosmic Rays Measured by the hybrid technique in Telescope Array", D. Ikeda and W. Hanlon (Telescope Array Collaboration), ICRC 2015: 34th International Cosmic Ray Conference, Netherlands, July 30 - August 6, 2015.
31. "Studies on Time Profiles of EAS Particles Observed with the Telescope Array Surface Detectors", N. Inoue, R. Abe, R. Cady, M. Fukushima, J.N. Matthews, T. Nonaka, H. Sagawa and T. Suzawa (Telescope Array Collaboration), ICRC 2015: 34th International Cosmic Ray Conference, Netherlands, July 30 - August 6, 2015.
32. "Summary of UHECR Composition Measurements by the Telescope Array Experiment", J. Belz (Telescope Array Collaboration), ICRC 2015: 34th International Cosmic Ray Conference, Netherlands, July 30 - August 6, 2015.
33. "Ultra-High-Energy Cosmic-Ray Hotspot Observed with the Telescope Array Surface Detectors", K. Kawata, M. Fukushima, D. Ikeda, D. Ivanov, E. Kido, J. N. Matthews, S. Nagataki, T. Nonaka, T. Okuda, G. Rubtsov, H. Sagawa, N. Sakurai, B. T. Stokes, M. Takeda, R. Takeishi, A. Taketa, G. B. Thomson, P. Tinyakov, I. Tkachev, H. Tokuno (Telescope Array Collaboration), ICRC 2015: 34th International Cosmic Ray Conference, Netherlands, July 30 - August 6, 2015.
34. "Cosmic Ray Shower Profile Track Finding for Telescope Array Fluorescence Detectors", J.P. Lundquist (Telescope Array Collaboration), ICRC 2015: 34th International Cosmic Ray Conference, Netherlands, July 30 - August 6, 2015.
35. "Fluorescence Detection of Cosmic Ray Air Showers Between $10^{16.5}$ eV and $10^{18.5}$ eV with the Telescope Array Low Energy Extension (TALE)", . Zundel (Telescope Array Collaboration), ICRC 2015: 34th International Cosmic Ray Conference, Netherlands, July 30 - August 6, 2015.
36. "TA anisotropy summary", M. Fukushima, D. Ikeda, D. Ivanov, K. Kawata, E. Kido, J.N. Matthews, S. Nagataki, T.Nonaka, T. Okuda, G. Rubtsov, H. Sagawa, N. Sakurai, B.T. Stokes, M. Takeda, R. Takeishi, A. Taketa, G.B., Thomson, P. Tinyakov, I. Tkachev, H. Tokuno, S. Troitsky (Telescope Array Collaboration), ICRC 2015: 34th International Cosmic Ray Conference, Netherlands, July 30 - August 6, 2015.
37. "TA Spectrum Summary", D. Ivanov (Telescope Array Collaboration), ICRC 2015: 34th International Cosmic Ray Conference, Netherlands, July 30 - August 6, 2015.
38. "Search for EeV Protons of Galactic Origin", D. Ivanov, M. Pshirkov, G. Thomson, P. Tinyakov, A. Tirone, F. Urban (Telescope Array Collaboration), ICRC 2015: 34th International Cosmic Ray Conference, Netherlands, July 30 - August 6, 2015.
39. "Report of the Working Group on the Composition of Ultra-High Energy Cosmic Rays", M. Unger for the Pierre Auger Collaboration and the Telescope Array Collaboration, ICRC 2015: 34th International Cosmic Ray Conference, Netherlands, July 30 - August 6, 2015.
40. "Calibration of a fluorescence detector using a flying standard light source for the Telescope Array", M. Hayashi, Y. Tameda, Y. Tsunesada, T. Tomida (Telescope Array Collaboration), ICRC 2015: 34th International Cosmic Ray Conference, Netherlands, July 30 - August 6, 2015.

41. "Calibration of the TA Fluorescence Detectors with Electron Light Source", B. Shin, T. Shibata, D. Ivanov, M. Fukushima, G. Thomson, J. Matthews, B. Cheon, H. Sagawa (Telescope Array Collaboration), ICRC 2015: 34th International Cosmic Ray Conference, Netherlands, July 30 - August 6, 2015.
42. "The NICHE Array: Status and Plans", D.R. Bergman, J.F. Krizmanic, Y. Tsunesada (Telescope Array Collaboration), ICRC 2015: 34th International Cosmic Ray Conference, Netherlands, July 30 - August 6, 2015.
43. "Imaging and non-imaging Cherenkov hybrid reconstruction", D.R. Bergman and T. Abu-Zayyad (Telescope Array Collaboration), ICRC 2015: 34th International Cosmic Ray Conference, Netherlands, July 30 - August 6, 2015.
44. "Performance and Operational Status of Muon Detectors in the Telescope Array Experiment", T. Nonaka, R. Cady, D. Ivanov, J.N. Matthews, S. Ogio, T. Okuda, H. Sagawa, N. Sakurai, B.T. Stokes, and R. Takeishi (Telescope Array Collaboration), ICRC 2015: 34th International Cosmic Ray Conference, Netherlands, July 30 - August 6, 2015.
45. "Test for the Radio Detection of the Extensive Air Shower using the Electron Beam in Telescope Array", D. Ikeda (Telescope Array Collaboration), ICRC 2015: 34th International Cosmic Ray Conference, Netherlands, July 30 - August 6, 2015.
46. "Development of the TALE Surface Detector Array", S. Ogio, S. Konishi, Y. Nishimoto, R. Onogi, Y. Takahashi and T. Goto (Telescope Array Collaboration), ICRC 2015: 34th International Cosmic Ray Conference, Netherlands, July 30 - August 6, 2015.
47. "Initial results of a direct comparison between the Surface Detectors of the Pierre Auger Observatory and the Telescope Array", R. Takeishi, R. Cady, J. N. Matthews, T. Nonaka, S. Ogio, H. Sagawa for the Telescope Array Collaboration, C. Covault, T. Fujii, J. Johnsen, P. Lebrun, R. Lorek, P. Mantsch, J. A. J. Matthews, P. Mazur, S. Quinn, F. Sarazin, R. Sato, for the Pierre Auger Collaboration, S. Collonges, B. Courty, B. Genolini, L. Guglielmi, M. Marton, E. Raully, T. Trung, L. Smith, O. Wolf, ICRC 2015: 34th International Cosmic Ray Conference, Netherlands, July 30 - August 6, 2015.
48. "Burst Shower Events Observed by the Telescope Array Surface Detector", T. Okuda, J. Belz, W. Hanlon, M. Fukushima, K. Kawata, E. Kido, T. Nonaka, H. Sagawa, M. Takeda, A. Taketa, H. Tokuno (Telescope Array Collaboration), ICRC 2015: 34th International Cosmic Ray Conference, Netherlands, July 30 - August 6, 2015.
49. "Search for a correlation between the UHECRs measured by the Pierre Auger Observatory and the Telescope Array and the neutrino candidate events from IceCube", The IceCube Collaboration, The Pierre Auger Collaboration, The Telescope Array Collaboration, ICRC 2015: 34th International Cosmic Ray Conference, Netherlands, July 30 - August 6, 2015.
50. "Recent Results from the Telescope Array Project", W.F. Hanlon (Telescope Array Collaboration), CRIS 2015: Cosmic Ray International Seminar 2015, Italy, September 14-16, 2015.
51. "Telescope Array extension", H. Sagawa (Telescope Array Collaboration), CRIS 2015: Cosmic Ray International Seminar 2015, Italy, September 14-16, 2015.
52. id0246 "Observation of intense fluxes of charged particles in association with thundercloud in Tibet", M. Amenomori et al., 34th International Cosmic Ray Conference (ICRC2015), July 30 - August 6, 2015, The Hague, The Netherlands.
53. id0279 "Sidereal anisotropy of Galactic cosmic ray observed by the Tibet Air Shower experiment and the IceCube experiment", M. Amenomori et al., 34th International Cosmic Ray Conference (ICRC2015), July 30 - August 6, 2015, The Hague, The Netherlands.
54. id0421 "Observation of primary cosmic rays with the new Tibet hybrid experiment(YAC-II + Tibet-III + MD)", M. Amenomori et al., 34th International Cosmic Ray Conference (ICRC2015), July 30 - August 6, 2015, The Hague, The Netherlands.
55. id0424 "YAC sensitivity for measuring the light-component spectrum of primary cosmic rays at the "knee" energies", L. M. Zhai et al., 34th International Cosmic Ray Conference (ICRC2015), July 30 - August 6, 2015, The Hague, The Netherlands.
56. id0430 "Shower reconstruction performance of the new Tibet hybrid experiment consisting of YAC-II, Tibet-III and MD arrays", D. Chen et al., 34th International Cosmic Ray Conference (ICRC2015), July 30 - August 6, 2015, The Hague, The Netherlands.
57. id0431 "Investigation of hadronic interaction models from *10TeV to 1 PeV with the Tibet AS-core", M. Amenomori et al., 34th International Cosmic Ray Conference (ICRC2015), July 30 - August 6, 2015, The Hague, The Netherlands.

58. id0432 "Simulation Study On High Energy Electron and Gamma-ray Detection With the Newly Upgraded Tibet AS-gamma Experiment", Xu Chen et al., 34th International Cosmic Ray Conference (ICRC2015), July 30 - August 6, 2015, The Hague, The Netherlands.
59. id0546 "On the primary model to explain the relation between a rigidity-dependent spectral hardening of proton and helium spectra and a sharp knee of the all-particle spectrum", Ying Zhang et al., 34th International Cosmic Ray Conference (ICRC2015), July 30 - August 6, 2015, The Hague, The Netherlands.
60. id0833 "Search for gamma rays above 100 TeV from the Crab Nebula using the Tibet air shower array and the 100 m^2 muon detector", M. Amenomori et al., 34th International Cosmic Ray Conference (ICRC2015), July 30 - August 6, 2015, The Hague, The Netherlands.
61. id0935 "Energy Determination and Gamma/Hadron Separation using the Lateral Distribution of EAS for the 100 TeV Gamma-Ray Astronomy", K. Kawata et al., 34th International Cosmic Ray Conference (ICRC2015), July 30 - August 6, 2015, The Hague, The Netherlands.
62. id0969 "The TIBET AS+MD Project; progress report 2015", M. Amenomori et al., 34th International Cosmic Ray Conference (ICRC2015), July 30 - August 6, 2015, The Hague, The Netherlands.
63. "Gamma Ray Bursts in the HAWC Era", Peter Meszaros, Katsuaki Asano, Kohta Murase, Derek Fox, He Gao, Nicholas Senno, the HAWC inauguration conference, Puebla, Mexico, March 19-20, 2015, Pubs. Academia de Ciencias de Mexico, arXiv:1506.02707 (2015).
64. "Resolving the Extragalactic Background Light with Multi-field Deep ALMA Data", Fujimoto, S.; Ouchi, M.; Ono, Y.; Shibuya, T.; Ishigaki, M.; Momose, R., REVOLUTION IN ASTRONOMY WITH ALMA: THE THIRD YEAR, Tokyo, Japan, 8-11 December 2014, Vol.499(2015), p.21.
65. "Probing composite Higgs models by measuring phase shifts at LHC", Kunio Kaneta, Contribution to the proceedings of the 2nd Toyama International Workshop on Higgs as a Probe of New Physics (HPNP 2015), February 11-15, 2015.
66. "Charged Q-balls in gauge mediated SUSY breaking models", Jeong-Pyong Hong, Masahiro Kawasaki, and Masaki Yamada, Contribution to the proceedings of the 2nd LeCosPA Symposium, December 14-18, 2015

(c) ICRR Reports

1. ICRR-Report-700-2015-1
"Spontaneous thermal Leptogenesis via Majoron oscillation"
Masahiro Ibe, Kunio Kaneta.

D. Doctoral Theses

1. " 8B solar neutrino spectrum measurement using Super-Kamiokande IV",
Yuuki Nakano,
Ph.D Thesis, Feb. 2016
2. "Studies of the energy, azimuthal, and time spectra of the atmospheric neutrino flux at Super-Kamiokande",
Euan Richard,
Ph.D Thesis, Sep. 2015
3. "Simultaneous multi-wavelength observation of giant radio pulses from the Crab pulsar",
Ryo Mikami,
Ph.D Thesis, Mar. 2016.
4. "I-ball formation and its evolution for an oscillating scalar field during reheating",
Naoyuki Takeda,
Ph.D Thesis, Mar. 2016.
5. "Visible and dark matter genesis through the Affleck-Dine mechanism",
Masaki Yamada,
Ph.D Thesis, Mar. 2016

E. Public Relations

(a) ICRR News

ICRR News is a quarterly publication written in Japanese about scientific and educational activities at ICRR. It includes:

1. reports on scientific activities of ICRR staff members and those conducted at one or more of its facilities,
2. reports of international conferences on topics relevant to ICRR's research activities,
3. reports on topics discussed at ICRR's Committees,
4. list of publications published by ICRR [ICRR-Report],
5. list of seminars held at ICRR,
6. announcements, and
7. other items of relevance.

Below lists the main topics in the issues published in FY 2015:

No.93 (June 30, 2015)

- The First CTA LST (Large Size Telescope) will be constructed at La Palma in Canary Island, Masahiro Teshima
- Awards
- ICRR Spring School 2015 Report
- Staff reassignment
- ICRR-Report
- ICRR-Sminar

No.94 (September 30, 2015)

- Subaru Telescope Detects Sudden Appearance of Galaxies in the Early Universe, Akira Konno, Masami Ouchi
- Pick-Up: Construction site for first CTA LST (Large Size Telescope) has been fixed
- Staff reassignment
- ICRR-Report
- ICRR-Seminar

No.95 (December 31, 2015)

- Nobel Prize in Physics 2015, Masayuki Nakahata
- Report on the tour, the inauguration ceremony and the celebration in commemoration of the completion of initial KAGRA experimental facility, Shinji Miyoki
- Report of the groundbreaking ceremony for the fist CTA LST (Large Size Telescope), Masahiro Teshima
- Open Campus 2015 Report
- Awards
- Staff reassignment
- ICRR-Seminar

(b) Public Lectures

- "Rikei Saizensen," Aug. 22, 2015, Kavli IPMU, Kashiwa-city, Chiba, Michiko Ohishi (ICRR, the University of Tokyo).
- "Nobel Prize commemorative Lecture," Nov. 21, 2015, Nagoya University, Nagoya-city, Aichi, Takaaki Kajita (ICRR, the University of Tokyo).
- "Neutrino and Gravitational Wave," Nov. 27, 2015, Toyama University, Toyama-city, Toyama, Takaaki Kajita (ICRR, the University of Tokyo).
- "Nobel Prize Commemorative Lecture," Jan. 13, 2016, Higashimatsuyama-city, Saitama, Takaaki Kajita (ICRR, the University of Tokyo).
- "Nobel Prize Commemorative Lecture," Jan. 17, 2016, Toyama-city, Toyama, Takaaki Kajita (ICRR, the University of Tokyo).
- "Nobel Prize Commemorative Lecture," Feb. 4, 2016, Koshigaya-city, Saitama, Takaaki Kajita (ICRR, the University of Tokyo).
- "SSH Kawagoe High School," Feb. 15, 2016, Kawagoe-city, Saitama, Takaaki Kajita (ICRR, the University of Tokyo).
- "Photo detection in neutrino related researches," Feb. 24, 2016, Grand Hotel Hamamatsu, Hamamatsu-city, Shizuoka, Takaaki Kajita (ICRR, the University of Tokyo).
- "Nobel Prize Commemorative Lecture," Feb. 28, 2016, Toyama-city, Toyama, Takaaki Kajita (ICRR, the University of Tokyo).
- "Nobel Prize Commemorative Symposium," Mar. 29, 2016, Yurakucho Asahi Hall, Chiyoda-ku, Tokyo, Takaaki Kajita (ICRR, the University of Tokyo).
- "Nobel Prize Commemorative Symposium," Mar. 39, 2016, JP Tower, Chiyoda-kum Tokyo, Takaaki Kajita (ICRR, the University of Tokyo).
- "Particle Physics and Neutrino," Feb. 13, 2016, Asahi Culture Center Shonan, Kimihiro Okumura (ICRR, the University of Tokyo).
- "Particle Physics and Neutrino," Mar. 6, 2016, Chiba City Museum of Science, Kimihiro Okumura (ICRR, the University of Tokyo).
- "SSH, Shizuoka Kita High School," Apr. 24, 2015, Kamioka Observatory, ICRR, University of Tokyo, Hiroyuki Sekiya (Kamioka Observatory, ICRR, the University of Tokyo).
- "Sciencecafe Gifu," Apr. 26, 2015, Gifu-city, Gifu, Yoichiro Suzuki (Kamioka Observatory, ICRR, the University of Tokyo).
- "The Graduate University for Advanced Studies," Jun. 24, 2015, Kamioka Observatory, ICRR, the University of Tokyo, Masayuki Nakahata (Kamioka Observatory, ICRR, the University of Tokyo).
- "Sciencecafe," Jul. 12, 2015, Toyama-city, Toyama, Masato Shiozawa (Kamioka Observatory, ICRR, the University of Tokyo).
- "Geo Space Adventure," Jul.18-19, 2015, Super-Kamiokande, Masayuki Nakahata, Shigetaka Moriyama, Yoshinari Hayato, Jun Kameda, Roger Wendell, Yumiko Takanega (Kamioka Observatory, ICRR, the University of Tokyo).
- "SSH, Momoyama High School," Jul.27, 2015, Kamioka Observatory, ICRR, University of Tokyo, Roger Wendell (Kamioka Observatory, ICRR, the University of Tokyo).
- "Hirameki Tokimeki Science," Aug. 3 and 7, 2015, Kamioka Observatory, ICRR, University of Tokyo, Jun Kamenda, Masaki Yamashita (Kamioka Observatory, ICRR, the University of Tokyo).
- "SSH, Ashikaga High School," Aug. 3, 2015, Kamioka Observatory, ICRR, University of Tokyo, Ko Abe (Kamioka Observatory, ICRR, the University of Tokyo).
- "SSH, Sapporo Nishi High School," Aug. 4, 2015, Kamioka Observatory, ICRR, University of Tokyo, Yasuhiro Kishimoto (Kamioka Observatory, ICRR, the University of Tokyo).

- "SSH, Ritsumeikan High School," Aug. 5, 2015, Kamioka Observatory, ICRR, University of Tokyo, Ko Abe (Kamioka Observatory, ICRR, the University of Tokyo).
- "Yume-no-Tamago-Juku," Aug. 7, 2015, Hida-city, Gifu, Atsushi Takeda (Kamioka Observatory, ICRR, the University of Tokyo).
- "SSH, Kyoto Kyouiku University High School ," Aug. 19, 2015, Kamioka Observatory, ICRR, University of Tokyo, Makoto Miura (Kamioka Observatory, ICRR, the University of Tokyo).
- "SSH, Ochanomizu High School," Aug. 26, 2015, Kamioka Observatory, ICRR, University of Tokyo, Motoyasu Ikeda, Kamioka Observatory, ICRR, the University of Tokyo.
- "Kamioka Junior High School," Oct. 15, 2015, Hida-city, Gifu, Hiroyuki Sekiya (Kamioka Observatory, ICRR, the University of Tokyo).
- "Sciencecafe in Kashiwa Open Campus," Oct. 23-24, 2015, Kashiwa-city, Chiba, Yoshinari Hayato, Yasuhiro Kishimoto (Kamioka Observatory, ICRR, the University of Tokyo).
- "Sciencecafe," Nov. 7, 2015, Toyama-city, Toyama, Masaki Yamashita (Kamioka Observatory, ICRR, the University of Tokyo).
- "Open lecture in Namerikawa-shi Fukuju University," Nov. 28, 2015, Namerikawa-city, Toyama, Masayuki Nakahata (Kamioka Observatory, ICRR, the University of Tokyo).
- "Sciencecafe Gifu," Dec. 5, 2015, Gifu-city, Gifu, Masayuki Nakahata (Kamioka Observatory, ICRR, the University of Tokyo).
- "Public Lecture," Dec. 14, 2015, Toyama-city, Toyama, Yasuhiro Kishimoto (Kamioka Observatory, ICRR, the University of Tokyo).
- "Shinsyu Sciencepot," Jan. 9, 2016, Shinsyu University, Masayuki Nakahata (Kamioka Observatory, ICRR, the University of Tokyo).
- "Sciencecafe," Jan. 15, 2016, Toyama-city, Toyama, Masayuki Nakahata (Kamioka Observatory, ICRR, the University of Tokyo).
- "Radiation safety management workshop," Feb. 23, 2016, Bunkyo-ku, Tokyo, Masayuki Nakahata (Kamioka Observatory, ICRR, the University of Tokyo).
- "SSH, Keio High School," Feb. 24, 2016, Kamioka Observatory, ICRR, University of Tokyo, Yoshinari Hayato (Kamioka Observatory, ICRR, the University of Tokyo).
- "Sciencecafe, Hida," Feb. 27, 2016, Hida-city, Gifu, Masato Shiozawa (Kamioka Observatory, ICRR, the University of Tokyo).
- "Public Lecture," Mar. 7, 2016, Toyama-city, Toyama, Yoshinari Hayato (Kamioka Observatory, ICRR, the University of Tokyo).
- "Spring School," Mar. 9, 2016, Kashiwa-city, Chiba, Shigetaka Moriyama (Kamioka Observatory, ICRR, the University of Tokyo).
- "Public lecture," Mar. 20, 2016, Sendai-city, Miyagi, Masayuki Nakahata (Kamioka Observatory, ICRR, the University of Tokyo).
- "Radiation safety management workshop," Mar. 4, 2016, Osaka-city, Osaka, Yasuhiro Kishimoto (Kamioka Observatory, ICRR, the University of Tokyo).
- "Science Cafe on Cosmic Rays," Jan. 11, 2016, Tamarokuto Science Center, Nishitokyo-city, Tokyo, Daisuke Ikeda (ICRR, the University of Tokyo).
- "Cutting-Edge Space Science Research" for Science-Nerd High School Students, October 31, 2015, Saitama Prefectural Education Center, Masami Ouchi (ICRR, the University of Tokyo).
- "Cosmic History Studied with the Large Telescopes," November 18, 2015, Tokyo Metropolitan Musashi High School, Yoshiaki Ono (ICRR, the University of Tokyo).

- "Studying the Universe and its history," November 6, 2015, Kagawa prefectural Sakurai high school, Florent Duval (ICRR, the University of Tokyo).
- "ICRR-Kavli IPMU Joint Public Lecture," Apr. 18, 2015, Kashiwa-city, Chiba, Shinji Miyoki (ICRR, the University of Tokyo).
- "SSH Shizuoka Kita High school," Apr. 24, 2015, Kamioka-cho, Hida-city, Gifu, Keiko Kokeyama (ICRR, the University of Tokyo).
- "Science Seminar at GSA - Constructing KAGRA to detect Gravitational Waves -," Jul. 18, 2015, Kamioka-cho, Hida-city, Gifu, Masatake Ohashi (ICRR, the University of Tokyo).
- "Public Lecture - Constructing KAGRA to detect Gravitational Waves -," Jul. 28, 2015, Kamioka-cho, Hida-city, Gifu, Masatake Ohashi (ICRR, the University of Tokyo).
- "Science Cafe - More about KAGRA and Gravitational Waves -," Jul. 31, 2015, Kamioka-cho, Hida-city, Gifu, Masatake Ohashi, Osamu Miyakawa, Keiko Kokeyama (ICRR, the University of Tokyo).
- "KAGRA Tour for Public," Aug. 1, 2015, Kamioka-cho, Hida-city, Gifu, GWPO (Gravitational Wave Project Office) (ICRR, the University of Tokyo).
- "Chiba Science School; Yume Challenge - Gravitational Wave, Melody from the Universe -," Aug. 19-20, 2015, ICRR, Kashiwa-city, Chiba, Keiko Kokeyama (ICRR, the University of Tokyo).
- "SSH Yoshiki High School," Sep. 7, 2015, , Keiko Kokeyama (ICRR, the University of Tokyo).
- "Public Lecture - Einstein's Melody from the Universe -," Nov. 7, 2015, Hiroshima University, Higashihiroshima-city, Hiroshima, Seiji Kawamura (ICRR, the University of Tokyo).
- "Public Lecture in commemoration of 100th anniversary of the General Theory of Relativity," Nov. 14, 2015, Kamioka-cho, Hida-city, Gifu, Masatake Ohashi (ICRR, the University of Tokyo).
- "Up until now and From now on about KAGRA Project," Nov. 14, 2015, Toyama-city, Toyama, Shinji Miyoki (ICRR, the University of Tokyo).
- Workshop; Let's build your mini Michelson Interferometers," Mar. 26, 2016, Tamarokuto Science Center, Nishitokyo-city, Tokyo, Keiko Kokeyama (ICRR, the University of Tokyo).
- "Asahigaoka High School," Jan. 29, 2016, Nagoya-city, Aichi, Osamu Miyakawa (ICRR, the University of Tokyo).
- "Lecture at Vacuum 2015 - Constructing the Large-scale Cryogenic Gravitational Wave Telescope KAGRA -," Pacifico Yokohama, Yokohama-city, Kanagawa, Yoshio Saito (ICRR, the University of Tokyo)
- "Public Lecture," Tamarokuto Science Center, Nishitokyo-city, Tokyo, Kazuaki Kuroda (ICRR, the University of Tokyo).

(c) Visitors

Kashiwa Campus (Total: 84 groups, 5,452 people)

- Elementary, Junior High and High schools: 6 groups
- Universities and Graduate schools: 2 groups
- Researchers: 0 group
- Inspections: 1 group
- Press: 72 groups
- Others: 3 groups

KAMIOKA Observatory (Total: 182 groups, 2,433 people)

- Elementary, Junior High and High schools: 17 groups
- Universities and Graduate schools: 31 groups

- Researchers: 18 groups
- Inspections: 18 groups
- Press: 16 groups
- Others: 82 groups

KAGRA Observatory (Total: 126 groups, 1,244 people)

- Junior High and High schools: 4 groups
- Universities and Graduate schools: 11 groups
- Researchers: 27 groups
- Inspections: 18 groups
- Press: 15 groups
- Others: 51 groups

F. Inter-University Research Activities

Numbers of Researchers

	Number of Applications	Number of Adoptions	Number of Researchers
Facility Usage			
Kamioka Observatory	39	39	866
Akeno Observatory	8	7	180
Norikura Observatory	11	11	91
Low-Level Radioisotope Measurement Facility	3	3	20
Cryogenic Laser Interferometer in Kashiwa	19	19	476
Laboratorial Facility in Kashiwa	9	9	134
Computer Facility in Kashiwa	12	12	253
Conference Facility in Kashiwa	10	10	254
Over Sea Facilities	13	13	255
Annual Sums	124	123	2,529
Joint Research			
Neutrino and Astroparticle Research	39	39	865
High Energy Cosmic Ray Research	51	50	1,021
Astrophysics and Gravity Research	26	26	560
Research Center for Cosmic neutrinos	8	8	83
Annual Sums	124	123	2,529

Research Project Titles

1. Study of simulation for atmospheric neutrino
2. Study of atmospheric neutrino flux and neutrino oscillations
3. Three-flavor oscillation study in atmospheric neutrinos
4. Study of flavor identification of atmospheric and beam neutrinos

5. Improving the sensitivity to atmospheric neutrino oscillations using external constraints
6. Study of solar neutrino energy spectrum
7. Precise measurement of Day/Night effect for B8 solar neutrinos
8. Solar neutrino measurement at Super-Kamiokande
9. Study for Supernova monitor
10. Study of Supernova Relic Neutrinos
11. Study of proton decay $p \rightarrow \nu K^+$
12. Search for proton decay via $e^+ \pi^0$ mode
13. Study in upward-going muons and high energy neutrinos
14. Sidereal daily variation of ~ 10 TeV galactic cosmic ray intensity observed by the Super-Kamiokande
15. Tokai to Kamioka Long Baseline Experiment T2K
16. Neutrino interaction study using accelerator data
17. Study for the electron neutrino appearance measurement in the T2K experiment
18. Energy calibration for Super-Kamiokande
19. Development of low concentration radon detection system
20. R&D of Megaton scale water Cherenkov Detector Hyper-Kamiokande
21. Development of the Hybrid Photodetector for a next-generation neutrino detector
22. A search for Dark Matter using Liquid Xenon Detector
23. Study of annual modulation for dark matter search with XMASS
24. Study for upgrade of XMASS detector
25. Development of calibration system for XMASS detector
26. Micro-analysis of gaseous contamination in Xe
27. R&D for low temperature rubber for XMASS
28. Radon emanation measurement from material for ultra-low background experiment
29. A study on near-ultraviolet emission of liquid xenon scintillator
30. Study of double beta decay of ^{48}Ca
31. Direction-sensitive dark matter search experiment
32. Study for lowering backgrounds of radioisotopes in large volume detectors
33. Studies on the evaluation of noble gas impurities using laser resonance ionization
34. Development of a radioactivity assay system for underground experiments
35. Development of radon detector for purified gases
36. Dark Matter Search with double-phase Argon detector
37. Integration of crustal activity observation around the Atotsugawa fault
38. Strain, tilt, seismic measurement in Kamioka-mine
39. Keeping nuclear emulsion plates in a box made of lead blocks at Kamioka Underground Lab
40. Research and development of the surface detectors for the TALE experiment

41. Development of new surface detector for observation of ultra high energy cosmic ray at Telescope Array site
42. Calibration for TA FD with RC helicopter
43. Characteristics of extensive air showers induced by ultra-high energy cosmic rays observed with AGASA
44. Observation of Galactic Cosmic Ray Intensities using Large Area Muon Telescopes
45. Multi-Color Imager for Transients, Survey and Monstrous Explosions
46. Observation of solar neutrons in solar cycle 24
47. Space weather observation using muon hodoscope at Mt. Norikura
48. Development of high energy proton irradiation technique for devices used in spaceship
49. Study of secondary cosmic rays from Thundercloud at Mt. Norikura
50. Dynamics of *Abies mariesii* forests of forest line of Mt. Norikura
51. Monitoring of secondary cosmic-ray neutrons at Norikura Observatory
52. Observation of cosmogenic nuclides concentrations with temporal variability at Mt. Norikura
53. Investigation of alpine plants on Mt. Norikura
54. Observation of total ozone and UV solar radiation with Brewer spectrophotometer on the Norikura mountains
55. Effect of forest fragmentation on the belowground microbial communities
56. Population study of Rock Ptarmigan on Mt. Norikura
57. R&D of a Compton Camera using Scintillators for Measurement of Astronomical Gamma-Ray Lines
58. Study on High Energy Cosmic Ray Sources by Observation in Space
59. R&D for the CTA Project
60. CTA-Japan Physics Research
61. Development of Foal Plane Instruments for the CTA Large Scale Telescope
62. Development of the readout system for the CTA large sized telescopes
63. Site preparation for the first Large Size Telescope of CTA in La Palma, Canary Islands, Spain
64. Development for ultra-light segmented mirror for CTA Large Size Telescope
65. Development of an ultra-fast data acquisition system for the CTA Large Sized Telescope
66. Development of camera for CTA small-sized telescopes
67. CTA Monte Carlo simulation
68. Development of advanced photon counter for the future IACT
69. Study of High Energy Gamma-ray Objects with the MAGIC telescopes
70. R&D for a Small Atmospheric Cherenkov Telescope in Akeno Observatory
71. Experimental Study of High-energy Cosmic Rays in the Tibet AS γ Experiment
72. Sidereal daily variation of ~ 10 TeV galactic cosmic ray intensity observed by the Tibet air shower array
73. Study of the composition of cosmic-rays at the Knee
74. Study of High Energetic Radiation from Thundercloud in Tibet
75. A study on variation of interplanetary magnetic field with the cosmic-ray shadow by the sun
76. Bolivian Air Shower Joint Experiment

77. Cosmic ray interactions in the knee and the highest energy regions
78. Observation with Ashra
79. Integration of the optical fiber trigger system for Ashra
80. Study of Extremely-high Energy Cosmic Rays by Telescope Array
81. The observation of abnormal shower event with lightning by TA surface particle detector
82. Study of absolute energy calibration of air shower by a compact electron linac
83. Study of radio detection of highest energy cosmic rays
84. Observation of airshower fluorescence light at the TA FD site by using an Imaging UV telescope
85. Calibration of TA-EUSO 64ch multi-anode PMT and comparison with CRAYS
86. Development of a new code for cosmic-ray air shower simulation
87. Comparative study of astrophysical particle acceleration processes
88. The extreme Universe viewed in very high energy gamma-rays 2015
89. Local organization of the International Workshop TeVPA2015
90. Gravitational Wave Detector in Kamioka (XIV)
91. Numerical simulation of electro-Magnetic Wave Propagation in Gravitational wave Detector III
92. Development of optical cavities for ultranarrow stable lasers
93. Application of geophysical observations in the Kamioka mine to the dynamics of snow and water
94. Research of Large-scale Gravitational wave Telescope (V)
95. Data analysis using CLIO dataVI
96. Research and Development for Next-Generation Ultra-High Sensitive Quantum Interferometer in KAGRA III
97. Development of Sapphire Mirror Suspension for KAGRA (LCGT) (XI)
98. Development of Very Low Vibration CryoCooler System
99. Development of High Performance Cryogenic Mirror Control System
100. FEA based investigation of cryogenic sapphire suspension system for the KAGRA detector
101. Research on cryogenic payload for KAGRA
102. Development of low mechanical loss coating for sapphire mirrors for KAGRA
103. Research on ultra-low frequency anti-vibration system for KAGRA
104. Development of KAGRA detector diagnostics system
105. Study for simulated plants for KAGRA control system
106. Analysis of impurities in sapphire mirror for KAGRA using low-temperature electron spin resonance
107. Development of the output mode-cleaner for KAGRA
108. Development of precision profiler for mirrors of LCGT interferometer 5
109. Development of precise adjustment mechanism for alignment evaluation of KAGRA (LCGT)
110. R&D for the intensity stabilization of the laser system in KAGRA
111. Construction of KAGRA data transfer and storage system
112. Data analysis of KAGRA detector

113. R&D of a free-fall type gravity gradiometer
114. Cosmic Reionization Probed with Large Optical Near-Infrared Telescopes
115. Evolution of the universe and particle physics
116. Frontier of the planetary material science
117. Continuous Measurement of Underground Laboratory Environment
118. Evaluation of the erupted radioactivities into the environment
119. Detection of time variations for cosmogenic nucleid Be-7
120. Simulation study for the IceCube Neutrino Observatory
121. Precise calculation of the atmospheric neutrino flux
122. Neutrino workshop
123. CRC workshop for future plans in cosmic ray research (2)

G. List of Committee Members

(a) Board of Councillors

KAJITA, Takaaki	ICRR, the University of Tokyo
KAWAMURA, Seiji,	ICRR, the University of Tokyo
TESHIMA, Masahiro	ICRR, the University of Tokyo
NAKAHATA, Masayuki	ICRR, the University of Tokyo
FUKUDA, Hiroo	The University of Tokyo
HOTATE, Kazuo	The University of Tokyo
TOKUSHUKU, Katsuo	KEK
SASAKI, Misao	YITP, Kyoto University
HAYASHI, Masahiko	National Astronomical Observatory of Japan
NAKAMURA, Takashi	Kyoto University
OKAMURA, Sadanori	Hosei University
TORII, Shoji	Waseda Research Institute for Science and Engineering
TSUNETA, Saku	Institute of Space and Astronautical Science
SUGIYAMA, Naoshi	Nagoya University
KOMAMIYA, Sachio	ICEPP, the University of Tokyo

(b) Advisory Committee

KAJITA, Takaaki	ICRR, the University of Tokyo
HISANO, Junji	Nagoya University
SHIBATA, Masaru	YITP, Kyoto University
HAZUMI, Masashi	KEK
KISHIMOTO, Tadafumi	Osaka University
YOKOYAMA, Masashi	The University of Tokyo
KANDA, Nobuyuki	Osaka City University
ITOW, Yoshitaka	Nagoya University
OGIO, Shoichi	Osaka City University
MUNAKATA, Kazuoki	Shinshu University
TERASAWA, Toshio	ICRR, the University of Tokyo
KAWASAKI, Masahiro	ICRR, the University of Tokyo
OHASHI, Masatake	ICRR, the University of Tokyo
FUKUSHIMA, Masaki	ICRR, the University of Tokyo
TESHIMA, Masahiro	ICRR, the University of Tokyo
NAKAHATA, Masayuki	ICRR, the University of Tokyo

(c) Inter-University Research Advisory Committee

NISHIJIMA, Kyoshi	Tokai University
YAMAMOTO, Tokonatsu	Konan University
TAJIMA, Hiroyasu	Nagoya University
KUBO, Hidetoshi	Kyoto University
MUNATAKA, Kazuoki	Shinshu University
TAKEUCHI, Yasuo	Kobe University
TOMARU, Takayuki	KEK
MASUDA, Kimiaki	Nagoya University
TERASAWA, Toshio	ICRR, the University of Tokyo
TAKITA, Masato	ICRR, the University of Tokyo
SAGAWA, Hiroyuki	ICRR, the University of Tokyo
MORIYAMA, Shigetaka	ICRR, the University of Tokyo
MIYOKI, Shinji	ICRR, the University of Tokyo

H. List of Personnel

Director	KAJITA, Takaaki,		
Vice-Director	NAKAHATA, Masayuki,	TERASAWA, Toshio,	
Kamioka Observatory (Neutrino and Astroparticle Division)			
Scientific Staff	ABE, Ko, ICHIMURA, Koichi, KISHIMOTO, Yasuhiro, MORIYAMA, Shigetaka, OGAWA, Hiroshi, TAKEDA, Atsushi, WENDELL, Roger Alexandre,	HAYATO, Yoshinari, IKEDA, Motoyasu, KOBAYASHI, Kazuyoshi, NAKAHATA, Masayuki, SEKIYA, Hiroyuki, TANAKA, Hidekazu, YAMASHITA, Masaki,	HIRAIDE, Katsuki, KAMEDA, Jun, MIURA, Makoto, NAKAYAMA, Shoei, SHIOZAWA, Masato, TOMURA, Tomonobu, YANG, Byeongsu,
Administrative Staff	OIDA, Yoshihito,		
Technical Staff	FURUTA, Hajime,	HIGASHI, Tetsuji,	TAMORI, Yukio,
Research Fellow	BAI, Lili,	SATO, Kazufumi,	TASAKA, Shigeki,
Public Relations Staff	TAKENAGA, Yumiko,		
Secretary	DOI, Kyoko, YONEZAWA, Keiko,	EJIRI, Midori,	KAMIKAWATO, Rie,
Research Center for Cosmic Neutrinos (Neutrino and Astroparticle Division)			
Scientific Staff	KAJITA, Takaaki, OKUMURA, Kimihiro,	MASUDA, Kimiaki,	NISHIMURA, Yasuhiro,
Technical Staff	SHINOHARA, Masanobu,		
Secretary	KITSUGI, Atsuko,	WATANABE, Keiko,	
High Energy Cosmic Ray Division			
Scientific Staff	ASANO, Katsuaki, ENOMOTO, Ryoji, IKEDA, Daisuke, MAZIN, Daniil Mihajlovic, OHISHI, Michiko, TAKEDA, Masahiro, TESHIMA, Masahiro,	DELGADO MENDEZ, Carlos Jose, FUKUSHIMA, Masaki, KAWATA, Kazumasa, NAKAJIMA, Daisuke, OHNISHI, Munehiro, TAKITA, Masato, TOKUNO, Hisao,	DOMINIS PRESTER, Dijana, HAYASHIDA, Masaaki, KIDO, Eiji, NONAKA, Toshiyuki, SASAKI, Makoto, TERASAWA, Toshio, YOSHIKOSHI, Takanori,
Technical Staff	AOKI, Toshifumi, NIWA, Hiroki, TOYOSHIMA, Yoshiaki,	IKEBA, Kiriko, OOKI, Kaoru,	MATSUBAYASHI, Nobuko, TAMURA, Akiko,
Research Fellow	FUJII, Toshihiro, SAKO, Takashi,	HADASCH, Daniela, TANAKA, Syuta,	NAGAOKA, Yoichi,
Secretary	KOKUBUN, Yayoi,	SHIRAGA, Ryoko	SUGAHARA, Midori,
Akeno Observatory (High Energy Cosmic Ray Division)			
Scientific Staff	SAGAWA, Hiroyuki,		
Technical Staff	KOBAYASHI, Ryoichi, SHIMIZU, Kanetoshi,	OHOKA, Hideyuki,	SEKINO, Koichi,
Norikura Observatory (High Energy Cosmic Ray Division)			
Technical Staff	AWAI, Kyosuke, OKAZAKI, Nao,	IMANISHI, Hidenori, SHIMODAIRA, Hideaki,	ISHITSUKA, Hideki, USHIMARU, Tsukasa,

Astrophysics and Gravity Division

Scientific Staff	HAYAMA, Kazuhiro, KAWAMURA, Seiji, KOKEYAMA, Keiko, OHASHI, Masatake, SAITO, Yoshio, UCHIYAMA, Takashi,	HIROSE, Eiichi, KAWASAKI, Masahiro, MIYAKAWA, Osamu, ONO, Yoshiaki, SUZUKI, Toshikazu, YAMAMOTO, Kazuhiro,	IBE, Masahiro, KIMURA, Nobuhiro, MIYOKI, Shinji, OUCHI, Masami, TOMARU, Takayuki
Administrative Staff	TAKAYAMA, Kyouichi,		
Technical Staff	DOI, Kohei, SHIMIZU, Mitsufumi,	FURUTA, Kiyoshi,	KAMIIZUMI, Masahiro,
Research Fellow	CRAIG, Kieran,	DUVAL, Florent Marcel Di- dier,	HAGEN, Alex,
	HARIGAYA, Keisuke, KUBO, Mariko, SAITO, Ryo, CHIDA, Ai, KAWAKAMI, Akiko, OKINAKA, Mihoko,	HIGUCHI, Ryo, KURODA, Kazuaki, SHIBUYA, Takatoshi, HARA, Yayoi, KIKUCHI, Rie,	KANETA, Kunio, OHYAMA, Yoshihiko, YANO, Michael, IDOMURA, Takako, MASHIMA, Chieko,
Secretary			

Graduate Students

Doctor	HAYAKAWA, Taku, ISHIO, Kazuma, KONNO, Akira, NAKANO, Masayuki, ORII, Asato, SHIN, Heungsu, TAKEDA, Naoyuki, TO, Sho,	HONG, Jeong Pyong, IYOGI, Kazuki, MIKAMI, Ryo, NAKANO, Yuuki, RICHARD, Euan Neil, TAKACHIO, Osamu, TAKEISHI, Ryuji, TSUI, Kaming,	ISHIGAKI, Masafumi, KOBAYASHI, Masatoshi, NAKAJIMA, Takeo, ONO, Kenji, SEKIGUCHI, Takanori, TAKAHASHI, Mitsunari, TAMAZAWA, Hiroko, YAMADA, Masaki, FUJIMOTO, Seiji, HASEGAWA, Kunihiko, INOMATA, Keisuke, KATAOKA, Atsunori, KOJIMA, Takashi, MIYO, Koseki, NAKANO, Wakutaka, SONODA, Yutaro, TANAKA, Hiroki,
Master	AKUTSU, Ryosuke, FUKAMI, Satoshi, HIROSHIMA, Nagisa, ISHIZAKI, Wataru, KATAYAMA, Junko, LIU, Yingtao, MUKAE, Shiro, NORITA, Takayuki, SUGAHARA, Yuma, TOKUNAGA, Kyosuke	ENOMOTO, Yutaro HARIKANE, Yuichi, INADA, Tomohiro, IWAMURA, Yuki, KATO, Sho, MIYAMOTO, Takahiro, NAGANO, Koji, SAITO, Koki, SUZUKI, Motoo, YAMANAKA, Yuji,	

Administrative Division

Administrative Staff	AKIYAMA, Makiko, KOBAYASHI, Toyoki, NAMATAME, Kaneo, SATO, Yu, YAMAGUCHI, Akiko, FUJIE, Tamiko,	ASAKA, Sadako, KONDO, Hitomi, OKANO, Yuka, WATANABE, Wataru, NAKAMURA, Saori,	FUKUHARA, Nana, MARUMORI, Yasuko, SAITO, Akiko, YAJIMA, Yuki, YAGI, Yoriko,
Research Administrator	SATO, Ritsuko,		
Public Relations Staff	FUKUDA, Hironobu,	HAYASHIDA, Misato,	ITO, Yoriko,